



**UNIVERSITY OF  
BIRMINGHAM**

# **Improvement of the structural response of steel tubular wind turbine towers by means of stiffeners**

**By**

**Yu Hu**

**A thesis submitted to  
The University of Birmingham  
For the degree of  
DOCTOR OF PHILOSOPHY**

**School of Civil Engineering  
College of Engineering and Physical Sciences  
University of Birmingham  
June 2015**

UNIVERSITY OF  
BIRMINGHAM

**University of Birmingham Research Archive**

**e-theses repository**

This unpublished thesis/dissertation is copyright of the author and/or third parties. The intellectual property rights of the author or third parties in respect of this work are as defined by The Copyright Designs and Patents Act 1988 or as modified by any successor legislation.

Any use made of information contained in this thesis/dissertation must be in accordance with that legislation and must be properly acknowledged. Further distribution or reproduction in any format is prohibited without the permission of the copyright holder.

# ABSTRACT

Renewable energy has been developed rapidly with the awareness on the protection of the environment increases. Wind energy has also been widely used as a clean energy since it does not emit greenhouse gases and less than land intensive than conventional fuels. Thus, wind turbine systems have attracted more attentions as energy converters that transfer the kinetic energy from the flowing air mass into mechanical energy. Wind turbine towers are the main structures that can support the nacelles including rotors, blades and generators etc.

In the thesis the structural response of steel tubular wind turbine towers with various design configurations is analysed using FEM modelling. First, a structural response simulation model was validated by comparison with the existing experimental data. This was then followed with a mesh density sensitivity analysis to obtain the optimum element size. Based on this outcome, towers of various heights between 50-250m are considered and investigated with three different design options as follows: (i) thick walled tower with internal horizontal stiffening rings, (ii) thick walled tower without stiffening rings and (iii) thin walled tower with stiffening rings. Based on this analysis, weight reduction ratios are examined in relation to the horizontal sway and von Mises stress increase ratios in order to identify a more efficient design approach between reducing the wall thickness and adopting internal stiffeners. All studied design solutions satisfy the strength and serviceability requirements as specified by the design codes of practice.

Then, the dynamic characteristics of these three types of independent towers and towers with concentrated mass have been examined to obtain the natural frequencies and mode shapes of the towers. The recommendations to avoid resonance for each height case are proposed. In the meantime, the local buckling behaviours of the three height towers have been performed. The effect of stiffening rings and wall thickness on the stability strength of wind turbine towers is reported.

An extensive parametric study on the structural response of tubular steel wind turbine towers enhanced by internal stiffening rings was performed. The wall thickness and the spacing of the

stiffening rings were considered as the critical design variables for towers of various heights between 50m and 250m. The parametric analysis results provide information on the effect of these parameters on the structural response of wind turbine towers of various heights.

Two alternative stiffening methods, employing horizontal or vertical stiffeners, for steel tubular wind turbine towers have been studied. In particular, two groups of three wind turbine towers of 50m, 150m and 250m in height, stiffened by horizontal rings and vertical strips respectively, were analysed. Following an extensive parametric study, these strengthening techniques were compared with each other and relevant conclusions about their effect on the overall strength and cost were obtained.

**KEY WORDS:** wind turbine tower; wind loading; shell structures; finite element analysis; stiffening rings; dynamic analysis; parametric study; sensitivity analysis; buckling; vertical stiffeners; Finite Element Analysis.

## **ACKNOWLEDGEMENTS**

The author greatly acknowledges his academic supervisors, Professor Charalampos Baniotopoulos and Dr. Jian Yang, for their continuous guidance, support and advice during the development of the research described in the present thesis. Also, the author would like to thank Professor Luís Simões da Silva and Dr. Marios Theofanous for their constructive comments to improve the quality of the thesis.

The author would like to gratefully thank Professor Dr. C. Rebelo, University of Coimbra for the data from his tower monitoring activity that he generously provided to him and all the people who provided help and constructive comments for the improvement of the quality of the thesis.

The author acknowledges with thanks China Scholarship Council (CSC) and the University of Birmingham.

Very special thanks to the author's parents, sister and younger brother, for their continuous encouragement and support during the PhD study of the author. Also, thanks to all the people not involved directly in this research who provided essential support to the author during his stay at the University of Birmingham.

<b>CHAPTER 1: INTRODUCTION.....</b>	<b>1</b>
1. 1 Background .....	1
1. 2 Aims and objectives .....	2
1. 3 Layout of thesis .....	3
<b>CHAPTER 2: LITERATURE REVIEW .....</b>	<b>5</b>
2.1 Wind energy .....	5
2.1.1 Global demand for energy .....	5
2.1.2 The wind.....	5
2.1.2 Current status of wind energy .....	7
2.2 Wind turbine towers.....	12
2.2.1 History of wind turbine towers .....	12
2.2.2 Modern wind turbine towers.....	15
2.2.3 Development of wind turbine technologies .....	18
2.3 Summary and identification of knowledge gaps.....	37
2.3.1 Summary .....	37
2.3.2 Knowledge gaps.....	38
<b>CHAPTER 3: METHODOLOGY.....</b>	<b>40</b>
3.1 Finite element method.....	40
3.1.1 Discretisation .....	40
3.1.2 Sensitivity of meshing.....	40
3.1.3 Interactions and constraints .....	41
3.1.4 Shell element .....	42
3.1.5 Continuum element .....	43

3.2 Wind load .....	44
3.2.1 50m towers .....	44
3.2.1 150m towers .....	48
3.2.2 250m towers .....	49
3.3 Experimental validations .....	50
3.3.1 Experiment description .....	50
3.3.2 Sensitivity analysis .....	54
3.3.3 Result comparison .....	55
3.4 Conclusions .....	58
<b>CHAPTER 4: FE ANALYSIS OF TOWER .....</b>	<b>59</b>
4.1 Introduction .....	59
4.2 Models of 50m tower .....	61
4.2.1 50m tower I .....	61
4.2.3 50m tower II .....	64
4.2.3 50m tower III .....	66
4. 3 Models of 150m tower .....	68
4.3.1 150m tower I .....	68
4.3.2 150m tower II .....	71
4.3.3 150m tower III .....	73
4. 4 Models of 250m tower .....	75
4.4.1 250m tower I .....	75
4.4.2 250m tower II .....	77
4.4.3 250m tower III .....	80

4. 5 Results and discussion .....	81
4. 6 Conclusions .....	85
<b>CHAPTER 5: DYNAMIC AND BUCKLING ANALYSIS .....</b>	<b>87</b>
5. 1 Dynamic analysis of tower .....	87
5.1.1 Introduction .....	87
5.1.2 Towers with concentrated mass .....	89
5. 2 Buckling analysis of towers .....	97
5.2.1 Introduction .....	97
5.2.2 Loading states .....	99
5.2.3 50m towers .....	100
5.2.4 150m towers .....	101
5.2.5 250m towers .....	102
5.2.6 Results and discussion.....	103
5. 3 Conclusions .....	104
<b>CHAPTER 6: PARAMETRIC ANALYSIS.....</b>	<b>106</b>
6. 1 Introduction .....	106
6. 2 50m towers .....	108
6.2.1 Models of 50m towers.....	108
6.2.2 Effect of the thickness T on the overall structural response .....	114
6.2.3 Effect of the spacing H of stiffening rings on the overall structural response .....	120
6. 3 150m towers .....	127
6.3.1 Models of 150m towers.....	127
6.3.2 Effect of the thickness T on the overall structural response .....	132

6.3.3 Effect of the spacing H of stiffening rings on the overall structural response .....	137
6. 4 250m towers .....	142
6.4.1 Models of 250m towers .....	142
6.4.2 Effect of the thickness T on the overall structural response .....	147
6.4.3 Effect of the spacing H of stiffening rings on the overall structural response .....	153
6. 5 Conclusions .....	158
<b>CHAPTER 7: VERTICAL STIFFENERS.....</b>	<b>159</b>
7. 1 Introduction .....	159
7. 2 On the mass of the vertical stiffeners.....	161
7. 3 Towers of 50m height .....	163
7.3.1 Model description .....	163
7.3.2 Effect of the number of vertical stiffeners .....	165
7.3.3 Effect of the central angle of the vertical stiffeners .....	168
7.3.4 Buckling analysis .....	169
7. 4 Towers of 150m height .....	172
7.4.1 Model description .....	172
7.4.2 Effect of the number of vertical stiffeners .....	174
7.4.3 Effect of the central angle of the vertical stiffeners .....	177
7.4.4 Buckling analysis .....	177
7. 5 Towers of 250m height .....	180
7.5.1 Model description .....	180
7.5.2 Effect of the number of vertical stiffeners .....	182
7.5.3 Effect of the central angle of the vertical stiffeners .....	185

7.5.4 Buckling analysis .....	185
7. 6 Conclusions .....	188
<b>CHAPTER 8: CONCLUSIONS AND RECOMMENDATIONS.....</b>	<b>189</b>
8. 1 Conclusions .....	189
8. 2 Recommendations for future work .....	193
<b>REFERENCES.....</b>	<b>195</b>

# LIST OF FIGURES

Figure 2.1 Wind circulation (WMO, 1981) .....	6
Figure 2.2 Scheme of the atmospheric boundary layer .....	7
Figure 2.3 Installed wind power capacity of main countries and regions (Dixon and Hall, 2014) .....	9
Figure 2.4 Wind energy installations: 2011-2020 (GW) (Perveen <i>et al.</i> , 2014) .....	10
Figure 2.5 Profile of a wipmolen mill (Gasch and Twele, 2012).....	14
Figure 2.6 First wind turbine for electricity generation by James Blyth in 1887 (Price, 2005).....	14
Figure 2.7 Smith-Putnam wind turbine (Wikipedia, 2014a).....	15
Figure 2.8 Composition of wind turbine tower system .....	16
Figure 2.9 Common types of wind turbine tower.....	17
Figure 2.10 Design variables of steel shell tower (Perelmuter and Yurchenko, 2013) .....	20
Figure 2.11 FE models of a tubular steel tower (Lavassas <i>et al.</i> , 2003).....	22
Figure 2.12 Dimensions of the 53m wind turbine tower (Guo <i>et al.</i> , 2011).....	23
Figure 2.13 Welding joint between tower and bottom flange (Jiang <i>et al.</i> , 2010).....	24
Figure 2.14 FE models of cantilevered shells with door openings and stiffening rings (Dimopoulos and Gantes, 2012).....	26
Figure 2.15 The prototype and door opening cut-out of the wind turbine tower (Dimopoulos and Gantes, 2013).....	26
Figure 2.16 Four stiffening types around cut-outs for tubular wind turbine towers (Dimopoulos and Gantes, 2013).....	27
Figure 2.17 Tower base configurations (Trung Q. Do <i>et al.</i> , 2014b).....	28
Figure 2.18 Geometry of lower segments of the tower (Tran <i>et al.</i> , 2013).....	29
Figure 2.19 Three types of support structures for offshore towers (Zaaijer, 2006).....	31
Figure 2.20 Wind turbine tower on the shake table: a) Parallel configuration. b) Perpendicular configuration (Prowell <i>et al.</i> , 2012) .....	32
Figure 2.21 118m height wind turbine tower with tripod foundation (Häckell and Rolfes, 2013) .....	36
Figure 2.22 The three measured wind turbine towers (Swartz <i>et al.</i> , 2010) .....	36

Figure 3.1 The discretisation process of one plate .....	40
Figure 3.2 Precision and running time with respect to density of meshing .....	41
Figure 3.3 The geometrical pattern and FEM models of shell elements .....	43
Figure 3.4 Continuum (Solid) element pattern.....	43
Figure 3.5 Ring with tetrahedron meshing .....	44
Figure 3.6 Load states of wind turbine towers .....	45
Figure 3.7 Distribution of wind loads along the tower height and around the circumference .....	45
Figure 3.8 Pressure distribution for circular cylinders .....	46
Figure 3.9 Simplified distribution pattern of wind load along tower height and around the circumference.....	47
Figure 3.10 Simplified distribution pattern of wind load along 250m tower height and around the circumference.....	49
Figure 3.11 The geometrical data and the FEM model of the 76m wind turbine tower.....	51
Figure 3.12 Wind speed of the 76m tower during testing period at Level 3 (2012b; 2012c) .....	54
Figure 3.13 Maximum von Mises stresses and horizontal sways of the 76m tower for different element sizes .....	55
Figure 3.14 Maximum vertical stresses of 76m tower at level 0 (2012b; 2012c) .....	56
Figure 3.15 Maximum vertical stresses of 76m tower at level 1 (2012b; 2012c) .....	56
Figure 3.16 Vertical stress contour plot at the cross-sections of the 76m tower at levels 0 .....	57
Figure 3.17 Vertical stress contour plot at the cross-sections of the 76m tower at levels 1 .....	57
Figure 3.18 Horizontal sway contour of the cross-section of the 76m tower at level 3 .....	58
Figure 4.1 Prototypes of 50m tower I: geometrical data and FEM models .....	62
Figure 4.2 Typical cross-section of the 50m height tower (in mm) .....	62
Figure 4.3 Contour plots of stress and sway for 50m tower I .....	63
Figure 4.4 Stress contour of flange of 50m tower I.....	64
Figure 4.5 Prototypes of 50m tower II: geometrical data and FEM models .....	65

Figure 4.6 Contour plots of stress and sway for 50m tower II.....	66
Figure 4.7 Stress contour of ring of 50m tower II.....	66
Figure 4.8 Contour plots of stress and sway for 50m tower III.....	67
Figure 4.9 Stress contour of ring of 50m tower III.....	68
Figure 4.10 Prototypes of 150m tower I: geometrical data and FEM models .....	69
Figure 4.11 Contour plots of stress and sway for 150m tower I .....	70
Figure 4.12 Stress contour of ring of 150m tower I .....	70
Figure 4.13 Prototypes of 150m tower II: geometrical data and FEM models .....	71
Figure 4.14 Contour plots of stress and sway for 150m tower II .....	73
Figure 4.15 Stress contour of ring of 150m tower II .....	73
Figure 4.16 Contour plots of stress and sway for 150m tower III.....	74
Figure 4.17 Stress contour of ring of 150m tower III.....	75
Figure 4.18 Prototypes of 250m tower I: geometrical data and FEM models .....	76
Figure 4.19 Contour plots of stress and sway for 250m tower I .....	77
Figure 4.20 Stress contour of ring of 250m tower I .....	77
Figure 4.21 Prototypes of 250m tower II: geometrical data and FEM models .....	78
Figure 4.22 Contour plots of stress and sway for 250m tower II.....	79
Figure 4.23 Stress contour of ring of 250m tower II .....	80
Figure 4.24 Contour plots of stress and sway for 250m tower III.....	80
Figure 4.25 Stress contour of ring of 250m tower III.....	81
Figure 4.26 50m tower horizontal sway and von Mises stress variation ratios of tower I/II and tower II/III .....	83
Figure 4.27 150m tower horizontal sway and von Mises stress variation ratios of tower I/II and tower II/III .....	84
Figure 4.28 250m tower horizontal sway and von Mises stress variation ratios of tower I/II and tower II/III .....	84
Figure 5.1 Structural design approaches for wind turbine towers .....	89

Figure 5.2 50m wind turbine tower I.....	90
Figure 5.3 50m wind turbine tower II.....	90
Figure 5.4 50m wind turbine tower III .....	91
Figure 5.5 150m wind turbine tower I.....	92
Figure 5.6 150m wind turbine tower II.....	93
Figure 5.7 150m wind turbine tower III .....	93
Figure 5.8 250m wind turbine tower I.....	95
Figure 5.9 250m wind turbine tower II.....	95
Figure 5.10 250m wind turbine tower III .....	96
Figure 5.11 Buckling behaviour of the shell structure.....	99
Figure 5.12 First local buckling modes of the 50m towers.....	100
Figure 5.13 First local buckling modes of the 150m towers.....	101
Figure 5.14 First local buckling modes of the 250m towers.....	102
Figure 6.1 The 50m-towers: geometrical data and FEM models (in mm).....	109
Figure 6.2 Typical ring cross-sections of the towers (in mm) .....	110
Figure 6.3 The von Mises stress of the shell and ring and the horizontal sway of the 50T <sub>ii</sub> R <sub>i</sub> H <sub>i</sub> tower .....	111
Figure 6.4 Maximum von Mises stress and horizontal sway versus T of the 50H <sub>i</sub> .....	114
Figure 6.5 Maximum von Mises stress and horizontal sway versus T of the 50H <sub>ii</sub> .....	115
Figure 6.6 Maximum von Mises stress and horizontal sway versus T of the 50H <sub>iii</sub> .....	115
Figure 6.7 Maximum von Mises stress and horizontal sway versus T of the 50H <sub>iv</sub> .....	116
Figure 6.8 $\Delta S/\Delta T$ and $\Delta D/\Delta T$ of the 50H <sub>i</sub> with respect to T .....	119
Figure 6.9 $\Delta S/\Delta T$ and $\Delta D/\Delta T$ of the 50H <sub>ii</sub> with respect to T.....	119
Figure 6.10 $\Delta S/\Delta T$ and $\Delta D/\Delta T$ of the 50H <sub>iii</sub> with respect to T .....	119
Figure 6.11 $\Delta S/\Delta T$ and $\Delta D/\Delta T$ of the 50H <sub>iv</sub> with respect to T .....	120
Figure 6.12 Maximum von Mises stresses and horizontal sways versus H of the 50T <sub>i</sub> .....	121
Figure 6.13 Maximum von Mises stresses and horizontal sways versus H of the 50T <sub>ii</sub> .....	121

Figure 6.14 Maximum von Mises stresses and horizontal sways versus H of the 50T <sub>iii</sub> .....	122
Figure 6.15 Maximum von Mises stresses and horizontal sways versus H of the 50T <sub>iv</sub> .....	122
Figure 6.16 The $\Delta S/\Delta H$ and $\Delta D/\Delta H$ graphs of the 50T <sub>i</sub> with respect to H.....	125
Figure 6.17 The $\Delta S/\Delta H$ and $\Delta D/\Delta H$ graphs of the 50T <sub>ii</sub> with respect to H.....	125
Figure 6.18 The $\Delta S/\Delta H$ and $\Delta D/\Delta H$ graphs of the 50T <sub>iii</sub> with respect to H .....	126
Figure 6.19 The $\Delta S/\Delta H$ and $\Delta D/\Delta H$ graphs of the 50T <sub>iv</sub> with respect to H .....	126
Figure 6.20 The 150m-towers: geometrical data and FEM models (in mm) .....	128
Figure 6.21 The von Mises stress of shell and ring and the horizontal sway of 150T <sub>iii</sub> R <sub>i</sub> H <sub>i</sub> tower ....	128
Figure 6.22 Maximum von Mises stress and horizontal sway versus T of the 150H <sub>i</sub> .....	132
Figure 6.23 Maximum von Mises stress and horizontal sway versus T of the 150H <sub>ii</sub> .....	132
Figure 6.24 Maximum von Mises stress and horizontal sway versus T of the 150H <sub>iii</sub> .....	133
Figure 6.25 Maximum von Mises stress and horizontal sway versus T of the 150H <sub>iv</sub> .....	133
Figure 6.26 $\Delta S/\Delta T$ and $\Delta D/\Delta T$ of the 150H <sub>i</sub> with respect to T .....	135
Figure 6.27 $\Delta S/\Delta T$ and $\Delta D/\Delta T$ of the 150H <sub>ii</sub> with respect to T.....	136
Figure 6.28 $\Delta S/\Delta T$ and $\Delta D/\Delta T$ of the 150H <sub>iii</sub> with respect to T .....	136
Figure 6.29 $\Delta S/\Delta T$ and $\Delta D/\Delta T$ of the 150H <sub>iv</sub> with respect to T .....	137
Figure 6.30 Maximum von Mises stresses and horizontal sways versus H of the 150T <sub>i</sub> .....	137
Figure 6.31 Maximum von Mises stresses and horizontal sways versus H of the 150T <sub>ii</sub> .....	138
Figure 6.32 Maximum von Mises stresses and horizontal sways versus H of the 150T <sub>iii</sub> .....	138
Figure 6.33 Maximum von Mises stresses and horizontal sways versus H of the 150T <sub>iv</sub> .....	138
Figure 6.34 The $\Delta S/\Delta H$ and $\Delta D/\Delta H$ graphs of the 150T <sub>i</sub> with respect to H.....	141
Figure 6.35 The $\Delta S/\Delta H$ and $\Delta D/\Delta H$ graphs of the 150T <sub>ii</sub> with respect to H.....	141
Figure 6.36 The $\Delta S/\Delta H$ and $\Delta D/\Delta H$ graphs of the 150T <sub>iii</sub> with respect to H .....	142
Figure 6.37 The $\Delta S/\Delta H$ and $\Delta D/\Delta H$ graphs of the 150T <sub>iv</sub> with respect to H .....	142
Figure 6.38 The 250m-towers: geometrical data and the FEM models (in mm) .....	143
Figure 6.39 The von Mises stress of the shell and the ring, and the horizontal sway of 250T <sub>i</sub> R <sub>i</sub> H <sub>i</sub> tower .....	144
Figure 6.40 Maximum von Mises stress and horizontal sway versus T of the 250H <sub>i</sub> .....	147

Figure 6.41 Maximum von Mises stress and horizontal sway versus T of the 250H <sub>ii</sub> .....	148
Figure 6.42 Maximum von Mises stress and horizontal sway versus T of the 250H <sub>iii</sub> .....	148
Figure 6.43 Maximum von Mises stress and horizontal sway versus T of the 250H <sub>iv</sub> .....	149
Figure 6.44 $\Delta S/\Delta T$ and $\Delta D/\Delta T$ of the 250H <sub>i</sub> with respect to T .....	151
Figure 6.45 $\Delta S/\Delta T$ and $\Delta D/\Delta T$ of the 250H <sub>ii</sub> with respect to T .....	151
Figure 6.46 $\Delta S/\Delta T$ and $\Delta D/\Delta T$ of the 250H <sub>iii</sub> with respect to T .....	152
Figure 6.47 $\Delta S/\Delta T$ and $\Delta D/\Delta T$ of the 250H <sub>iv</sub> with respect to T .....	152
Figure 6.48 Maximum von Mises stresses and horizontal sways versus H of the 250T <sub>i</sub> .....	153
Figure 6.49 Maximum von Mises stresses and horizontal sways versus H of the 250T <sub>ii</sub> .....	153
Figure 6.50 Maximum von Mises stresses and horizontal sways versus H of the 250T <sub>iii</sub> .....	154
Figure 6.51 Maximum von Mises stresses and horizontal sways versus H of the 250T <sub>iv</sub> .....	154
Figure 6.52 The $\Delta S/\Delta H$ and $\Delta D/\Delta H$ graphs of the 250T <sub>i</sub> with respect to H.....	157
Figure 6.53 The $\Delta S/\Delta H$ and $\Delta D/\Delta H$ graphs of the 250T <sub>ii</sub> with respect to H.....	157
Figure 6.54 The $\Delta S/\Delta H$ and $\Delta D/\Delta H$ graphs of the 250T <sub>iii</sub> with respect to H .....	158
Figure 6.55 The $\Delta S/\Delta H$ and $\Delta D/\Delta H$ graphs of the 250T <sub>iv</sub> with respect to H .....	158
Figure 7.1 Profile of the wind turbine tower in two perpendicular planes .....	162
Figure 7.2 Prototypes of the 50m towers <i>a</i> , <i>b</i> and <i>c</i> (mm).....	164
Figure 7.3 Typical cross-section of the 50m tower <i>a</i> with V <sub>i</sub> .....	164
Figure 7.4 Contour plots of 50m tower <i>a</i> with V <sub>i</sub> .....	166
Figure 7.5 Contour plots of 50m tower <i>b</i> with V <sub>i</sub> .....	166
Figure 7.6 Contour plots of 50m tower <i>c</i> with V <sub>i</sub> .....	167
Figure 7.7 Maximum von Mises stresses and horizontal sways of the 50m towers with V <sub>i</sub> , V <sub>ii</sub> and V <sub>iii</sub> .....	168
Figure 7.8 Maximum von Mises stresses and horizontal sways of the 50m towers <i>a</i> , <i>b</i> and <i>c</i> .....	169
Figure 7.9 First local buckling modes of the 50m towers <i>a</i> , <i>b</i> and <i>c</i> with V <sub>i</sub> .....	170
Figure 7.10 First local buckling modes of the 50T <sub>iv</sub> R <sub>iv</sub> H <sub>iv</sub> .....	170
Figure 7.11 Local buckling eigenvalues of the 50m towers .....	171

Figure 7.12 Prototypes of the 150m towers <i>a</i> , <i>b</i> and <i>c</i> (mm).....	173
Figure 7.13 Typical cross-section of the 150m tower <i>c</i> with $V_i$ .....	173
Figure 7.14 Contour plots of the 150m towers <i>a</i> with $V_i$ .....	174
Figure 7.15 Contour plots of the 150m towers <i>b</i> with $V_i$ .....	174
Figure 7.16 Contour plots of the 150m towers <i>c</i> with $V_i$ .....	175
Figure 7.17 Maximum von Mises stresses and horizontal sways of 150m towers with $V_i$ , $V_{ii}$ and $V_{iii}$ .....	176
Figure 7.18 Maximum von Mises stresses and horizontal sways of the 150m towers <i>a</i> , <i>b</i> and <i>c</i> .....	177
Figure 7.19 Local buckling modes of the 150m towers <i>a</i> , <i>b</i> and <i>c</i> with $V_i$ .....	178
Figure 7.20 First local buckling modes of the 150T <sub>iv</sub> R <sub>iv</sub> H <sub>iv</sub> .....	178
Figure 7.21 Buckling eigenvalues of the 150m towers .....	179
Figure 7.22 Prototypes of 250m towers <i>a</i> , <i>b</i> and <i>c</i> (mm) .....	181
Figure 7.23 Typical cross-section of the 250m tower <i>b</i> with $V_i$ .....	181
Figure 7.24 Contour plots of the 250m tower <i>a</i> with $V_i$ .....	182
Figure 7.25 Contour plots of the 250m tower <i>b</i> with $V_i$ .....	183
Figure 7.26 Contour plots of the 250m tower <i>c</i> with $V_i$ .....	183
Figure 7.27 Maximum von Mises stresses and horizontal sways of the 250m towers with $V_i$ , $V_{ii}$ and $V_{iii}$ .....	184
Figure 7.28 Maximum von Mises stresses and horizontal sways of the 250m towers <i>a</i> , <i>b</i> and <i>c</i> .....	185
Figure 7.29 First local buckling modes of 250m towers <i>a</i> , <i>b</i> and <i>c</i> with $V_i$ .....	186
Figure 7.30 First local buckling modes of 250T <sub>iv</sub> R <sub>iv</sub> H <sub>iv</sub> .....	186
Figure 7.31 Buckling eigenvalues of the 250m towers .....	187

# LIST OF TABLES

Table 2.1 Offshore and onshore wind capacities in the EU (EWEA, 2008).....	11
Table 3.1 The cross-section characteristics along the tower height (2012b; 2012c).....	51
Table 3.2 Maximum von Mises stresses and horizontal sways of the 76m tower for different element sizes .....	55
Table 4.1 Material properties of structural steel of the wind turbine tower .....	63
Table 4.2 50m wind turbine towers: maximum von Mises stress and horizontal sway .....	68
Table 4.3 Shell thickness of the 150 tower I.....	69
Table 4.4 Stiffening ring spacing for the 150m tower II .....	72
Table 4.5 Shell thickness of the 150 tower III .....	74
Table 4.6 150m wind turbine towers: maximum von Mises stress and horizontal sway.....	75
Table 4.7 Shell thickness of the 250 tower I.....	76
Table 4.8 Stiffening ring spacing for the 250m tower II .....	78
Table 4.9 Shell thickness of the 250 tower III .....	81
Table 4.10 250m wind turbine towers: maximum von Mises stress and horizontal sway.....	81
Table 4.11 Wind turbine tower mass characteristics .....	82
Table 4.12 Wind turbine towers horizontal sway and von Mises stress variation .....	83
Table 5.1 Natural frequencies for 50m wind turbine towers (Hz).....	91
Table 5.2 Natural frequencies for 150m wind turbine towers (Hz).....	94
Table 5.3 Natural frequencies for 250m wind turbine towers (Hz).....	96
Table 5.4 Buckling eigenvalues of 50m towers I, II and III .....	100
Table 5.5 Buckling eigenvalues of 150m towers I, II and III .....	102
Table 5.6 Buckling eigenvalues of 250m towers I, II and III .....	103

Table 5.7 Wind turbine towers eigenvalues variation .....	103
Table 6.1 Parameter details of the 50m-towers .....	110
Table 6.2 Maximum von Mises stresses and horizontal sways of 50m towers.....	111
Table 6.3 Rate of change $\Delta S/\Delta T$ and $\Delta D/\Delta T$ for the $50H_i/H_{ii}/H_{iii}/H_{iv}$ with respect to $T$ .....	116
Table 6.4 Rate of change $\Delta S/\Delta H$ and $\Delta D/\Delta H$ of the $50T_i/T_{ii}/T_{iii}/T_{iv}$ with respect to $H$ .....	123
Table 6.5 Parameter details of the 150m-towers .....	127
Table 6.6 Maximum von Mises stress and horizontal sway of 150m-towers .....	129
Table 6.7 Rate of change $\Delta S/\Delta T$ and $\Delta D/\Delta T$ for the $150H_i/H_{ii}/H_{iii}/H_{iv}$ with respect to $T$ .....	133
Table 6.8 The $\Delta S/\Delta H$ and $\Delta D/\Delta H$ of the $150T_i/T_{ii}/T_{iii}/T_{iv}$ with respect to $H$ .....	139
Table 6.9 Parameter details of the 250m-towers .....	144
Table 6.10 Maximum von Mises stress and horizontal sway of 250m towers.....	145
Table 6.11 Rate of change $\Delta S/\Delta T$ and $\Delta D/\Delta T$ for the $250H_i/H_{ii}/H_{iii}/H_{iv}$ with respect to $T$ .....	149
Table 6.12 Rate of change $\Delta S/\Delta H$ and $\Delta D/\Delta H$ of the $250T_i/T_{ii}/T_{iii}/T_{iv}$ with respect to $H$ .....	155
Table 7.1 Thickness of the vertical stiffeners of the 50m towers.....	163
Table 7.2 Maximum von Mises stress and horizontal sway of the 50m towers $a, b$ and $c$ .....	167
Table 7.3 First buckling eigenvalues of the 50m towers $a, b$ and $c$ .....	171
Table 7.4 Thickness of the vertical stiffeners of the 150m towers.....	173
Table 7.5 Maximum von Mises stress and horizontal sway of the 150m towers $a, b$ and $c$ .....	175
Table 7.6 Buckling eigenvalues of the 150m towers $a, b$ and $c$ .....	179
Table 7.7 Thickness of the vertical stiffeners of the 250m towers.....	180
Table 7.8 Maximum von Mises stress and horizontal sway of the 150m towers $a, b$ and $c$ .....	184
Table 7.9 Buckling eigenvalues of the 250m towers $a, b$ and $c$ .....	187

# NOMENCLATURE

$A$	the swept area of blade
$A_i$	the cross sectional area
$\Delta a_1$	the horizontal sway and von Mises stress augmentation percentage of tower I to II
$\Delta a_2$	the horizontal sway and von Mises stress augmentation percentage of tower II to III
$C_T$	the thrust coefficient
$C_D$	the cylindrical drag coefficient
$c_{p,o}$	the external pressure coefficient without free-end flow
$D_o$	the diameter at height $H$ of wind tower
$D_i$	the middle surface diameter of the $i^{th}$ segment
$D$	the diameter of cross-section of tower
$dh$	the differential height of the cross-section C-C
$\Delta E_R$	the eigenvalue augmentation percentage of tower I to II
$\Delta E_S$	the eigenvalue augmentation percentage of tower II to III
$EI$	tower bending stiffness
$F$	thrust force
$f$	first natural frequency
$f_r$	the rotational frequency of the rotor speed
$f_b$	the blade passing frequency
$f_0$	the natural frequency of the tower
$G$	the weight of conic tower
$h$	the distance between two stiffening rings

$H$	the height of the vertical stiffener
$h_s$	the height of the $i^{th}$ segment
$L$	the tower height
$l$	the thickness of the cross-section C-C of the vertical stiffener
$m_1$	the mass of towers I
$m_2$	the mass of towers II
$m_3$	the mass of towers III
$\Delta m_R$	the mass reduction ratio between $m_1$ and $m_2$
$\Delta m_S$	the mass reduction ratio between $m_2$ and $m_3$
$m$	the tower mass per meter
$M$	the top mass
$M_{i,k}$	the design bending moment of the $i^{th}$ segment
$N_i$	the design axial force of the $i^{th}$ segment
$n_s$	the $i^{th}$ segment
$Q$	the wind pressure
$r_{OA}$	the inner radius of the vertical stiffener
$r_{OB}$	the outer radius of the vertical stiffener
$S$	the cross-section area of vertical stiffener at the cross-section C-C
$t_i$	the thickness of the $i^{th}$ segment
$v$	the speed to the height $H$
$v_0$	the speed to the height $H_0$
$v_H$	the wind velocity at height $H$ of wind tower
$V$	the wind speed
$V(z)$	the calibrated wind speed
$V_{hub}$	the wind speed at hub height
$W$	the produced capacity of generator

$W_i$	the second moment of cross-section inertia of the $i^{th}$ segment
$z_0$	the roughness coefficient length
$z$	the critical height of wind turbine
$z_{hub}$	the hub height
$\alpha$	the exponent value determined to be 0.20
$\alpha_A$	the position of the flow separation
$\beta$	the central angle of the cross-section C-C of the vertical stiffener around the circumference
$\varphi_{\lambda\alpha}$	the end-effect factor
$\varphi_\lambda$	the end-effect factor
$\rho_a$	air density
$\rho_s$	steel density
$\sigma_i$	compression stress of the $i^{th}$ segment
$\omega$	the natural frequency of structure system
[C]	damping matrix
[F(t)]	excitation force from the thrust forces
[K]	stiffening matrix
[M]	mass matrix
[ $\ddot{\mathbf{x}}$ ]	tower top acceleration
[ $\dot{\mathbf{x}}$ ]	tower top velocity
[ $\mathbf{x}$ ]	tower top displacement matrix

# CHAPTER 1: INTRODUCTION

## 1.1 Background

Due to a growing awareness of the need for environmental protection, during the last decade renewable energy has become increasingly significant due to the fact that renewable energy sources do not emit greenhouse gases. Wind energy has rapidly developed as a clean and renewable energy source in recent years in order to meet the increasing demand for power. It is worth mentioning that Europe and North America accounted for more than 60% of global wind power capacity at the end of 2012. Developed countries including China and India generated over 95% of global installed capacity at the end of 2012 (Timilsina *et al.*, 2013). The European Union has already installed over 50GW of wind power generating capacity and has planned to increase the use of wind energy in order to reduce carbon dioxide emissions by 20% by the year 2020 (Tabassum *et al.*, 2014). It is estimated that more than 20% of the world's electricity demand will be met by wind energy by 2050.

The use of wind turbines is nowadays the principal technology for generating electrical power from wind, and therefore wind energy converters need to be thoroughly investigated with respect to their capacity, effectiveness and integrity. Economic efficiency is also a key parameter that needs to be considered in the design of a wind turbine tower. The steel towers account for about 15 to 20% of the total manufacturing cost. The efficiency of the design parameter variation should therefore be analysed in order to provide a more efficient approach to strengthening the towers in the most economical way.

Due to the rapid development of wind turbine technology, the size of wind turbines and the height of the towers have increased substantially. Energy yield is related to the height of the wind turbine towers. One of the standard design solutions to overcome local buckling problems in the latter is the incorporation of stiffening rings in the interior of the tower. These stiffening rings are added to the inner side of the tower wall to improve the buckling resistance of the towers. Therefore the numbers

of the stiffening rings for towers of various heights need to be considered as variables in the design of wind turbine towers. All design solutions need to satisfy the strength and serviceability requirements as specified by the structural Design Codes. In this thesis, the relevant Design Codes is EN 1993-1-6. The steel wind turbine towers have been designed against the relevant limit states: buckling limit states, fatigue limit states and serviceability limit states.

## **1. 2 Aims and objectives**

The main aim of this thesis is to investigate the structural response of steel wind turbine towers subjected to combined wind loads, and to propose different stiffening solutions to optimise the structural response. In particular, this aim will be achieved by considering the following objectives:

1. To propose an approach to calculating the structural response of wind turbine towers under wind loads by means of numerical simulation, to simplify the complicated load states in accordance with the relevant Eurocodes, and to validate the FE models that simulate the towers by comparing the numerical results with existing data from monitoring exercises.
2. To analyse the structural behaviour of towers of various heights under wind loads, and to propose an effective design for very high wind turbine towers, because towers higher than 200m have not yet been erected in practice, but have been scheduled for manufacture in the near future.
3. To assess the effect of stiffening rings and wall thickness on the strength of towers of various heights and to explore the most efficient method between adopting stiffening rings and reducing wall thickness in increasing the strength of towers. Additionally, to determine the most efficient range of the parameters including the wall thickness, and the dimensions and quantity of the stiffening rings, in the design of wind turbine towers.
4. To evaluate the natural frequencies and mode shapes of each independent tower structure without the nacelle-rotor system, and of the nacelle-tower systems, considering the concentrated mass, and to propose an approach to avoid resonance for each specific height case.

5. To estimate the effect of stiffening rings and wall thickness on the stability of towers of three typical heights, and to analyse their buckling modes and eigenvalues.

6. To obtain the structural behaviour of vertically stiffened towers and to improve the type of stiffener by comparing the effect of vertical and horizontal stiffeners on the structural response of towers under wind loads to guide the design of vertically stiffened towers.

### **1.3 Layout of thesis**

This thesis is organised in eight chapters.

Chapter 1 presents the project background regarding wind turbine towers, and introduces the aims and objectives of the thesis.

Chapter 2 comprises a detailed literature review in the field of wind turbine towers, which includes the current status of wind energy, and the history and development of wind turbine towers. Chapter 2 also reports the optimisation problems and a serviceability analysis of the design of towers. In addition, a dynamic analysis and the monitoring of wind turbine towers are also described. Finally, knowledge gaps in the aforementioned topics are defined.

Chapter 3 discusses the methodology used to numerically simulate the models of the wind turbine towers. Types of finite element meshes are discussed, and a relevant sensitivity analysis is performed. Chapter 3 also describes an approach to simplifying wind loads using appropriate software, and presents the verification of numerical solutions in the structural response of towers under wind loads by comparing the numerical results with existing data from monitoring exercises.

Chapter 4 concerns the analysis of three representative towers, of 50m, 150m and 250m in height, subjected to wind loads, and investigates the effect of stiffening rings and wall thickness on the strength of the three height cases.

Chapter 5 analyses the dynamic characteristics of the 50m, 150m and 250m towers for both the independent towers and for the nacelle-tower systems. This chapter also provides recommendations

## CHAPTER 1: INTRODUCTION

for the corresponding solutions to avoid resonance for the independent towers and for the nacelle-tower systems. A buckling analysis of the selected towers is then carried out to investigate the effect of stiffening rings and wall thickness on the shell stability.

Chapter 6 presents a parametric study of the towers performed by considering the wall thickness, and numbers of stiffening rings as design variables. As a result of this study, the most efficient range of variation for each parameter of the three heights of tower is obtained.

Chapter 7 introduces the novel vertical stiffened wind turbine tower concept and compares the effects of vertical and horizontal stiffeners on the structural response of towers under wind loads. A parameter study with respect to variations in the vertical stiffeners in order to study their effect on the strength and stability of wind turbine towers is then performed.

Chapter 8 summarises the conclusions of the present research and proposes effective design solutions for each height case.

## CHAPTER 2: LITERATURE REVIEW

### 2.1 Wind energy

#### 2.1.1 Global demand for energy

Due to global population increases and economic growth, demand for power is continuously increasing. The major contributors to global increasing demand for energy are the United States, China and India. The current global population is 7.1 billion people (UN, 2014), and this will probably exceed 9 billion by 2050. Global GDP was about 85 trillion dollars in 2012 and is likely to expand to 250 to 300 trillion dollars by 2050 (WB, 2014). Global consumption and supply of energy has surged over the past few decades, doubling since 1973, from 6115.21Mtoes (million tons of oil equivalent) to 12267.38Mtoes (IEA, 2010a). Nowadays, the vast energy demands are met through conventional fuels and renewable energy which sustain our industries and meet our day to day needs for heat and light (Breeze, 2004, 2008; Erdos, 2012). The global demand for electricity was about  $20.2 \times 10^{12}$  kWh in 2008, which was mainly produced from fossil fuels and nuclear power, and the global energy demand is expected to increase by 36 percent from 2008 to 2035. It is difficult to calculate exactly how long the remaining fossil fuels will last, but researchers predict that there is only approximately 60 years' worth of oil and 100 years' worth of gas remaining. The International Energy Agency (IEA) assumes that some countries should implement relevant energy policies to reduce green-house gas emissions with the aim of protecting the natural environment (IEA, 2010b). As a consequence, human beings are confronted with urgent challenges in developing renewable energy.

#### 2.1.2 The wind

As the earth is a sphere, the atmosphere in the equatorial zones can obtain the energy closer than that in the polar zones causing the difference in the intensity of solar radiation in the different zones as shown in Figure 2.1a. The heat is delivered through the air flow from the equator to the two poles of the earth with exchanging the air mass of the global wind systems as displayed in Figure 2.1b. Thus,

wind can be created by the air motion relative to the earth caused by atmospheric pressure gradient (Al-Bahadly, 2009).

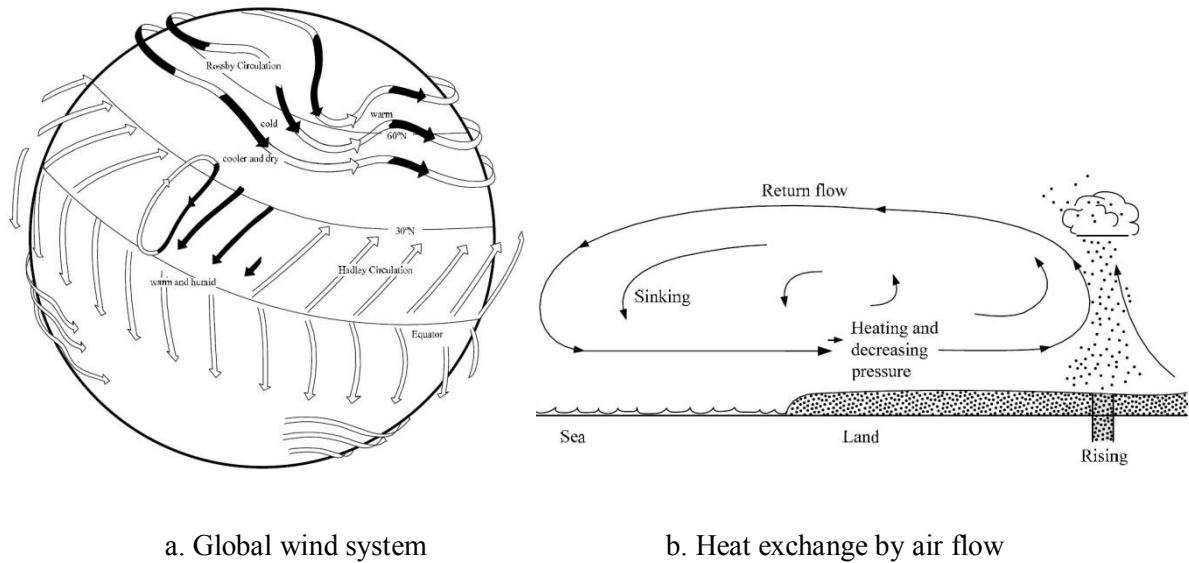


Figure 2.1 Wind circulation (WMO, 1981)

The atmospheric boundary layer is the lowest part of the atmosphere. The atmosphere boundary layer directly influences most of the human daily activities of all life on the planet Earth. Typically, the boundary layer extends in the range of several hundreds to 1500m. In this layer, the air flow can be affected by these parameters such as the friction at the ground, the orography, the topography, the flow velocity, temperature, moisture, etc. (Garratt, 1992). The geostrophic wind above the boundary layer is not disturbed by the friction of ground. Therefore, the wind speed varies in the layer between geostrophic wind and the ground with the height above ground increases as shown in Figure 2.2.

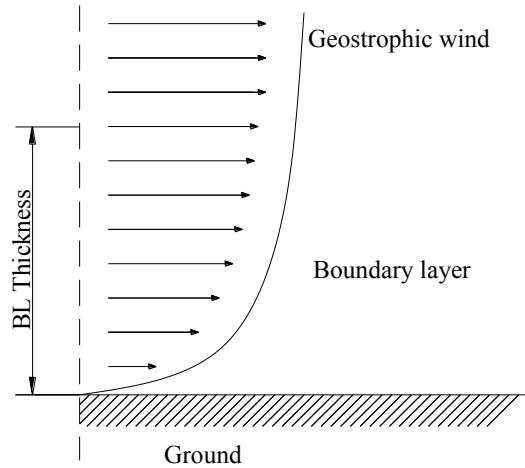


Figure 2.2 Scheme of the atmospheric boundary layer

Wind turbine tower assemblies have to be erected in the atmosphere boundary layer. The energy yield of a wind turbine depends on the vertical wind profile as displayed in Figure 2.2 involving the properties and the intensity of the air flow in the atmosphere surface layer. The vertical wind profile can be influenced by the surface roughness, the topography and temperature, etc. The surface boundary layer is defined as a magnitude of approx. 10% of the height of the full atmospheric boundary layer, and it can be affected by vertical temperature profile (Geernaert, 2003). However, if the air temperature in the surface boundary layer decreases by approx. 1°C per 100m height, the thermal stratification of the atmosphere is named as neutrally stable. (Bañuelos-Ruedas *et al.*, 2010; K. Chen *et al.*, 2014)

## 2.1.2 Current status of wind energy

### 2.1.2.1 Development of wind energy

The awareness of environmental protection has been growing due to an increasing number of climatic disasters caused by global warming. Specifically, lightning, floods, landslides, tropical cyclones and sea level rise caused by global warming are the main disasters that affect public health and quality of life. In the 1980s there were 1498 climatic disasters worldwide and 3217 climatic disasters in 2000-2008, accounting for more than 75% of all natural disasters that include a rise in extreme weather events, including storms, floods, droughts, heat waves, sea waves, heavy rainfall, and wet

## CHAPTER 2: LITERATURE REVIEW

groundslides can be referred to as climatic disasters (Oh and Reuveny, 2010). In particular, the carbon dioxide generated from the burning of fossil fuels is one of the main contributors to global warming. China and India are two of the largest carbon dioxide emitters, being among the world's developing countries, and the United States was the second highest total emitter in 2009. The other major emitters include Japan, Germany, Russia, and the United Kingdom (Chang, 2013; Leung and Yang, 2012). In order to reduce carbon dioxide emissions, many countries have signed the international treaty, the Kyoto Protocol (UNFCCC, 2013). Thus, renewable energy from wind, water and the sun has become increasingly important since renewables do not emit greenhouse gases. Other advantages are that renewable energy production generally requires less land in terms of power produced per square metre than conventional fuels, and conventional energy production and supply often faces financial or other crises (M. Dolores Esteban *et al.*, 2011).

Wind energy has developed rapidly as a clean and renewable energy in recent years, in order to meet increasing demand for power. At the end of 2012, Europe and North America accounted for more than 60% of global wind power capacity. Overall, developed countries plus China and India generated over 95% of global installed capacity (Timilsina *et al.*, 2013). Although there have been high growth rates in recent years, the current role of wind power in meeting global electricity demand remains small, accounting for about 2-3% of the global electricity supply (REN21, 2012). China is expected to remain the biggest producer of wind energy in the foreseeable future, having just replaced the United States in 2010 as shown in Figure 2.3 (Dixon and Hall, 2014). The capacity of installed wind power in China achieved 42.3GW in 2010 and increased by 64% over the last year 2009. China is expected to produce 200GW of wind power by 2020. The United States installed wind power has reached 35.2GW, with more than 10GW installed in one year (Bilgili *et al.*, 2011). It is estimated that more than 20% of the world's electricity demand will be met by wind energy by 2050. The European Union still leads the world wind power market, although America and China have a high growth rate of installed wind power capacity (Kaldellis and Zafirakis, 2011). The European Union has installed over 50GW of wind power capacity according to Figure 2.3, and has plans to increase the use of wind energy in order to reduce carbon dioxide emissions by 20% by the year 2020 (Tabassum *et al.*, 2014).

Germany and Spain are the first two leading wind power producers in Europe. Installed wind power capacity in Germany reached 27.2GW in 2010, adding 1.5GW of installed capacity over the year (GWEC, 2011a). Spain, as the second highest wind power producer, brought the total installed capacity up to 20.7GW in 2010. According to Spanish Wind Power, it is predicted that Spain plans to install a capacity of 45GW wind power by 2020 (2011b). India is the fifth highest wind power producer in the world, and had created about 13GW of installed capacity of wind energy by the end of 2010 (Atul Sharma *et al.*, 2012). It is predicted that the installed capacity of wind power may reach 19GW, 25GW or 29GW by 2015 in accordance with three different scenarios, referred to as ‘reference’, ‘moderate’ and ‘advanced’, respectively (Sahu *et al.*, 2013). For the UK, the total installed capacity of wind power achieved 5.2GW in 2011, and the growth rate of wind power use is up by 79% over the period 2005-2011 (Islam *et al.*, 2013). The expected maximum installed capacity of wind power in the world is  $1.9 \times 10^9$  kW by 2030-2050 (Joselin Herbert *et al.*, 2007).

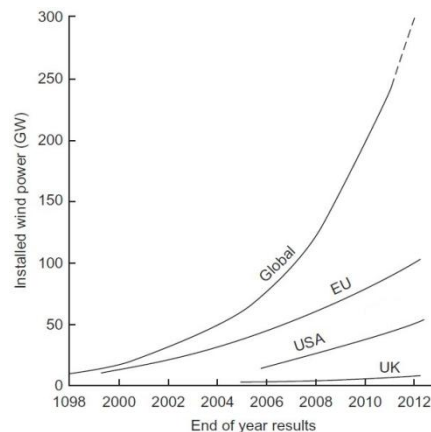


Figure 2.3 Installed wind power capacity of main countries and regions (Dixon and Hall, 2014)

### 2.1.2.2 Onshore and offshore wind energy

Onshore and offshore are the two different alternatives for wind energy. Onshore wind energy has been used for over 2000 years. Onshore wind is the strongest performing renewable sector. The bar chart given in Figure 2.4 shows wind energy installation at present levels and its estimated future use in total throughout the world (Perveen *et al.*, 2014).

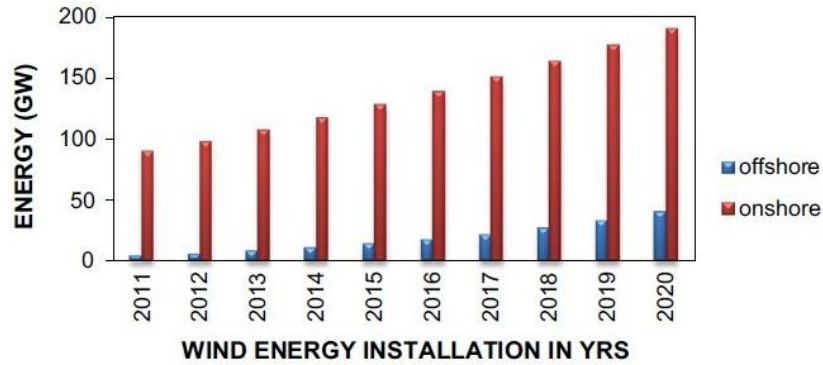


Figure 2.4 Wind energy installations: 2011-2020 (GW) (Perveen *et al.*, 2014)

The US is dominated by onshore wind according to the project database of the Energy Industries Council (Patel, 2014). As renewable electricity is the cheapest source of generating power, onshore wind will be the largest contributor to producing the 34% share of renewable electricity required by 2020 in the EU (Rajgor, 2010). Offshore wind energy production has just started to develop in recent years. Gradually, as some countries do not have enough space on land for the development of onshore wind power, and as the technology of offshore wind energy generation also matures, offshore wind farms are beginning to flourish.

In general, offshore wind farms are built on the continental shelf area, about 10km off the coast and 10m deep on the seabed. Compared with onshore facilities, offshore wind installations are much more complex, both in the system design and in the construction process (M. Dolores Esteban *et al.*, 2011). Wind turbines should be fixed on the seabed and the foundation should be a strong supporting structure. Therefore, offshore wind farms need a more developed technology so that the offshore installations can resist high loads and adapt to the corrosion conditions in the humid marine environment. Submarine cables and other electricity transmission systems are required for erection and maintenance work, which results in high costs for offshore installations compared to onshore towers (UNEP Centre, 2013). Offshore wind units are double or triple the cost of onshore wind units (M. Dolores Esteban *et al.*, 2011; Wu *et al.*, 2014), depending on the region. However, the wind resource offshore is of a higher quality than that on land. Wind speeds are higher, more consistent and there is less turbulence, therefore the generating lifetime of an offshore wind turbine is increased under stable wind conditions. The space used for offshore wind farms is more flexible than that on

## CHAPTER 2: LITERATURE REVIEW

land. Specifically, the installations are set up far from densely populated areas, which reduces the noise impact on communities. Also, the large distances between offshore installations contributes to reducing the visual impact on communities living by the coast. Due to the sea surface being level compared to land, turbulence propagation between turbines in offshore conditions is higher than that in onshore conditions (Herman *et al.*, 2003; 2006; Sheng, 2008).

Table 2.1 Offshore and onshore wind capacities in the EU (EWEA, 2008)

Country	2008 capacity (GW)		2020 national plan (GW)		2020 EWEA high capacity (GW)	
	Onshore	Offshore	Onshore	Offshore	Onshore	Offshore
UK	2.7	0.59	14.9	13.0	14.0	20.0
Germany	23.9	0.01	35.8	10.0	42.0	10.0
France	3.4	-	19.0	6.0	20.0	6.0
Netherlands	2.0	0.25	6.0	5.18	5.4	6.0
Sweden	0.9	0.13	4.37	1.82	8.0	3.0
Denmark	2.8	0.41	2.62	1.34	4.0	2.5
Belgium	0.4	0.03	2.1	1.8	2.5	2.0
Spain	16.7	-	35.0	3.0	41.0	1.5
Italy	3.7	-	12.0	0.7	17.0	1.0
Greece	1.0	-	7.2	0.3	12.0	0.2
Others	6.1	0.05	17.8	2.1	47.8	2.8
EU	63.5	1.47	168.1	45.2	210.0	55.0

Table 2.1 (EWEA, 2008; Green and Vasilakos, 2011), shows both the conservative and ambitious scenarios for the installed capacities of onshore and offshore wind generation for the main EU countries by 2020. All main EU countries intend to utilise more onshore and offshore wind power by 2020. Specifically, the UK plans to retain its leading position in terms of offshore wind generation in the EU, followed by Germany with a potential offshore capacity of 10GW. Germany produced onshore wind power of 23.9GW in 2008 and is expected to generate 35 to 42GW of onshore wind

power by 2020. By 2020, the cost of investment in annual wind power capacity will reach 17 billion Euros with around half of investments going to the offshore market. By 2030, the twenty-seven EU countries will invest almost 20 billion Euros in the wind power market, with 60% of offshore market investments (EWEA, 2009a). In addition, more than 375,000 people will be employed in the European wind power market, with 160,000 in the onshore market, and 215,000 in the offshore market (EWEA, 2009b).

Currently, the development of offshore wind power generation is not limited to Europe, and the offshore wind industry in the Asia-Pacific area is also booming (GEWEC, 2014). The advantage of offshore energy for China is that offshore wind farms are close to densely populated areas, in contrast with onshore wind farms which are located far from the main cities. It is estimated that there is around 200GW of offshore wind power resource, almost 10 times than of the onshore installed capacity at present, indicating the huge potential of generating offshore power in China (Zhou, 2010). The first offshore wind farm in the Asia-Pacific area is located in Shanghai, and it generates a total of 102MW of installed capacity. A further large scale wind farm with around 1GW of installed capacity is planned for Shanghai by 2020 (Miguel Esteban and Leary, 2012).

## **2.2 Wind turbine towers**

### **2.2.1 History of wind turbine towers**

In ancient times, humankind invented the windmill as a tool in agriculture. As early as the seventh century, the first recorded windmills with a vertical axis of rotation were used in a region which is today part of Afghanistan to grind grain, and were made with sails similar to those used on boats. The sails were fixed to a vertical axis wheel that could turn horizontally when the wind blew on the sails. Grindstones were attached to the wheel, so that the grain could be ground when the sails were rotating. Later, by 1000 AD, Persian and Chinese windmills were similarly created with braided mats as sails, and using a vertical axis (Koeppel, 1982). The oldest windmill of a lift-driven horizontal axis device, known as a post windmill, was found in England from about the twelfth century. The rapid

## CHAPTER 2: LITERATURE REVIEW

development of windmills is likely to have been influenced by Crusaders bringing the knowledge of windmills from the Middle East to Europe. The post windmill spread from England to France, the Netherlands, Germany, Denmark, and some other European countries during the twelfth and thirteenth centuries (Ackermann and Soder, 2000).

Between the 12<sup>th</sup> and the 19<sup>th</sup> centuries, windmill technology improved continuously in Europe. The tower mill gained popularity as the first type of mill used for irrigation in Southern Europe as early as the 13<sup>th</sup> century. The main characteristics of the tower mills are a cylindrical stone construction with a fixed roof, and a guyed rotor with eight sails. In the 15<sup>th</sup> century, the Dutch attempted to modify the old post mill into a structure known as a 'wipmolen' which was used to drive drainage pumps, as shown in Figure 2.5. Later, the Dutch smock mill was also developed for drainage purposes and was made of lighter wooden material in the 16<sup>th</sup> century. Paltrock mills were made to utilise wind energy as a driving force in the 17<sup>th</sup> century (Gasch and Twele, 2012). By the 18<sup>th</sup> century, around 20,000 modern windmills were in operation in France alone. 90% of the power used in the industry at this time was related to wind energy in the Netherlands. Up until the 19<sup>th</sup> century, typical European windmills consisted of a 25m diameter rotor and 30m height stocks (Ackermann and Soder, 2000). At this time, windmills were not only used for agricultural purposes, but also for industrial purposes. In 1887, Professor James Blyth (Price, 2005) in Marykirk, Scotland, applied the use of wind energy for generating electricity as shown in Figure 2.6. Later, Poul LaCour also built a wind turbine with the aim of generating electricity in Denmark in 1891.

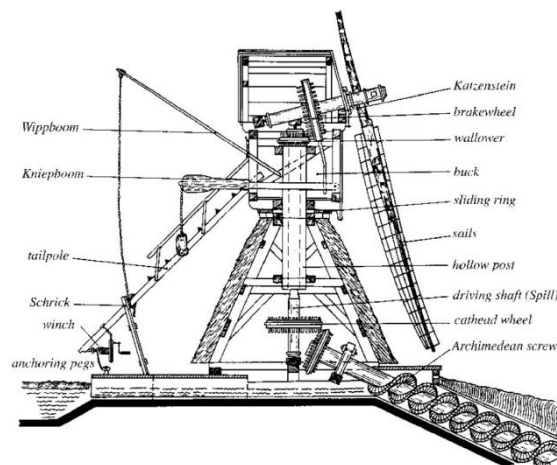


Figure 2.5 Profile of a wipmolen mill (Gasch and Twele, 2012)

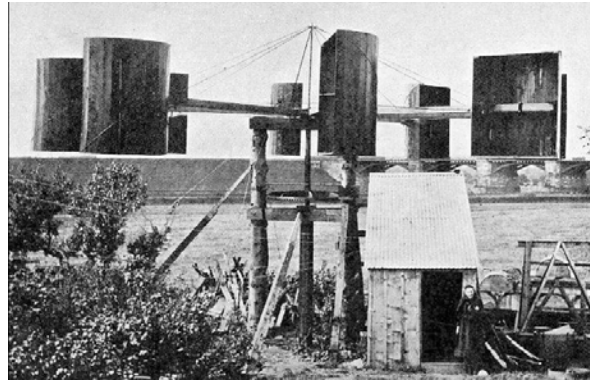


Figure 2.6 First wind turbine for electricity generation by James Blyth in 1887 (Price, 2005)

By the time industrialisation in Europe led to a gradual decline in windmills, and European windmills started to disappear, windmills spread to North America. In the early settlement period, the European immigrants erected small windmills to pump water for raising livestock. The European windmills usually had to be protected from extreme wind speeds, to avoid damage to the windmill (Tabassum *et al.*, 2014). The early American windmills were designed to be fully self-regulated, hence they could be left to operate unattended (Hills, 1994; Johnson, 1985; Righter, 1996). They were the first windmill type that had an automatically controlled yaw system including storm control (Gasch and Twele, 2012). The total number of windmills installed was about 600,000 units, reaching a peak between 1920 and 1930. The historical development of wind turbine technology has been documented by Baker (1982), Shepherd (1990), Ancona (1989), Golding (1991) and Kealey (1987).

During World Wars I and II, Danish engineers improved wind turbine technology and produced a type of turbine to overcome energy shortages (Petersen and Thorndahl, 1993). American engineer Palmer Putnam designed and built the first grid-connected wind turbine with a diameter of 53m, as shown in Figure 2.7. However, the economic costs for conventional power generation were 50% lower than the power production costs of Putnam's wind turbine. Therefore, his wind turbine failed commercially and was dismantled in 1945 (Paul, 1995 #1464; Koepl, 1982 #1447). After World War II, Johannes Juul developed a Danish wind turbine design, and installed a turbine in Denmark generating about 2.2 million kWh between 1956 and 1967. Hutter invented an innovative turbine

comprising a tower and slender fibreglass blades, with the wind turbine mounted downwind of the tower on a flexible teetering hub (Ackermann and Soder, 2000; Gipe, 1995). At the beginning of the 1960s, the electricity generated from wind turbines was too expensive to compete with conventional fossil fuel generation due to the cheap oil coming to Europe from the Near East, which led to the breakdown of wind energy use. With the oil crisis in the beginning of the 1970s, wind power began to revive in some countries (Carmoy, 1978; Gipe, 1995; Thomas and Robbins, 1980). The governments in the USA, Germany, Sweden and some other countries provided financial support to develop wind power. However, most of these projects did not perform very successfully due to technical problems. Nevertheless, due to the special government support policy in Denmark, further development of wind energy generation progressed. Some small Danish manufacturers of wind turbines produced wind turbines with a rotor diameter between 12 and 15m, which were technically and economically successful enough to meet market demand (Meyer, 1995).



Figure 2.7 Smith-Putnam wind turbine (Wikipedia, 2014a)

## 2.2.2 Modern wind turbine towers

### 2.2.2.1 Introduction

Wind turbines are the energy converters that can convert the kinetic energy of the wind into the mechanical energy of rotation. In engineering practice, wind turbine size has increased rapidly in the past 20 years, and tower height has also been increasing with developments in technology (IPCC, 2011). The most important application of modern wind turbines is the generation of electrical energy (IPCC, 2011). Wind turbine towers are mainly composed of rotor, blades, generator and tower as

shown in Figure 2.8. The rotor converts the wind energy into the mechanical energy of rotation as the essential function of the wind turbine. The blades are linked via the nacelle to the rotor shaft. The three-bladed rotor is a general type of wind turbine. There are two types of rotors in terms of rotor position in relation to the tower. One type of rotor is the upwind rotor, which is located in front of the tower, and this dominates the wind power market. The other type of rotor is the downwind rotor, which is placed behind the tower. This type has the main disadvantage of the rotor blade creating noise when it passes through the disturbed flow caused in the wake of the tower. The function of generators coupled to the grid is to generate electrical power, with the electricity then being transmitted directly to the grid.

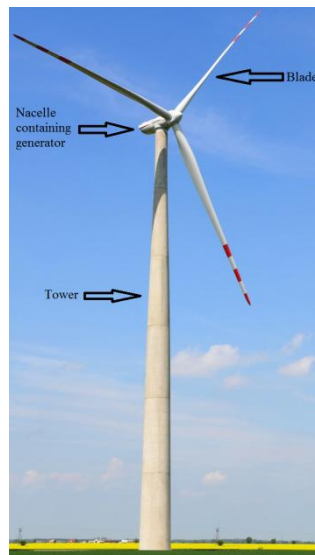


Figure 2.8 Composition of wind turbine tower system

The towers are the main support structures that carry the rotor and the power transmission and control systems. The tower is relevant to the economic efficiency of a wind turbine. Firstly, it accounts for a significant proportion (approximately 15 to 20%) of the wind turbine's costs, and it also determines the costs of transport and erection. Secondly, the wind turbine's hub height determines the energy yield at each site. A hub height above the surface boundary layer delivers a constantly higher energy yield.

Therefore, the choice of the optimum hub height has to be made for each site individually. In order to facilitate certification and selection, the manufacturers offer each wind turbine with several set tower heights. Generally, the higher the tower is, the more energy the wind turbine produces. Therefore, higher towers are needed in engineering practice as the technology develops. However, the challenge is that higher towers should be designed at a reasonable cost while satisfying the strength and serviceability requirements as specified by the design codes. Further challenges arise in transporting high towers, and large cranes are needed to erect the whole tower.

### 2.2.2.2 Types of wind turbine tower

The lattice tower is composed of trusses or frames which are bolted or welded together as shown in Figure 2.9a. The initial material cost to build a lattice tower is less than that to build the equivalent tubular tower structure of similar stiffness. A lattice tower has many joints in terms of its structural characteristics (Agbayani and Vega, 2012). As each bolted joint needs to be torqued to satisfy the specification requirements, and checked periodically, the assembly and maintenance costs are higher. Moreover the structural damping is higher than that of a steel tower. However, the foundation cost of lattice towers is less than that of tubular towers.



a. Lattice tower (Knight, 2014)      b. Tubular tower (Wikipedia, 2014b)      c. Hybrid tower (Gasch and Twele, 2012)

Figure 2.9 Common types of wind turbine tower

The tubular tower is manufactured with circular or polygonal cross sections with tapering conical sections or plain cylindrical sections in order to resist the increasing bending moment from top to base (Manwell *et al.*, 2009). Bolted flanges are used to connect the different sections of the tubular tower, and their function is not only to strengthen the whole tower but to simplify transport and erection as shown in Figure 2.9b.

The hybrid tower combines different configurations of wind turbine tower or tower materials, such as concrete and steel. The tower base section is made in-situ from concrete due to the transportation limits, and the upper tower part is made from cylindrical steel sections as shown in Figure 2.9c. Tension anchors are used to connect the two tower parts and to pre-stress the concrete (Malcolm, 2004). For the wind turbine cost components, the tower in the height range from 40m up to more than 100m accounts for 26.3% of the overall wind turbine cost (Krohn *et al.*, 2009), whereas for higher tower, the tower cost is assumed to be approximate 20% due to more transportation and manufacture cost.

### **2.2.3 Development of wind turbine technologies**

As mentioned above, it has been a very long time since humans began to utilise wind energy. Wind turbine technologies are continuously developing as energy demand increases. In the future, more attention should be paid to wind turbine systems in order to decrease manufacturing costs and improve energy yields. Recently, many advances have been made in the field of wind turbine tower systems. These are introduced below under the headings of optimal design, serviceability analysis and dynamic analysis, and monitoring of wind turbine towers.

#### **2.2.3.1 Optimal design of wind turbine towers**

Negm and Maalawi (2000) considered the cross-sectional area, the radius of gyration and the height of each segment as the key design variables, and suggested five design options before reaching the final one. The design variables are formulated as a nonlinear mathematical programming problem. They achieved the optimum solutions which incorporated significant improvements to the overall tower system design. They also optimised a typical blade structure of horizontal-axis wind turbines by using similar optimal design criteria to those used in maximum frequency design. Maalawi (2007)

developed a novel design model for yawing dynamic optimisation of a wind turbine structure, in order to find a way to reduce large amplitudes caused by yawing-induced vibrations, which might damage the whole wind turbine tower system. He investigated the relationship between yawing fundamental frequency and design variables including cross sectional properties of the tower, yawing stiffening and rotor/nacelle inertia ratios.

Uys *et al.* (2007) calculated the cost formulation of a conical steel wind turbine tower under dynamic loads while meeting the structural requirements of slender structures. They undertook a cost minimisation study for the steel tower where the cost function was formulated by including materials and manufacturing costs. They concluded that the minimum cost solution corresponds to the minimum number of ring-stiffeners. Silva *et al.* (2008) proposed nonlinear dynamic models of reinforced concrete wind turbine towers in order to minimise the cost of towers with different heights by formulating the construction costs whilst meeting the strength and stiffness requirements. They considered a linear static analysis and a linear/nonlinear dynamic analysis for the towers. The cost of tower erection was expressed as the function of the tip diameter and taper.

Karpat (2013) offered an optimisation algorithm in the MATLAB programming language to minimise the cost of a wind turbine tower with stiffening rings. He considered the wall thickness of the shell segments and the dimensions of the stiffening rings as the design variables, and used the limits of local buckling for the stiffening rings, the local shell buckling limit, the panel ring buckling limit and the limitation of the frequency as the design constraints. The optimisation algorithm was validated by the structural design of wind turbine towers presented by Uys *et al.* (2007). It was found that variations in the wall thickness and the diameter of towers have an important effect on the mass and cost of wind turbine towers. Perelmuter and Yurchenko (2013) reported a parametric study of a procedure which employs steel conic shell towers for high capacity wind turbines. They considered the minimum weight of the tower as the purpose function, and the height of the tower, and the diameters and thickness of the tower shell as design variables as shown in Figure 2.10. The objective function of target capacity,  $W$ , and weight were expressed as

$$W = 0.0742\pi\rho_a v_H^3 D_\omega^2 \quad (2.1)$$

where  $W$ = produced capacity of generator;

$\rho_a$ = air density;

$v_H$  = wind velocity at height  $H$  of wind tower;

$D_\omega$  = diameter at height  $H$  of wind tower.

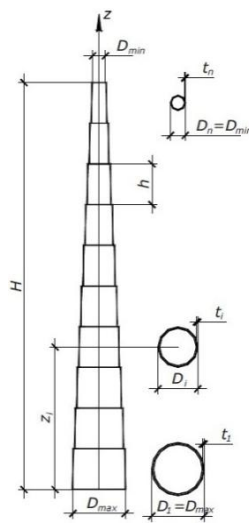


Figure 2.10 Design variables of steel shell tower (Perelmuter and Yurchenko, 2013)

$$G = \pi\rho_s h_s \sum_{i=1}^{n_s} t_i D_i \quad (2.2)$$

where  $G$ = weight of conic tower;

$\rho_s$  = steel density;

$h_s$  = height of the  $i^{th}$  segment;

$t_i$  = thickness of the  $i^{th}$  segment;

$n_s$  = the  $i^{th}$  segment;

$D_i$  = middle surface diameter of the  $i^{th}$  segment.

The critical compression stress was considered as the constraint of ultimate limit for each segment of the conic tower to avoid local buckling.

$$\sigma_i = \frac{N_i}{A_i} + \frac{M_{i,k}}{W_i} \leq \sigma_{cr,i} \quad (2.3)$$

Where  $\sigma_i$  = compression stress of the  $i^{th}$  segment;

$N_i$  = design axial force of the  $i^{th}$  segment;

$A_i$  = cross sectional area;

$M_{i,k}$  = design bending moment of the  $i^{th}$  segment;

$W_i$  = second moment of cross-section inertia of the  $i^{th}$  segment.

The formulated optimisation problem for optimum height and weight of the tower was therefore solved.

Urbano *et al.* (2013) presented the weight increase and energy yield ratios of two 120m tower examples designed as soft and stiff towers respectively, and for one 95m tower with a larger rotor diameter, compared to a baseline 95m tower. The weight increase and energy yield ratios of the three specific towers compared to the baseline tower were compared to obtain an optimal tower design. Lim *et al.* (2013) devised an optimal design for a 2MW wind turbine tower made of composite materials. They minimised the cost of the composite tower whilst satisfying the strength and serviceability requirements. The composite tower was compared with existing similar steel towers in terms of manufacturing cost in order to investigate the cost effectiveness. Gencturk *et al.* (2014) optimised a lattice tower under seismic loading by providing a cost effective solution for small and medium size combined turbines. Gencturk *et al.* (2014) found that an average reduction of total weight of approximately 30% can be obtained by optimising the section sizes, connections and the foundation.

Abdalla *et al.* (2014) investigated the structural response of the steel telecommunication lattice masts subjected to wind loading.

### 2.2.3.2 Serviceability analysis of wind turbine towers

Grant *et al.* (2000) conducted an experimental programme using a wind tunnel for an operational, horizontal axis wind turbine in two phases. Quantitative laser sheet visualisation was used to monitor the wakes of wind turbines operating in wind tunnels. The predicted results from the basic prescribed wake model without the inclusion of wind-tunnel wall effects were compared with the experimental ones. A good agreement between the predicted and the measured downstream movement of the vortex was achieved. Bazeos *et al.* (2002) described the prototype of a wind turbine steel tower and a corresponding FE model, and analysed its static and dynamic behaviours and other destabilizing effects. The refined and simplified models developed for static and seismic analyses were compared with each other and were in close agreement. Lavassas *et al.* (2003) analysed and presented the detailed design of a prototype of a tubular shaped 1MW steel wind turbine tower, with a variable wall thickness along the height of the tower. They developed two different finite element models (FEM) to simulate the structural response of a tubular tower with stiffening rings subjected to combined loads including gravity, seismic and wind loads as shown in Figure 2.11. The tower models were designed to resist fatigue to meet the requirement of relevant Eurocodes.

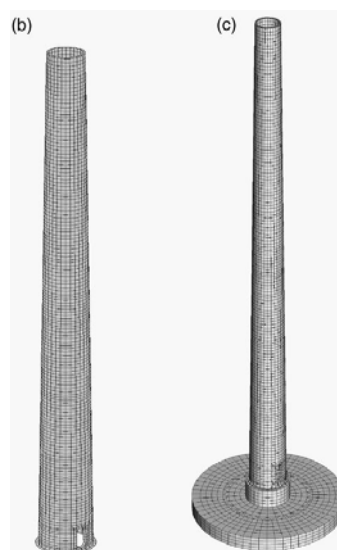


Figure 2.11 FE models of a tubular steel tower (Lavassas *et al.*, 2003)

## CHAPTER 2: LITERATURE REVIEW

Binh *et al.* (2008) proposed the equivalent static method considering the dynamic effects based on a peak factor to evaluate wind load on wind turbines. They estimated the nonlinearity of the wind load by using the peak factor based on a non-Gaussian assumption of high turbulence intensity. The formula for the peak factor was simplified to a function of skewness. The formulas were verified by using FEM simulation of a stall-regulated wind turbine. Recently, Veljkovic *et al.* (2010a; 2010b) comprehensively studied the friction connection with open slotted hole for a steel wind turbine tower by using static and fatigue tests and performed the feasibility study of the friction connection by using FE model. Chou and Tu (2011) investigated the collapse mechanism of a large wind turbine tower in Taiwan, and reviewed similar accidents in other countries to identify potential risk factors affecting the lifecycle of wind turbines. Experiments were conducted on intact and fractured bolts in order to identify the likely reasons for the tower collapse accident occurring. Kwon (2012) introduced models of wind turbine tower systems under gust loading, which is a type of extreme loading. He devised a new formula to assess the gust load effect on wind turbine tower systems. Nuta *et al.* (2011) assessed the seismic risk of tubular steel wind turbine towers in a Canadian seismic environment by using FE analysis and incremental dynamic analysis of a 1.65MW wind tower. A methodology was proposed to study the probability of reaching a predetermined damage state under seismic loading. Guo *et al.* (2011) numerically simulated a pushover analysis of a 53m wind turbine tower as shown Figure 2.12. Local buckling of the tower occurred under peak load. Guo *et al.* (2011) compared the deformation shape based on pushover analysis with that based on seismic excitation. It was found that the earthquake resistance can be evaluated using the pushover analysis results for the wind tower.

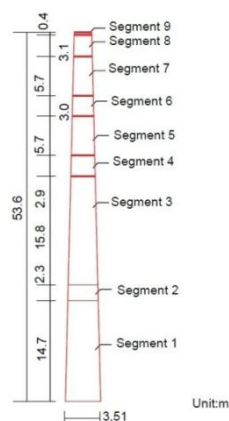


Figure 2.12 Dimensions of the 53m wind turbine tower (Guo *et al.*, 2011)

Jiang *et al.* (2010) numerically simulated the welded joints between the tower and the base flanges in a wind turbine by taking the residual stress into consideration. Their results show that complex residual stresses are generated in the fillet weld. The bevel type of fillet weld is optimised in order to assure the strength and safe operation of wind turbines. They concluded that the K type bevel, with an internal concave fillet and an external convex fillet, provides the minimal residual stress as shown in Figure 2.13. Quilligan *et al.* (2012) investigated the relative performance of steel and pre-stressed concrete tower solutions for a range of typical tower heights from 88 to 120m, and for various wind speeds, by means of a numerical model. A comparison is presented of the relative performance of the two tower solutions by using fragility curves.

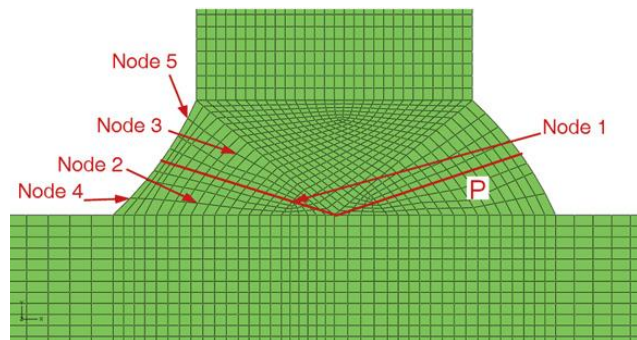


Figure 2.13 Welding joint between tower and bottom flange (Jiang *et al.*, 2010)

Lee and Bang (2012) described an accident involving a 600 kW wind turbine in Korea, and provided a buckling analysis method for the slender shell structures. They found the buckling limit load of the wind turbine tower and the wind speed at buckling point. They gave the following formulas to illustrate this process:

$$F = 0.5\rho C_T V^2 A \quad (2.4)$$

where  $F$  = Thrust force;

$\rho$  = Air density;

$C_T$  = Thrust coefficient;

$V$  = Wind speed;

$A$  = Swept area of blade.

$$V(z) = V_{hub}(z/z_{hub})^\alpha \quad (2.5)$$

where  $V(z)$  = Calibrated wind speed;

$V_{hub}$  = Wind speed at hub height;

$z$  = Critical height of wind turbine;

$z_{hub}$  = Hub height;

$\alpha$  = exponent value determined to be 0.20.

$$Q = 0.5C_D\rho V^2 A \quad (2.6)$$

where  $Q$  = Wind pressure;

$C_D$  = Cylindrical drag coefficient;

$\rho$  = Air density;

$V$  = Wind speed;

$A$  = Swept area of blade.

According to Lee and Bang (2012), the rotor thrust and aerodynamic force are estimated to be 1283.6 kN and 68.7 kN respectively. The buckling of the tower occurred at a wind speed of 34.6m/s. The analysis of a nonlinear FEM shell model found it to exhibit similar behaviour to the actual accident situation during buckling.

Dimopoulos and Gantes (2012) carried out an experimental and numerical study of the buckling behaviour of cantilevered shells with door openings and stiffening rings as shown in Figure 2.14. They presented load-displacement curves and strain measurements of tubular wind towers with opening and stiffening obtained from the experimental study. It was found that there was a good

agreement between the numerical and the experimental results in terms of load-displacement curves and ultimate load.

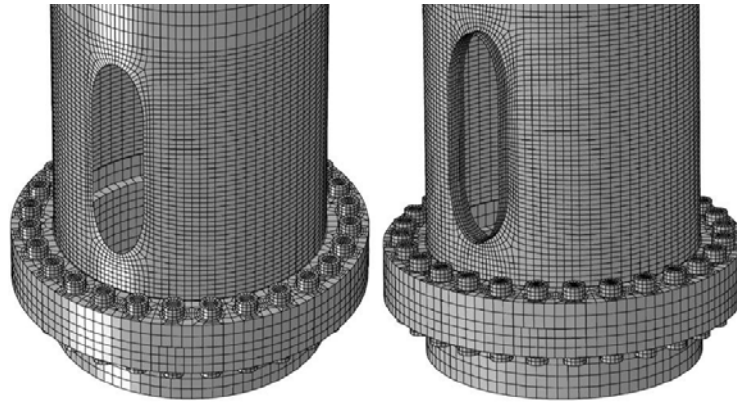


Figure 2.14 FE models of cantilevered shells with door openings and stiffening rings (Dimopoulos and Gantes, 2012)

Dimopoulos and Gantes (2013) also compared different stiffening methods involving four types of stiffening around the door openings near the base of the tubular wind tower as shown in Figure 2.15. Figure 2.16 shows the four types of cut-outs: a) type 1- peripheral frame; b) type 2- two stringers and a ring; c) type 3- two stringers, a frame and a ring; d) type 4- two stringers, a frame, a ring and comb stiffeners. It was found that simple stiffening types around cut-outs, consisting of either a peripheral frame or two vertical stringers and a ring, are particularly efficient and can be used instead of more complex ones.

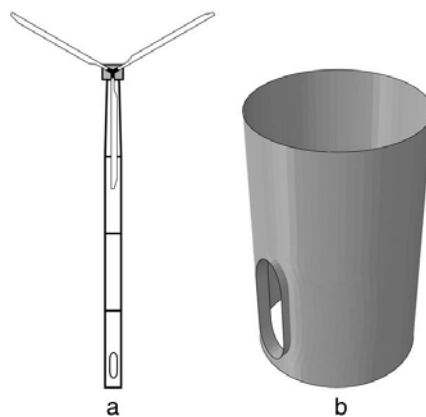


Figure 2.15 The prototype and door opening cut-out of the wind turbine tower (Dimopoulos and Gantes, 2013)

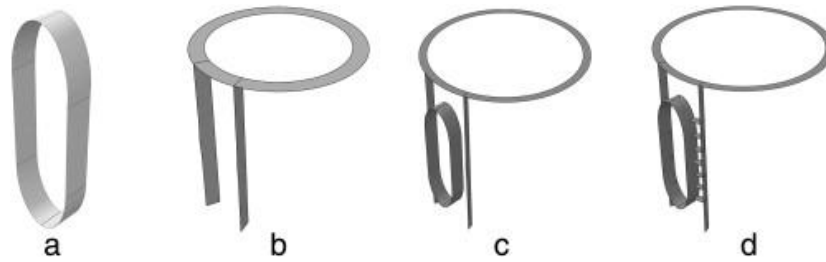


Figure 2.16 Four stiffening types around cut-outs for tubular wind turbine towers (Dimopoulos and Gantes, 2013)

Sim and Uang (2011) investigated the cause of failure of welded sleeve connections in cantilevered steel structures, employing FE models developed using ABAQUS software to evaluate the strain and stress field in the sleeve connection. Two alternative connection details were proposed to mitigate weld cracking. Sim *et al.* (2014) then conducted a full-scale static failure test on a 21.9m long 65 kW wind turbine tower to evaluate its flexural strength and failure mode. Sim *et al.* (2014) also developed a parametric study including initial geometric imperfections and the tower base boundary condition using FEM analysis. FE models of the wind turbine tower with and without a local dent were employed to investigate its effect on the flexural response of the tower. A good correlation between the structural response and the failure mode was found.

Do *et al.* (2014a; 2014c) described a model fatigue assessment including fatigue crack propagation which was used for the analysis of wind turbine tower base connections. It was shown that the fatigue life of wind towers, and the amount of energy generated, both depend heavily on the wind distribution at each site. The concept of performance-based design was developed and was used to develop the design of a typical 5MW wind turbine tower taking into consideration two design variables including the external diameter and the thickness of the tower base. Do *et al.* (2014b) then discussed the fatigue analysis of a wind turbine tower base subjected to wind loading as shown in Figure 2.17. They applied the concept of performance-based design to optimise the design parameters of the tower base in order to enhance the fatigue life of the tower, with the aim of minimising the quantity and cost of steel used.

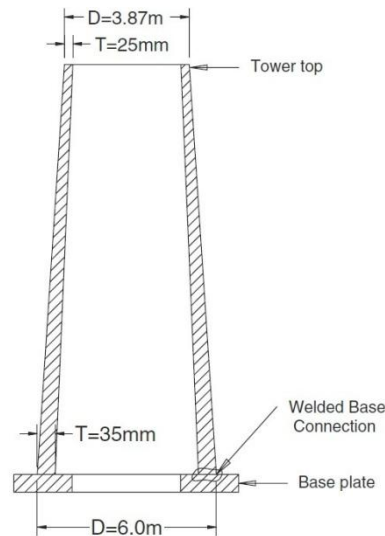


Figure 2.17 Tower base configurations (Trung Q. Do *et al.*, 2014b)

Jay and Myers (2014) discussed the current design standards for wind turbine towers to resist buckling and fatigue and evaluated their applicability to shells manufactured by spiral welding. Spiral welding may affect buckling and the fatigue strength of wind turbine towers, therefore fatigue tests should be performed to determine the weld detail and the design of the tower within the Eurocode framework. Rebelo (2014) and Gervásio (2014) considered the design of steel, concrete, and hybrid steel-concrete tubular towers which supported multi-megawatt turbines of 2, 3.6 and 5MW power with hub heights of 80m, 100m and 150m respectively. Rebelo (2014) presented design approaches for these towers and their foundations under extreme loadings in accordance with the relevant Eurocodes. It was concluded that the most suitable solution using steel tubular sections and flange connections was for the 80m towers. Also, Gervásio (2014) performed a life cycle analysis of the designed solutions. Gervásio (2014) considered the life cycle of the three different heights of tower during 20 years of use. It was found that the 100m hybrid towers with friction connections were the most efficient solution. Gervásio (2014) determined that the service life of the towers could be extended for another period of 20 years. For steel towers, the use of friction connections raised the possibility of dismantling and reusing the tower.

Tran *et al.* (2013) described the influence of door opening on the strength of wind turbine towers by means of full scale FE models. The door openings on the lower segments of the tower were

strengthened by increasing the shell thickness around the door, and using the stiffener to stiffen the door as shown in Figure 2.18. A buckling analysis of the towers with and without a door opening was performed. The ultimate strength of the shell structure was also estimated by means of a geometrically and materially nonlinear analysis with imperfection modes.

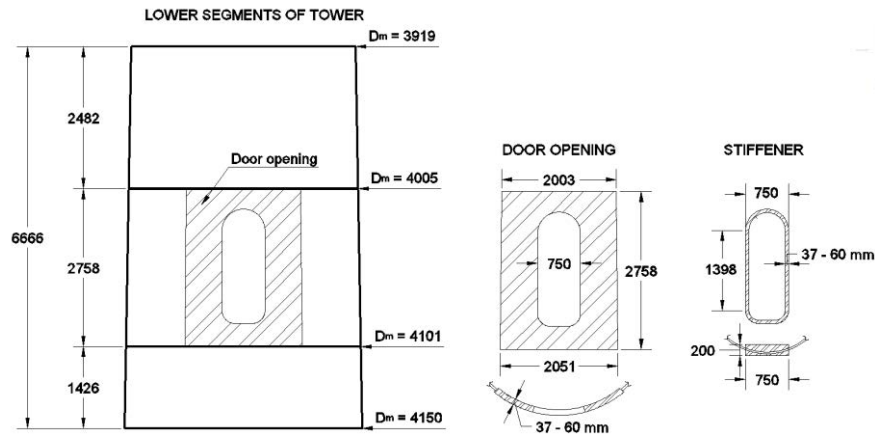


Figure 2.18 Geometry of lower segments of the tower (Tran *et al.*, 2013)

Dong Hyawn Kim *et al.* (2014) performed a seismic fragility analysis of a 5MW offshore wind turbine tower considering a nonlinear soil-pile interaction model. Two different loading plans to apply ground motion were compared with each other. Ground motion could be applied to obtain a reasonable seismic response from the wind turbine tower assemblies. They therefore concluded that layer by layer seismic loading from a free field analysis should be applied in the seismic design of offshore wind turbines. Dong Hyawn Kim *et al.* (2014) also carried out a pushover analysis to obtain the critical displacement of the nacelle. Pramod Kumar Sharma *et al.* (2014) simulated the dynamic characteristics and performed a buckling analysis of a 150m wind monitoring tower in India, and verified its stability.

### 2.2.3.3 Dynamic analysis of wind turbine towers

Tempel and Molenaar (2002) simplified the structural dynamic analysis of a flexible wind turbine tower system into a slender tower structure with top concentrated mass. The base of the tower structure was considered to be fixed. An expression of the first natural frequency of the simplified tower was provided as follows:

$$f^2 = (3.04EI) / [4\pi^2 L^3 (M + 0.227mL)] \quad (2.7)$$

where  $f$  = First natural frequency;

$M$  = Top mass;

$m$  = Tower mass per meter;

$L$  = Tower height;

$EI$  = Tower bending stiffness.

Murtagh *et al.* (2004) analysed the dynamic characteristics of a lattice tower with a lumped mass on the top. Two different methods were employed to calculate the mode shapes and natural frequencies of the tower-mass model, the characteristics were compared with each other and the values were found to be in close agreement. Murtagh *et al.* (2005) subsequently investigated the forced vibration response of a wind turbine tower with blades subjected to rotational wind loading. The dynamic responses of the tower/nacelle assemblies excluding the blade/tower interaction, and those of the tower including the blade/tower interaction, were calculated and compared. A new approach was then proposed based on the gust response factor (GRF) with the aim of evaluating the dynamic response of wind turbine towers under gust loads. Murtagh *et al.* (2007) also compared the GRFs for the two models, one of which considered the blade/tower interaction, and the other which ignored the blade/tower interaction. It was shown that the GRFs obtained by excluding the blade/tower interaction were lower than those obtained by including the blade/tower interaction.

Zaaijer (2006) assessed the dynamic behaviour of different types of foundations for offshore wind turbines as shown in Figure 2.19. The dynamic models of the foundations were simplified, while sufficient accuracy was maintained in the results. The experimental data was used to validate the accuracy of the modelling results and the applicability of the numerical techniques.

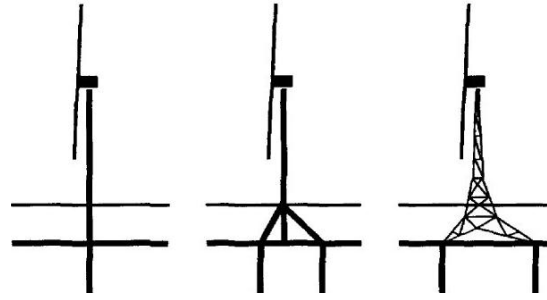


Figure 2.19 Three types of support structures for offshore towers (Zaaijer, 2006)

Haenler *et al.* (2006) developed a new simulation code for the design of a horizontal-axis wind turbine subjected to dynamics loads due to earthquake. The tower structure was simulated into a number of elastically connected lumped masses. They found that higher tower modes for earthquake analyses were much more important than lower ones for normal operation conditions. Reinhard Harte and Van Zijl (2007) presented the high-cycle dynamic loading and fatigue behaviour in terms of classical wind turbines, and found that fracturing and cracking of concrete heavily influenced the long-term durability of the tower systems. The dynamic response of an innovative solar chimney under wind loading was also investigated. It was predicted that the classical wind turbine towers and the novel chimney design would be developed to increase energy supplies in the future.

Xiao-bo Chen *et al.* (2009) investigated the wind-induced response analysis of a wind turbine tower considering the blade-tower coupling effect using the finite element method. One case, including the effect of blade-tower coupling on the top of the tower, and another case, only applying the mass of blades and the hub at the tower top, were developed and compared. It was concluded that the blade-tower coupling effect should be considered in the design of wind turbine towers to obtain more precise results. Makarios and Baniotopoulos (2015; 2012) performed modal analysis by using continuous model approach of a wind turbine tower. Prowell *et al.* (2012; 2009) tested the structural response characteristics and the modal parameters of two full-scale towers on a shake table, testing both parallel and perpendicular configurations to the rotation axis of the rotor as shown in Figure 2.20. They pointed out that the structural response and demand parameters of the two configurations tested were nearly the same. It was observed that higher mode behaviour may be important for large turbines.



Figure 2.20 Wind turbine tower on the shake table: a) Parallel configuration. b) Perpendicular configuration (Prowell *et al.*, 2012)

Bhattacharya and Adhikari (2011) carried out a novel experiment to analyse the dynamic behaviour of a wind turbine tower supported by a monopile foundation, and acquired the corresponding parameters necessary for the analytical solutions. They also simulated the wind turbine tower and compared the numerical results with experimental and analytical solutions, and found that the three different solutions matched each other well. Adhikaria and Bhattacharya (2012) considered a dynamic analysis of offshore wind turbine towers with flexible foundations, subjected to wind and wave loadings. The foundations were simplified into rotational and lateral springs. Andersen *et al.* (2012) analysed the first natural frequency of an offshore wind turbine tower with a monopile by using a simple model. The deterministic design of the pile was then given using two different approaches. M. Harte *et al.* (2012) performed a vibration analysis of an onshore wind turbine including the soil-structure interaction. By examining the displacement of the turbine and the bending moment of the base of the tower under wind loads, it was found that soil-structure interaction can affect the dynamic response of the wind turbine tower. Bisoi and Haldar (2014) reported a parametric study with the aim of investigating the effect of various parameters on the dynamic characteristics of soil-monopile-tower systems under wind and wave loads.

Valamanesh and Myers (2014) considered the aerodynamic damping of horizontal axis wind turbine towers in the fore-aft and side-to-side directions under seismic loads. A good correlation between the predictions made using the specific software FAST and the analysis of a 1.5MW baseline wind tower developed by the National Renewable Energy Laboratory in the US was achieved. The influence of aerodynamic damping on the seismic response of the horizontal axis wind turbine towers was demonstrated for a dynamic model. Van der Woude and Narasimhan (2014) estimated the effect of vibration isolation, with the aim of reducing the dynamic response of wind turbine tower systems under wind and seismic loadings. They conducted a parametric study to analyse the effect of vibration isolators on the response of wind tower structures. It was shown that some key parameters of the tower structural response can be reduced by using the isolation systems, which could contribute to design solutions for wind turbine assemblies.

Brodersen and Høgsberg (2014) investigated vibrations in an offshore wind turbine tower which had dampers at the base of the tower. The damper stroke was increased by employing a toggle-brace system, meaning that the feasibility of installing dampers inside the tower wall was increased. Mensah and Dueñas-Osorio (2014) improved the reliability of wind turbine tower systems equipped with tuned liquid column dampers (TLCD). Specifically, the structural response and the failure risk of the wind turbine tower assemblies could be reduced by adjusting the TLCDs, which could be used to control excessive vibrations of the tower structures. Kjørlaug *et al.* (2014) tested the dynamic response of a 65kW wind turbine tower on a shake table, and compared the experimental results with their numerical findings. They developed a numerical model of a 5MW wind turbine tower taking into account the soil-structure interaction. The dynamic characteristics of a 5MW wind turbine tower subjected to combined seismic loads in the horizontal and vertical directions were investigated. It was shown that the soil-structure interaction should be taken into account in order to obtain the displacement of the tower.

### **2.2.3.4 Monitoring of wind turbine towers**

Structural damage can occur in any part of a wind turbine, but the most common types of damage are rotor or blade damage and tower damage (CWIF, 2005). Therefore, in order to reduce maintenance

and repair costs, and to extend the operational life and improve the profitability of wind turbine systems, wind turbine tower systems should be monitored in the long-term, and more attention should be paid to continuous monitoring technology for wind turbines.

Adams *et al.* (2011) described a structural health monitoring process for a horizontal axis wind turbine tower, and acquired modal vibration and operating data from the monitoring system. They then compared the simulated response of the wind tower with the experimental one. It was concluded that a 25% reduction of stiffness at the root of one blade only contributed to a less than 4% change in the natural frequencies of the wind turbine.

Pieraccini *et al.* (2008) carried out dynamic testing of wind turbine towers by using a microwave sensor. They measured the structural response of towers subjected to light and strong wind loads. The sensors were placed at selected points on each tower. The horizontal displacement and a spectral analysis of these points were recorded.

Hartmann *et al.* (2011) evaluated the lifespan and reliability of a 500kW wind turbine tower by updating the finite element model with parameters obtained from structural health monitoring systems. Smarsly *et al.* (2012) developed an autonomous software based on multi-agent technology to monitor installed displacement, strain and acceleration sensors, and installed a decentralized monitoring system on a 500kW wind turbine. It was demonstrated that the autonomous software can be utilised to undertake long-term monitoring.

Ozbek *et al.* (2010) described the use of photogrammetry to monitor a large wind turbine tower, and estimated the measurement accuracy by comparing the amplitudes of the expected deformations with the measured ones. The monitoring data could be rendered more precise by employing data processing methods. It was shown that photogrammetric data could be also used to identify some of the turbine modes, and the main challenges of testing and monitoring the dynamic characteristic of wind turbines were analysed. Ozbek *et al.* (2013) measured a 2.5MW wind turbine in operation and out of operation by means of three different gauge systems. It was found that the wind speed and rotational speed could affect the identified modal parameters for the rotating wind turbines.

W. H. Chen *et al.* (2011) and Ni *et al.* (2009) developed the structural health monitoring systems for the Guangzhou New TV Tower (GNTVT), which is considered to be a super-tall structure. Three types of parameters including loading sources, structural responses and environmental effects were comprehensively measured by a distributed sensor system on the GNTVT. They updated the finite element model of the super-tall tower with the measured parameters from the monitoring systems. The improved finite element model could serve for the future health monitoring of the tower. Ni *et al.* (2009) executed a structural health and condition assessment strategy based on the static and dynamic monitoring data. Also, some monitoring data from the GNTVT under some extreme loads was collected during its construction.

Antunes *et al.* (2012) monitored the dynamic behaviour of two slender steel telecommunication towers by using FBG (Fiber Bragg Grating) accelerometers. Numerical modelling was also performed to illustrate the feasibility of dynamic monitoring. They concluded that the optical accelerometer is effective in monitoring the tall slender steel towers, as there was a good agreement between the experimental and the numerical results, and the first natural frequency of the monitored tower had a relative error of 12.1% compared with 8.8% for that of the numerical model.

Ciang *et al.* (2008) reviewed the structural health monitoring of wind turbine towers, listed some typical causes of damage to wind turbine tower systems, and discussed the advantages and disadvantages of different monitoring methods. Häckell and Rolfes (2013) described the sensor level distributions on a 118m height wind turbine tower with a tripod foundation as shown in Figure 2.21. Twenty-four channels at six different levels were chosen to collect the parameters, which included wind speed, relative wind to nacelle direction, rotor speed, nacelle position, air temperature, air pressure and wind turbulence intensity. The collected data was used for the extraction of modal parameters and the estimation of condition parameters.

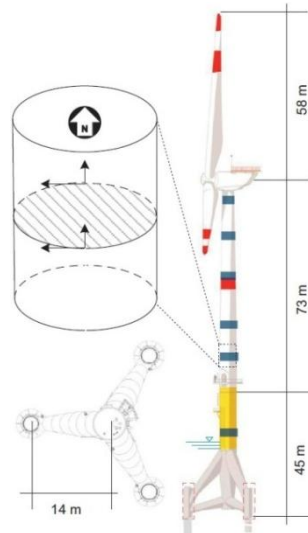


Figure 2.21 118m height wind turbine tower with tripod foundation (Häckell and Rolfes, 2013)

Swartz *et al.* (2010) utilised wireless sensor networks to monitor two 78m towers and one 40m tower. The wireless sensors were placed at four levels on the first and third wind turbine towers, as shown in Figure 2.22a and 2.22c. The acceleration data was recorded in the first wind turbine installation. The strain gauge data was collected by wireless sensors located at three levels for the second wind turbine installation, as shown in Figure 2.22b. The mode shapes of the third wind turbine installation were also tested using data from the wireless sensors. For offshore wind turbine towers, the implementation of the wireless sensors was necessary to measure the dynamic response of wind turbine towers exposed to wind and wave loads, because requirements for an economical design had to be met.

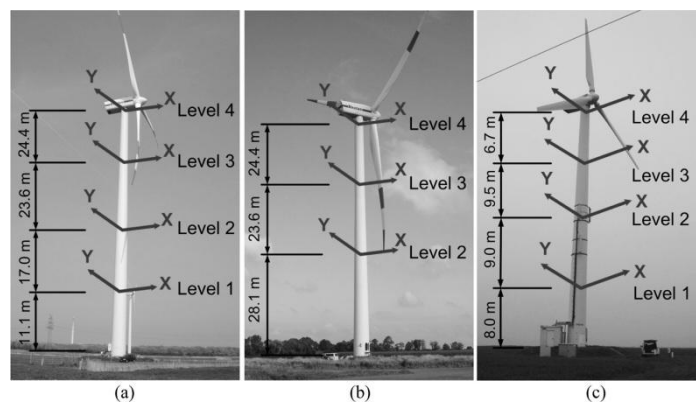


Figure 2.22 The three measured wind turbine towers (Swartz *et al.*, 2010)

Carlos Rebelo *et al.* (2012a) introduced the preliminary results of monitoring system of a steel wind turbine tower. Rolfes *et al.* (2014) introduced several main monitoring methods including modal-

based methods, acoustic emission, and ultrasound wave propagation. They presented some monitoring systems currently on the market and the monitoring technology for the support structures of wind turbine assemblies. Structural health monitoring technology is therefore very promising as an area in which significant future repair cost savings could be made.

## **2.3 Summary and identification of knowledge gaps**

### **2.3.1 Summary**

From the examination of the literature discussed above, it can be seen that much effort has been put into the development of wind turbine technologies. The recent development of wind turbine tower systems can be summarised as follows:

1. Various optimal designs of wind turbine towers have been developed as a function of the design variables to minimise manufacturing costs. Some optimisation approaches have been programmed to calculate the corresponding magnitudes of the design variables.
2. The finite element method has been applied using commercial software to analyse and verify the strength, stiffness and stability of wind turbine towers. The basic load situations include wind loads, gravity and seismic loadings for the tower structures.
3. The dynamic characteristics of wind turbine tower systems have been obtained through numerical simulations and experimental testing involving the whole tower systems. Some simplified models for wind turbine assemblies which take into account the soil-foundation interactions have been implemented in order to obtain more precise predictions.
4. Many novel monitoring approaches have been put forward to measure the wind turbine tower system parameters. The parameters in tower structures can be measured to update the finite element models of towers, and the improved models can then be employed to predict the reliability of tower structures.

### 2.3.2 Knowledge gaps

Although many innovative contributions have been made to the field of wind turbine systems, there are still many uncertain issues which need to be resolved. Several knowledge gaps have been identified:

1. Wind turbine size has increased rapidly in the past 30 years. As the energy yield significantly depends on the turbine's hub height, the choice of the optimum hub height has to be made for each site individually. In engineering practice, towers higher than 200m have not yet been erected, but will perhaps be manufactured in future. Therefore, towers of different heights, particularly higher towers, should be studied for potential future towers.
2. Wind load is very complicated for the wind turbine tower in engineering practice due to its variable direction and magnitude. An effective method should be proposed to simplify the wind load for use in numerical simulations. The numerical results should then be compared with the experimental data in order to evaluate whether the numerical method to simplify tower structure and wind loads is accurate. The sensitivity of element size should be validated by comparing the structural response of different meshed models subjected to wind loads.
3. Economic efficiency is a key point that needs to be considered in the design of wind turbine towers. Stiffening rings are added to resist local buckling for tower shell structures, and the effect of cost reduction measures, such as varying the number of stiffening rings and shell thickness, on the structural response of towers should be analysed in order to formulate appropriate codes of practice.
4. For the design of tower structures, the parametric analysis of wind turbine towers is significant. Specifically, the distance between two stiffening rings, the thickness of the tower shell and the cross section of the flanges should be decided according to the corresponding design rule. However, the parametric effect of wind turbine towers has not been discussed here.
5. Tower structures are slender structures subjected to gravity, seismic and wind loads. The effect of internal stiffening rings and their thickness on the buckling behaviour of wind turbine towers should

be analysed for towers of various heights. Dynamic analysis of wind turbine towers should also be simulated, and the implementation of resonance avoidance should be proposed for each height solution.

6. Stiffening rings are adopted in most designs of wind turbine towers to provide resistance to local buckling. However, vertical stiffeners are also employed, but their use is less widespread than stiffening rings in engineering practice. The effect of vertical stiffeners on the structural response of wind turbine towers should therefore be analysed. A comparison of stiffening rings and vertical stiffeners should be performed to obtain a better design solution.

## CHAPTER 3: METHODOLOGY

### 3.1 Finite element method

#### 3.1.1 Discretisation

A continuous elastic body can be partitioned into many shaped elements, which can transfer the elastic body into one assembly composed of finite elements. Neighbouring elements can only be connected by the nodes. Thus, the forces applied to one element can be delivered to the other adjacent elements through the nodes. There are diverse types of meshing, such as triangle, rectangle and quadrilateral. The degrees of freedom refer to the number of components of translation and rotation at each node. Degrees of freedom are the fundamental variables for the finite element analysis. In one plane, each node includes two degrees of freedom in the x and y directions, as shown in Figure 3.1. The components of translation and rotation are calculated at the nodes of the elements. For the displacements at the other points in each element, these can be obtained by interpolating from the nodal displacements.

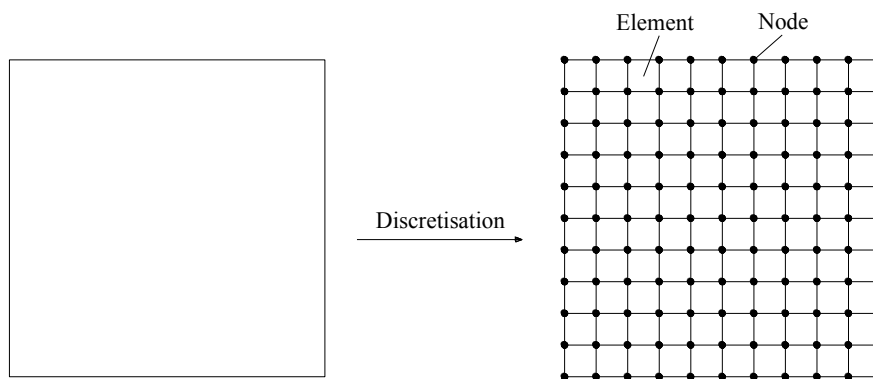


Figure 3.1 The discretisation process of one plate

#### 3.1.2 Sensitivity of meshing

The density of the meshing can be selected by the global and local sizing control for the models. The density of the meshing can affect both the accuracy of the solution and the computation time. It is better for the models to be meshed in refined elements to fit the geometrical boundary of the model rather than

using rough element models, as the accuracy is in general increased as the density of the meshing grows, up to a limit. Also, the interpolating functions of the refined elements can approach the exact solution more accurately than those of the rough elements, and the refined elements can reflect precise stress variations in the area of stress concentration. However, the accuracy may be reduced due to the accumulated errors from the computation iterations, and computation time may also be increased in the case where the quantity of elements and nodes is too great.

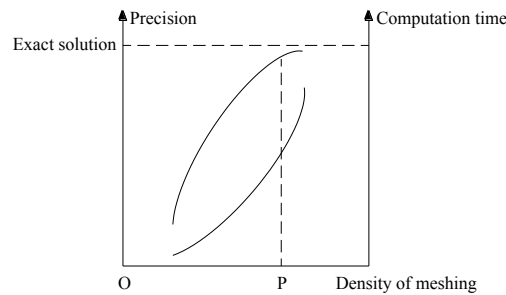


Figure 3.2 Precision and running time with respect to density of meshing

Figure 3.2 shows the variations of precision and computing time with respect to the density of the meshing. The precision varies very slightly, and the computation time increases greatly after the meshing density increases beyond a certain point, as shown in Figure 3.2. Therefore, both the accuracy and the calculation efficiency should be taken into account. The optimum size of elements should be chosen by conducting a sensitivity analysis on each model. The numerical results for the models meshed in various element sizes should be compared with each other. Thus, the optimum element size for the models should be decided where the numerical results of models meshed in two different element sizes are sufficiently close to each other.

### 3.1.3 Interactions and constraints

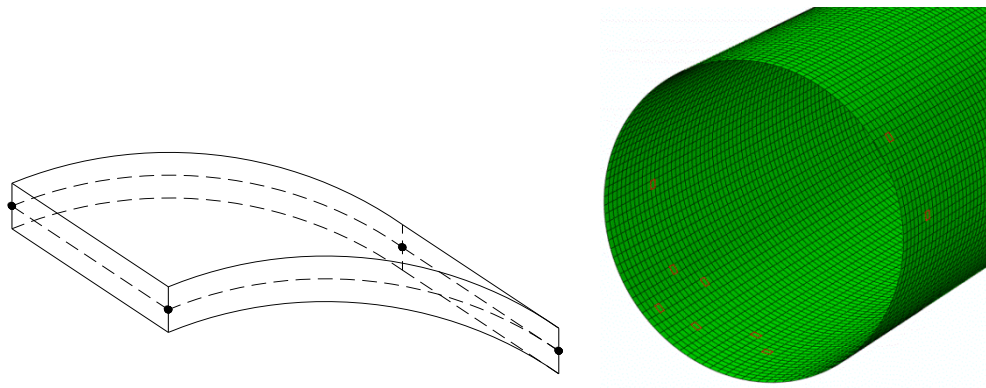
Tie constraints can constrain each node at the master surface and the slave surface, thus, the displacements of each node are equal to each other at both surfaces. The advantage of tie constraints is that they eliminate the degrees of freedom on the slave surface, and simplify the running time. Rotational and translational degrees of freedom can be tied together.

Coupling constraints can couple the motion of a group of nodes on a surface to a reference node. This is useful in the case where many nodes are constrained to the rigid body of a single node. To facilitate the application of the axial, transverse and torsional loads at the top of the tower, a reference node was introduced with a rigid constraint to the top cross-section of the tower. The reference node for the coupling constraint contains both translational and rotational degrees of freedom. The loads are applied to the top of the tower by employing coupling constraints.

### **3.1.4 Shell element**

A shell element can be used in the case where the value of one dimension is less than that of the other dimensions, and the representative stresses in the thickness direction are negligible. The geometric patterns of a shell element are displayed in Figure 3.3a. The shell element may be a plane or a curved surface. Six degrees of freedom for each node of the shell element are included in the three translational and three rotational directions. The thickness and material properties of the shell element should be defined.

For a wind turbine tower, the wall thickness is relatively small in relation to its diameter and height. Therefore, the tower wall can be simulated using the S4R shell element, which is a 4-node doubly-curved thin or thick shell, with a reduced integration finite element with hourglass control, which is capable of finite membrane strains, as shown in Figure 3.3b. In the ABAQUS software, the element type S4R is a general-purpose shell element, which can provide robust and accurate solutions for numerical simulation. Reduced integration is usually used to obtain more accurate results, whilst it significantly reduces the computation time.



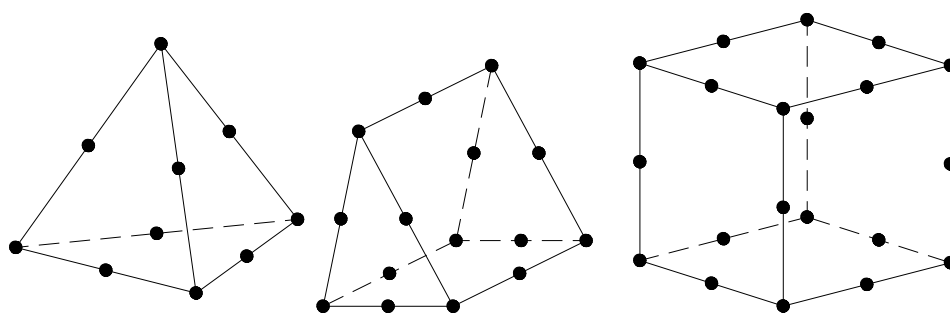
a. Shell element pattern

b. Tower in shell elements

Figure 3.3 The geometrical pattern and FEM models of shell elements

### 3.1.5 Continuum element

The solid elements are the standard volume elements which can be used to solve general 3D problems. The types of solid element are usually tetrahedron, pentahedron and hexahedron as shown in Figure 3.4. The tetrahedron is used for models with a complex boundary shape, but the pentahedron and hexahedron are usually meshed for regular shaped models. The solid elements can be meshed into linear and quadratic elements in full-integration or reduced-integration elements. Each node of the solid elements has three translational degrees of freedom. Thus, the solid elements do not transfer the bending moment from one to another.



a. Tetrahedron

b. Pentahedron

c. Hexahedron

Figure 3.4 Continuum (Solid) element pattern

The stiffening rings in the tower model are simulated by means of C3D10 continuum finite elements, which are 10-node quadratic tetrahedrons as shown in Figure 3.5. The regular second-order tetrahedron

elements usually give accurate results. The shell and solid elements are tied together, and the tie constraint is simulated to 'glue' each of the nodes to the slave surface with the master surface, so that displacements of the nodes between the slave and the master surfaces are equal to each other.

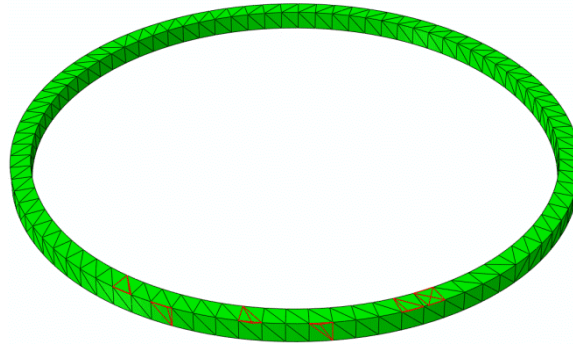


Figure 3.5 Ring with tetrahedron meshing

## 3.2 Wind load

### 3.2.1 50m towers

In the structural model, the self-weight of the towers is calculated directly using the FE analysis software ABAQUS by considering the dimensions of the tower and the material density. The contribution of the platforms and the ancillary equipment (ladders, cable racks etc.) to the total weight of the tower are neglected. The load states of 50m tower are shown in Figure 3.6. On the top of the tower, the weight of the nacelle, together with the blades and the rotor, will induce the vertical force and moment that act on the top of the tower, which are 750kN and 400kNm, respectively. The moment on the top of tower is caused by eccentric gravity of wind turbine. In addition, there is a horizontal wind load applied on the blades of the towers, with the data being provided by the rotor manufacturer (Baniotopoulos *et al.*, 2011; Seer *et al.*, 2013). For the 50m tower, the horizontal force is 80kN.

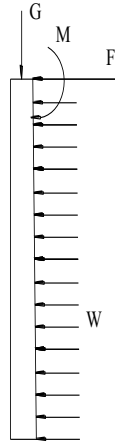


Figure 3.6 Load states of wind turbine towers

According to BS EN 1991-1-4, the wind loads over the tower stem are calculated based on the specific dynamic characteristics and geometry of the tower structure. The distribution function of basic wind pressure along the height,  $z$  of the 50m tower stem is related to the diameter,  $D$  as given by Eqs. (3.1, 3.2) ( $z, D$  are in m;  $f_b$  is in kN/m):

$$z \leq 2.00\text{m}: f_b = 0.51 \cdot D \quad (3.1)$$

$$z > 2.00\text{m}: f_b = 0.013 \cdot \ln(20 \cdot z) \cdot [\ln(20 \cdot z) + 7] \cdot D \quad (3.2)$$

where  $D = -0.0266 \cdot z + 3.7$  (variation of tower diameter along the height). Figure 3.7 shows the distribution of wind loads along the tower height and circumferential circle.

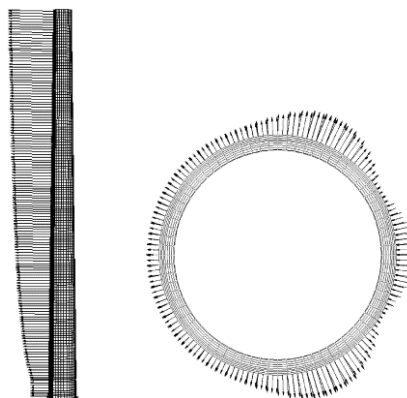


Figure 3.7 Distribution of wind loads along the tower height and around the circumference

According to BS EN 1991-1-4, the external pressure coefficients  $c_{pe}$  of the circular tower can be obtained by Eqs (3.3).

$$c_{pe} = c_{p,o} \cdot \varphi_{\lambda\alpha} \quad (3.3)$$

where  $c_{p,o}$  is the external pressure coefficient without free-end flow,  $\varphi_{\lambda\alpha}$  is the end-effect factor. The end-effect factor  $\varphi_{\lambda\alpha}$  is given by expression (3.4).

$$\begin{aligned} \varphi_{\lambda\alpha} &= 1 & [0^\circ, \alpha_{min}] \\ \varphi_{\lambda\alpha} &= \varphi_\lambda + (1 - \varphi_\lambda) \cos\left[\frac{\pi}{2} \cdot \frac{(\alpha - \alpha_{min})}{(\alpha_A - \alpha_{min})}\right] & [\alpha_{min}, \alpha_A] \\ \varphi_{\lambda\alpha} &= \varphi_\lambda & [\alpha_A, 180^\circ] \end{aligned} \quad (3.4)$$

where  $\alpha_A$  is the position of the flow separation,  $\varphi_\lambda$  is the end-effect factor. The parameters of wind load distribution around the circumference can be shown in Figure 3.8. According to the BS EN 1991-1-4 and Figure 3.8, the coefficients can be obtained as follows:  $\varphi_\lambda = 0.99$ ;  $\alpha_{min} = 75^\circ$ ;  $\alpha_A = 105^\circ$ ;  $c_{p0,min} = -1.5$ ;  $c_{p0,h} = -0.8$ .

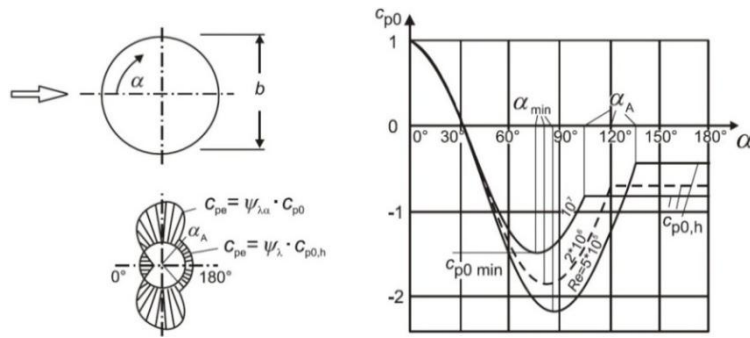


Figure 3.8 Pressure distribution for circular cylinders

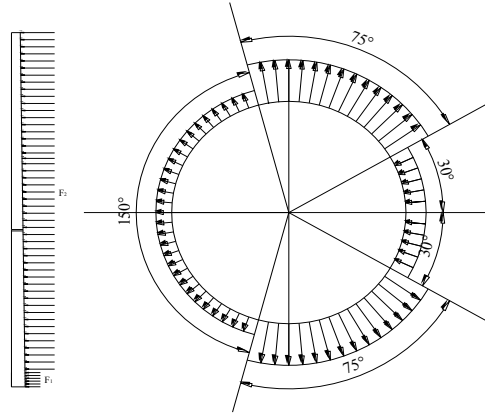


Figure 3.9 Simplified distribution pattern of wind load along tower height and around the circumference

Simplified distribution patterns of the wind loads used in the present analysis are presented in Figure 3.9 in accordance with BS EN 1991-1-4. As shown in Figure 3.9, the wind load distribution profile along the vertical axes of the 50m and 150m towers is divided into two parts where the wind pressure of each part is equal to the maximum load within the corresponding zone. The wind pressure on the circumferential surface of the tower is symmetrical with respect to the horizontal axis of the cross-section. The distributions of wind load coefficients around the circumference are divided into four parts as shown in Figure 3.9.

For the wind pressure, according to Equations (3.1) and (3.2), the applied wind pressure  $p$  on the surface of the tower shell can be obtained by Equation (3.5):

$$p = f_b / [\theta \cdot (D/2)] \quad (3.5)$$

where  $\theta$  is equal to  $\pi/3$  (see Figure 3.9). The wind pressure can be calculated by using Equations (3.6) and (3.7):

$$z \leq 2.00\text{m}: p = 0.975 \times 10^{-3} \text{N/mm}^2 \quad (3.6)$$

$$z > 2.00\text{m}: p = 0.025 \cdot \ln(20 \cdot z) \cdot [\ln(20 \cdot z) + 7] \quad (3.7)$$

According to BS EN 1991-1-4 and Figure 3.9, for the 50m tower, the maximum wind pressure  $p_1$  at the bottom 2m zone is calculated by Eq. (3.1), where the negative value represents wind suction (in  $\text{N/mm}^2$ ):

$$p_1 = \begin{cases} c_{p,o} \cdot \varphi_{\lambda\alpha} \cdot p = 0.975 \times 10^{-3} \text{ N/mm}^2 & [0^\circ, 30^\circ] \\ c_{p,o} \cdot \varphi_{\lambda\alpha} \cdot p = -1.455 \times 10^{-3} \text{ N/mm}^2 & (30^\circ, 105^\circ) \\ c_{p,o} \cdot \varphi_{\lambda\alpha} \cdot p = -0.768 \times 10^{-3} \text{ N/mm}^2 & (105^\circ, 180^\circ) \end{cases} \quad (3.8)$$

where  $c_{p,o}$  is the external pressure coefficient without free-end flow,  $\varphi_{\lambda\alpha}$  is the end-effect factor.

Similarly, the maximum wind pressure  $p_2$  of the upper 48m zone is calculated by Eq. (3.2) (in  $\text{N/mm}^2$ ):

$$p_2 = \begin{cases} c_{p,o} \cdot \varphi_{\lambda\alpha} \cdot p = 2.39 \times 10^{-3} \text{ N/mm}^2 & [0^\circ, 30^\circ] \\ c_{p,o} \cdot \varphi_{\lambda\alpha} \cdot p = -3.585 \times 10^{-3} \text{ N/mm}^2 & (30^\circ, 105^\circ) \\ c_{p,o} \cdot \varphi_{\lambda\alpha} \cdot p = -1.893 \times 10^{-3} \text{ N/mm}^2 & (105^\circ, 180^\circ) \end{cases} \quad (3.9)$$

### 3.2.1 150m towers

The load states of 150m tower are identical to those of 50m tower as shown in Figure 3.6. On the top of the tower, the vertical force and moment are incurred from the weight of the blades and rotor. As for 150m towers, the gravity of nacelle and moment are 2300kN and 3550kN·m respectively. Similarly, the horizontal force produced by wind load applied on the blades of the towers is 280kN.

Wind load distribution of 150m tower is also similar with the 50m tower whatever along the height or around the circumference as shown in Figure 3.7 and 3.9. According to BS EN 1991-1-4 and Equations (3.1-3.5), and the express  $D = -0.0186 \cdot z + 8.5$  is the diameter variation of 150m tower along the height.

Using the same calculation procedure as the 50m tower, the maximum wind pressure at the height of 150m towers from 0m to 2m can be obtained by Eq. (3.1) as follows:

$$p_1 = \begin{cases} c_{p,o} \cdot \varphi_{\lambda\alpha} \cdot p = 0.975 \times 10^{-3} \text{ N/mm}^2 & [0^\circ, 30^\circ] \\ c_{p,o} \cdot \varphi_{\lambda\alpha} \cdot p = -1.4625 \times 10^{-3} \text{ N/mm}^2 & (30^\circ, 105^\circ) \\ c_{p,o} \cdot \varphi_{\lambda\alpha} \cdot p = -0.7722 \times 10^{-3} \text{ N/mm}^2 & (105^\circ, 180^\circ) \end{cases} \quad (3.10)$$

The maximum wind pressure of the upper 148m zone is (in  $\text{N/mm}^2$ ):

$$p_2 = \begin{cases} c_{p,o} \cdot \varphi_{\lambda\alpha} \cdot p = 2.98 \times 10^{-3} \text{ N/mm}^2 & [0^\circ, 30^\circ] \\ c_{p,o} \cdot \varphi_{\lambda\alpha} \cdot p = -4.47 \times 10^{-3} \text{ N/mm}^2 & (30^\circ, 105^\circ) \\ c_{p,o} \cdot \varphi_{\lambda\alpha} \cdot p = -2.36 \times 10^{-3} \text{ N/mm}^2 & (105^\circ, 180^\circ) \end{cases} \quad (3.11)$$

### 3.2.2 250m towers

The vertical force and moment from the gravity of rotor are applied to the circular centre of top cross-section of the 250m tower. The load situation of wind blowing the blades can be simplified into a horizontal force applied to the top circular centre of the tower. The magnitude of moment and the horizontal force are 9800kN·m and 3800kN as displayed in Figure 3.6.

According to BS EN 1991-1-4, the simplified distribution of wind load along the tower height and around the circumference of 250m tower is shown in Figure 3.10. Due to higher height of the 250m tower, the wind load distribution of 250m tower need be divided into three parts where the wind pressure of each part is equal to the maximum load within the corresponding zone along the tower height. The first part is from the height of 0m to 2m, the second part is from the height of 2m to 100m and the third part is from 100m to 250m. The distribution of wind load around the circumference of 250m tower is identical to that of 50m and 150m towers.

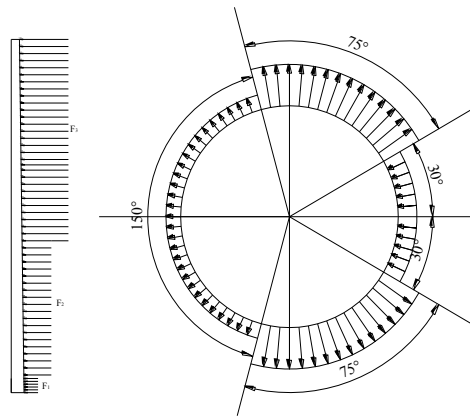


Figure 3.10 Simplified distribution pattern of wind load along 250m tower height and around the circumference

According to BS EN 1991-1-4 and Equations (3.1-3.5), and the express  $D = -0.018 \cdot z + 14$  is the diameter variation of 250m tower along the height. Thus, as for the 250m tower, the distribution of maximum wind pressure of the lower 2m tower is (in  $N/mm^2$ ):

$$p_1 = \begin{cases} c_{p,o} \cdot \varphi_{\lambda\alpha} \cdot p = 0.975 \times 10^{-3} \text{ N/mm}^2 & [0^\circ, 30^\circ] \\ c_{p,o} \cdot \varphi_{\lambda\alpha} \cdot p = -1.4625 \times 10^{-3} \text{ N/mm}^2 & (30^\circ, 105^\circ] \\ c_{p,o} \cdot \varphi_{\lambda\alpha} \cdot p = -0.7722 \times 10^{-3} \text{ N/mm}^2 & (105^\circ, 180^\circ] \end{cases} \quad (3.12)$$

Similarly, the distribution of maximum wind pressure of the upper 2m to 100m tower is (in N/mm<sup>2</sup>):

$$p_2 = \begin{cases} c_{p,o} \cdot \varphi_{\lambda\alpha} \cdot p = 2.575 \times 10^{-3} \text{ N/mm}^2 & [0^\circ, 30^\circ] \\ c_{p,o} \cdot \varphi_{\lambda\alpha} \cdot p = -3.8625 \times 10^{-3} \text{ N/mm}^2 & (30^\circ, 105^\circ] \\ c_{p,o} \cdot \varphi_{\lambda\alpha} \cdot p = -2.0394 \times 10^{-3} \text{ N/mm}^2 & (105^\circ, 180^\circ] \end{cases} \quad (3.13)$$

The distribution of maximum wind pressure of the upper 100m to 250m tower is (in N/mm<sup>2</sup>):

$$p_3 = \begin{cases} c_{p,o} \cdot \varphi_{\lambda\alpha} \cdot p = 3.283 \times 10^{-3} \text{ N/mm}^2 & [0^\circ, 30^\circ] \\ c_{p,o} \cdot \varphi_{\lambda\alpha} \cdot p = -4.9245 \times 10^{-3} \text{ N/mm}^2 & (30^\circ, 105^\circ] \\ c_{p,o} \cdot \varphi_{\lambda\alpha} \cdot p = -2.6 \times 10^{-3} \text{ N/mm}^2 & (105^\circ, 180^\circ] \end{cases} \quad (3.14)$$

where  $\alpha_A$  is the position of the flow separation. The wind pressure on the cross-section of the tower is symmetrical with respect to horizontal axis of the cross-section of tower.

### 3.3 Experimental validations

An extensive numerical investigation was performed to study the effect of stiffening rings on the overall response of wind turbine towers. The numerical models were developed using the commercial package ABAQUS. The models were first validated with respect to existing data recently obtained by Rebelo *et al.* (2012b; 2012c) who monitored the structural response of an actual wind turbine tower of 76m height.

#### 3.3.1 Experiment description

The tubular cylindrical tower that was monitored is composed of three segments with lengths 21.77m, 26.62m and 27.76m respectively, as shown in Figure 3.11. The segments are connected to each other by bolted flanges. The mid-section widths of the upper and lower level flanges are 105mm and 120mm respectively and the corresponding thicknesses are 120mm and 175mm. The diameter varies linearly from 4.3 m at the base to 2.95m at the top, and the shell thickness decreases linearly from 30mm to 12mm along its height. The self-weight of the wind turbine is 106.73t and the turbine is placed at the top of the tower with an eccentricity of 0.72m. Sensors are fixed at four levels as displayed in Figure

## CHAPTER 3: METHODOLOGY

3.11. Levels 0, 1, 2 and 3 in Figure 3.11 are located at heights 5.8m, 17.97m, 44.59m and 71.15m, respectively.

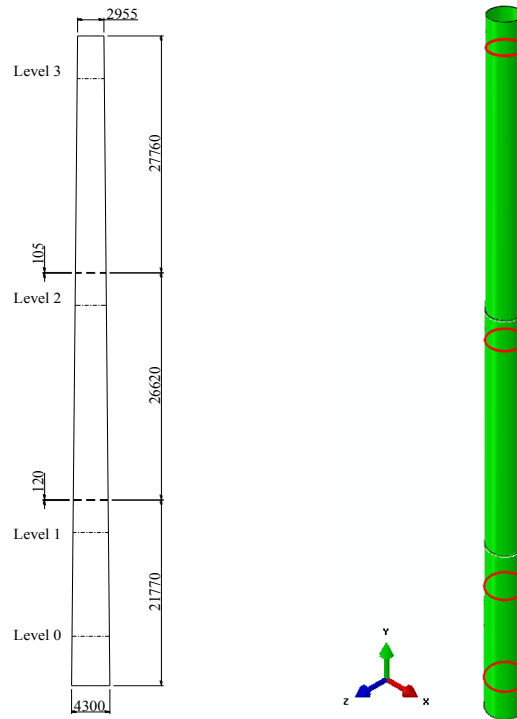


Figure 3.11 The geometrical data and the FEM model of the 76m wind turbine tower

Table 3.1 The cross-section characteristics along the tower height (2012b; 2012c)

Height(m)	Diameter(m)	Thickness(m)
0	4.3	0.03
2	4.276	0.03
3.082	4.257	0.03
5.412	4.215	0.03
5.802	4.208	0.026
7.789	4.173	0.026
9.302	4.147	0.027
11.502	4.108	0.024
12.582	4.089	0.023

## CHAPTER 3: METHODOLOGY

15.172	4.043	0.022
17.362	4.004	0.022
17.972	3.993	0.022
19.752	3.962	0.022
22.182	3.917	0.021
22.362	3.917	0.02
25.252	3.864	0.02
28.002	3.816	0.02
30.752	3.768	0.02
31.982	3.746	0.019
34.382	3.704	0.019
36.252	3.671	0.019
39.002	3.622	0.018
41.752	3.574	0.018
43.982	3.535	0.017
44.592	3.524	0.017
46.382	3.492	0.017
48.817	3.448	0.016
48.967	3.448	0.015
51.552	3.4	0.015
53.812	3.36	0.015
55.502	3.33	0.014
58.252	3.28	0.014
58.622	3.277	0.013
61.022	3.231	0.013
63.752	3.182	0.013
65.842	3.144	0.013

### CHAPTER 3: METHODOLOGY

66.502	3.133	0.012
69.252	3.083	0.012
71.152	3.049	0.012
72.002	3.034	0.012
73.082	3.015	0.012
75.492	2.971	0.014
75.64	2.955	0.018

In the numerical model, different wall thicknesses were used in four different sections, i.e. 28mm thickness for heights from 0 m to 8.8m, 22mm from 8.8m to 21.77m, 18mm from 21.77m to 48.39m and 13mm from 48.39m to 76.15m. The tower shell is simulated by the S4R shell element, which is a 4-node doubly-curved thin or thick shell element, with a reduced integration finite element with hourglass control, and is capable of considering finite membrane strains. The flanges are simulated by means of the C3D10 continuum finite element, which is a 10-node quadratic tetrahedron element. The interaction between the flange and the tower wall is considered by using tie constraints. The support of the tower is considered as fully fixed. A reference node was introduced with a rigid constraint to the top cross-section of the tower to apply all possible loadings at the top of the tower. The elastic modulus and the Poisson's ratio of steel are 200GPa and 0.3 respectively, and the density of steel is 7.85g/cm<sup>3</sup>.

Due to the complexity of the load combinations, the wind load profile along the tower height and around the circumference is simulated by using a simplified method: the tower is divided into two parts along the tower height, and separated into four parts around the circumference in accordance with section 3.2, based on BS EN 1991-1-4 (1991). The wind speed was taken at the four levels of the tower, and the maximum wind speed during the testing period was 25m/s as displayed in Figure 3.12. Wind pressure can be expressed as a function of wind speed by means of the following formula:

$$p = 0.5 \cdot \rho_a \cdot v^2 \quad (3.15)$$

where air density,  $\rho_a$  is equal to  $1.25 \text{ kg/m}^3$ , wind speed,  $v$  is expressed in  $\text{m/s}$ , and the wind pressure,  $p$  in  $\text{N/m}^2$ .

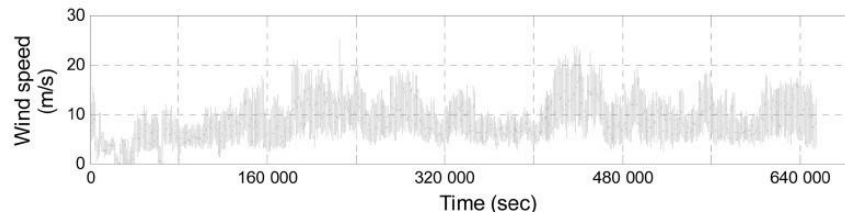


Figure 3.12 Wind speed of the 76m tower during testing period at Level 3 (2012b; 2012c)

According to Rebelo *et al.* (2012b; 2012c), the magnitude of the average maximum bending moment at the base of the tower under monitoring is  $29000 \text{ kN}\cdot\text{m}$ . The self-weight of the tower is calculated by the software, based on the dimensions of the tower and the material density.

### 3.3.2 Sensitivity analysis

Since the simulation accuracy and the calculation efficiency of the developed numerical models are affected by the mesh density, a study of the mesh sensitivity is essential. The refined elements may lead to a low efficiency, whereas the rough elements may lead to erroneous results. To obtain the optimum element size for such a tower model, the shell should initially be simulated by means of finite elements of various element sizes. The maximum von Mises stresses and the horizontal sways of the tower under consideration have been calculated using models of rough to refined elements, which in turn have been examined to attain convergence. The size of the S4R shell element is chosen as between 400mm and 50mm. The size of the C3D10 element of the two flanges is discretised at the size of 50mm. The maximum von Mises stresses and horizontal sways of the 76m tower structures modelled with different element sizes are presented in Table 3.2.

According to the results (Table 3.2 and Figure 3.13), the maximum von Mises stresses and horizontal sways of this tower are evidently affected by the size of the finite element selected when the element size is reduced from 400mm to 100mm. In Table 3.2 and Figure 3.13, the maximum von Mises stresses and the horizontal sways of the 76m tower remain almost constant with element sizes reducing from 100mm to 50mm. The maximum von Mises stresses and horizontal sways of the towers converge to

101.6MPa and 568.5mm, respectively when the size of the shell elements is reduced to 100mm. Therefore, the optimum size of the applied S4R shell element of the tower is approximately 100mm.

Table 3.2 Maximum von Mises stresses and horizontal sways of the 76m tower for different element sizes

Size of elements (mm)	Max. von Mises stress (MPa)	Max. Horizontal sway (mm)
400	102.64	575.13
300	103.9	572.8
200	102	570.7
100	101.6	568.5
80	101.6	568.5
50	101.6	568.5

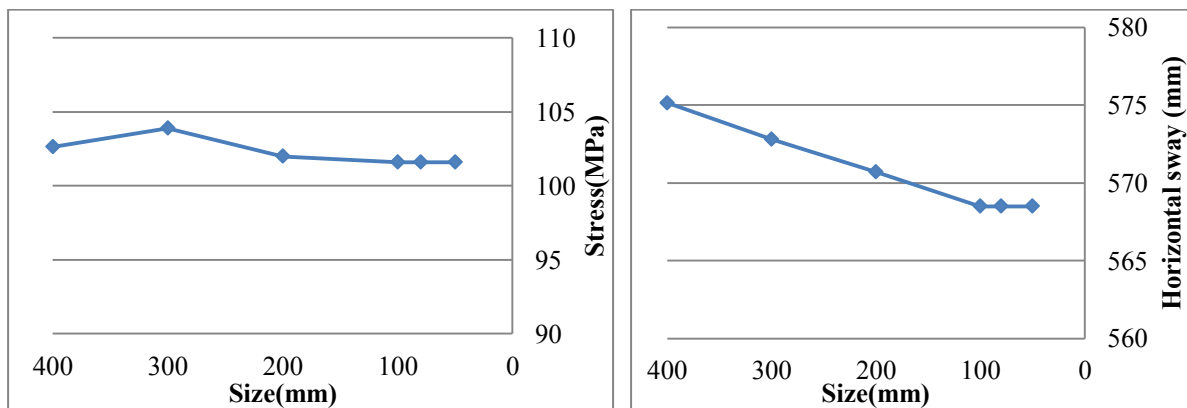


Figure 3.13 Maximum von Mises stresses and horizontal sways of the 76m tower for different element sizes

### 3.3.3 Result comparison

As previously mentioned, the tower which was studied by Rebelo *et al.* (2012b; 2012c) was monitored by sensors placed at four different levels. The measured stress at each level is compared with the numerical results of the present model. As wind loading is variable in engineering practice, the stress values should be fluctuating at different wind speeds. Thus, the combination of mean stress value and

its standard deviation for each wind speed should be compared with the monitored data to validate the model. According to this data inventory (2012b; 2012c), the sum of average vertical stresses and corresponding standard deviation of levels 0 and 1 are respectively 68MPa and 73MPa respectively, both being achieved at a wind speed of 12m/s as shown in Figure 3.14 and 3.15. In the data inventory, it just describes the stress at levels 0 and 1 and the displacement at level 2. Hence these given values need to be compared with the corresponding results of numerical models.

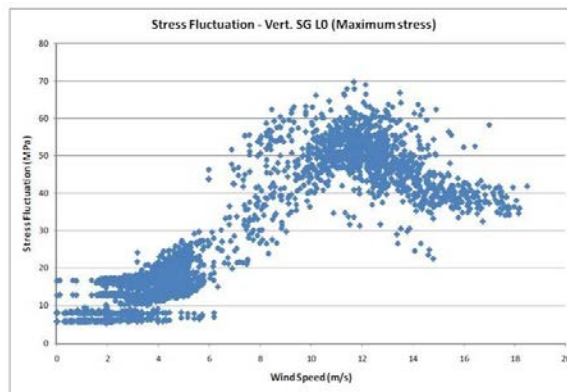


Figure 3.14 Maximum vertical stresses of 76m tower at level 0 (2012b; 2012c)

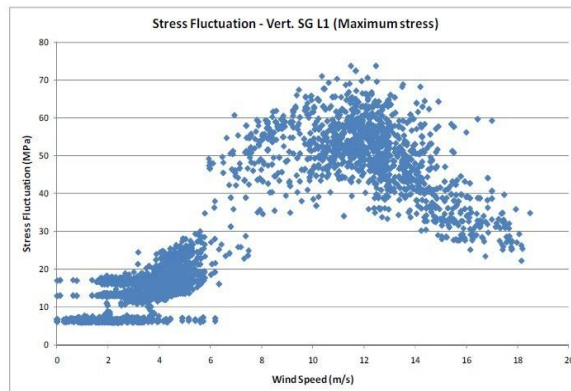


Figure 3.15 Maximum vertical stresses of 76m tower at level 1 (2012b; 2012c)

The vertical stress contours at the cross-sections at levels 0 and 1 are depicted in Figure 3.16 and 3.17. In the cross-section at level 0, the maximum vertical stress is 66.41MPa, which is close to the measured stress of 68MPa. Similarly, the maximum stress in the cross-section at level 1 is 72.99MPa, which is almost identical to the measured stress of 73MPa at the monitored tower (Figure 3.17).

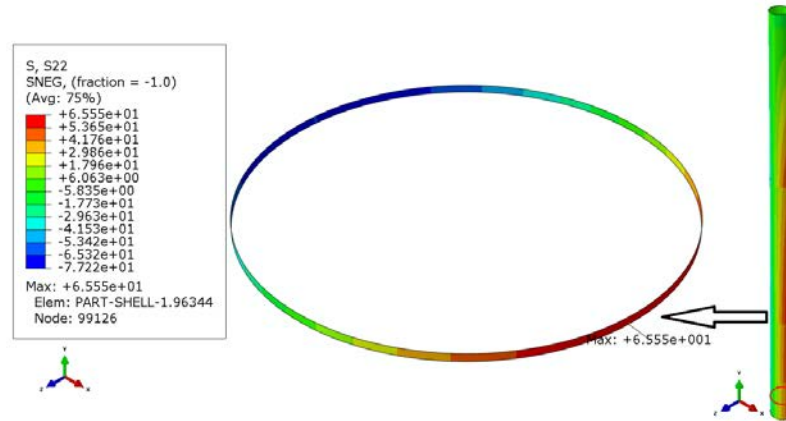


Figure 3.16 Vertical stress contour plot at the cross-sections of the 76m tower at levels 0

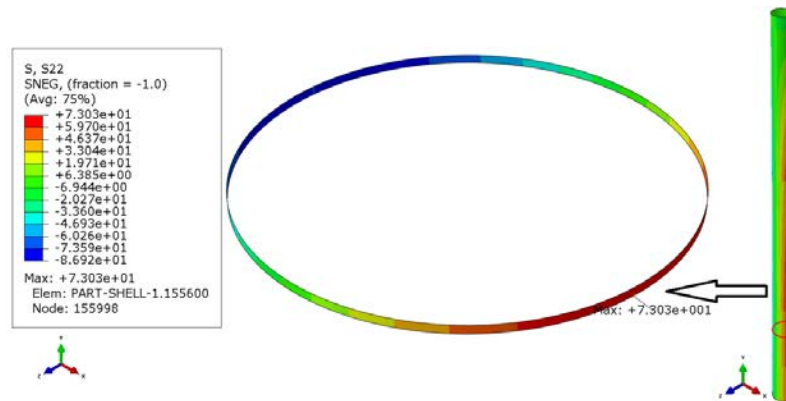


Figure 3.17 Vertical stress contour plot at the cross-sections of the 76m tower at levels 1

The measured dynamic horizontal sway of the tower fluctuates. According to Rebelo *et al.* (2012b; 2012c), the average maximum horizontal sway of the tower obtained from the experimental monitoring data at level 3 is 534.23mm. The maximum horizontal sway from the numerical model is 534.8mm, which is almost identical to the measured average maximum displacement of 534.23mm as depicted in Figure 3.18. Thus, a good correlation for maximum vertical stress and horizontal sway between the numerical and the experimental results has been achieved.

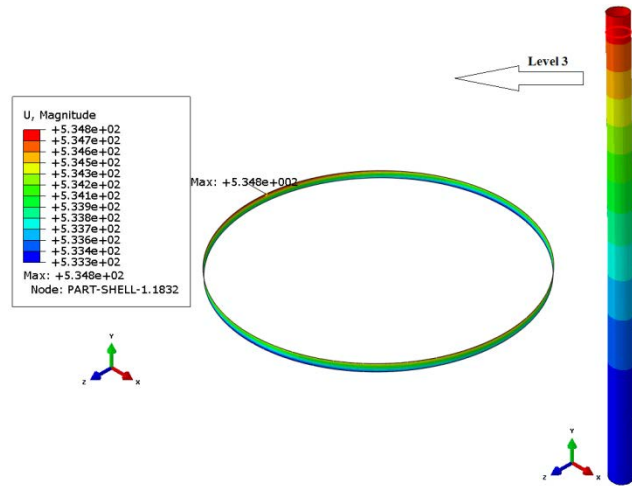


Figure 3.18 Horizontal sway contour of the cross-section of the 76m tower at level 3

### 3.4 Conclusions

In this study, an effective numerical model has been validated against experimental data. In addition, a sensitivity analysis of the FE models used has been performed so that the optimum element size can be defined. The simulated maximum stresses of the monitored towers are fairly close to the measured ones in the instrumented tower at the same heights. The maximum horizontal sways measured by the sensors are fairly close to the maximum horizontal displacements modelled using a numerical simulation method. Thus, the numerical simulation method appears to be sufficiently effective to simulate the structural response of tubular steel wind turbine towers.

## CHAPTER 4: FE ANALYSIS OF TOWER

### 4.1 Introduction

The use of renewable energy and in particular, wind energy, mitigates the rate of environmental deterioration as it minimises the emission of greenhouse gases. Wind energy appears as a clean and appropriate solution to cope with a great part of this energy demand. Currently, wind energy is extensively used and the underpinning technology is developing very rapidly. In Denmark, for example, 20% of electricity had produced from wind by 2007, and it is planned that 50% of Danish electricity needs will be met by wind generation by 2025 (DEA, 2006). China's wind market has continued its high growth rates in the past few years, and an additional capacity of 6.3GW of wind power has been installed in China, bringing the total capacity to 12.2GW by 2008 (Wenyi Liu *et al.*, 2010). Wind turbines are energy converters that convert kinetic energy from the moving air to electrical power; they are attached to supporting towers that also support the rotor and the power transmission and control systems. One of the most common design options for wind turbine towers is a tubular steel structure manufactured in sections of 20-30m with flanges at both ends facilitating the bolting of these sections *in situ*.

Economic efficiency is a key parameter that needs to be considered in the design of a wind turbine tower. As a proportion of the total cost, the construction cost of the wind turbine makes up a considerable percentage, i.e. approximately 15 to 20%. The materials used, and subsequently the weight of the system, determine the costs incurred during transport and erection. On top of this, the height of a tower directly determines the energy yield, and hence will be determined before the design process commences (Gasch and Tvele, 2012).

A successful structural design of a tower should meet the design criteria of cost effectiveness, safety and functionality. Given the proportion of steel material cost in the total cost of the wind tower, a material efficient design with satisfactory performance becomes an important step in the wind turbine

tower construction. Li *et al.* (2013) analysed the reasons of wind turbine tower collapses under extreme wind loads and proposed a robust design of wind turbine towers against typhoons. Kilic and Unluturk (2015) measured and predicted the behaviour of wind turbine towers by using wireless sensor networks and accelerometers. Binh *et al.* (2008) proposed evaluation formulas of design wind load on the supporting structure in complex terrains, whereas the respective formulas have been validated by comparing analytical solutions with the respective FEM simulation. Dong Hyawn Kim *et al.* (2014) carried out seismic fragility analysis of offshore wind turbine towers by considering soil-pile interaction. The critical displacement was obtained to assess the structural safety under seismic loads by using pushover analysis. Van der Woude and Narasimhan (2014) investigated parametric studies of base isolation systems to improve the structural response of wind turbine structures during strong earthquake events; it was concluded that the use of base isolation system reduces excessive dynamic displacements of the structures in seismic zones. Tran *et al.* (2013) described the influence of the door opening on the strength of wind turbine towers by means of detailed FE models. Trung Q. Do *et al.* (2014b) studied the structural response of towers taking into account fatigue due to wind loadings; aiming to minimise the cost of steel to optimise design parameters of the tower base and achieve fatigue life of tower have been obtained. Polyzois *et al.* (2009) presented the experiments and the numerical simulations for GFRP wind turbine towers under static and dynamic loadings. Valamanesh and Myers (2014) compared the predicted results with those from a baseline wind turbine tower in operation and in rest, where a reasonable agreement seems to have been achieved. Guo *et al.* (2013) performed a series of bending tests of tower tubes with stiffeners to inspect the effect of section slenderness on the behaviour of the steel tower tubes and the respective experimental results are in accordance to the AS4100 design code.

In this paper, wind towers of three different heights have been numerically modelled by means of the finite element program ABAQUS (2008). In each height case, towers have three design options, namely, the intermediately thick shell structure without rings (named as “tower I”) or with rings (named as “tower II”), and the thin shell structure with strong rings (named as “tower III”). The weights of the shell structure and rings associated with each tower construction have also been

considered. Thus, the three design options for each height case are compared in order to identify the efficient design solutions by either increasing the thickness or adopting ring stiffeners. Given the high percentage of the material cost in the total construction cost, the weight of tower is considered as the key criteria when carrying out the comparison. In addition to the von Mises stress and the horizontal sway behaviour, the dynamic characteristics of these independent tower structures that do not involve the mass of nacelle-rotor system are also examined and the suggestions to avoid resonance for each height case are proposed.

## **4.2 Models of 50m tower**

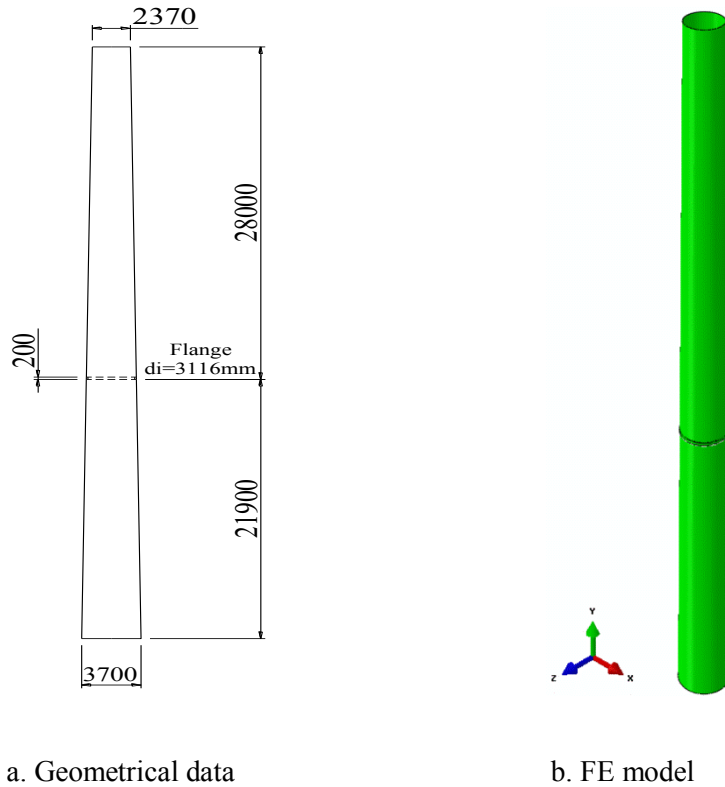
### **4.2.1 50m tower I**

In engineering practice, the choice of the tower height is pre-determined based on the energy yield requirement. Generally, tower should be connected together by flanges and rings, which is convenient to transport and erect the towers. Therefore, different height towers with or without rings are researched respectively.

The geometric and FEM models of 50m wind turbine tower are shown in Figure 4.1. A typical cross-section and flange arrangement of the 50m height tower are presented in Figure 4.2. The thickness and central spacing of flange are 200mm and 100mm respectively. The tower is composed of the lower and upper parts as displayed in Figure 4.1, thickness of which is 25mm and 15mm respectively. The material properties of the steel towers are displayed in Table 4.1, whereas the thickness and mid-section width of the flanges are shown in Figure 4.2. The diameters of the towers' cross-sections from bottom to top vary linearly.

As the heights and diameters of the towers are far greater than the thicknesses of the tower walls, the shell of a tower is simulated via the S4R shell element, which is a 4-node doubly-curved thin or thick shell, with reduced integration finite element with hourglass control and capable of finite membrane strains. The flanges are designed to be on the inner side of the shell, thus permitting easy access for the maintenance of the bolts. The flange in the model is simulated by means of C3D10 continuum

finite elements, which are a 10-node quadratic tetrahedron. The interaction between the flange and the tower wall is via the tie constraint. The nodes and element numbers of the 50m tower I are 51874 and 49732, respectively. To facilitate the application of the axial, transverse and torsional loads at the top of tower, a reference node was introduced with a rigid constraint to the top cross section of the tower. The support of the tower is considered as fixed.



a. Geometrical data  
b. FE model  
Figure 4.1 Prototypes of 50m tower I: geometrical data and FEM models

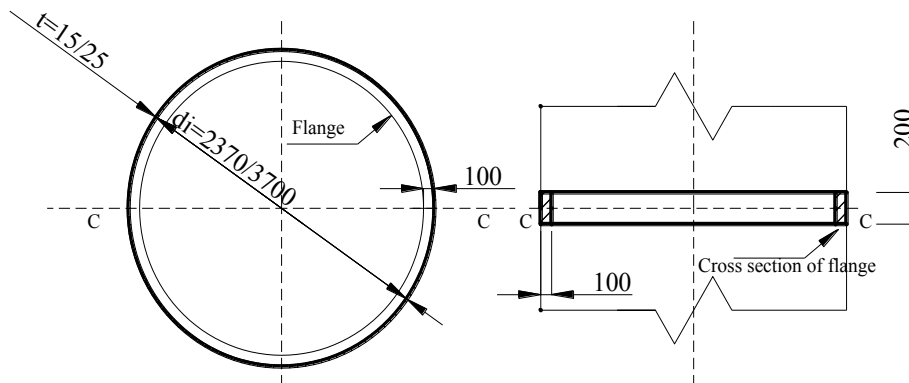
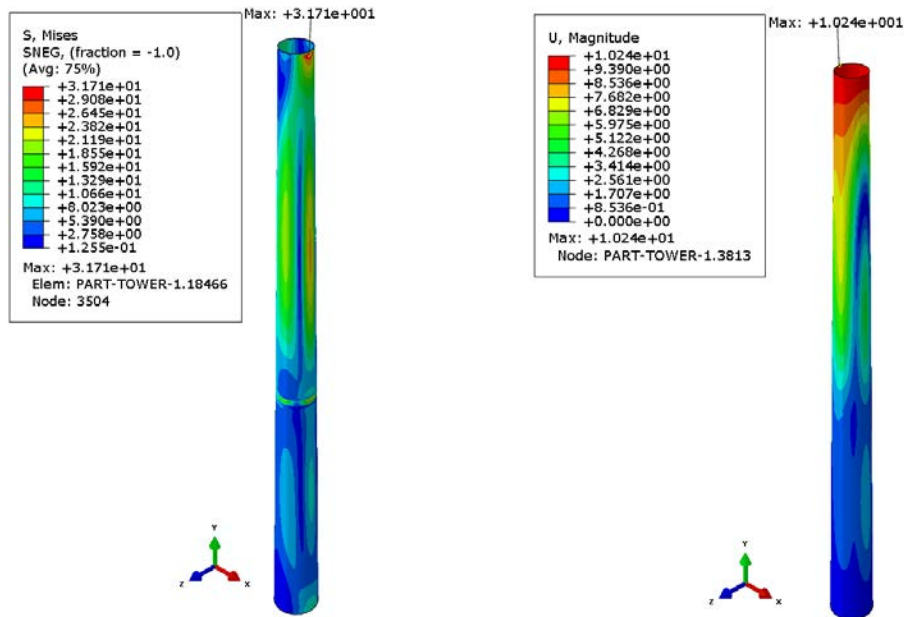


Figure 4.2 Typical cross-section of the 50m height tower (in mm)

CHAPTER 4: FE ANALYSIS OF TOWER

Table 4.1 Material properties of structural steel of the wind turbine tower

Material property	Elastic modulus	Density	Poisson's ratio
Steel	205GPa	7.85g/cm <sup>3</sup>	0.3



a. Von Mises stress of shell

b. Horizontal sway

Figure 4.3 Contour plots of stress and sway for 50m tower I

The contour plots of the von Mises stress and horizontal sway of the shell structure and the horizontal sway of the shell structure of the 50m tower I is depicted in Figure 4.3 where the stress concentration in the vicinity of the bottom of the tower is observed. The maximum von Mises stress of the 50m tower I is 31.71MPa, which is less than that of the flange, at 43.65MPa as displayed in Figure 4.4. The maximum horizontal sway of the 50m tower I at the top is 10.24mm as shown in Figure 4.3b.

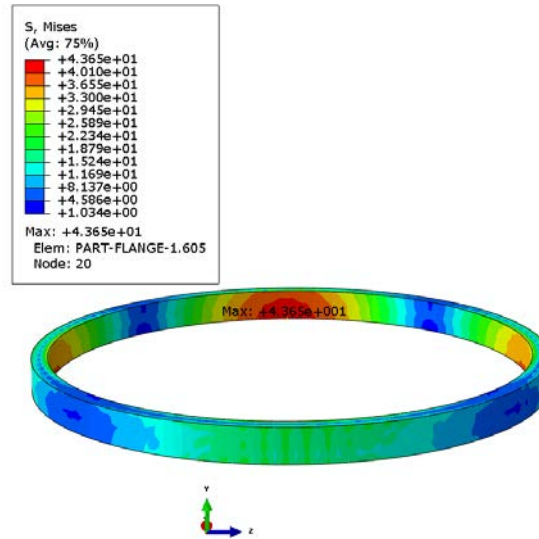
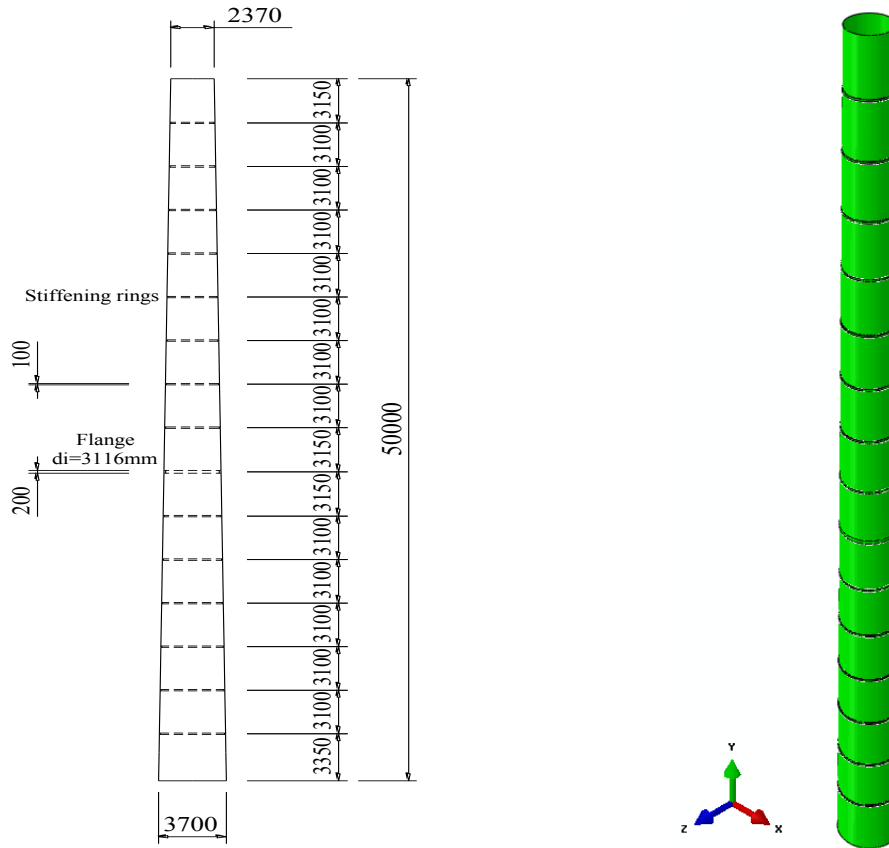


Figure 4.4 Stress contour of flange of 50m tower I

### 4.2.3 50m tower II

Steel shells are regularly stiffened by means of stiffening rings to prevent local buckling. The stiffening rings are added to the inner surface of the shell. The dimensions and FE models of 50m tower II are presented in Figure 4.5. The location and dimension of flange are the same as the 50m tower I. Specifically, all stiffening rings of the 50m tower II are 100mm high and have a trapezoidal cross-sectional shape with 50mm width at the mid-section. The other dimensions are identical to those of the 50m tower I, so are the loads. The ring spacing of the 50m tower II is displayed in Figure 4.5a. The shell thickness of the 50m tower II is identical to that of corresponding tower I.

Similarly, the bases of the towers of this type are considered to be fixed. The shell structure of tower II is also simulated by using the S4R element, which is a 4-node doubly-curved thin or thick shell type element with reduced integration and hourglass control and capable of allowing for the finite membrane strain. The numbers of node and element of the 50m tower II are 63486 and 46179, respectively. Circular stiffeners are placed at regular intervals. The contact interaction between the shell and rings is modelled as being tied together. The flanges and rings in the models are both simulated by using the C3D10 continuum finite element, which is a 10-node quadratic tetrahedron. The towers' cross-sections also vary linearly from the bottom to the top.

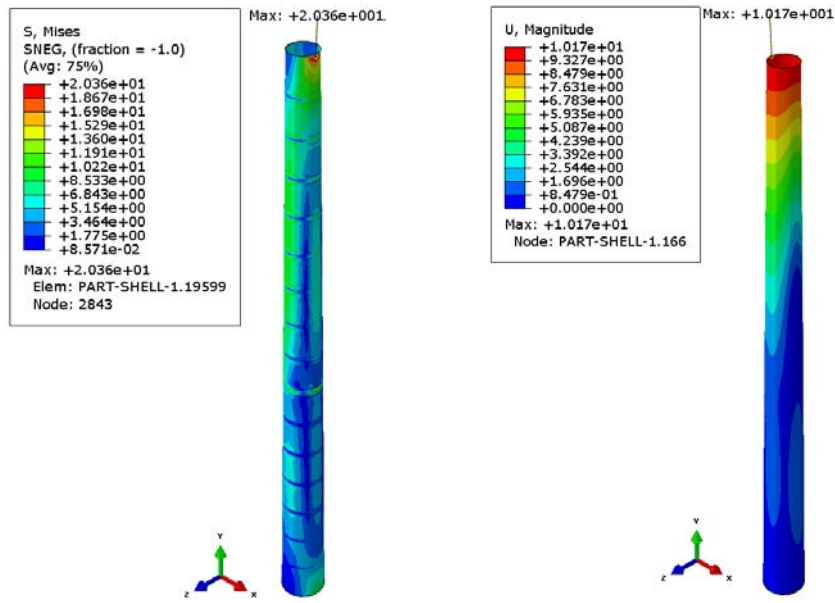


a. Geometrical data

b. FE model

Figure 4.5 Prototypes of 50m tower II: geometrical data and FEM models

The von Mises stress contour plot of the shell and rings of the 50m tower II is shown in Figure 4.6, together with the horizontal sway. The stress distribution in the 50m tower II is obviously different from its counterpart 50m tower I. The maximum shell von Mises stress is only 20.36MPa, which is less than the von Mises stress 30.71MPa in the previous model. The maximum horizontal sway of the 50m tower II is 10.17mm at the top of the tower. The maximum von Mises stress of the rings occurs in the inner surface of the sixth ring and is 39.22Mpa, which is less than the maximum von Mises stress of 43.65MPa in the flange of 50m tower I as shown in Figure 4.7.



a. Von Mises stress of shell

b. Horizontal sway

Figure 4.6 Contour plots of stress and sway for 50m tower II

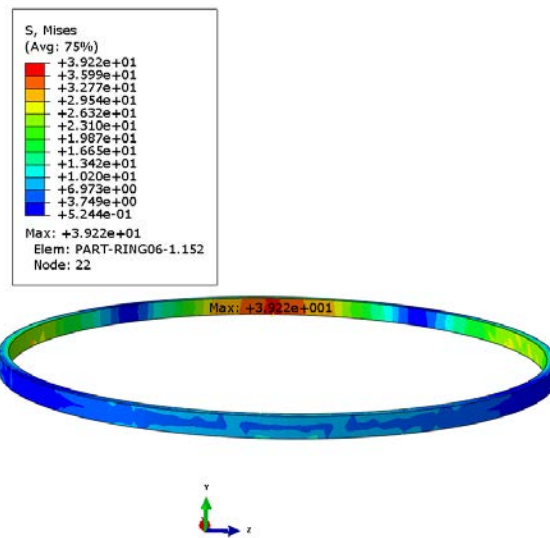


Figure 4.7 Stress contour of ring of 50m tower II

### 4.2.3 50m tower III

In the case of the thin-walled tower with stiffening rings, the thickness of the shells is reduced appropriately taking into account strength, stiffness and stability constraints. The shell thickness of these three types of tower is considered to be reduced to certain extent. The shell thickness of thin-walled towers is 20mm in the height range from 0 to 21.9m and 10mm in the height from 21.9mm to

50m. The other parameters are identical to those of the thick shell towers including the spacing of stiffening rings.

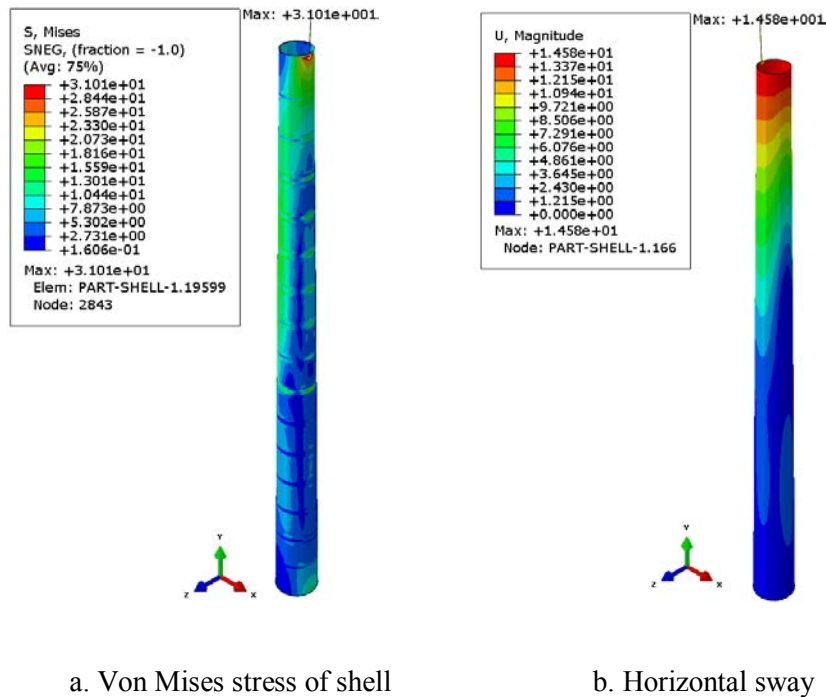


Figure 4.8 Contour plots of stress and sway for 50m tower III

The horizontal sway and von Mises stress contours of the 50m tower III are presented in Figure 4.8. The maximum von Mises stress of the tower is 31.01MPa. The horizontal sway of the tower increases nonlinearly along the height, from 0mm at the base to a maximum of 14.58mm at the top. The maximum von Mises stress of the rings also occurs in the inner surface of the fifth ring and is 51.12MPa as shown in Figure 4.9. The maximum von Mises stress and horizontal sway of 50m tower III are less than those of 50m tower II. The maximum von Mises stresses and horizontal sways of the 50m towers are displayed in Table 4.2.

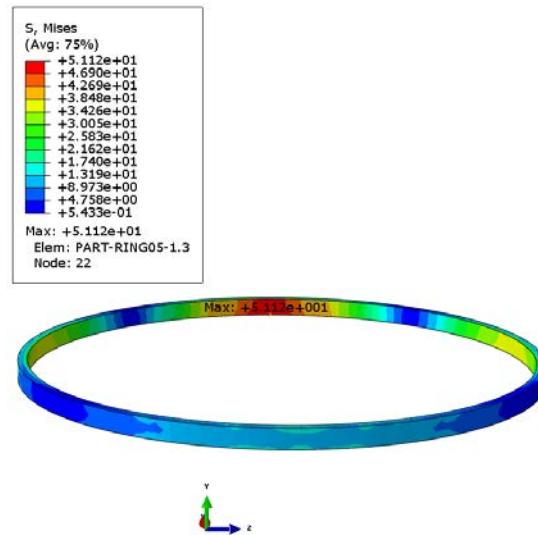


Figure 4.9 Stress contour of ring of 50m tower III

Table 4.2 50m wind turbine towers: maximum von Mises stress and horizontal sway

Variables	Tower I	Tower II	Tower III
Max. von Mises stress (MPa)	31.71	20.36	31.01
Max. horizontal sway (mm)	10.24	10.17	14.58

### 4.3 Models of 150m tower

#### 4.3.1 150m tower I

As for the 150m wind turbine towers, the schematic and FE model of 150m tower I are shown in Figure 4.10. Five flanges are mounted to the inner side of 150m tower I as shown in Figure 4.10b. The dimension and distribution of the five flanges are displayed in Figure 4.10a. Thickness and mid-section width of the flanges are respectively 300mm and 150mm. The diameter of tower cross-section varies linearly from 8.5m at the base to 5.7m at the top. Shell thickness of the 150m tower is displayed in Table 4.3.

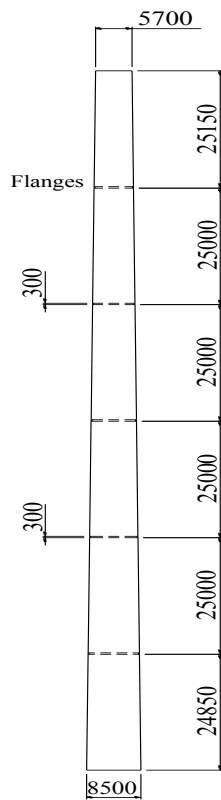
The 150m tower is also made of steel whose material property is the same with the 50m one as displayed in Table 4.1. The element types of shell and flange are also S4R shell element and C3D10

CHAPTER 4: FE ANALYSIS OF TOWER

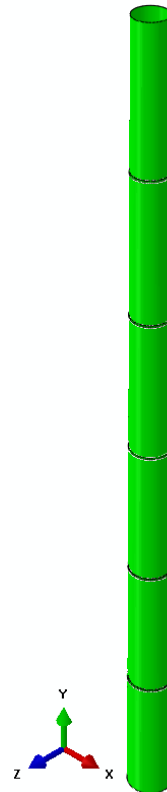
continuum element. The bottom of the tower is considered to be fixed. The connection between flanges and shell is tie constraint. Also, the top cross section of the 150m tower is coupled to the circular centre via coupling constraint to apply the axial, transverse and torsional loads.

Table 4.3 Shell thickness of the 150 tower I

Height range of tower	0-49.85m	49.85m-99.85m	99.85m-150m
Shell thickness	40mm	30mm	25mm



a. Geometrical data



b. FE model

Figure 4.10 Prototypes of 150m tower I: geometrical data and FEM models

## CHAPTER 4: FE ANALYSIS OF TOWER

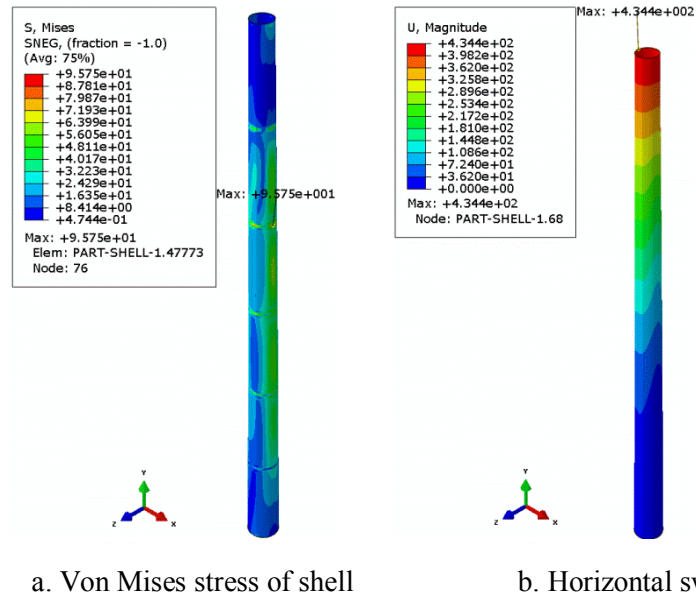


Figure 4.11 Contour plots of stress and sway for 150m tower I

According to Figure 4.11, the maximum von Mises stress and horizontal sway of 150m wind turbine tower can be obtained. The maximum von Mises stress locates in the connection area between the second ring and shell, and is 95.75MPa as shown in Figure 4.11a. The maximum horizontal sway of the 150m tower is 434.4mm at the top. The maximum von Mises stress of the 150m tower occurs in the inner side of the second ring and its magnitude is 211.8MPa as shown in Figure 4.12.

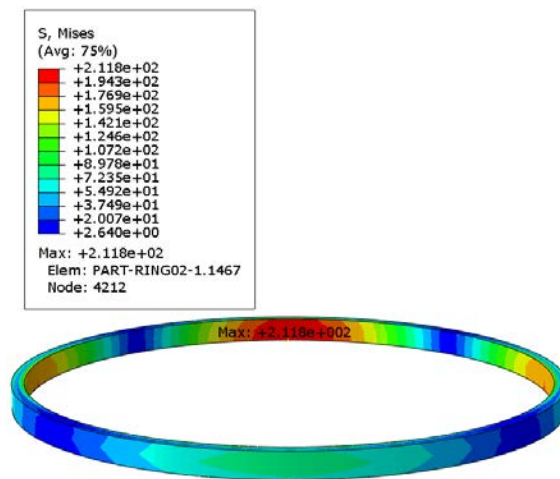


Figure 4.12 Stress contour of ring of 150m tower I

### 4.3.2 150m tower II

Similarly, stiffening rings are added into shell of the 150m tower II in order to strengthen the tower and to investigate the behaviour of the 150m tower II subjected to wind loads. The dimensions and FE models of the 50m tower II are depicted in Figure 4.12. The distributions of stiffening rings of 150m tower II are represented in Table 4.4. The other dimensions are identical to the ones of the 150m tower I, so are loads. The thickness and mid-section width of stiffening rings of 150m towers are respectively 250mm and 150mm. The ring spacing of sections 1 and 36 of the 150m tower II are 4050mm and 3850mm, respectively; the spacing of sections 6, 12, 18, 24 and 30 are 3700mm, and the remaining are all 3900mm. The wall thickness of 150m towers II are also the same with the 50m towers I.

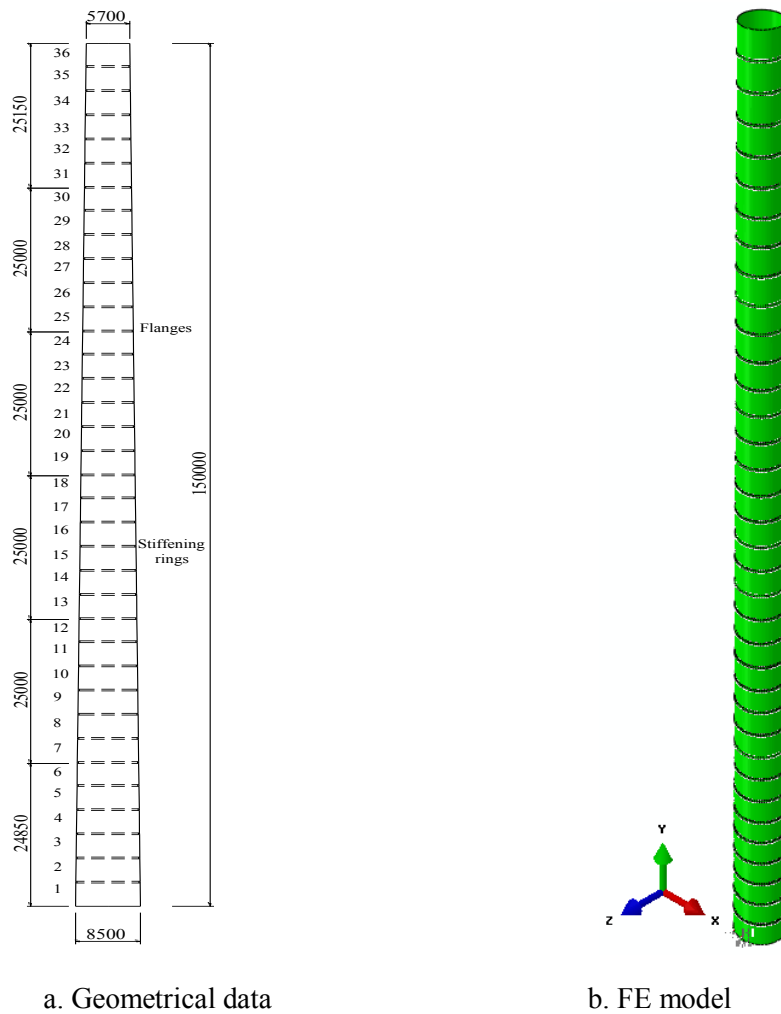


Figure 4.13 Prototypes of 150m tower II: geometrical data and FEM models

## CHAPTER 4: FE ANALYSIS OF TOWER

The bottom of the 150m tower is fixed in Figure 4.13b, wall of the 150m tower is created into S4R element, and the element types of flange and stiffening ring are C3D10 element. The interaction between shell and ring is simulated via tie constraint. The cross-section diameters of the tower linearly reduce from the bottom to the top. Wall thickness is identical to the 150m tower I as shown in Table 4.3. The aforementioned moment, vertical and horizontal force can be applied to the circular centre of the top cross-section of the tower, the magnitudes of which are referred to the Chapter 3.

Table 4.4 Stiffening ring spacing for the 150m tower II

Section	1	2	3	4	5	6
Spacing (mm)	4050	3900	3900	3900	3900	3700
Section	7	8	9	10	11	12
Spacing (mm)	3900	3900	3900	3900	3900	3700
Section	13	14	15	16	17	18
Spacing (mm)	3900	3900	3900	3900	3900	3700
Section	19	20	21	22	23	24
Spacing (mm)	3900	3900	3900	3900	3900	3700
Section	25	26	27	28	29	30
Spacing (mm)	3900	3900	3900	3900	3900	3700
Section	31	32	33	34	35	36
Spacing (mm)	3900	3900	3900	3900	3900	3850

The maximum von Mises stress and horizontal sway of the 150m tower II is represented in Figure 4.14. Maximum von Mises stress of the 150m tower II is 64.43MPa less than that of 150m tower I and maximum horizontal sway of 150m tower II is 430.8mm at the top of the tower, which is close to that of 150m tower I. Concerning maximum von Mises stress on the stiffening rings, its magnitude is only 44.08MPa, which is less than that of 150m tower I and exist on the twenty-first stiffening ring as shown in Figure 4.15.

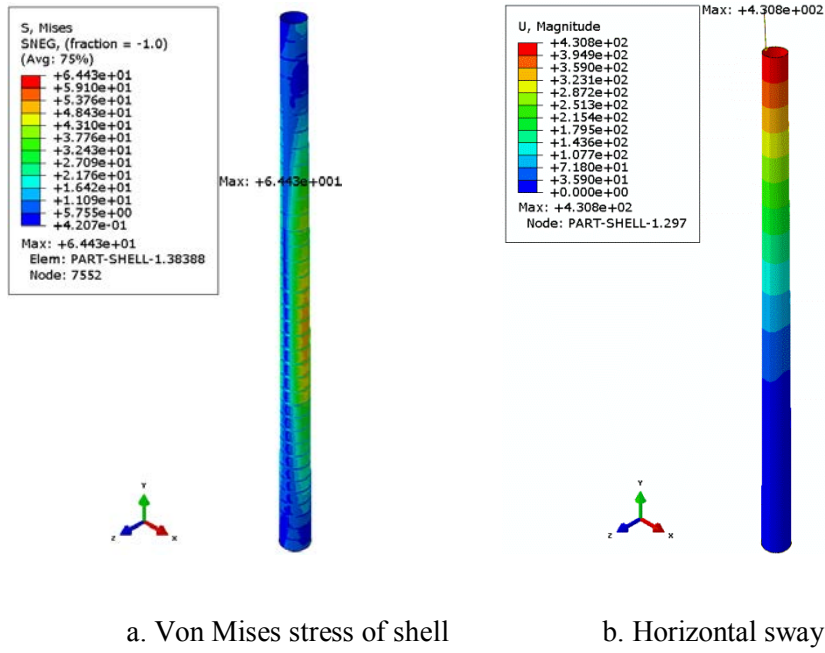


Figure 4.14 Contour plots of stress and sway for 150m tower II

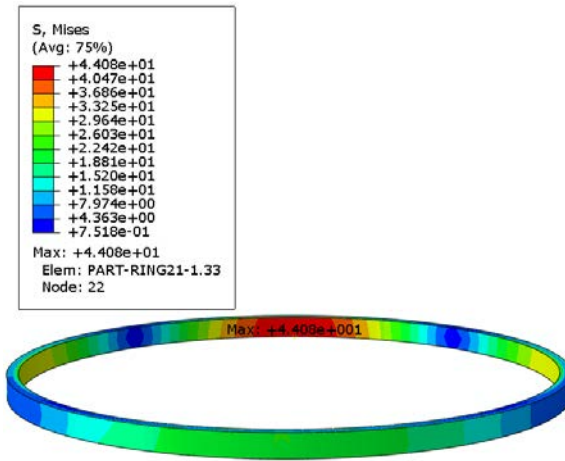


Figure 4.15 Stress contour of ring of 150m tower II

### 4.3.3 150m tower III

As for 150m thin wind turbine tower, the thickness is reduced properly in the range of strength, stiffness and stability constraints. The new thickness of the 150m tower III is 35mm from 0m to 49.85m height, 25mm from 49.85m to 99.85m height and 20mm from 99.85m to 150m height respectively as displayed in Table 4.5. The other parameters including the FE model and loads are the same with those of the 150m tower II.

CHAPTER 4: FE ANALYSIS OF TOWER

Table 4.5 Shell thickness of the 150 tower III

Height range of tower	0-49.85m	49.85m-99.85m	99.85m-150m
Shell thickness	35mm	25mm	20mm

The von Mises stress and horizontal sway contour of the 150m tower III are described in Figure 4.16. The maximum von Mises stress of the 150m tower III is 84.6MPa and maximum horizontal sway of the 150m tower III is 508.9mm on the top of the tower. The maximum von Mises stress of rings is shown in Figure 4.17. The maximum von Mises stress on the twenty-second ring is 41.95MPa less than that of 150m tower II. All maximum von Mises stress and horizontal sway of three types of towers are displayed in Table 4.6.

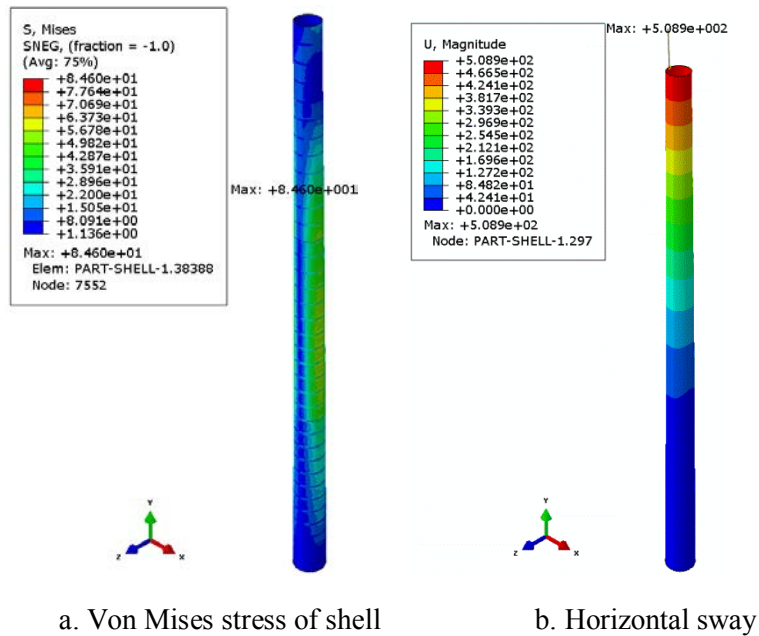


Figure 4.16 Contour plots of stress and sway for 150m tower III

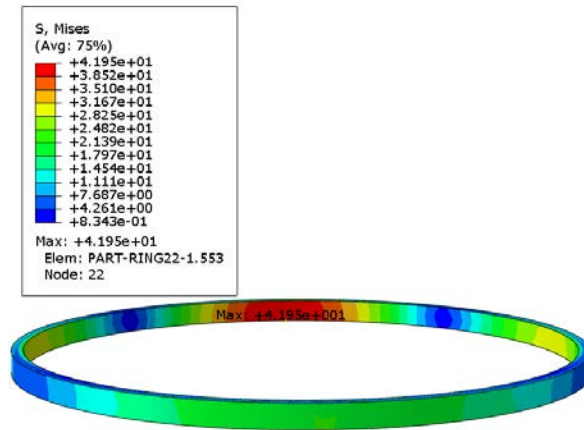


Figure 4.17 Stress contour of ring of 150m tower III

Table 4.6 150m wind turbine towers: maximum von Mises stress and horizontal sway

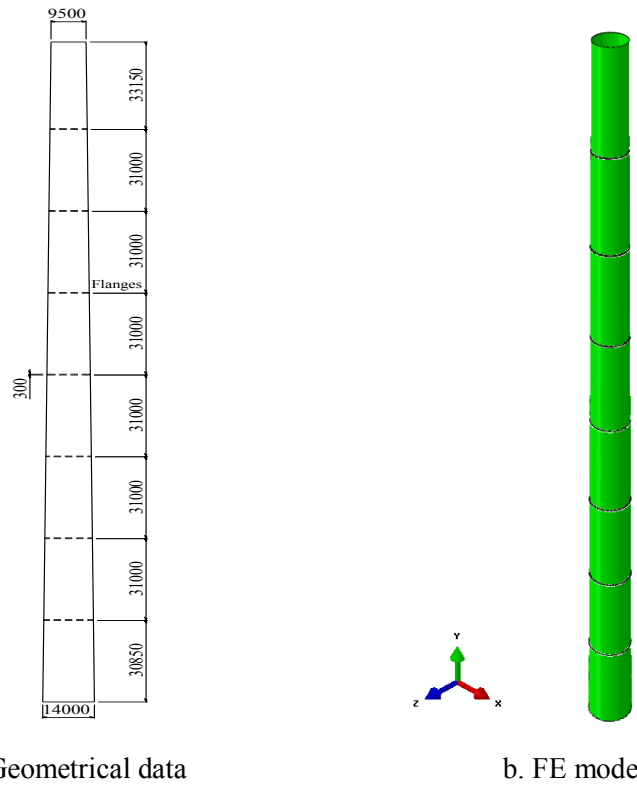
Variables	Tower I	Tower II	Tower III
Max. von Mises stress (MPa)	95.75MPa	64.43MPa	84.60MPa
Max. horizontal sway (mm)	434.4mm	430.8mm	508.9mm

## 4. 4 Models of 250m tower

### 4.4.1 250m tower I

The schematic and FE model of 250m tower I are represented in Figure 4.18. The flanges distribution of 250m tower can be shown in Figure 4.18a. The thickness and mid-section width of flanges are respectively 300mm and 150mm. The diameter of cross-section varies linearly from 14m at the base to 9.5m at the top. The thickness of the 250m tower I are displayed in Table 4.7, the first thickness is 60mm in the height range from 0m to 92.85m, the second thickness is 50mm in the height range from 92.85mm to 185.85m and the third thickness is 45mm in the height range from 185.85mm to 250m.

For the FE model, the element types of shell and flange are also S4R element and C3D10 continuum finite element referring to the Chapter 3. The flanges and tower wall are connected by tie constraint. The top cross-section of the 250m tower I is coupled to circular centre on the top of the 250m tower via coupling constraint. The base of the 250m tower I is simulated to be fixed.



a. Geometrical data

b. FE model

Figure 4.18 Prototypes of 250m tower I: geometrical data and FEM models

Table 4.7 Shell thickness of the 250 tower I

Height range of tower	0-92.85m	92.85m-185.85m	185.85m-250m
Shell thickness	60mm	50mm	45mm

The maximum von Mises stress and horizontal sway of 250m tower are depicted in Figure 4.19. The maximum von Mises stress of the 250m tower wall is 83.96MPa, which locates in the vicinity of connection area between the second flange and tower wall. The maximum horizontal sway of the 250m tower I is 193.3mm in the leeward surface of the tower wall. The maximum von Mises stress of flange occurs on the third flange, magnitude of which is 269.8MPa far greater than that of tower wall as shown in Figure 4.20.

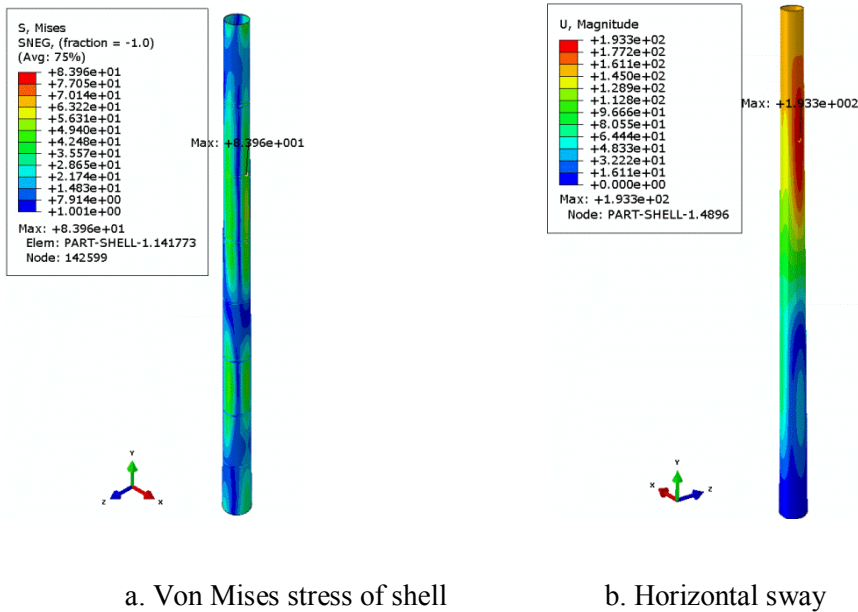


Figure 4.19 Contour plots of stress and sway for 250m tower I

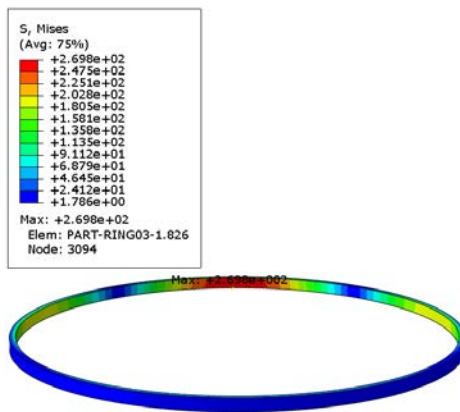


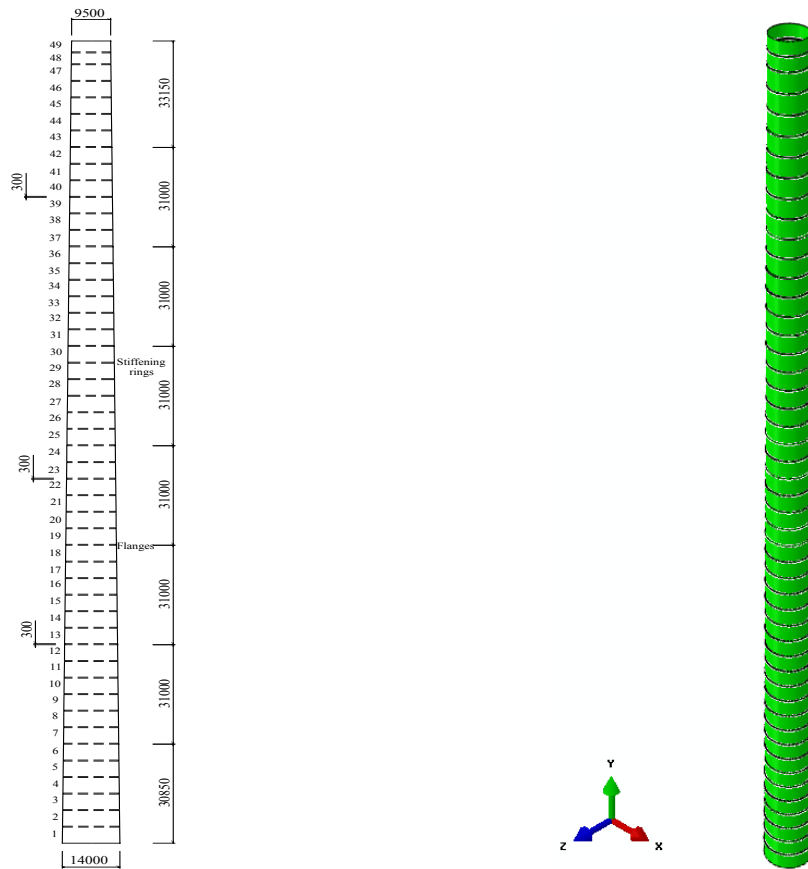
Figure 4.20 Stress contour of ring of 250m tower I

#### 4.4.2 250m tower II

The distribution of stiffening rings of the 250m tower II is shown in Figure 4.21. The 250m tower is separated into 49 sections as displayed in Figure 4.21a and distances between stiffening rings are presented in Table 4.8, the ring spacing of section 1 is 5000mm; of sections 6, 12, 18, 24, 30, 36 and 42 are 4950mm; of sections 48 and 49 are 3400mm and of the remaining sections are 4850mm. The shell thickness of the tower II is identical to that of corresponding tower I. The other parameters of the 250m tower II are same with those of 250m tower I. As for FE model of the 250m tower II, the

## CHAPTER 4: FE ANALYSIS OF TOWER

interaction between stiffening rings and tower wall, the element types, boundary condition, loads states and wall thickness are considered to be identical to the 250m tower I.



a. Geometrical data

b. FE model

Figure 4.21 Prototypes of 250m tower II: geometrical data and FEM models

Table 4.8 Stiffening ring spacing for the 250m tower II

Section	1	2	3	4	5	6	7
Spacing (mm)	5000	4850	4850	4850	4850	4950	4850
Section	8	9	10	11	12	13	14
Spacing (mm)	4850	4850	4850	4850	4950	4850	4850
Section	15	16	17	18	19	20	21
Spacing (mm)	4850	4850	4850	4950	4850	4850	4850
Section	22	23	24	25	26	27	28

CHAPTER 4: FE ANALYSIS OF TOWER

Spacing (mm)	4850	4850	4950	4850	4850	4850	4850
Section	29	30	31	32	33	34	35
Spacing (mm)	4850	4950	4850	4850	4850	4850	4850
Section	36	37	38	39	40	41	42
Spacing (mm)	4950	4850	4850	4850	4850	4850	4950
Section	43	44	45	46	47	48	49
Spacing (mm)	4850	4850	4850	4850	4850	3400	3400

In Figure 4.22, von Mises stress and horizontal sway contour of 250m tower II are described. The maximum von Mises stress of shell is 49.83MPa in the vicinity of tower base. However, the maximum von Mises stress of the 250m tower II in inner side of the thirty-second stiffening ring, and the magnitude of maximum von Mises stress is 104.9MPa as shown in Figure 4.23. The maximum horizontal sway of 250m tower II is 136.6mm in Figure 4.22b.

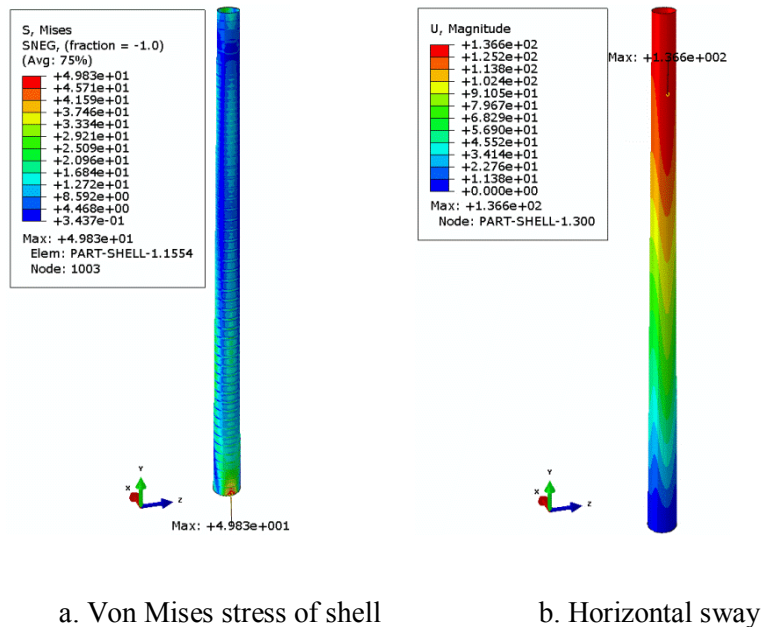


Figure 4.22 Contour plots of stress and sway for 250m tower II

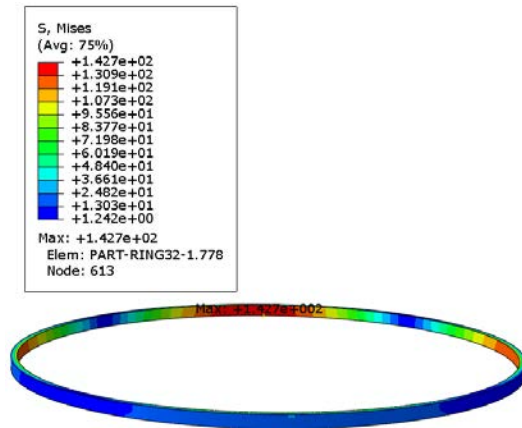
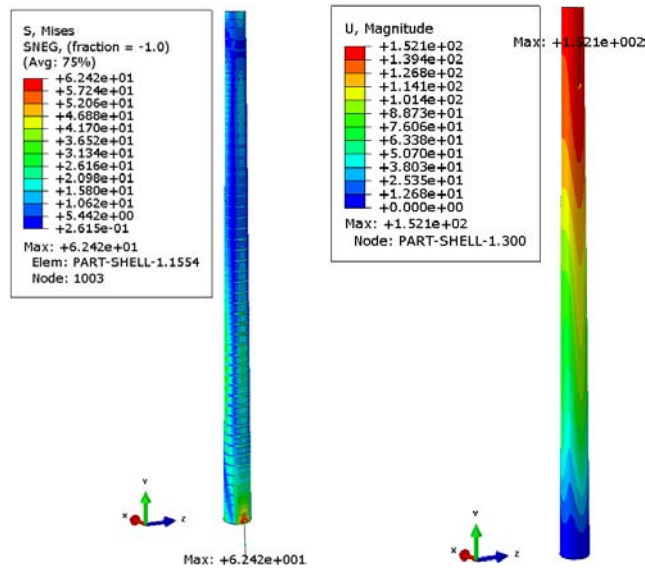


Figure 4.23 Stress contour of ring of 250m tower II

### 4.4.3 250m tower III

To analyse the effect of thickness variation of tower under wind load, the thickness of 250m tower is reduced in proper range. In the case of the 250m tower III, the wall thickness is 55mm in the range of 0m to 92.85m, 45mm from 92.85m to 185.85m and 40mm from 185.85m to 250m as shown in Table 4.9. The other all parameters are the same with those of the 250m tower II.



a. Von Mises stress of shell

b. Horizontal sway

Figure 4.24 Contour plots of stress and sway for 250m tower III

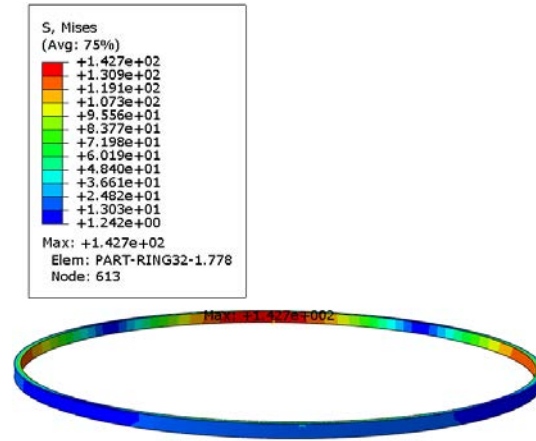


Figure 4.25 Stress contour of ring of 250m tower III

Table 4.9 Shell thickness of the 250 tower III

Height range of tower	0-92.85m	92.85m-185.85m	185.85m-250m
Shell thickness	55mm	45mm	40mm

According to Figure 4.24, von Mises stress and horizontal sway contours of 250m tower III are similar to those of 250m tower II. The maximum von Mises stress is 62.42MPa close to tower base at leeward side. The maximum von Mises stress of stiffening rings also exists in the thirty-second ring, its magnitude is 142.7MPa. The maximum horizontal sway of the 250m tower III is 152.1mm. The numerical simulation results of 250m towers are represented in Table 4.10.

Table 4.10 250m wind turbine towers: maximum von Mises stress and horizontal sway

Variables	Tower I	Tower II	Tower III
Max. von Mises stress (MPa)	83.96	49.83	62.42
Max. horizontal sway (mm)	193.3	136.6	152.1

## 4.5 Results and discussion

The cases of three wind turbine towers of different heights, with or without stiffening rings have been modelled by means of the finite element method. The results of numerical simulation are displayed in

CHAPTER 4: FE ANALYSIS OF TOWER

Table 4.2, 4.6 and 4.10 which show the maximum von Mises stress and horizontal sway of these towers. As discussed earlier, the overall construction cost is related to the weight of the tower. So, in order to reduce the cost, material weights can be reduced as much as possible whilst still meeting the stiffness and strength requirement. Taking into account dimensions and material properties, the weights of the towers can be calculated. The masses of the three different towers are shown in Table 4.11.

Table 4.11 Wind turbine tower mass characteristics

Height of tower (m)	$m_1$ (t)	$m_2$ (t)	$m_3$ (t)	$\Delta m_R$	$\Delta m_S$
50	76.02	81.09	62.38	6.25%	23.07%
150	887.17	1118.50	987.17	20.68%	11.74%
250	3934.29	4460.52	4098.28	11.8%	8.12%

Where  $m_1$  is the mass of towers I;

$m_2$  is the mass of towers II;

$m_3$  is the mass of towers III;

$\Delta m_R$  is the mass reduction ratio between  $m_1$  and  $m_2$ ;

$\Delta m_S$  is the mass reduction ratio between  $m_2$  and  $m_3$ .

The numerical results for all the three towers are analysed and listed in Table 4.12, where the horizontal sway and von Mises stress variation ratios are calculated in accordance with the data in Table 4.2, 4.6 and 4.10. In order to estimate marginal increase/decrease, the differential horizontal sway and von Mises stress are divided by the corresponding differential mass.

CHAPTER 4: FE ANALYSIS OF TOWER

Table 4.12 Wind turbine towers horizontal sway and von Mises stress variation

Height of tower (m)	Variables	$\Delta a_1$	$\Delta a_2$	$\Delta a_1/\Delta m_R$	$\Delta a_2/\Delta m_S$
50	Horizontal sway	0.69%	43.4%	0.11	1.88
	Von Mises stress	55.75%	52.31%	8.92	2.27
150	Horizontal sway	0.84%	18.13%	0.04	1.54
	Von Mises stress	48.61%	31.3%	2.35	2.67
250	Horizontal sway	41.51%	11.35%	3.52	1.4
	Von Mises stress	68.49%	25.27%	5.8	3.11

$\Delta a_1$  is the horizontal sway and von Mises stress augmentation percentage of tower II to I;

$\Delta a_2$  is the horizontal sway and von Mises stress augmentation percentage of tower II to III.

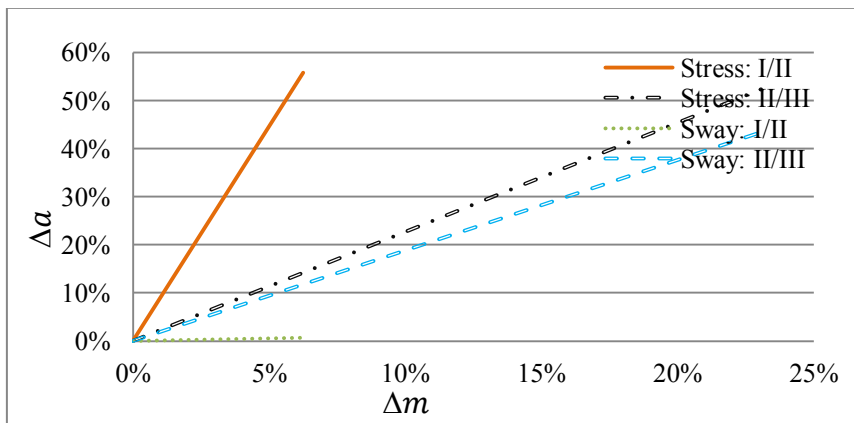


Figure 4.26 50m tower horizontal sway and von Mises stress variation ratios of tower I/II and tower

II/III

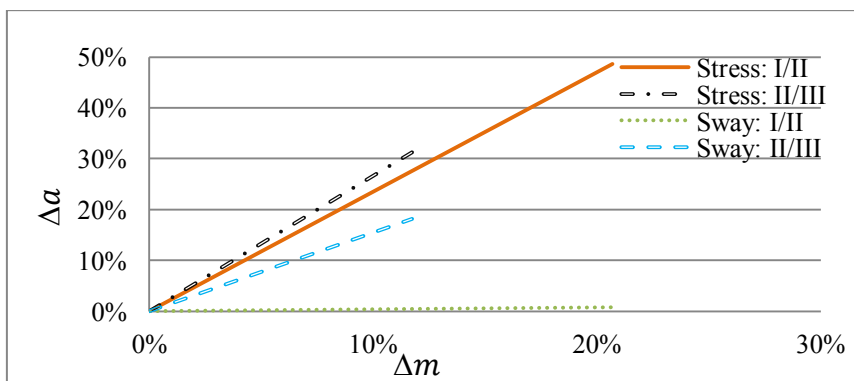


Figure 4.27 150m tower horizontal sway and von Mises stress variation ratios of tower I/II and tower

II/III

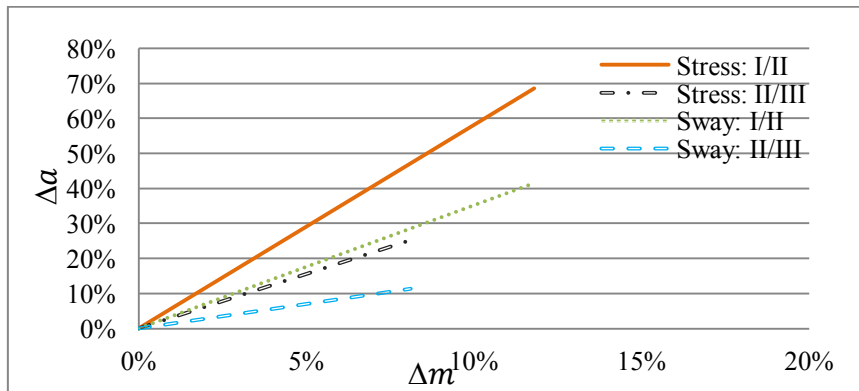


Figure 4.28 250m tower horizontal sway and von Mises stress variation ratios of tower I/II and tower

II/III

In addition, according to Figure 4.26 to 4.28, the graphs present horizontal sway and von Mises stress augmentation ratios of three types of towers when thickness and number of rings of these towers are reduced. As the  $\Delta a_1/\Delta m_R$  and  $\Delta a_2/\Delta m_S$  are positive with reference to the slopes of the function curves in Figure 4.26 to 4.28, the slope magnitudes of function curves reflect the variation rate of horizontal sway and von Mises stress augmentation ratios when the weight reduction ratios are increased. Specifically, if the slope magnitudes of the function curves are greater, this indicates that the variation rate of horizontal sway and von Mises stress augmentation ratios with weight reduction ratios growth is higher, which is a more effective way to change the loading resistance of a tower structure. The cost is related to weight of steel. In other words, the greater the slope magnitudes of function curves are, the more efficient savings there are in cost.

At the 50m height level, the mass reduction ratio of tower II to III is 23.07%, which is more than that of tower II to I, 6.25% as shown in Table 4.11. However, the magnitudes of horizontal sway and von Mises stress augment ratios of tower II to III is 43.4% and 52.31%, respectively, and the magnitudes of horizontal sway and von Mises stress augment ratios of tower II to I, 0.69% and 55.75% as indicated in Table 4.12. Meanwhile, the  $\Delta a_1/\Delta m_R$  is equal to 0.11 and 8.92, and the  $\Delta a_2/\Delta m_S$  is at 1.88 and 2.27 in Table 4.12, respectively. For von Mises stress variation rate, the magnitude of tower II to I

$(\Delta a_1/\Delta m_R)$  is 8.92 greater than that of tower II to III ( $\Delta a_2/\Delta m_S$ ) is 2.27. However, the horizontal sway variation rate of the tower II to I ( $\Delta a_1/\Delta m_R$ ) is 0.11 less than that of tower II to III ( $\Delta a_2/\Delta m_S$ ) is 1.88. For the 50m tower, the maximum von Mises stress can be affected more than maximum horizontal sway, which indicates that varying ring space is more sensitive to the strength variation of the tower structure than varying the thickness. As for the 50m height level, reducing the number of rings is a better way to save cost than reducing thickness.

At the 150m height level, the horizontal sway reduction ratio of tower II to I is quite small at only 0.84%, which is lower than that of tower II to III, which is 18.13%. The mass reduction ratio of tower II to III is 11.74%, and that of tower II to I is 20.68% as shown in Table 4.11. The horizontal sway and von Mises stress variation rate of tower II to III ( $\Delta a_2/\Delta m_S$ ) are 1.54 and 2.67, respectively, which are both greater than those of tower II to I ( $\Delta a_1/\Delta m_R$ ), at 0.04 and 2.35 as shown in Table 4.12, respectively. It is noted that the variation rate of the horizontal sway of tower II to I is minimal at only 0.04 (see Table 4.12). Considering the cost efficiency, it is advantageous to reduce the thickness to achieve better cost saving.

At the 250m height level, Table 4.11 shows the mass reduction ratio of tower II to III is 8.12%, which is less than that of tower II to I, 11.8%. Also, the horizontal sway and von Mises stress variation ratios of tower II to III are 11.35% and 25.27%, respectively, which are both smaller than the respective ratios of tower II to I, that is, 41.51% and 68.49%, as shown in Table 4.12. The horizontal sway and von Mises stress variation rate of tower II to I ( $\Delta a_1/\Delta m_R$ ) are 3.52 and 5.8, respectively, which are greater than those of tower II to III ( $\Delta a_2/\Delta m_S$ ) 1.4 and 3.11 in Table 4.12. Reducing the number of rings is a more efficient method to satisfy the strength and stiffness requirements of the tower structure of the similar height range.

## 4. 6 Conclusions

The present research work concerns the investigation of the behaviour of wind turbine towers under wind loads. The horizontal sway and von Mises stress variation ratios are analysed when the tower thickness and the stiffening ring numbers are reduced. Three representative tower heights have been

## CHAPTER 4: FE ANALYSIS OF TOWER

examined separately in order to identify a more efficient design between increasing the wall thickness and adding stiffening rings in order to save manufacturing cost. In the 50m and 250m tower heights, reducing the number of rings is a more efficient way to save material use; whereas in the 150m high tower, reducing the thickness of the tower shell is more efficient.

# CHAPTER 5: DYNAMIC AND BUCKLING ANALYSIS

## 5. 1 Dynamic analysis of tower

### 5.1.1 Introduction

As the nacelle mass is placed on the top of the tower, wind turbines can be vibrated very easily under wind loads. The behaviour of the vibration has a large influence on the deformations, the inner stresses and the resulting ultimate limit state, the fatigue and the operating life of the wind turbine. The excitations or the external loads acting on the wind turbine may be distinguished in terms of their historic loadings, for example, quasi-steady, periodic, random and transient loads. Loads from earthquakes are relevant for the tower design at specific sites.

Dynamic analysis usually involves the calculation of natural frequency and mode shapes, which can provide the parameters for avoiding resonance when the turbine operates. There are several types of vibration modes; for example, lateral bending mode and torsional vibration mode. The slender tower is particularly flexible in the directions of lateral and axial bending. Only the horizontal sway of the top of the tower is considered in this simplified model. The motion differential equation of multiple degrees of freedom is as follows:

$$[\mathbf{M}][\ddot{\mathbf{x}}]+[\mathbf{C}][\dot{\mathbf{x}}]+[\mathbf{K}][\mathbf{x}]=[\mathbf{F}(\mathbf{t})] \quad (5.1)$$

Where  $[\mathbf{M}]$ ,  $[\mathbf{C}]$  and  $[\mathbf{K}]$  represent the mass matrix, the damping and the stiffening matrix, respectively.

$[\ddot{\mathbf{x}}]$ ,  $[\dot{\mathbf{x}}]$  and  $[\mathbf{x}]$  are the acceleration of the top of the tower, the velocity of the top of the tower and the displacement matrix, respectively.  $[\mathbf{F}(\mathbf{t})]$  is the excitation force from the thrust forces. If there is no excitation, the right side of the differential Equation (5.1) is zero. In this case, the vibration type is

referred to as natural vibration. As the structural damping has very little influence on natural frequency, damping can be ignored. The motion equation of the top of the tower displacement  $[\mathbf{x}]$  is:

$$[\mathbf{M}][\ddot{\mathbf{x}}] + [\mathbf{K}][\mathbf{x}] = \mathbf{0} \quad (5.2)$$

Equation (5. 2) can be written as follows:

$$([\mathbf{K}] - \omega^2 [\mathbf{M}])[\mathbf{x}] = \mathbf{0} \quad (5.3)$$

where  $\omega$  is the natural frequency of the structure system. Each  $\omega$  is related to the corresponding mode shape of the  $[\mathbf{x}]$ .

In recent years, many efforts have been made to develop the dynamic analysis of wind turbine tower systems. For instance, Manenti S. (2010) considered an offshore wind turbine as a relatively complex structural system, because several environmental factors affect its dynamic behaviour by generating both an active load and a resistant force to the structure's deformation. Also, the wind-waves' mutual interaction should be considered as a nonlinear interaction which is crucial for optimal and cost-effective design. Jerath and Austin (2013) simulated a 65kW wind turbine subjected to seismic load using FEM, and they compared the numerical results with experimental results obtained from existing literature. The effect of some parameters including wind turbine size, damping ratios and different seismic magnitudes were explored. W. Y. Liu (2013) calculated the natural frequency based on the coordinate system of a wind turbine blade-cabin-tower coupling system, and analysed the stochastic following wind vibration. AlHamaydeh and Hussain (2011) created a detailed 3D FEM of a tower-foundation-pile system with a reinforced concrete foundation. An optimised design was developed which has adequate separation between the natural and the operational frequencies, and which avoids damage to the structural system. Murtagh *et al.* (2005) presented the forced vibration of a wind turbine system subjected to wind loading. Farshidianfar *et al.* (2011) validated five theoretical solutions for the vibration characteristics of cylindrical shells by comparing with experimental results. Lopatin and Morozov (2015) considered the free vibration of a cantilever composite cylindrical shell by using analytical and numerical solutions. Three scenarios of tower structure design were examined for their dynamic performance, as shown in Figure 5.1, and these are referred to as the 'soft-soft',

‘soft-stiff’ and ‘stiff-stiff’ cases (Kuhn, 1997). A soft-soft tower design means that the natural frequency of the tower,  $f_0$  is less than the rotational frequency of the rotor speed,  $f_r$ . A soft-stiff tower design represents the case where the natural frequency,  $f_0$  of the tower is greater than the rotational frequency,  $f_r$  of the rotor speed, and is less than the blade passing frequency,  $f_b = N \cdot f_r$ , where  $N$  is the blade number and is equal to 3 for a three-bladed wind turbine. A stiff-stiff tower design refers to the case where the natural frequency  $f_0$  of the tower is greater than the blade passing frequency  $3f_r$ .

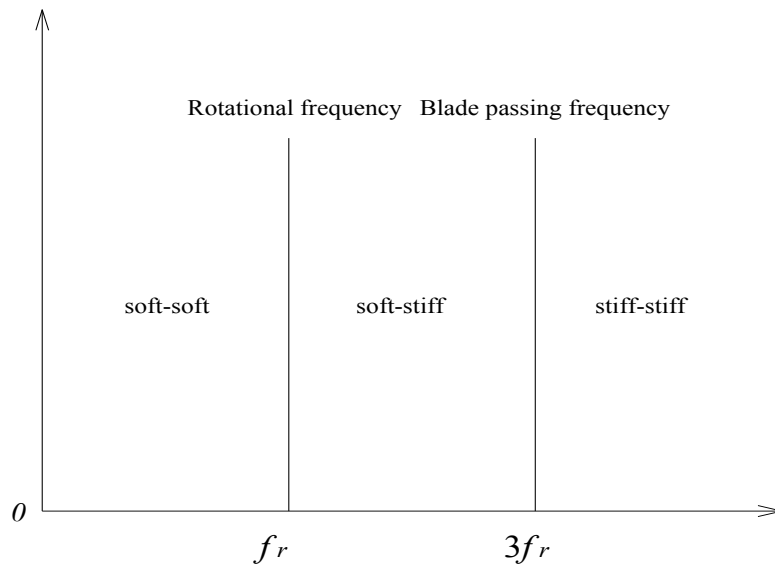


Figure 5.1 Structural design approaches for wind turbine towers

### 5.1.2 Towers with concentrated mass

To understand the dynamic behaviour of high wind turbine tower, the mode shapes and natural frequencies of all towers with concentrated mass were also modelled in order to analyse the dynamic characteristics. For wind turbine assemblies, the mass of the nacelle-rotor system is supported by the tower. Thus, the concentrated mass of the nacelle-rotor system at the top of the tower should be considered in terms of a dynamic analysis of a real wind turbine tower because the mass of the nacelle-rotor system accounts for more than 30% of the total mass of the wind turbine tower. Results can inform the design solution to avoid the resonance of tower under the cyclic loads. The bases of the tower models are still considered to be fixed. The other parameters including material property,

towers dimensions, types of elements and interaction between rings and shell are the same as corresponding models in Chapter 4. The eigen solver of frequency is the Lanczos method.

5.1.2.1 50m towers

The mass of the nacelle-rotor system is simplified into one point with a concentrated mass applied to the centre of the circular cross section at the top of the tower. The magnitude of the concentrated mass is 30t according to the data inventory (2009). The natural frequencies and mode shapes of the 50m towers I, II and III are shown in Figure 5.2 to 5.4 and in Table 5.4. Similarly, all the parameters of the 50m towers are identical to those of the previous 50m towers without the nacelle-rotor system. The bases of the 50m towers are considered to be fixed.

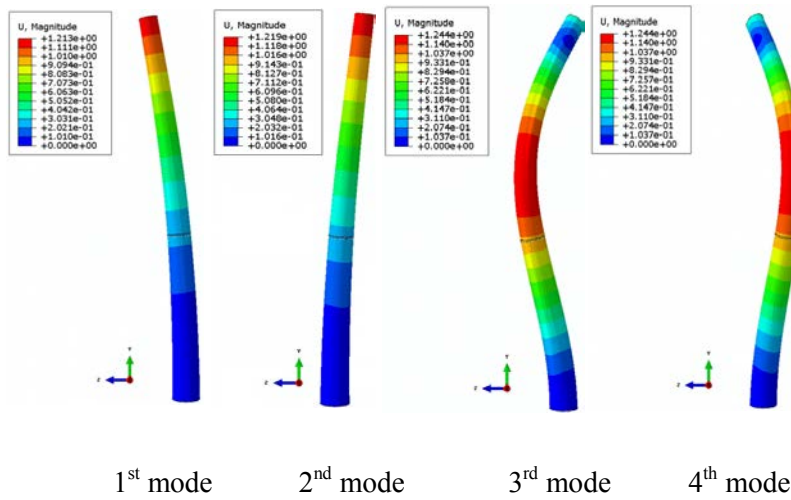


Figure 5.2 50m wind turbine tower I

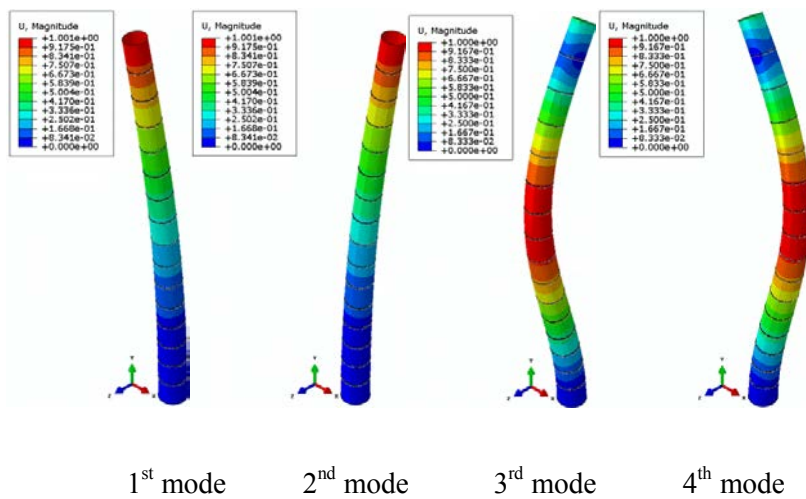


Figure 5.3 50m wind turbine tower II

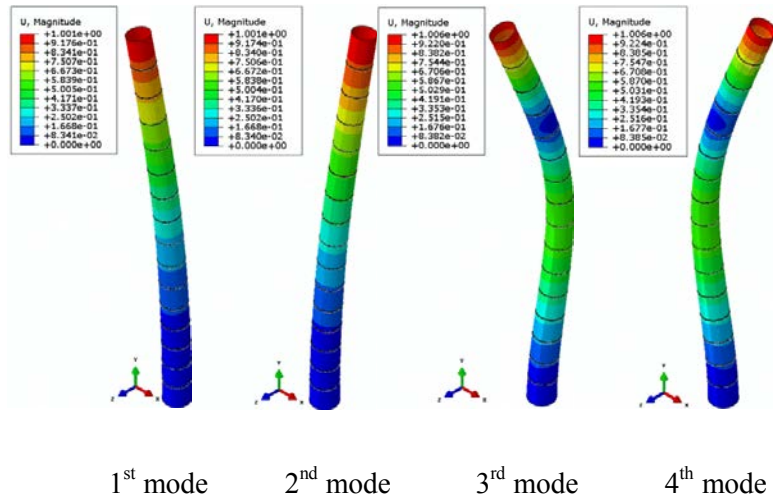


Figure 5.4 50m wind turbine tower III

The mode shapes of the 50m towers are shown in Figure 5.2 to 5.4. All four modes of the 50m towers I, II and III are bending modes. The first two mode shapes of the 50m towers are a symmetric pair, as are the second two mode shapes. The first and third mode shapes are vibrated in the x-y plane, and the second and fourth mode shapes are vibrated in the y-z plane. These two planes are perpendicular to each other in three-dimensional space. Clearly, the third and fourth mode shapes of the 50m tower I with a concentrated mass at the top of the tower are different from those of the 50m tower I without a concentrated mass.

Table 5.1 Natural frequencies for 50m wind turbine towers (Hz)

Towers	Variables	Vibration details in x-y plane		Vibration details in y-z plane	
tower I	Models	1 <sup>st</sup>	3 <sup>rd</sup>	2 <sup>nd</sup>	4 <sup>th</sup>
	Natural frequencies	0.983	6.099	0.983	6.099
tower II	Models	1 <sup>st</sup>	3 <sup>rd</sup>	2 <sup>nd</sup>	4 <sup>th</sup>
	Natural frequencies	0.976	5.925	0.976	5.925
tower III	Models	1 <sup>st</sup>	3 <sup>rd</sup>	2 <sup>nd</sup>	4 <sup>th</sup>
	Natural frequencies	0.880	5.778	0.880	5.778

In Table 5.4, the natural frequencies of the 50m towers I, II and III with a concentrated mass are displayed. The first frequencies of the 50m towers I, II and III are 0.983, 0.976 and 0.88 respectively.

The first and second frequencies are close and perpendicular to each other in three dimensional space. Also, the third and fourth frequencies are equal to each other as shown in Table 5.4. According to section 5.1.1, the 50m towers I, II and III, considering the mass of the nacelle-rotor system, are of a soft-stiff tower design in terms of the range of first frequencies. Thus, to avoid resonance for the soft-stiff tower design, the controller should be operated to omit the speed exclusion zone during the start-up and shut-down of the wind turbine.

**5.1.2.2 150m towers**

The magnitude of concentrated mass at the top of the tower is 300t Lindvig (2010). The other parameters of these 150m towers are same as those of the 150m towers without a concentrated mass on the top of tower. The mode shapes of the 150m towers I, II and III are represented in Figure 5.5 to 5.7.

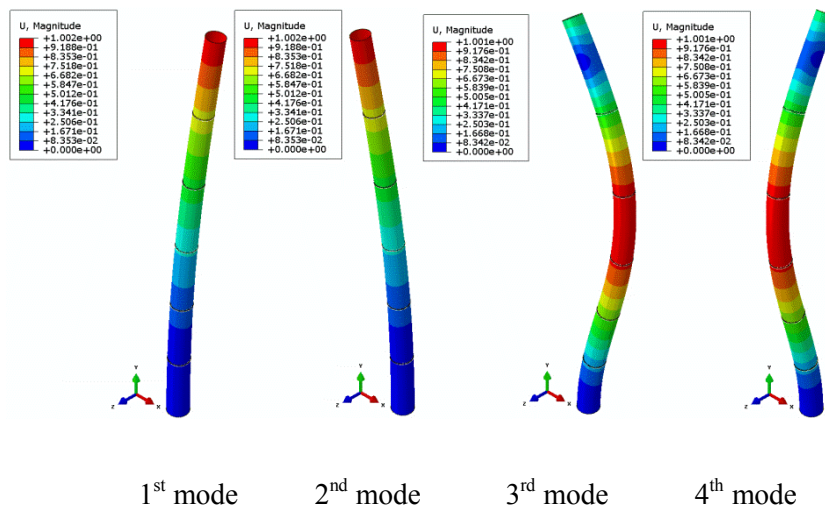


Figure 5.5 150m wind turbine tower I

## CHAPTER 5: DYNAMIC AND BUCKLING ANALYSIS

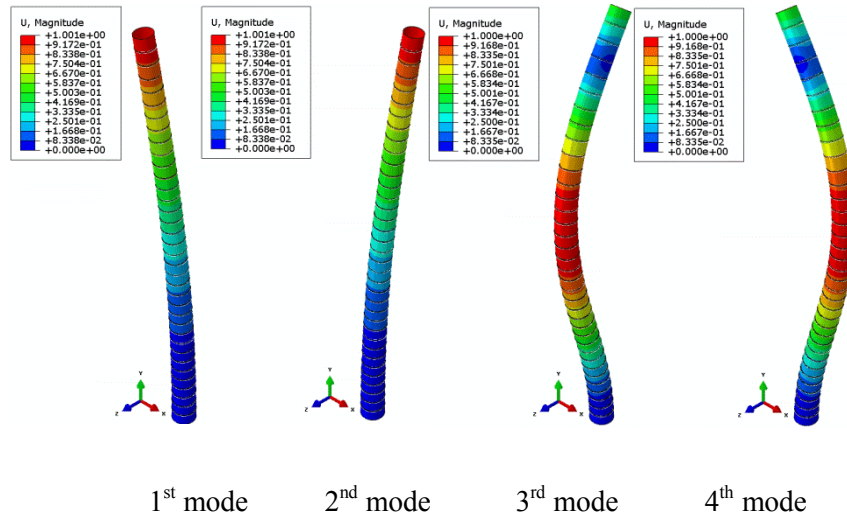


Figure 5.6 150m wind turbine tower II

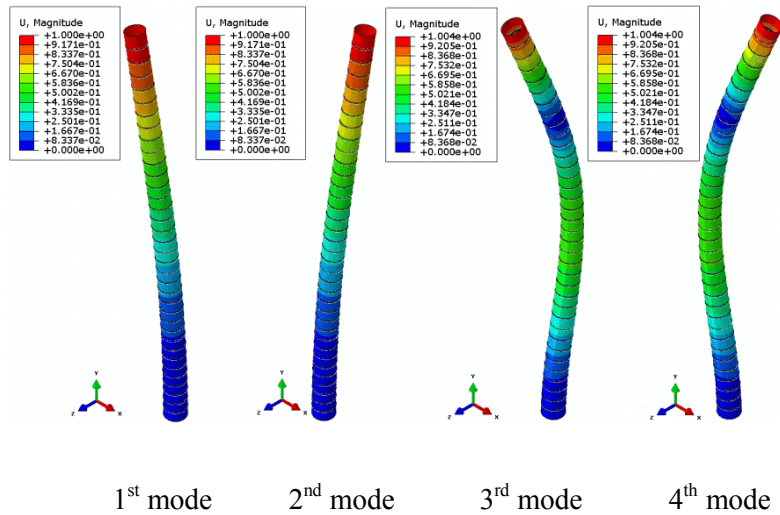


Figure 5.7 150m wind turbine tower III

The mode shapes of the 150m towers are all bending modes. The first and second mode shapes of the 150m towers are a symmetric pair. The natural frequencies of the 150m towers are displayed in Table 5.5. The first and second frequencies of the 150m tower I are equal to each other in the x-y and y-z planes, and the natural frequencies of the 150m towers are 0.261 Hz and 1.602 Hz, respectively. For the 150m tower II, the first and second frequencies are 0.252 and 1.458 Hz, respectively, in the x-y and y-z planes. Additionally, the first two frequencies of the 150m tower III are both 0.239 Hz.

Table 5.2 Natural frequencies for 150m wind turbine towers (Hz)

Towers	Variables	Vibration details in x-y plane		Vibration details in y-z plane	
tower I	Models	1 <sup>st</sup>	3 <sup>rd</sup>	2 <sup>nd</sup>	4 <sup>th</sup>
	Natural frequencies	0.261	1.602	0.261	1.602
tower II	Models	1 <sup>st</sup>	3 <sup>rd</sup>	2 <sup>nd</sup>	4 <sup>th</sup>
	Natural frequencies	0.252	1.458	0.252	1.458
tower III	Models	1 <sup>st</sup>	3 <sup>rd</sup>	2 <sup>nd</sup>	4 <sup>th</sup>
	Natural frequencies	0.239	1.412	0.239	1.412

The first three natural frequencies of the 150m towers I, II and III are 0.261 Hz, 0.252 Hz and 0.239 Hz respectively, as shown in Table 5.5. The first two natural frequencies are equal to each other, as are the second two. With reference to section 5.1.1, the first frequencies of the 150m towers I, II and III lie between the rotational and the blade passing frequencies. Thus, the 150m towers with concentrated mass are also a soft-stiff tower design, and the proposed corresponding method to avoid resonance is by operating the controller during start-up and shut-down of the wind turbine.

### 5.1.2.3 250m towers

Currently, 250m high towers are not erected in engineering practice. Therefore, it is estimated that the magnitude of the concentrated mass of the nacelle rotor system at the top of the tower is around 450t. The other parameters are identical to those of the 250m independent towers.

CHAPTER 5: DYNAMIC AND BUCKLING ANALYSIS

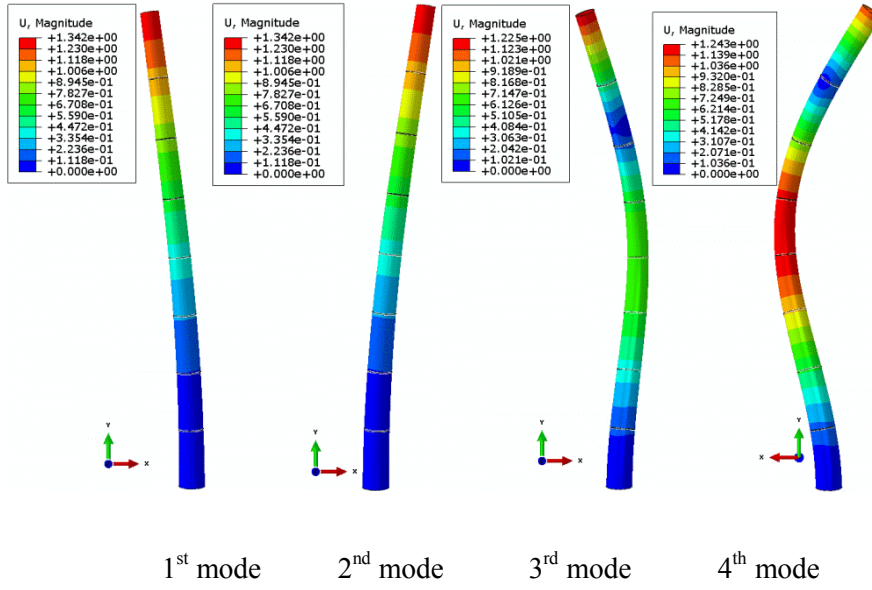


Figure 5.8 250m wind turbine tower I

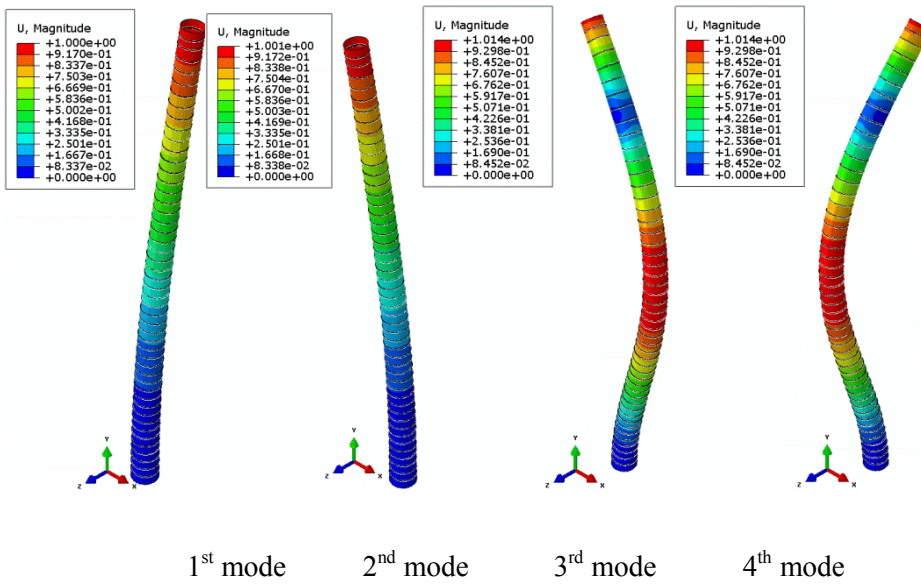


Figure 5.9 250m wind turbine tower II

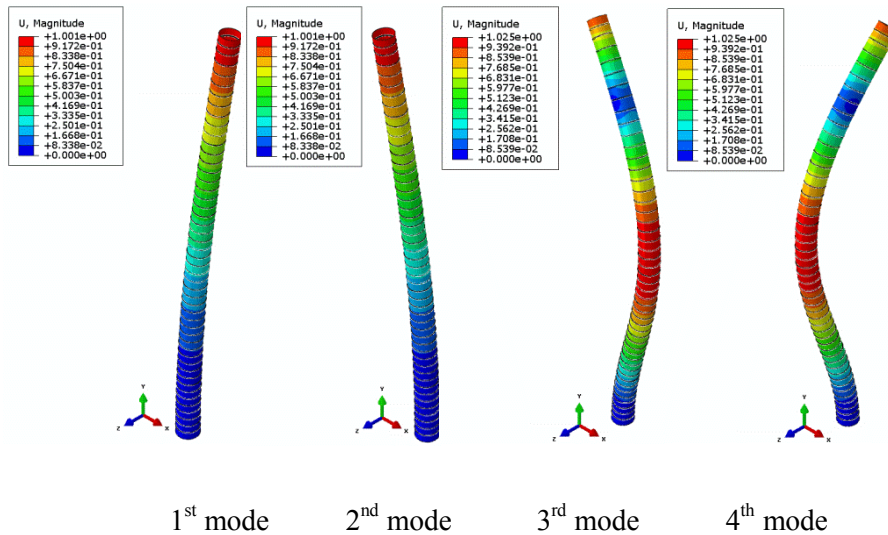


Figure 5.10 250m wind turbine tower III

The mode shapes of the 250m towers I, II and III are presented in Figure 5.8 to 5.10. The first two mode shapes of the 250m towers are a symmetric pair, as are the second two. All the mode shapes of the 250m towers are bending modes. The first two mode shapes of the 250m towers are vibrated in the x-y plane and the y-z plane, respectively. The natural frequencies of the 250m towers I, II and III are 0.204 Hz, 0.196 Hz and 0.193 Hz, respectively. The corresponding natural frequencies of the second two mode shapes of the 250m towers are 1.05 Hz, 1.0 Hz and 0.99 Hz, respectively, in the x-y plane and the y-z plane.

Table 5.3 Natural frequencies for 250m wind turbine towers (Hz)

Towers	Variables	Vibration details in x-y plane		Vibration details in y-z plane	
tower I	Models	1 <sup>st</sup>	3 <sup>rd</sup>	2 <sup>nd</sup>	4 <sup>th</sup>
	Natural frequencies	0.204	1.05	0.204	1.05
tower II	Models	1 <sup>st</sup>	3 <sup>rd</sup>	2 <sup>nd</sup>	4 <sup>th</sup>
	Natural frequencies	0.196	1.0	0.196	1.0
tower III	Models	1 <sup>st</sup>	3 <sup>rd</sup>	2 <sup>nd</sup>	4 <sup>th</sup>
	Natural frequencies	0.193	0.99	0.193	0.99

The natural frequencies of the 250m towers I, II and III with a concentrated mass are displayed in Table 5.6. The first frequencies of the 250m towers are 0.204 Hz, 0.196 Hz and 0.193 Hz respectively. According to section 5.1.1, the first frequencies of the 250m towers are less than the rotational frequencies, thus the 250m towers I, II and III with a concentrated mass are a soft-soft tower design. The corresponding resonant susceptible zone should be avoided during the start-up and shut-down of the wind turbine.

## 5.2 Buckling analysis of towers

### 5.2.1 Introduction

Towers are slender structures due to the small wall thickness of the tower in relation to their diameter and their height. Cylindrical shells have been widely used as tanks, silos, and bins. Steel cylindrical shells subjected to an asymmetrical lateral external pressure in practice are vulnerable to buckling failure. Lei Chen and Rotter (2012) investigated a linear and nonlinear buckling analysis of anchored cylindrical shells subjected to wind loadings. Empirical expressions were developed to guide the design of cylindrical shell structures against buckling. Winterstetter and Schmidt (2002) provided the solutions on how to simulate buckling behaviour using FEM for circular cylindrical steel shells, and proposed improved design guidelines by comparing with existing design codes. Gettel and Schneider (2007) compared a linear buckling analysis and a geometrically and materially nonlinear analysis (GMINA) of cylindrical shells subjected to transverse load. It was found that the GMINA concept may lead to a safe and economical design of cylindrical shells under combined loads. Shi *et al.* (2014) presented experiments on the column buckling of high strength steel tubes, and simulated the buckling behaviours of the steel column using FE models, and the numerical and experimental results achieved were in good agreement in terms of the Chinese, European and American codes for column design. Corona *et al.* (2006) studied the buckling behaviour of circular tubes under bending. Silvestre and Gardner (2011) introduced the buckling behaviour of elliptical hollow section tubes, and concluded that local buckling modes mainly occurred in the short to intermediate tubes, and distortional and global buckling modes respectively dominated the stability of intermediate to medium length tubes

and longer tubes. Yang Zhao and Lin (2014) studied the buckling of a thin-walled steel tank subjected to wind loads using numerical simulation. Chou and Tu (2011) introduced 715 cases of wind turbine tower accidents during 1999 to 2009, where the main causes that led to tower collapse were storms and strong winds. Sim *et al.* (2014) tested the flexural strength of a steel wind turbine tower and simulated the local buckling of the tower in different boundary conditions, achieving a good correlation between the experimental and analytical results. Y. T. Kim *et al.* (2013) explored the stability of a cracked cylindrical thin wall subjected to axial and internal pressure. Tafreshi and Bailey (2007) reported the buckling response of composite cylindrical shells under a combination of axial, torsional and bending loads using the Finite Element Method. Ghanbari Ghazijahani and Showkati (2013) carried out experiments on a cylindrical shell subjected to pure bending and external pressure. Houliara and Karamanos (2010) analysed the buckling of a transversely-isotropic cylindrical shell under bending loading. Javidruzi *et al.* (2004) examined the dynamic stability behaviour of a cracked cylindrical shell under a tension load.

Stiffening rings are added to the inner shell of cylindrical shell towers in order to improve their resistance to local buckling. It is known that the buckling capacity of cylindrical shells is proportional to the tower wall thickness. Thus, the effect of stiffening rings on the buckling behaviour of the tower wall should be investigated for various height cases. In this section, the buckling modes of towers of three different heights were selected to be simulated by means of the finite element program ABAQUS. The eigenvalues variation ratios divided by the corresponding mass reduction ratios of towers I to II and towers II to III are then compared with each other.

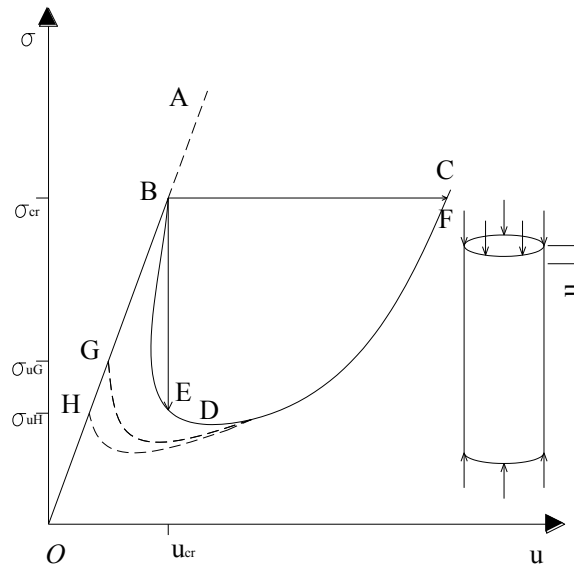


Figure 5.11 Buckling behaviour of the shell structure

Where  $\sigma$  represents the uniformly applied compressive stress,  $\sigma_{cr}$  refers to the critical stress and  $U$  is the decrease distance of the cylinder shell. For buckling behaviour of an perfect cylinder structure, when the maximum stress in the shell structure research to critical stress  $\sigma_{cr}$ , a sudden change from point B to point F occurs called th snap-through phenomenon as shown in Figure 5.11. However, for the imperfect cylinder structures, the shell would fail by local buckling long before the theoretical critical stress is reached. The limit point G or H (relevant to different values of the imperfection) refers to a more realistic lower load than the theoretical bifurcation load. Their corresponding critical stresses are represented by  $\sigma_{uG}$  and  $\sigma_{uH}$ , respectively. Hence the conclusions based on the linear eigenvalue buckling analysis are optimistic. Throughout the chapter, elastic critical buckling stress is assumed to be a good indicator of the buckling strength, whereas geometrically and materially nonlinear analysis should be conducted in future work.

### 5.2.2 Loading states

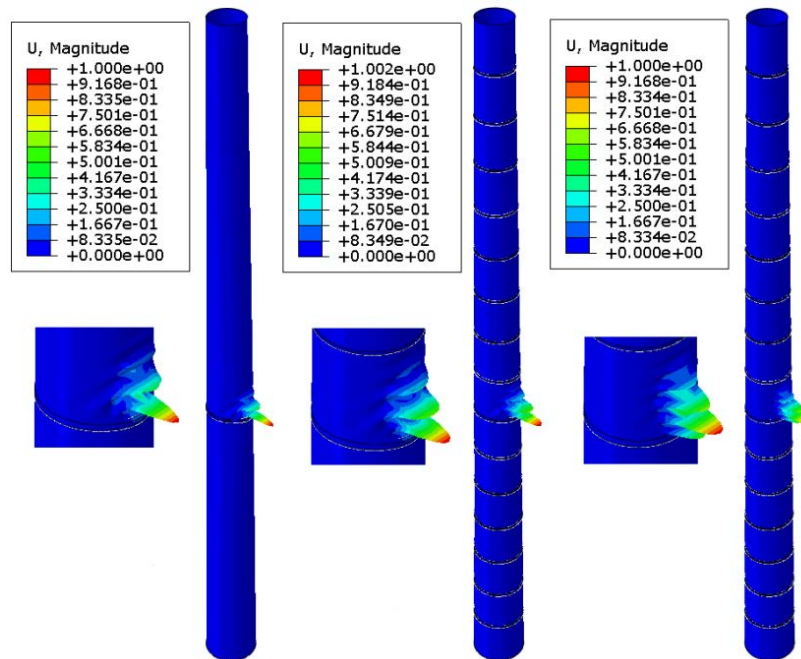
Axial, transverse and torsional loads act at the top of the tower, and these are equivalent to respectively, the weight of the nacelle, the blades and the rotor,  $f_n$ , a horizontal force,  $f_w$  from the manufacturer's data and the bending moment,  $f_m$  from the weight of the nacelle eccentricity relative to

the tower axis. In addition, the wind pressure,  $p$  is distributed along and around the surface of the tower wall. The loading states for each height case are combined into the expression:

$$f = f_n + f_m + f_w + p \tag{5.4}$$

### 5.2.3 50m towers

The bases of the 50m towers are considered as fixed. The other parameters including material properties, tower dimensions, types of element and interaction between stiffening rings and tower wall are the same as in the previous models corresponding to 50m towers I, II and III. The simulated results for the 50m towers I, II and III are presented in Figure 5.12:



a. Local buckling mode of 50m tower I      b. Local buckling mode of 50m tower II      c. Local buckling mode of 50m tower III

Figure 5.12 First local buckling modes of the 50m towers

Table 5.4 Buckling eigenvalues of 50m towers I, II and III

	Tower I	Tower II	Tower III
Eigenvalues	55.4	56.6	25.84

The first local buckling modes of 50m towers I, II and III occur in the vicinity of the flange as shown in Figure 5.12. All the buckling eigenvalues of 50m towers I, II and III are negative, as displayed in Table 5.7. Therefore, the corresponding local buckling modes of the towers are in the x positive direction, which is opposite to the horizontal force direction. According to Table 5.7, the absolute value of the buckling eigenvalue of the 50m tower II is greater than those of the 50m towers I and III, which indicates that the stability of the 50m tower II is greater than that of 50m towers I and III.

### 5.2.4 150m towers

Linear buckling analysis was performed on the 150m towers I, II and III, and all parameters of the 150m tower models are identical to the those of the 150m towers in the previous section. The wind load of the 150m tower models is also the same as that of the 150m towers described in Chapter 3.

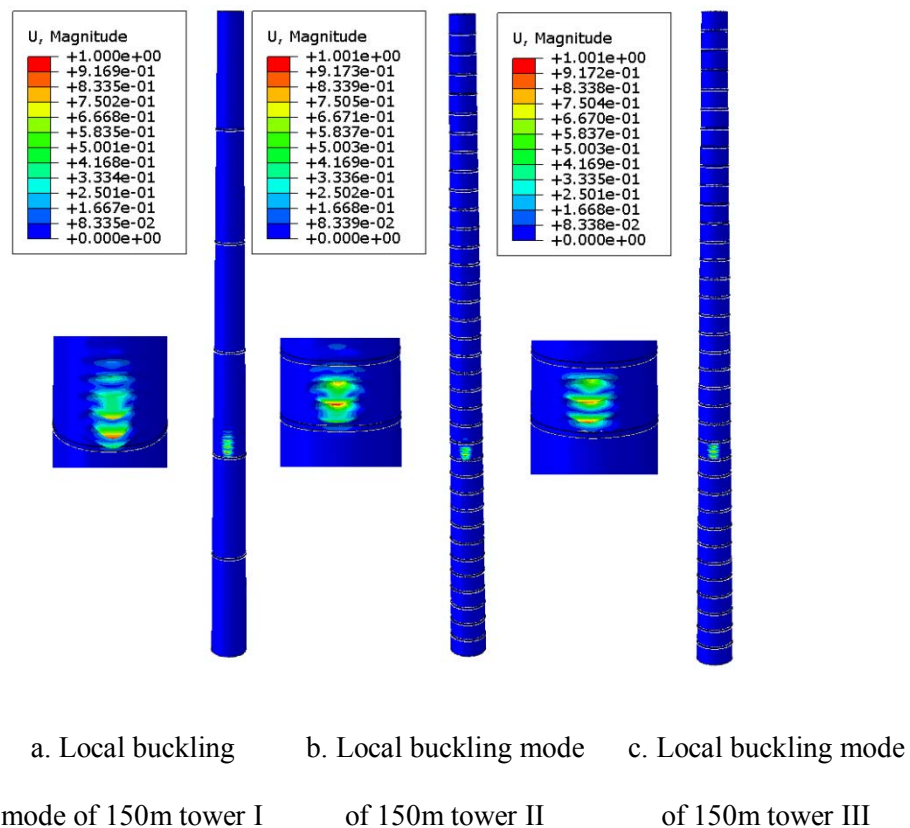


Figure 5.13 First local buckling modes of the 150m towers

The local buckling modes of the 150m towers I, II and III occur in the vicinity of the bases as shown in Figure 5.13. The absolute value of the corresponding local buckling eigenvalues of the 150m

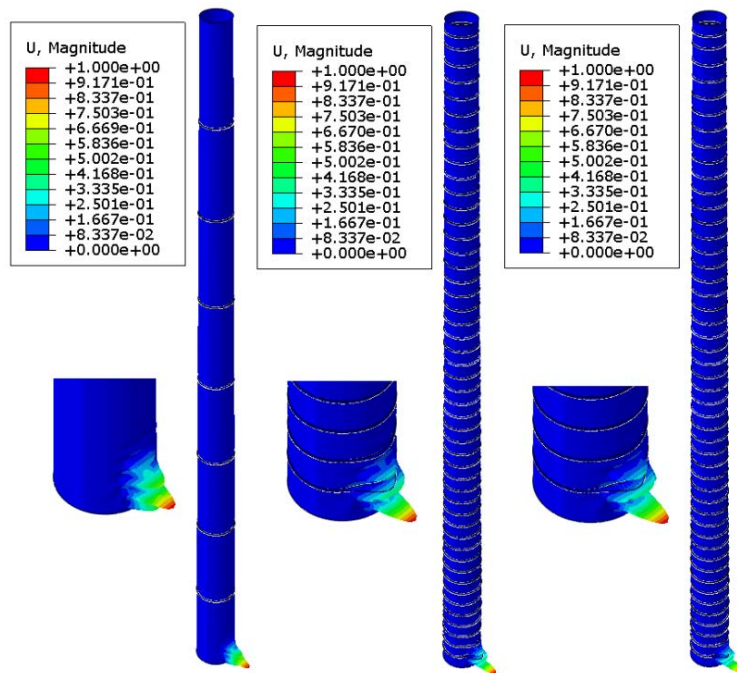
towers I, II and III are 14.38, 16.46 and 12.53, respectively as shown in Table 5.8. The buckling eigenvalue of the 150m tower II is greater than those of the 150m towers I and III.

Table 5.5 Buckling eigenvalues of 150m towers I, II and III

	Tower I	Tower II	Tower III
Eigenvalues	16.98	18.09	12.49

### 5.2.5 250m towers

Like the 150m towers above, the local buckling modes of the 250m towers I, II and III are simulated using the same parameters as the 250m towers in the previous section. The buckling modes of 250m towers I, II and III are presented in Figure 5.14.



a. Local buckling mode of 250m tower I      b. Local buckling mode of 250m tower II      c. Local buckling mode of 250m tower III

Figure 5.14 First local buckling modes of the 250m towers

The local buckling modes of the 250m towers I, II and III are all in the vicinity of the bases, and occur in the x positive direction, which means the direction of critical loads is opposite to the applied horizontal force. It was also found that the absolute value of the buckling eigenvalues of the 250m tower II are greater than those of the 250m towers I and III.

Table 5.6 Buckling eigenvalues of 250m towers I, II and III

	Tower I	Tower II	Tower III
Eigenvalues	18.0	19.0	14.71

### 5.2.6 Results and discussion

The buckling analysis of the three towers of different heights, I, II and III was performed by means of the Finite Element Method, and the eigenvalues of the three types of towers I, II and III are displayed in Table 5.7 to 5.9. Compared with tower II, the quantity of stiffening rings of tower I, and the wall thickness of tower III, are reduced. It can be seen that the buckling eigenvalues of the all three towers decrease as tower height increases as shown in Table 5.7 to 5.9. Therefore, the effect of stiffening rings and wall thickness on the structural stability of the towers can be investigated by comparing the eigenvalues variation ratios of tower II to I, and of tower II to III where the weight reduces. The mass characteristics of the towers are shown in Table 4.10. The numerical results for all three tower heights are analysed and are listed in Table 5.10, where the eigenvalue variation ratios are calculated in accordance with the data in Table 5.7 to 5.9.

Table 5.7 Wind turbine towers eigenvalues variation

Height of tower (m)	$\Delta E_R$	$\Delta E_S$	$\Delta E_R/\Delta m_R$	$\Delta E_S/\Delta m_S$
50	2.12%	54.35%	2.95	2.36
150	6.58%	30.96%	0.32	2.64
250	5.26%	22.6%	0.45	2.78

$\Delta E_R$  is the eigenvalue augmentation percentage of tower II to I ;

$\Delta E_S$  is the eigenvalue augmentation percentage of tower II to III;

$\Delta E_R/\Delta m_R$  represents the eigenvalue augmentation percentage per mass reduction ratios of tower II to I;

$\Delta E_S/\Delta m_S$  refers to the eigenvalue augmentation percentage per mass reduction ratios of tower II to III.

According to Table 5.10, for the 50m height level, the eigenvalue augmentation percentage from tower II to tower I is 2.12%, which is less than that from tower II to tower III, which is 54.35%. The mass reduction ratios of tower II to tower I, and tower II to tower III are 6.25% and 23.07% respectively.  $\Delta E_R/\Delta m_R$  is 2.95, which is greater than  $\Delta E_S/\Delta m_S$ , which is 2.36, and this indicates that the more efficient method for strengthening the stability of the 50m towers is to adjust the ring numbers. At the 150m height level, the eigenvalue augmentation percentages from tower II to tower I, and from tower II to tower III are 6.58% and 30.96%, respectively, as shown in Table 5.10. The mass reduction ratios of tower II to tower I, and of tower II to tower III are 20.68% and 11.74%, as shown in Table 4.10. The  $\Delta E_R/\Delta m_R$  of the 150m towers is 0.32, which is less than the  $\Delta E_S/\Delta m_S$  of the 150m towers, which is 2.64. Therefore, reducing the wall thickness is a more efficient way to strengthen the stability of the 150m towers. For the 250m height level, the mass reduction ratio of tower II to tower I is 11.8%, which is more than that of tower II to tower III, which is 8.12%, as shown in Table 4.10. The eigenvalue augmentation percentage for tower II to tower I is 5.26%, which is lower than that for tower II to tower III, which is 22.6%, as shown in Table 5.10. The  $\Delta E_R/\Delta m_R$  of the 250m towers is 0.45, which is less than the  $\Delta E_S/\Delta m_S$  of the 250m towers, which is 2.78, which implies that reducing the thickness of the 250m towers is more efficient to strengthen their stability.

### 5.3 Conclusions

For the dynamic analysis of independent towers, the mode shapes and the natural frequencies of the towers have been obtained in the case where the mass of the nacelle-rotor system at the top of the tower is not considered. The first two mode shapes for all cases are both bending modes. The first two and the second two mode shapes are perpendicular to each other. The 50m towers I, II and III, designed as stiff-stiff towers, will not experience resonance during the start-up and shut-down of the wind turbines because their natural frequencies are greater than the blade passing frequencies and the

rotational frequencies. However, the 150m soft-stiff towers and the 250m soft-soft towers should be controlled to prevent resonance effects during the start-up and shut-down of the wind turbines, as the natural frequencies of the 150m and 250m towers are both less than the corresponding blade passing frequencies and rotational frequencies.

As the mass of the nacelle-rotor system accounts for more than 30% of the total mass of the wind turbine tower, the concentrated mass at the top of the tower should be considered. Concerning the towers with a concentrated mass, the mode shapes of the 50m, 150m and 250m towers I, II and III are all bending modes. The first two mode shapes for each tower case are a symmetric pair perpendicular to each other, as are the second two mode shapes. The 50m and 150m towers I, II and III are designed as soft-stiff towers, because the natural frequencies of the 50m and 150m towers lie between the rotational frequencies  $f_r$  and the blade passing frequencies  $f_b$ , whereas the 250m towers I, II and III are of the soft-soft tower design in terms of the range of natural frequencies. The controller should therefore be operated to avoid the corresponding frequencies of the towers during the start-up and shut-down of the wind turbine.

In the buckling analysis, the buckling behaviour of the three heights of tower was investigated using the Finite Element Method. The buckling modes and eigenvalues for each height case were compared. For the 50m height level, increasing the number of stiffening rings is the more efficient way to improve their stability. However, for the 150m and 250m height levels, increasing the shell thickness is more efficient for reinforcing the towers against buckling.

## CHAPTER 6: PARAMETRIC ANALYSIS

### 6.1 Introduction

Wind turbines, being the principal technology for the generation of electrical power as wind energy converters, have been extensively investigated with respect to their capacity, effectiveness and safety. A large collection of research results has been accumulated with reference to the structural response of wind energy converters. For instance, Li *et al.* (2013) analysed the reasons for wind turbine tower collapse under extreme wind loads, and they proposed a robust design for wind turbine towers against typhoons. Kilic and Unluturk (2015) measured and predicted the behaviour of wind turbine towers by using wireless sensor networks and accelerometers. Binh *et al.* (2008) proposed evaluation formulas for the design wind load on the supporting structure in complex terrains, and these formulas have been validated by comparing analytical solutions with the respective FEM simulations. Dong Hyawn Kim *et al.* (2014) carried out seismic analysis of offshore wind turbine towers by considering the soil-pile interaction. The critical displacement was obtained to assess the structural safety under seismic loads by using pushover analysis. Tondini *et al.* (2013) reported the structural response of high strength steel circular columns subjected to fire loading by comparing numerical and experimental results. Van der Woude and Narasimhan (2014) performed parametric studies on base isolation systems to improve the structural response of wind turbine structures during strong earthquake events; it was concluded that the use of base isolation systems reduces possible excessive dynamic displacements of the structures in seismic zones. Tran *et al.* (2013) described the influence of the door opening on the strength of wind turbine towers by means of detailed FE models. Trung Q. Do *et al.* (2014b) studied the structural response of towers by taking into account fatigue due to wind loads, aiming to minimise the cost of structural steel, and to optimise the design parameters of the tower base and to achieve a longer fatigue life of the towers. Schneider and Zahlten (2004) presented the structural response of ring-stiffened cylindrical shells of 50m height under wind loads using Finite Element Analysis. Valamanesh and Myers (2014) compared the predicted results with those from a baseline wind turbine

tower in operation and at rest, where a reasonable agreement seems to have been achieved. Guo *et al.* (2013) performed a series of bending tests on tower tubes with stiffeners, to investigate the effect of section slenderness on the behaviour of the steel tower tubes, and the respective experimental results are in accordance with the AS4100 design code, whereas Ghanbari Ghazijahani *et al.* (2015) considered the effect of an opening on the structural response of a cylindrical shell under axial compression.

As the tower height is closely related to the energy yield, the appropriate supporting structure for a wind turbine, i.e. the tower, should be designed by taking into account cost effectiveness. To facilitate transportation, wind turbine towers are manufactured in sections that are connected *in situ* during the erection. Obviously, the geometric variation of the stiffening rings greatly affects both the strength and the stability of the towers. Typical tubular steel wind turbine towers are composed of cylindrical or conical shells interconnected by bolted flanges. To improve the economy in the design of such towers, the effect of cross-sectional dimensions and the quantity of stiffening rings used should also be considered. Sabouri-Ghomi *et al.* (2006) studied the relevant design parameters and in particular, the quantities and dimensions of the stiffening rings with the aim of analysing their effect on the structural stability of reinforced concrete cooling towers. By using numerical analysis, a method to determine the parameters of the stiffening rings which could increase the buckling capacity of the cooling towers was proposed. Perelmuter and Yurchenko (2013) formulated an optimisation problem for the design of steel wind turbine towers by considering the wall thickness, the diameters of the cross-section and the height as design variables. Sim *et al.* (2014) reported a parametric study in which a numerical simulation was compared with experimental results on the flexural buckling strength of a wind turbine tower. Hu *et al.* (2014) studied the effect of varying the number of stiffening rings with respect to wall thickness variation, on the structural response of steel wind turbine towers. Within this framework the most efficient method for selecting the number of stiffening rings and for reducing the wall thickness in order to strengthen the towers and minimise costs was proposed for each height case. Negm and Maalawi (2000) chose the cross-sectional area, radius of gyration and height of each segment as design variables, and formulated the design problem as a

nonlinear mathematical programming problem. Shi *et al.* (2014) investigated the overall buckling of tubular columns composed of high strength steel by applying experimental testing and numerical simulation, and the numerical and experimental results were compared with reference to the analytical solutions obtained by applying current code provisions. Zhu and Young (2012) studied the optimised mesh size and performed a parametric study of steel oval hollow section columns by using one hundred numerical models.

In this paper, a parametric study with reference to the design of wind turbine towers is numerically performed by means of the finite element software ABAQUS (2008). The wall thickness (referred to as  $t$ ), and the spacing of the stiffening rings (referred to as  $H$ ) are considered as the design variables for each height case. For the three height towers, the taper angle is designed to be  $89.5^\circ$ , which is equal to that of the 76m tower model in Chapter two. The effect of the chosen dimension of the stiffening rings on the overall structural response can not be captured, hence the effect of stiffener ring slenderness is ignored. To obtain a direct comparison, the maximum von Mises stresses and horizontal sways of the FEM towers are calculated for each height case. The rate of change of the maximum von Mises stresses and of the horizontal sways for three different tower heights with respect to each of the design parameters are compared to obtain the efficiency range of the parameters at hand.

## 6.2 50m towers

### 6.2.1 Models of 50m towers

The geometrical data and the FE models of four different distributions of stiffening rings for 50m towers are presented in Figure 6.1. The values of  $H$  for the 50m towers are 16.667m, 10m, 6.25m and 4.16m respectively (referred to as  $H_i$ ,  $H_{ii}$ ,  $H_{iii}$  and  $H_{iv}$  in Figure 6.1). The diameters reduce linearly from 3.7m at the base to 2.37m at the top. The widths of the stiffening rings are 50mm, 100mm, 200mm and 300mm respectively, and the mid-section thickness of the stiffening rings is 100mm. Their corresponding values of  $R$  are referred to as  $R_i$ ,  $R_{ii}$ ,  $R_{iii}$ , and  $R_{iv}$  (Figure 6.2). Concerning the thickness, four groups of thickness distributions for the 50m towers are depicted in

CHAPTER 7: VERTICAL STIFFENERS

Table 6.1. These are, for the lower and upper section, 15/5mm, 20/10mm, 25/15mm and 30/20mm (referred to as  $\text{H}_i$ ,  $\text{H}_{ii}$ ,  $\text{H}_{iii}$ ,  $\text{H}_{iv}$ ). The corresponding shell weights are also presented in Table 6.1, and these are 45.49t, 64.2t, 82.91t and 101.62t. The Young's modulus, the density and the Poisson's ratio of the steel are 205GPa, 7.85g/cm<sup>3</sup> and 0.3 respectively.

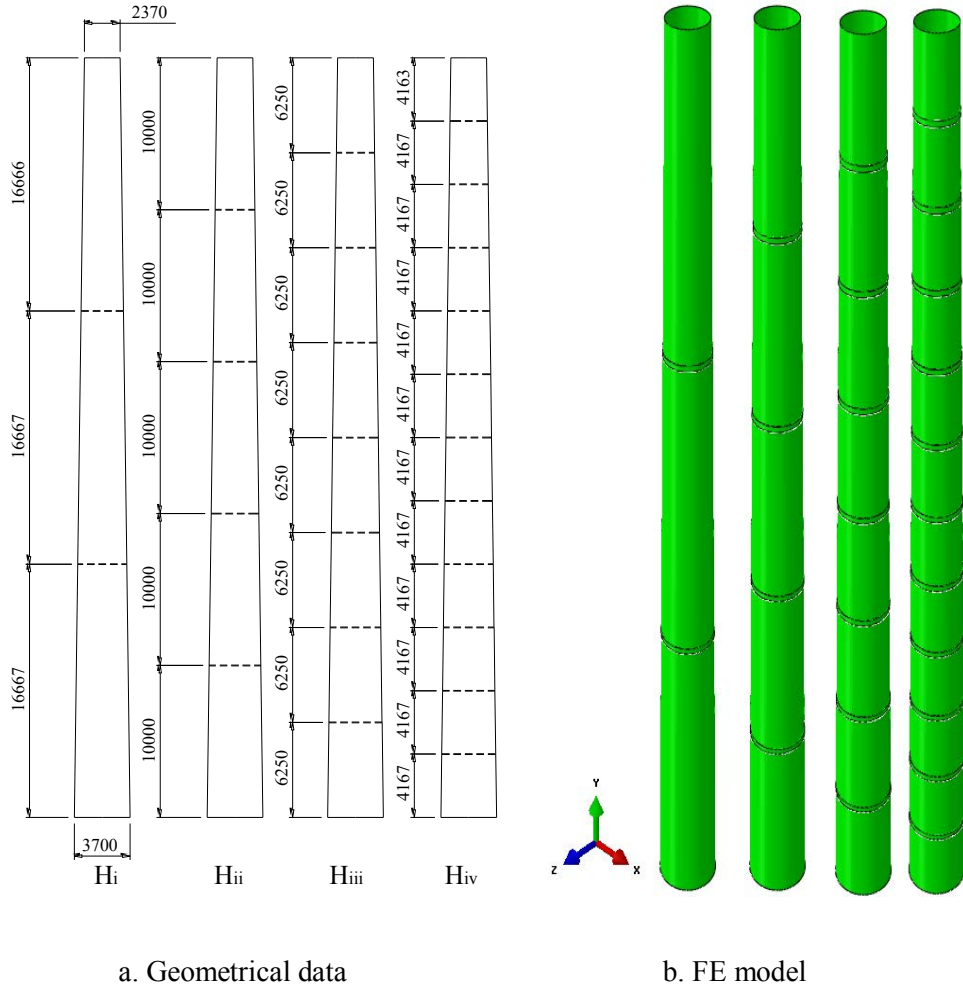


Figure 6.1 The 50m-towers: geometrical data and FEM models (in mm)

CHAPTER 7: VERTICAL STIFFENERS

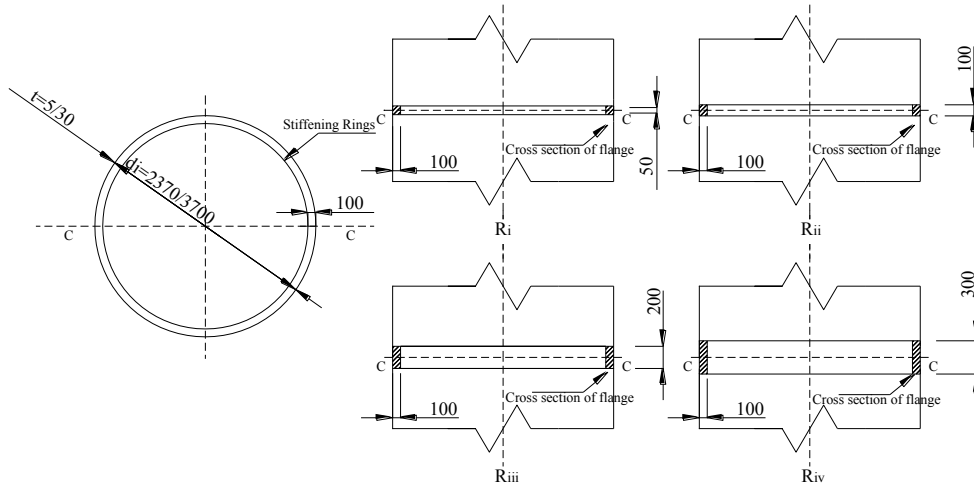


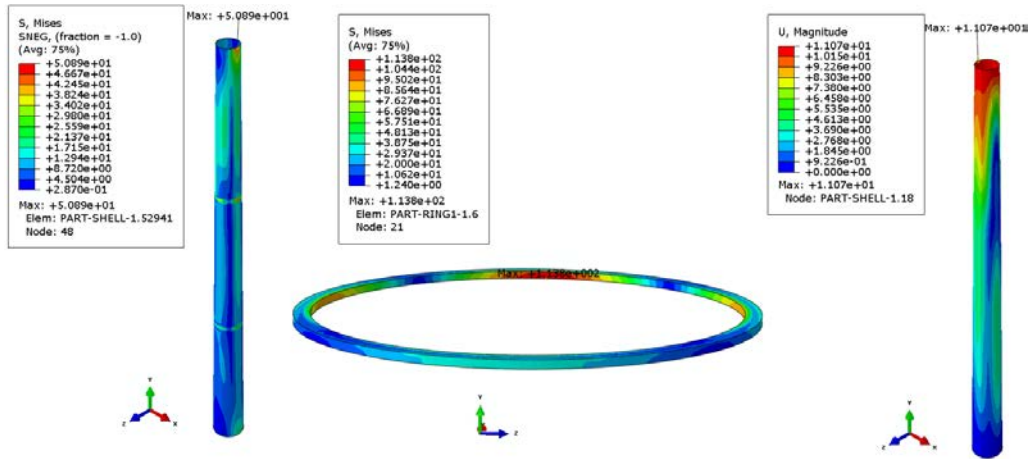
Figure 6.2 Typical ring cross-sections of the towers (in mm)

Table 6.1 Parameter details of the 50m-towers

50m towers	Height range of the towers		Weight of the shell (t)	Mid-section width-to-thickness ratio of rings		Spacing of rings (m)	
	0-33.334m	33.334m-50m					
	Thickness	Thickness					
T <sub>i</sub>	15mm	5mm	45.49	R <sub>i</sub>	0.5	H <sub>i</sub>	16.667
T <sub>ii</sub>	20mm	10mm	64.2	R <sub>ii</sub>	1	H <sub>ii</sub>	10
T <sub>iii</sub>	25mm	15mm	82.91	R <sub>iii</sub>	2	H <sub>iii</sub>	6.25
T <sub>iv</sub>	30mm	20mm	101.62	R <sub>iv</sub>	3	H <sub>iv</sub>	4.167

For the FE models, the 50m tower models are composed of S4R shell elements and C3D10 continuum elements. As described in the section three, the 50m tower models are discretized by the mesh having a shell element size of 100mm and a continuum element size of 50mm. The interaction between the flange and the tower wall is tie constrained, and the base of the tower is considered to be fully fixed. Concerning the loading states for the 50m towers, the axial, transverse and torsional loads at the top of the tower are applied to a reference node imported with a rigid constraint to the top cross-section of the towers. The magnitudes of the combined loads including wind pressure along the tower height and around the circumference follow the pattern proposed by Chapter 3.

## CHAPTER 7: VERTICAL STIFFENERS



a. von Mises stress: shell

b. von Mises stress: ring

c. Horizontal sway

Figure 6.3 The von Mises stress of the shell and ring and the horizontal sway of the  $50T_{ii}R_iH_i$  tower

The 50m tower with thickness  $T_{ii}$ , mid-section width to thickness ratio of the stiffening rings  $R_i$ , and ring spacing  $H_i$  is simplified as  $50T_{ii}R_iH_i$ , and its contour plots of von Mises stress and horizontal sway are shown in Figure 6.3. The maximum von Mises stress of  $50T_{ii}R_iH_i$  occurs in the inner side of the stiffening ring, and its magnitude is 113.8MPa, greater than that in the 50m tower shell which is 50.89MPa. The maximum horizontal sway of the 50m tower is 11.07mm at the top of the tower as expected (Figure 6.3). The maximum von Mises stresses and horizontal sway of the 50m towers are displayed in Table 6.2. As the analysis of stiffener ring slenderness could not capture its effect on the overall structural response, the stiffener ring slenderness is not included as the parameter according to Table 6.2.

Table 6.2 Maximum von Mises stresses and horizontal sways of 50m towers

Types of towers	Max. Stress (MPa)	Max. Stress of shell (MPa)	Max. Horizontal sway (mm)
$T_iR_iH_i$	171.2	113.38	20.96
$T_{ii}R_iH_i$	113.8	50.89	11.07
$T_{iii}R_iH_i$	76.1	31.30	8.47
$T_{iv}R_iH_i$	50.94	21.88	6.92

CHAPTER 7: VERTICAL STIFFENERS

$T_i R_{ii} H_i$	109.93	109.93	20.57
$T_{ii} R_{ii} H_i$	72.09	49.1	11.07
$T_{iii} R_{ii} H_i$	52.58	30.47	8.46
$T_{iv} R_{ii} H_i$	37.84	21.53	6.91
$T_i R_{iii} H_i$	107.7	107.7	20.23
$T_{ii} R_{iii} H_i$	47.75	47.75	11.03
$T_{iii} R_{iii} H_i$	33.61	29.70	8.43
$T_{iv} R_{iii} H_i$	26.11	21.15	6.88
$T_i R_{iv} H_i$	106.7	106.7	20.05
$T_{ii} R_{iv} H_i$	47.14	47.14	10.99
$T_{iii} R_{iv} H_i$	29.31	29.31	8.40
$T_{iv} R_{iv} H_i$	20.92	20.92	6.86
$T_i R_i H_{ii}$	110.7	80.93	16.84
$T_{ii} R_i H_{ii}$	83.88	41.21	11.07
$T_{iii} R_i H_{ii}$	60.39	27.33	8.47
$T_{iv} R_i H_{ii}$	44.68	20.05	6.92
$T_i R_{ii} H_{ii}$	77.65	77.65	16.84
$T_{ii} R_{ii} H_{ii}$	53.36	39.09	11.06
$T_{iii} R_{ii} H_{ii}$	41.83	25.95	8.46
$T_{iv} R_{ii} H_{ii}$	31.83	19.2	6.91
$T_i R_{iii} H_{ii}$	75.2	75.20	16.71
$T_{ii} R_{iii} H_{ii}$	37.4	37.4	10.99
$T_{iii} R_{iii} H_{ii}$	27.71	24.73	8.41
$T_{iv} R_{iii} H_{ii}$	22.68	18.36	6.87
$T_i R_{iv} H_{ii}$	74.24	74.24	16.62
$T_{ii} R_{iv} H_{ii}$	36.77	36.77	10.92
$T_{iii} R_{iv} H_{ii}$	24.24	24.24	8.36

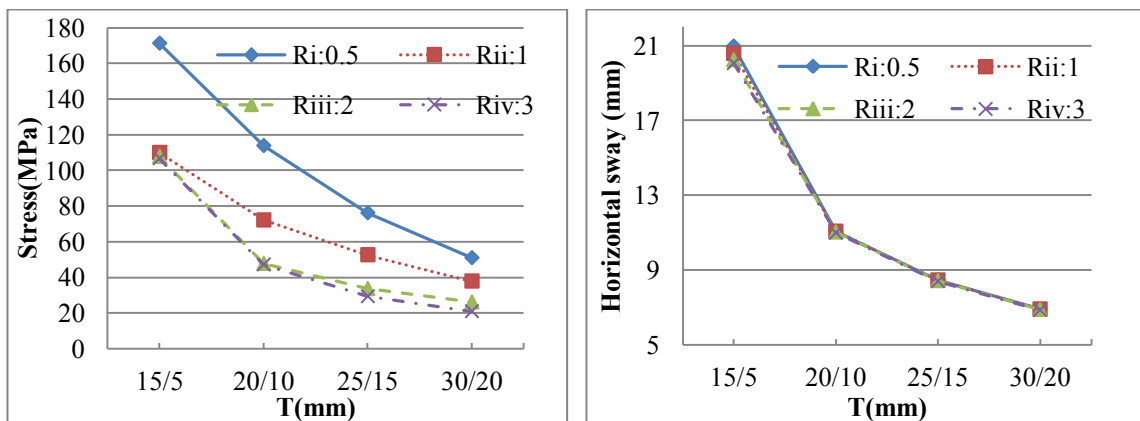
CHAPTER 7: VERTICAL STIFFENERS

$T_{iv}R_{iv}H_{ii}$	17.98	17.98	6.83
$T_iR_iH_{iii}$	78.00	62.69	16.77
$T_{ii}R_iH_{iii}$	63.39	34.37	11.05
$T_{iii}R_iH_{iii}$	50.34	24.01	8.46
$T_{iv}R_iH_{iii}$	40.2	18.35	6.91
$T_iR_{ii}H_{iii}$	59.53	59.53	16.73
$T_{ii}R_{ii}H_{iii}$	39.9	32.27	11.02
$T_{iii}R_{ii}H_{iii}$	33.34	22.49	8.44
$T_{iv}R_{ii}H_{iii}$	26.91	17.29	6.89
$T_iR_{iii}H_{iii}$	57.29	57.29	16.51
$T_{ii}R_{iii}H_{iii}$	30.66	30.66	10.90
$T_{iii}R_{iii}H_{iii}$	21.25	21.25	8.35
$T_{iv}R_{iii}H_{iii}$	18.09	16.34	6.83
$T_iR_{iv}H_{iii}$	56.29	56.29	16.35
$T_{ii}R_{iv}H_{iii}$	29.93	29.93	10.79
$T_{iii}R_{iv}H_{iii}$	20.66	20.66	8.28
$T_{iv}R_{iv}H_{iii}$	15.86	15.86	6.77
$T_iR_iH_{iv}$	52.42	52.42	16.48
$T_{ii}R_iH_{iv}$	38.68	27.41	10.80
$T_{iii}R_iH_{iv}$	32.20	18.15	8.22
$T_{iv}R_iH_{iv}$	26.68	13.29	6.67
$T_iR_{ii}H_{iv}$	49.88	49.88	16.38
$T_{ii}R_{ii}H_{iv}$	25.94	25.94	10.74
$T_{iii}R_{ii}H_{iv}$	19.79	17.15	8.17
$T_{iv}R_{ii}H_{iv}$	16.94	12.57	6.63
$T_iR_{iii}H_{iv}$	48.04	48.04	16.06
$T_{ii}R_{iii}H_{iv}$	24.78	24.78	10.59

$T_{iii}R_{iii}H_{iv}$	16.34	16.34	8.09
$T_{iv}R_{iii}H_{iv}$	11.99	11.99	6.58
$T_iR_{iv}H_{iv}$	47.17	47.17	15.83
$T_{ii}R_{iv}H_{iv}$	24.26	24.26	10.46
$T_{iii}R_{iv}H_{iv}$	15.99	15.99	8.0
$T_{iv}R_{iv}H_{iv}$	11.72	11.72	6.52

### 6.2.2 Effect of the thickness T on the overall structural response

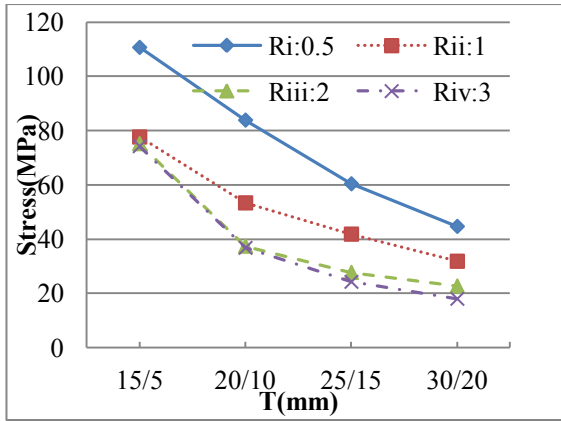
The maximum von Mises stresses in the tower shell and the maximum horizontal sways of the 50m towers for each group of thicknesses are presented in Table 6.2. For each R and H, the 50m towers with 15/5mm, 20/10mm, 25/15mm, and 30/20mm thickness were numerically simulated to obtain the maximum von Mises stresses and the horizontal sways (Table 6.2). Given that the shell wall thickness is a significant parameter in the design of the tower structure, it is evident that variations in thickness significantly affect the tower's strength and stiffness. Thus, the inherent relationship between thickness and strength/deflection of the structure was studied, and the efficiency range of tower thickness was identified. The maximum von Mises stresses and the horizontal sways of the tower plotted against T for the 50m-towers are presented in Figure 6.4 to 6.7.



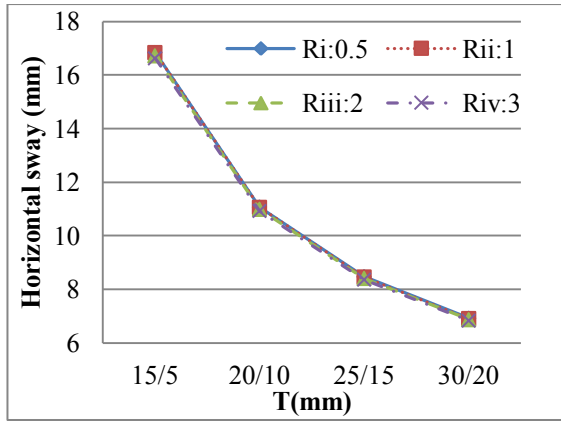
a. Maximum von Mises stress

b. Maximum horizontal sway

Figure 6.4 Maximum von Mises stress and horizontal sway versus T of the 50H<sub>i</sub>

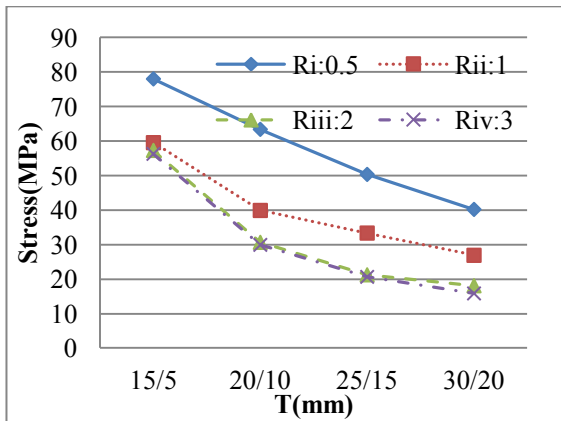


a. Maximum von Mises stress

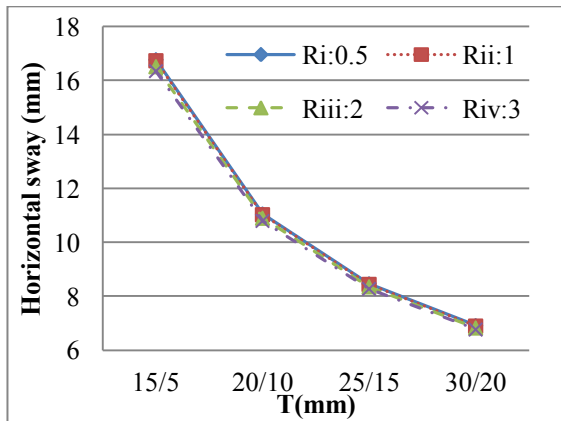


b. Maximum horizontal sway

Figure 6.5 Maximum von Mises stress and horizontal sway versus T of the 50Hii

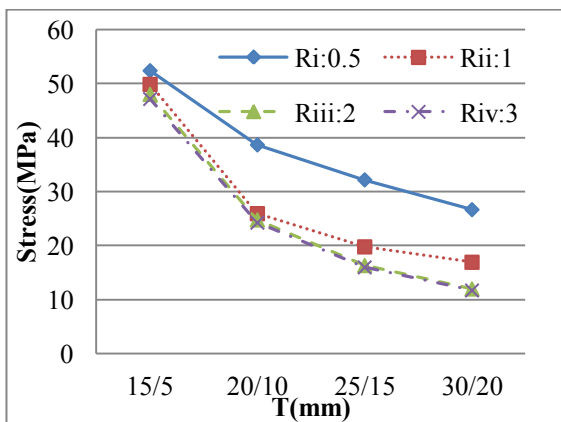


a. Maximum von Mises stress

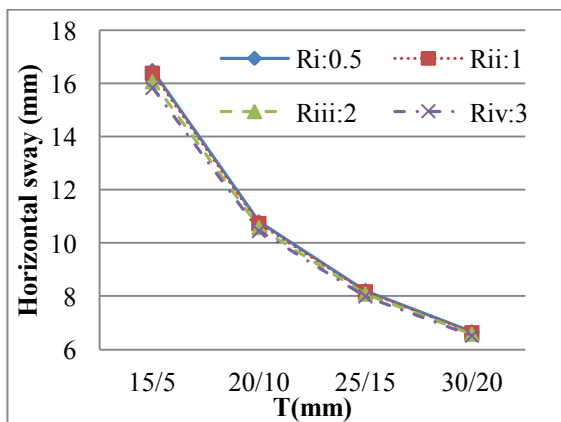


b. Maximum horizontal sway

Figure 6.6 Maximum von Mises stress and horizontal sway versus T of the 50Hiii



a. Maximum von Mises stress



b. Maximum horizontal sway

Figure 6.7 Maximum von Mises stress and horizontal sway versus T of the 50H<sub>iv</sub>

The 50m tower with a ring spacing of H<sub>i</sub> is denoted as 50H<sub>i</sub>. In Figure 6.4 to 6.7 (a) and (b) the horizontal axis represents the T of 50H<sub>i</sub> and the vertical axis corresponds to the maximum von Mises stresses or the horizontal sways of 50H<sub>i</sub>. Clearly, the maximum von Mises stress and the horizontal sway of the 50m towers reduce as the thickness increases from T<sub>i</sub> to T<sub>iv</sub> in accordance with Figure 6.4 to 6.7 and Table 6.2.

The rate of change of the maximum von Mises stress and of the horizontal sway of the 50m-towers with respect to T were investigated in order to obtain the efficiency range of thickness, based on its effect on the maximum von Mises stress and the sway of the towers. Where there is a high rate of change of the maximum von Mises stress and of the horizontal sway of the towers with respect to T, this indicates the significant range. The rate of change of the maximum von Mises stress and of the horizontal sway are given by the following general equations:

$$\frac{\Delta S}{\Delta T} = \begin{cases} (S_{T_i} - S_{T_{ii}}) / (T_{ii} - T_i) \\ (S_{T_{ii}} - S_{T_{iii}}) / (T_{iii} - T_{ii}) \\ (S_{T_{iii}} - S_{T_{iv}}) / (T_{iv} - T_{iii}) \end{cases} \quad (6.1)$$

$$\frac{\Delta D}{\Delta T} = \begin{cases} (D_{T_i} - D_{T_{ii}}) / (T_{ii} - T_i) \\ (D_{T_{ii}} - D_{T_{iii}}) / (T_{iii} - T_{ii}) \\ (D_{T_{iii}} - D_{T_{iv}}) / (T_{iv} - T_{iii}) \end{cases} \quad (6.2)$$

where the  $\Delta S/\Delta T$  and  $\Delta D/\Delta T$  respectively represent the rate of change of the maximum von Mises stress and of the horizontal sway of the wind tower with respect to T. S<sub>T<sub>i</sub></sub>, S<sub>T<sub>ii</sub></sub>, S<sub>T<sub>iii</sub></sub>, S<sub>T<sub>iv</sub></sub> refer to the maximum von Mises stress of the 50m-towers for each R and H. D<sub>T<sub>i</sub></sub>, D<sub>T<sub>ii</sub></sub>, D<sub>T<sub>iii</sub></sub>, D<sub>T<sub>iv</sub></sub> refer to the maximum horizontal sway of the 50m towers under the four specified values of R and H. Therefore, the  $\Delta S/\Delta T$  and  $\Delta D/\Delta T$  of the 50/150/250H<sub>i</sub> towers can be obtained by using Table 6.2 and Eqs. (6.1, 6.2), as shown in Table 6.3. In addition, the rate of change for the maximum von Mises stress and for the horizontal sway of the towers with different sizes and spacings of the stiffening rings can also be calculated substituting the results from Table 6.2 to Eqs. (6.1) and (6.2).

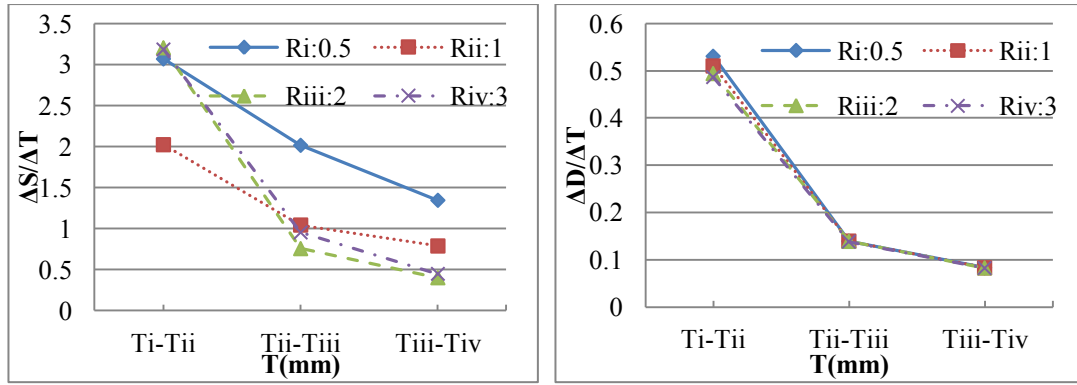
Table 6.3 Rate of change  $\Delta S/\Delta T$  and  $\Delta D/\Delta T$  for the 50H<sub>i</sub>/H<sub>ii</sub>/H<sub>iii</sub>/H<sub>iv</sub> with respect to T

CHAPTER 7: VERTICAL STIFFENERS

Types of rings	Ranges of thickness variations	$\Delta S/\Delta T$	$\Delta D/\Delta T$
$R_i H_i$	$T_i$ to $T_{ii}$	3.07	0.53
	$T_{ii}$ to $T_{iii}$	2.01	0.14
	$T_{iii}$ to $T_{iv}$	1.34	0.08
$R_{ii} H_i$	$T_i$ to $T_{ii}$	2.02	0.51
	$T_{ii}$ to $T_{iii}$	1.04	0.14
	$T_{iii}$ to $T_{iv}$	0.79	0.08
$R_{iii} H_i$	$T_i$ to $T_{ii}$	3.20	0.49
	$T_{ii}$ to $T_{iii}$	0.76	0.14
	$T_{iii}$ to $T_{iv}$	0.41	0.08
$R_{iv} H_i$	$T_i$ to $T_{ii}$	3.18	0.49
	$T_{ii}$ to $T_{iii}$	0.95	0.14
	$T_{iii}$ to $T_{iv}$	0.45	0.08
$R_i H_{ii}$	$T_i$ to $T_{ii}$	1.43	0.31
	$T_{ii}$ to $T_{iii}$	1.26	0.14
	$T_{iii}$ to $T_{iv}$	0.84	0.08
$R_{ii} H_{ii}$	$T_i$ to $T_{ii}$	1.30	0.31
	$T_{ii}$ to $T_{iii}$	0.62	0.14
	$T_{iii}$ to $T_{iv}$	0.53	0.08
$R_{iii} H_{ii}$	$T_i$ to $T_{ii}$	2.02	0.31
	$T_{ii}$ to $T_{iii}$	0.52	0.14
	$T_{iii}$ to $T_{iv}$	0.27	0.08
$R_{iv} H_{ii}$	$T_i$ to $T_{ii}$	2.00	0.30
	$T_{ii}$ to $T_{iii}$	0.67	0.14
	$T_{iii}$ to $T_{iv}$	0.33	0.08
$R_i H_{iii}$	$T_i$ to $T_{ii}$	0.78	0.31
	$T_{ii}$ to $T_{iii}$	0.70	0.14

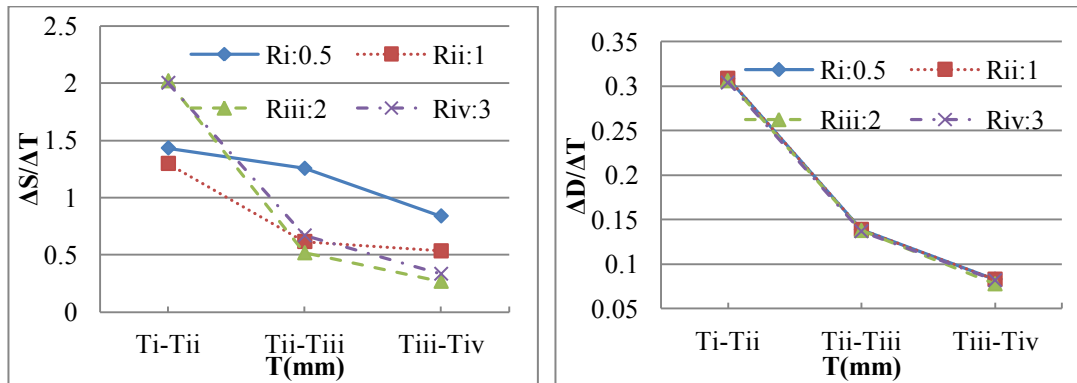
CHAPTER 7: VERTICAL STIFFENERS

	$T_{iii}$ to $T_{iv}$	0.54	0.08
$R_{ii}H_{iii}$	$T_i$ to $T_{ii}$	1.05	0.30
	$T_{ii}$ to $T_{iii}$	0.35	0.14
	$T_{iii}$ to $T_{iv}$	0.34	0.08
$R_{iii}H_{iii}$	$T_i$ to $T_{ii}$	1.42	0.30
	$T_{ii}$ to $T_{iii}$	0.50	0.14
	$T_{iii}$ to $T_{iv}$	0.17	0.08
$R_{iv}H_{iii}$	$T_i$ to $T_{ii}$	1.41	0.30
	$T_{ii}$ to $T_{iii}$	0.50	0.13
	$T_{iii}$ to $T_{iv}$	0.26	0.08
$R_iH_{iv}$	$T_i$ to $T_{ii}$	0.73	0.30
	$T_{ii}$ to $T_{iii}$	0.35	0.14
	$T_{iii}$ to $T_{iv}$	0.30	0.08
$R_{ii}H_{iv}$	$T_i$ to $T_{ii}$	1.28	0.30
	$T_{ii}$ to $T_{iii}$	0.33	0.14
	$T_{iii}$ to $T_{iv}$	0.15	0.08
$R_{iii}H_{iv}$	$T_i$ to $T_{ii}$	1.24	0.29
	$T_{ii}$ to $T_{iii}$	0.45	0.13
	$T_{iii}$ to $T_{iv}$	0.23	0.08
$R_{iv}H_{iv}$	$T_i$ to $T_{ii}$	1.22	0.29
	$T_{ii}$ to $T_{iii}$	0.44	0.13
	$T_{iii}$ to $T_{iv}$	0.23	0.08



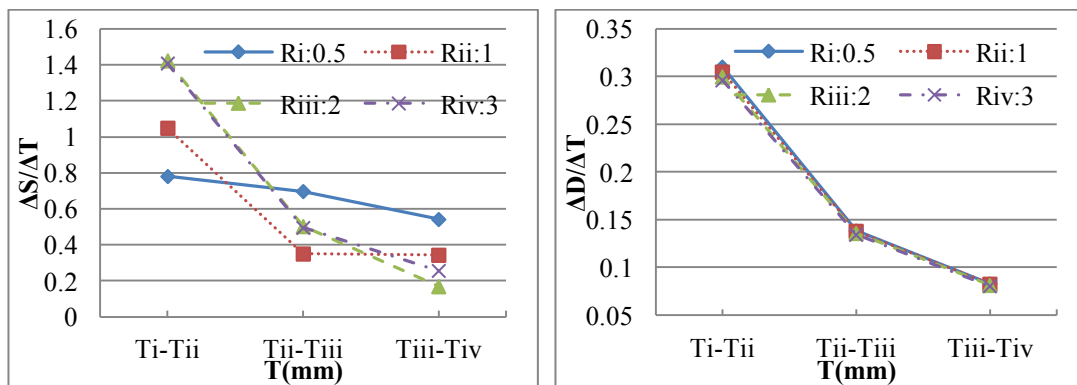
a. Rate of change of maximum von Mises stress      b. Rate of change of maximum horizontal sway

Figure 6.8  $\Delta S/\Delta T$  and  $\Delta D/\Delta T$  of the  $50H_i$  with respect to T



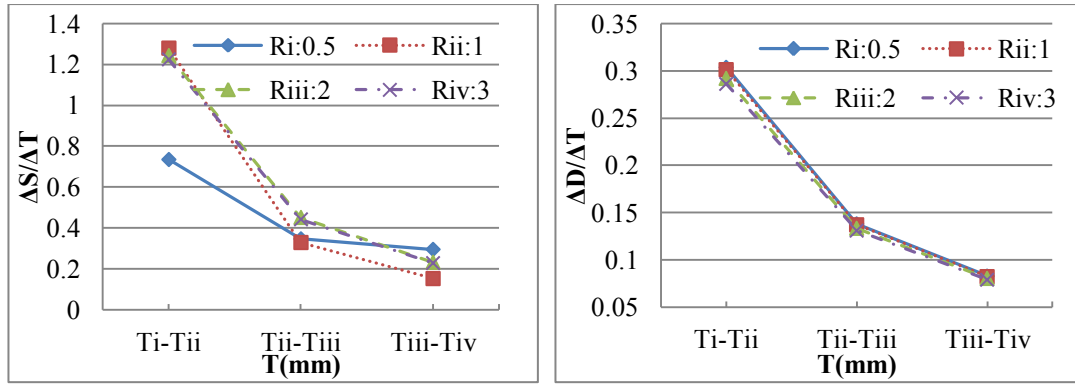
a. Rate of change of maximum von Mises stress      b. Rate of change of maximum horizontal sway

Figure 6.9  $\Delta S/\Delta T$  and  $\Delta D/\Delta T$  of the  $50H_{ii}$  with respect to T



a. Rate of change of maximum von Mises stress      b. Rate of change of maximum horizontal sway

Figure 6.10  $\Delta S/\Delta T$  and  $\Delta D/\Delta T$  of the  $50H_{iii}$  with respect to T



a. Rate of change of maximum von Mises stress      b. Rate of change of maximum horizontal sway

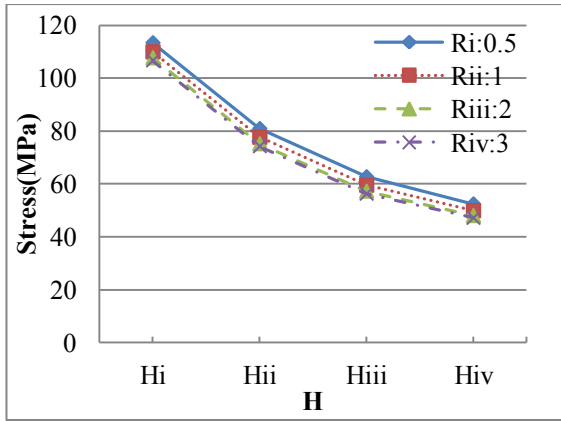
Figure 6.11  $\Delta S/\Delta T$  and  $\Delta D/\Delta T$  of the  $50H_{iv}$  with respect to T

The rate of change of the maximum von Mises stress and of the horizontal sway of the 50m-towers are presented in Figure 6.8 to 6.11. In general, the rate of change of the maximum von Mises stress and of the horizontal sway of the 50m towers for each R and H reduce as T increases from  $T_i$  to  $T_{iv}$ . For the maximum horizontal sway, the rate of change of the 50m-towers are very close for each T variation, which are 0.5 ( $T_i$  to  $T_{ii}$ ), 0.14 ( $T_{ii}$  to  $T_{iii}$ ) and 0.08 ( $T_{iii}$  to  $T_{iv}$ ). For the maximum von Mises stress, the rate of change for the 50m-towers as T increases from  $T_i$  to  $T_{ii}$ , are relatively greater than those when T increases from  $T_{ii}$  to  $T_{iv}$  (as shown in Figure 6.8 to 6.11 and Table 6.2). The most critical range of the shell wall thickness of the 50m towers based on the changing rate is from  $T_i$  to  $T_{ii}$ . For the low height tower, the efficiency range of thickness variation in thin walled towers is more critical than that in thick walled towers.

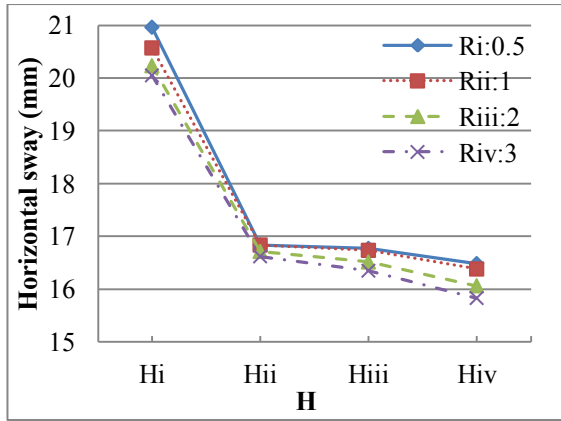
### 6.2.3 Effect of the spacing H of stiffening rings on the overall structural response

Stiffening rings are designed and manufactured to strengthen the tower against shell buckling. For these rings, an appropriately chosen distance between two neighbouring stiffening rings should be investigated for each height case. For each T and R, the maximum von Mises stresses in the shell of the towers are compared.

CHAPTER 7: VERTICAL STIFFENERS

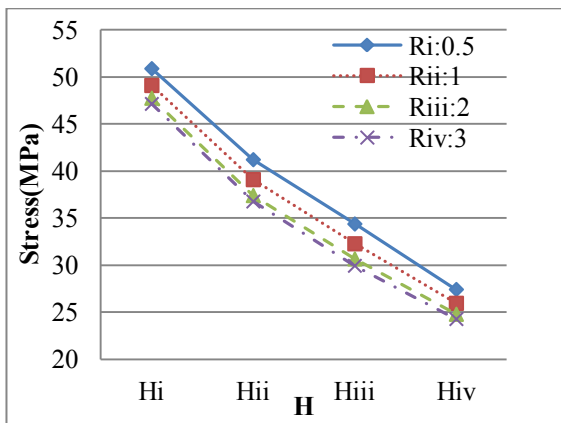


a. Maximum von Mises stress

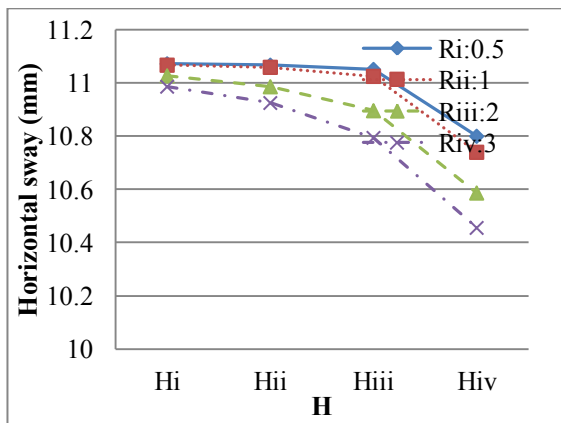


b. Maximum horizontal sway

Figure 6.12 Maximum von Mises stresses and horizontal sways versus H of the 50T<sub>i</sub>

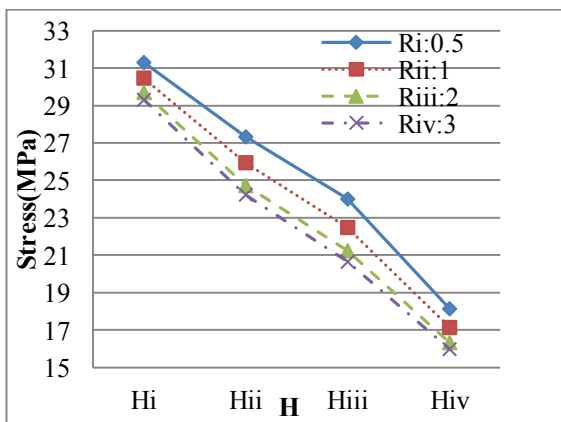


a. Maximum von Mises stress

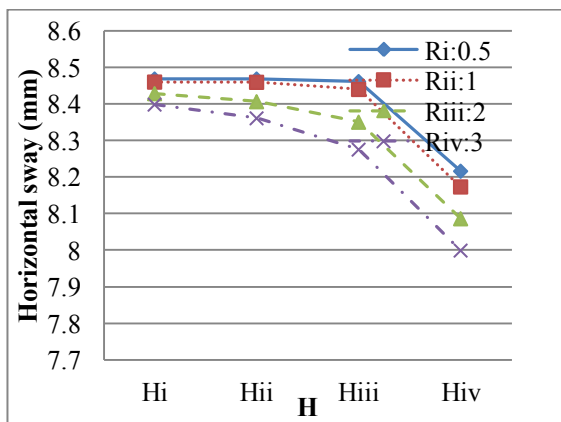


b. Maximum horizontal sway

Figure 6.13 Maximum von Mises stresses and horizontal sways versus H of the 50T<sub>ii</sub>

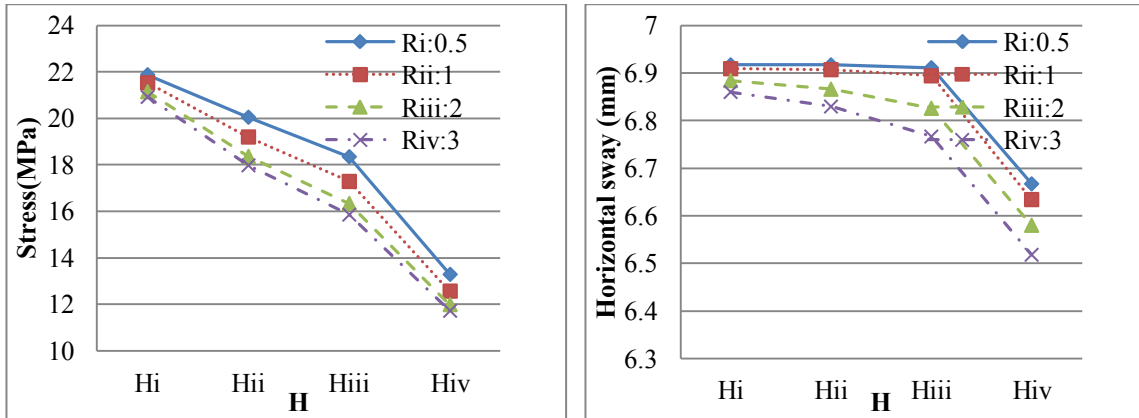


a. Maximum von Mises stress



b. Maximum horizontal sway

Figure 6.14 Maximum von Mises stresses and horizontal sways versus H of the 50T<sub>iii</sub>



a. Maximum von Mises stress

b. Maximum horizontal sway

Figure 6.15 Maximum von Mises stresses and horizontal sways versus H of the 50T<sub>iv</sub>

The 50m tower with thickness  $T_i$  is referred to as 50T<sub>i</sub>. The maximum von Mises stresses and the horizontal sways versus H for the 50T<sub>i</sub>/T<sub>ii</sub>/T<sub>iii</sub>/T<sub>iv</sub> are presented in Figure 6.12 to 6.15. At the horizontal axis, the H of the 50m-tower, and at the vertical axis the maximum von Mises stresses or the horizontal sways of each tower is depicted (Figure 6.12 to 6.15). Clearly, the maximum von Mises stresses and the horizontal sways reduce as H decreases, as can be seen in Table 6.2. The rate of change of the maximum von Mises stress and of the horizontal sway of the 50T<sub>i</sub>/T<sub>ii</sub>/T<sub>iii</sub>/T<sub>iv</sub> with respect to H can be obtained by referring to Eqs. (6.5) and (6.6) and Table 6.2. The greater the  $\Delta S/\Delta H$  and  $\Delta D/\Delta H$  of the towers, the more critical is the variation of the spacing, H, in the strengthening of the tower. The general equations:

$$\frac{\Delta S}{\Delta H} = \begin{cases} (S_i - S_{ii}) / (H_{ii} - H_i) \\ (S_{ii} - S_{iii}) / (H_{iii} - H_{ii}) \\ (S_{iii} - S_{iv}) / (H_{iv} - H_{iii}) \end{cases} \quad (6.5)$$

$$\frac{\Delta D}{\Delta H} = \begin{cases} (D_i - D_{ii}) / (H_{ii} - H_i) \\ (D_{ii} - D_{iii}) / (H_{iii} - H_{ii}) \\ (D_{iii} - D_{iv}) / (H_{iv} - H_{iii}) \end{cases} \quad (6.6)$$

are introduced, where the  $\Delta S/\Delta H$  and  $\Delta D/\Delta H$  represent the rate of change of the maximum von Mises stresses and of the horizontal sways of the towers respectively.  $S_i$ ,  $S_{ii}$ ,  $S_{iii}$  and  $S_{iv}$  are the maximum

CHAPTER 7: VERTICAL STIFFENERS

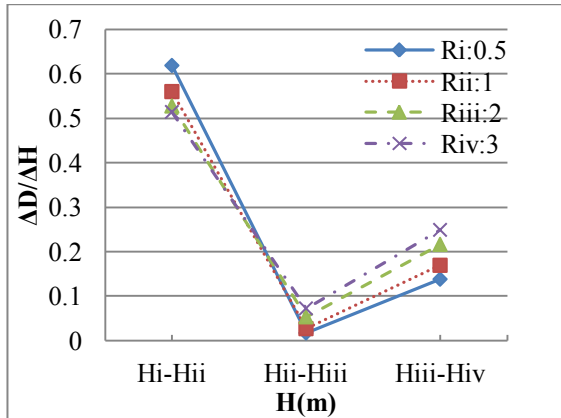
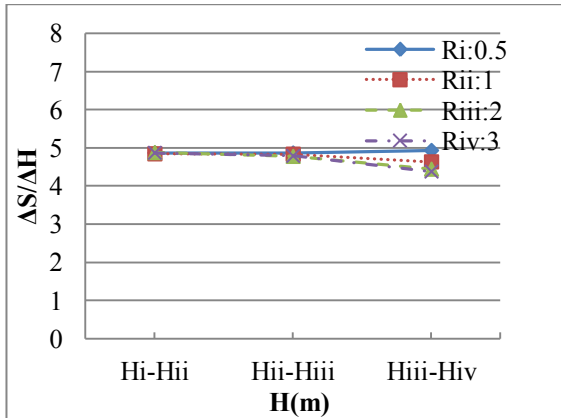
von Mises stresses of the towers.  $D_i$ ,  $D_{ii}$ ,  $D_{iii}$  and  $D_{iv}$  refer to the maximum horizontal sways of the towers, and  $H_i$ ,  $H_{ii}$ ,  $H_{iii}$  and  $H_{iv}$  are the four distances between neighbouring rings at each of the towers of height 50m.

Table 6.4 Rate of change  $\Delta S/\Delta H$  and  $\Delta D/\Delta H$  of the  $50T_i/T_{ii}/T_{iii}/T_{iv}$  with respect to H

Types of rings	Ranges of H variation	$\Delta S/\Delta H$	$\Delta D/\Delta H$
$T_i R_i$	$H_i$ to $H_{ii}$	4.87	0.62
	$H_{ii}$ to $H_{iii}$	4.86	0.017
	$H_{iii}$ to $H_{iv}$	4.93	0.14
$T_i R_{ii}$	$H_i$ to $H_{ii}$	4.84	0.56
	$H_{ii}$ to $H_{iii}$	4.83	0.027
	$H_{iii}$ to $H_{iv}$	4.63	0.17
$T_i R_{iii}$	$H_i$ to $H_{ii}$	4.87	0.53
	$H_{ii}$ to $H_{iii}$	4.78	0.054
	$H_{iii}$ to $H_{iv}$	4.44	0.22
$T_i R_{iv}$	$H_i$ to $H_{ii}$	4.87	0.51
	$H_{ii}$ to $H_{iii}$	4.79	0.073
	$H_{iii}$ to $H_{iv}$	4.38	0.25
$T_{ii} R_i$	$H_i$ to $H_{ii}$	1.45	0.00075
	$H_{ii}$ to $H_{iii}$	1.82	0.0043
	$H_{iii}$ to $H_{iv}$	3.34	0.12
$T_{ii} R_{ii}$	$H_i$ to $H_{ii}$	1.50	0.0012
	$H_{ii}$ to $H_{iii}$	1.82	0.0091
	$H_{iii}$ to $H_{iv}$	3.04	0.137
$T_{ii} R_{iii}$	$H_i$ to $H_{ii}$	1.55	0.0062
	$H_{ii}$ to $H_{iii}$	1.80	0.024
	$H_{iii}$ to $H_{iv}$	2.82	0.148

CHAPTER 7: VERTICAL STIFFENERS

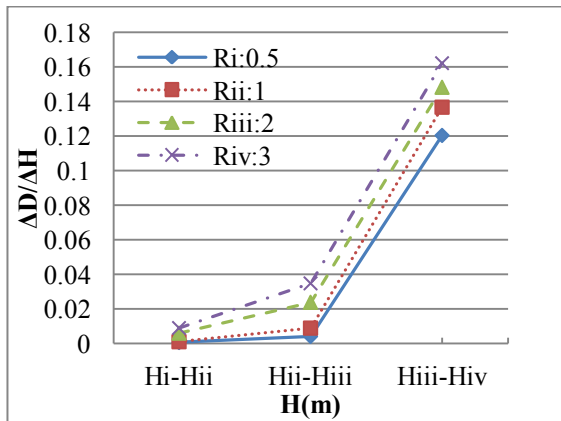
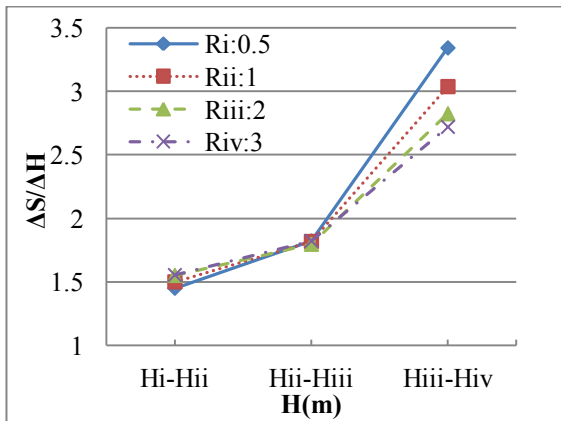
$T_{ii}R_{iv}$	$H_i$ to $H_{ii}$	1.56	0.00915
	$H_{ii}$ to $H_{iii}$	1.82	0.035
	$H_{iii}$ to $H_{iv}$	2.72	0.16
$T_{iii}R_i$	$H_i$ to $H_{ii}$	0.60	0
	$H_{ii}$ to $H_{iii}$	0.89	0.001867
	$H_{iii}$ to $H_{iv}$	2.82	0.118
$T_{iii}R_{ii}$	$H_i$ to $H_{ii}$	0.68	0
	$H_{ii}$ to $H_{iii}$	0.92	0.0052
	$H_{iii}$ to $H_{iv}$	2.56	0.128
$T_{iii}R_{iii}$	$H_i$ to $H_{ii}$	0.75	0.0033
	$H_{ii}$ to $H_{iii}$	0.93	0.015
	$H_{iii}$ to $H_{iv}$	2.36	0.127
$T_{iii}R_{iv}$	$H_i$ to $H_{ii}$	0.76	0.00561
	$H_{ii}$ to $H_{iii}$	0.95	0.023
	$H_{iii}$ to $H_{iv}$	2.24	0.13
$T_{iv}R_i$	$H_i$ to $H_{ii}$	0.27	0
	$H_{ii}$ to $H_{iii}$	0.45	0.0016
	$H_{iii}$ to $H_{iv}$	2.43	0.117
$T_{iv}R_{ii}$	$H_i$ to $H_{ii}$	0.35	0.0003
	$H_{ii}$ to $H_{iii}$	0.51	0.0035
	$H_{iii}$ to $H_{iv}$	2.27	0.125
$T_{iv}R_{iii}$	$H_i$ to $H_{ii}$	0.42	0.0027
	$H_{ii}$ to $H_{iii}$	0.54	0.011
	$H_{iii}$ to $H_{iv}$	2.09	0.118
$T_{iv}R_{iv}$	$H_i$ to $H_{ii}$	0.44	0.0046
	$H_{ii}$ to $H_{iii}$	0.57	0.0168
	$H_{iii}$ to $H_{iv}$	1.99	0.119



a. Rate of change of maximum von Mises stress

b. Rate of change of maximum horizontal sway

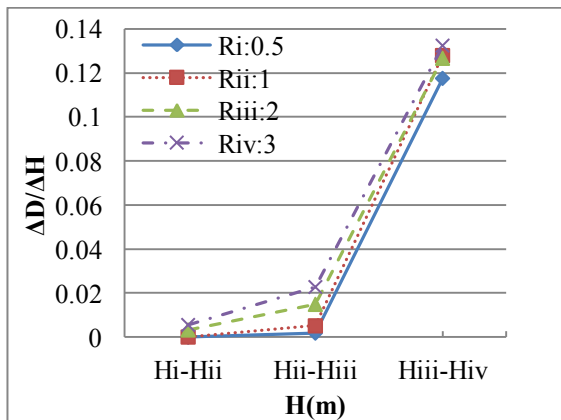
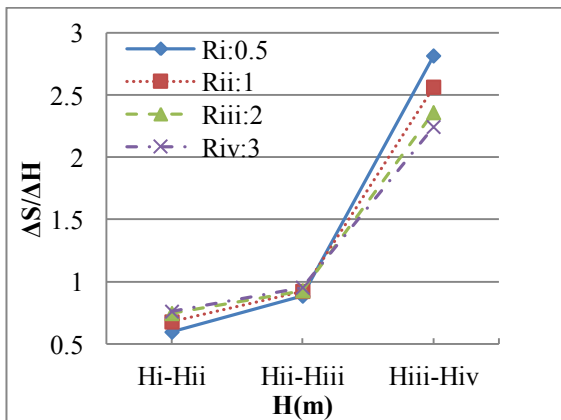
Figure 6.16 The  $\Delta S/\Delta H$  and  $\Delta D/\Delta H$  graphs of the  $50T_i$  with respect to H



a. Rate of change of maximum von Mises stress

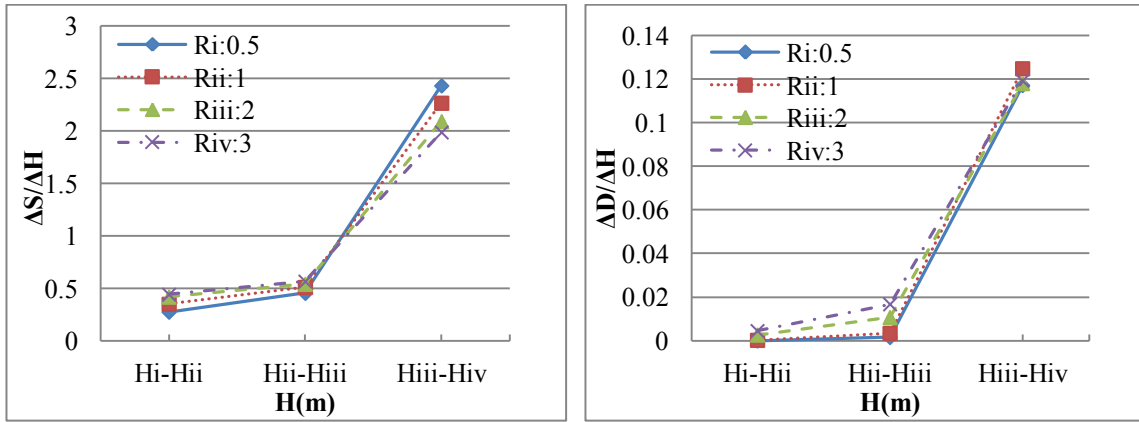
b. Rate of change of maximum horizontal sway

Figure 6.17 The  $\Delta S/\Delta H$  and  $\Delta D/\Delta H$  graphs of the  $50T_{ii}$  with respect to H



- a. Rate of change of maximum von Mises stress      b. Rate of change of maximum horizontal sway

Figure 6.18 The  $\Delta S/\Delta H$  and  $\Delta D/\Delta H$  graphs of the  $50T_{iii}$  with respect to H



- a. Rate of change of maximum von Mises stress      b. Rate of change of maximum horizontal sway

Figure 6.19 The  $\Delta S/\Delta H$  and  $\Delta D/\Delta H$  graphs of the  $50T_{iv}$  with respect to H

The rate of change of the maximum von Mises stresses and of the horizontal sways of the  $50T_i/T_{ii}/T_{iii}/T_{iv}$  towers with respect to H are displayed in Figure 6.16 to 6.19. The effect of varying H on the rate of change of the maximum von Mises stresses is more significant than the effect on the rate of change of the maximum horizontal sway as shown in Table 6.4. The rate of change of the maximum von Mises stresses of the  $50T_i$  tower with respect to H vary slightly (with a range of approx. 4.4 to 4.9) as shown in Figure 6.16(a). However, the rate of change of the maximum horizontal sways of the  $50T_i$  tower with H varying from  $H_i$  to  $H_{ii}$  are greater than those when H increases from  $H_{ii}$  to  $H_{iv}$ . Thus, the more significant range in H variation for  $50T_i$  is from  $H_i$  to  $H_{ii}$ . However, for  $50T_{ii}/T_{iii}/T_{iv}$ , the range from  $H_{iii}$  to  $H_{iv}$  is the most significant one when strengthening the 50m towers by decreasing rings spacing, as indicated in Figure 6.17 to 6.19. For thin walled towers, a greater gap between two neighbouring rings is a better option for strength enhancement, whereas for intermediate and thick walled towers, the effective range for enhancing tower strength is where the neighbouring rings are spaced at shorter intervals.

## 6.3 150m towers

### 6.3.1 Models of 150m towers

The ring spacings,  $H$ , for the case of the towers with height 150m are depicted in Figure 6.20. The ring distances of 18.75m, 15m, 11.544m and 9.375m are represented as  $-H_i$ ,  $-H_{ii}$ ,  $-H_{iii}$  and  $-H_{iv}$  respectively. The dimensions of width and mid-section thickness of the stiffening rings in the 150m towers are identical to those of the corresponding stiffening rings in the 50m towers as displayed in Figure 6.2 (referred to as  $-R_i$ ,  $-R_{ii}$ ,  $-R_{iii}$ ,  $-R_{iv}$ ). For each  $H$ , the four groups of wall thicknesses for the 150m towers are distributed from heights 0m to 50m, 50m to 100m, and 100m to 150m. The four groups of thicknesses of the 150m towers are presented in Table 6.5 as 40/30/25mm, 45/35/30mm, 50/40/35mm, and 55/40/35mm respectively, (referred to as  $-T_i$ ,  $-T_{ii}$ ,  $-T_{iii}$ ,  $-T_{iv}$ ), and their corresponding weights are 849.01t, 980.34t, 1111.67t and 1242.99t respectively. The diameters of the cross-sections of the tower wall vary linearly from 8.5m at the base to 5.7m at the top. The support of the 150m towers are considered to be fixed, and the types of elements, the material properties and the interaction between the shell and the rings are also similar to those of the 50m models.

Table 6.5 Parameter details of the 150m-towers

150m towers	Height range of the towers			Weight of the shell (t)	Ratio of mid-section width-to-thickness of rings		Spacing of rings (m)	
	0 to 50m	50m to 100m	100m to 150m					
	Thickness	Thickness	Thickness					
$T_i$	40mm	30mm	25mm	849.01	$R_i$	0.5	$H_i$	18.75
$T_{ii}$	45mm	35mm	30mm	980.34	$R_{ii}$	1	$H_{ii}$	15
$T_{iii}$	50mm	40mm	35mm	1111.67	$R_{iii}$	2	$H_{iii}$	11.544
$T_{iv}$	55mm	45mm	40mm	1242.99	$R_{iv}$	3	$H_{iv}$	9.375

# CHAPTER 7: VERTICAL STIFFENERS

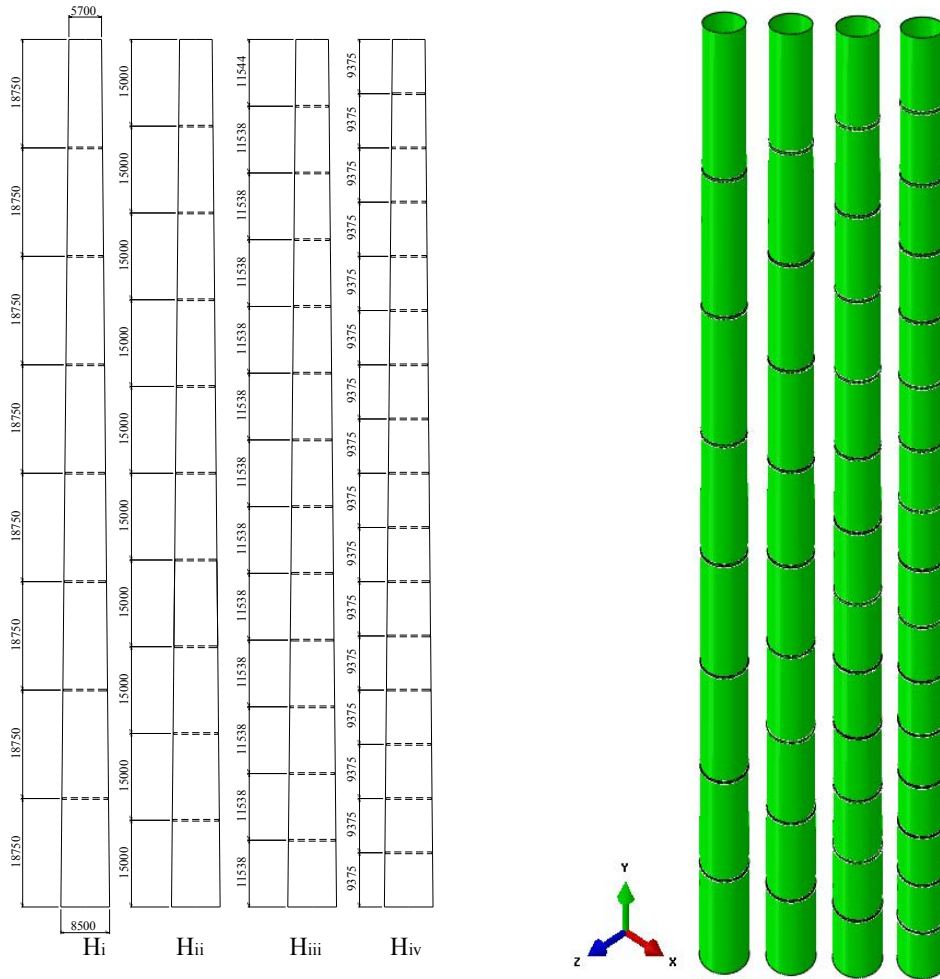
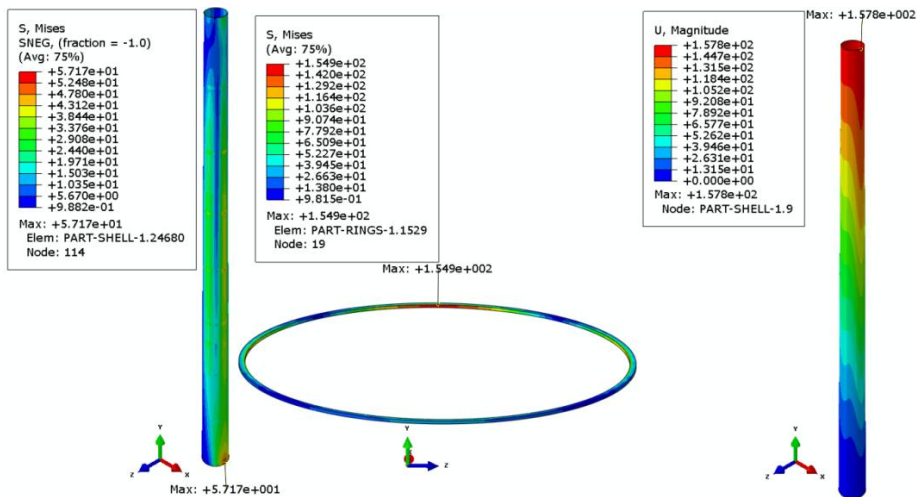


Figure 6.20 The 150m-towers: geometrical data and FEM models (in mm)



a. von Mises stress: shell

b. von Mises stress: ring

c. Horizontal sway

Figure 6.21 The von Mises stress of shell and ring and the horizontal sway of 150T<sub>iii</sub>R<sub>i</sub>H<sub>i</sub> tower

CHAPTER 7: VERTICAL STIFFENERS

The maxima for the von Mises stress of the shell and the ring, and the horizontal sway of 150T<sub>iii</sub>R<sub>i</sub>H<sub>i</sub> are presented in Figure 6.21. The maximum von Mises stress of the shell is 57.17MPa and occurs as expected at the base of the tower, whereas the maximum von Mises stress of the stiffening rings is 154.9MPa, occurring at the inner side of the rings. The horizontal sway increases nonlinearly from 0mm at the base to its maximum value of 157.8mm at the top. The maximum von Mises stresses in the tower shell and the maximum horizontal sways of the 150m towers are presented in Table 6.6. The stiffener ring slenderness is also not considered to be a parameter due to its negligible effect on the overall structural response.

Table 6.6 Maximum von Mises stress and horizontal sway of 150m-towers

Types of towers	Max. Stress (MPa)	Max. Stress of shell (MPa)	Max. Horizontal sway (mm)
T <sub>i</sub> R <sub>i</sub> H <sub>i</sub>	351.2	91.14	199.4
T <sub>ii</sub> R <sub>i</sub> H <sub>i</sub>	230.4	65.94	176.15
T <sub>iii</sub> R <sub>i</sub> H <sub>i</sub>	154.9	57.17	157.8
T <sub>iv</sub> R <sub>i</sub> H <sub>i</sub>	106.8	51.62	143.05
T <sub>i</sub> R <sub>ii</sub> H <sub>i</sub>	280.1	89.96	199.27
T <sub>ii</sub> R <sub>ii</sub> H <sub>i</sub>	194.4	64.75	176.04
T <sub>iii</sub> R <sub>ii</sub> H <sub>i</sub>	136.2	56.91	157.75
T <sub>iv</sub> R <sub>ii</sub> H <sub>i</sub>	96.71	51.49	142.97
T <sub>i</sub> R <sub>iii</sub> H <sub>i</sub>	210.5	83.08	198.97
T <sub>ii</sub> R <sub>iii</sub> H <sub>i</sub>	155.8	63.02	175.8
T <sub>iii</sub> R <sub>iii</sub> H <sub>i</sub>	114.7	56.47	157.55
T <sub>iv</sub> R <sub>iii</sub> H <sub>i</sub>	84.59	51.26	142.79
T <sub>i</sub> R <sub>iv</sub> H <sub>i</sub>	171.8	76.84	198.66
T <sub>ii</sub> R <sub>iv</sub> H <sub>i</sub>	132.5	62.37	175.55
T <sub>iii</sub> R <sub>iv</sub> H <sub>i</sub>	100.9	56.11	157.33
T <sub>iv</sub> R <sub>iv</sub> H <sub>i</sub>	76.45	51.07	142.61

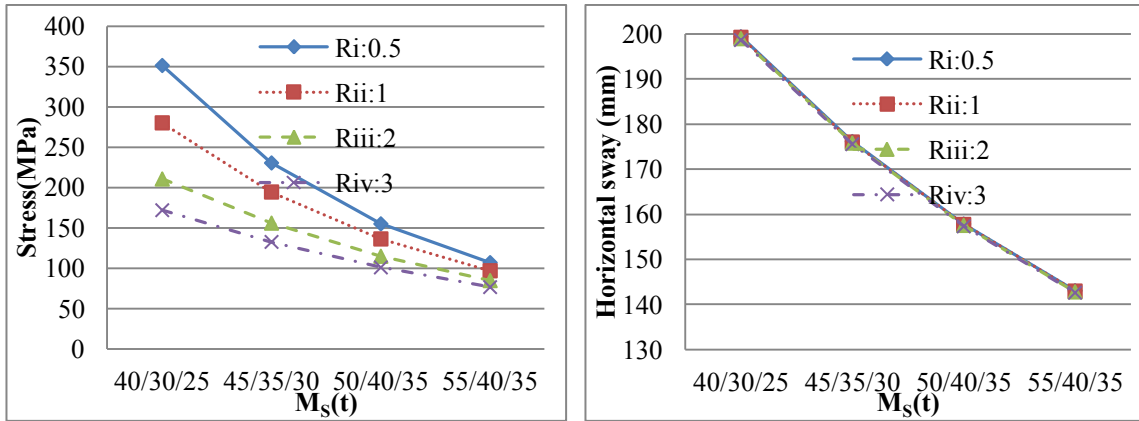
CHAPTER 7: VERTICAL STIFFENERS

$T_i R_i H_{ii}$	327.7	85.28	199.38
$T_{ii} R_i H_{ii}$	221.1	64.20	176.13
$T_{iii} R_i H_{ii}$	151.6	57.09	157.82
$T_{iv} R_i H_{ii}$	106.2	51.58	143.03
$T_i R_{ii} H_{ii}$	272.1	85.12	199.2
$T_{ii} R_{ii} H_{ii}$	195.5	63.56	175.98
$T_{iii} R_{ii} H_{ii}$	140.2	56.76	157.7
$T_{iv} R_{ii} H_{ii}$	101.3	51.41	142.92
$T_i R_{iii} H_{ii}$	187.3	76.53	198.84
$T_{ii} R_{iii} H_{ii}$	143.6	62.58	175.67
$T_{iii} R_{iii} H_{ii}$	109.2	56.23	157.44
$T_{iv} R_{iii} H_{ii}$	82.66	51.13	142.69
$T_i R_{iv} H_{ii}$	154.9	69.43	198.46
$T_{ii} R_{iv} H_{ii}$	122.5	61.82	175.36
$T_{iii} R_{iv} H_{ii}$	95.18	55.8	157.17
$T_{iv} R_{iv} H_{ii}$	73.28	50.89	142.46
$T_i R_i H_{iii}$	306.9	66.65	195.28
$T_{ii} R_i H_{iii}$	230.4	58.26	172.09
$T_{iii} R_i H_{iii}$	175.0	51.83	153.83
$T_{iv} R_i H_{iii}$	134.7	46.73	139.07
$T_i R_{ii} H_{iii}$	214.9	63.97	195.12
$T_{ii} R_{ii} H_{iii}$	169.8	56.54	171.94
$T_{iii} R_{ii} H_{iii}$	134.8	50.66	153.69
$T_{iv} R_{ii} H_{iii}$	107.7	45.92	138.94
$T_i R_{iii} H_{iii}$	137.0	61.25	194.79
$T_{ii} R_{iii} H_{iii}$	113.0	54.59	171.64
$T_{iii} R_{iii} H_{iii}$	93.31	49.25	153.42

CHAPTER 7: VERTICAL STIFFENERS

$T_{iv}R_{iii}H_{iii}$	77.38	44.89	138.7
$T_iR_{iv}H_{iii}$	101.4	59.71	194.44
$T_{ii}R_{iv}H_{iii}$	85.35	53.44	171.34
$T_{iii}R_{iv}H_{iii}$	71.96	48.39	153.16
$T_{iv}R_{iv}H_{iii}$	60.83	44.24	138.47
$T_iR_iH_{iv}$	274.9	65.68	195.24
$T_{ii}R_iH_{iv}$	211.1	57.71	172.05
$T_{iii}R_iH_{iv}$	163.3	51.46	153.79
$T_{iv}R_iH_{iv}$	127.6	46.48	139.04
$T_iR_{ii}H_{iv}$	188.0	62.92	195.03
$T_{ii}R_{ii}H_{iv}$	151.6	55.81	171.85
$T_{iii}R_{ii}H_{iv}$	122.6	50.15	153.62
$T_{iv}R_{ii}H_{iv}$	99.54	45.56	138.88
$T_iR_{iii}H_{iv}$	114.5	60.13	194.58
$T_{ii}R_{iii}H_{iv}$	96.26	53.77	171.46
$T_{iii}R_{iii}H_{iv}$	80.96	48.64	153.27
$T_{iv}R_{iii}H_{iv}$	68.47	44.44	138.56
$T_iR_{iv}H_{iv}$	86.74	58.63	194.13
$T_{ii}R_{iv}H_{iv}$	74.4	52.63	171.07
$T_{iii}R_{iv}H_{iv}$	63.89	47.77	152.92
$T_{iv}R_{iv}H_{iv}$	54.96	43.78	138.26

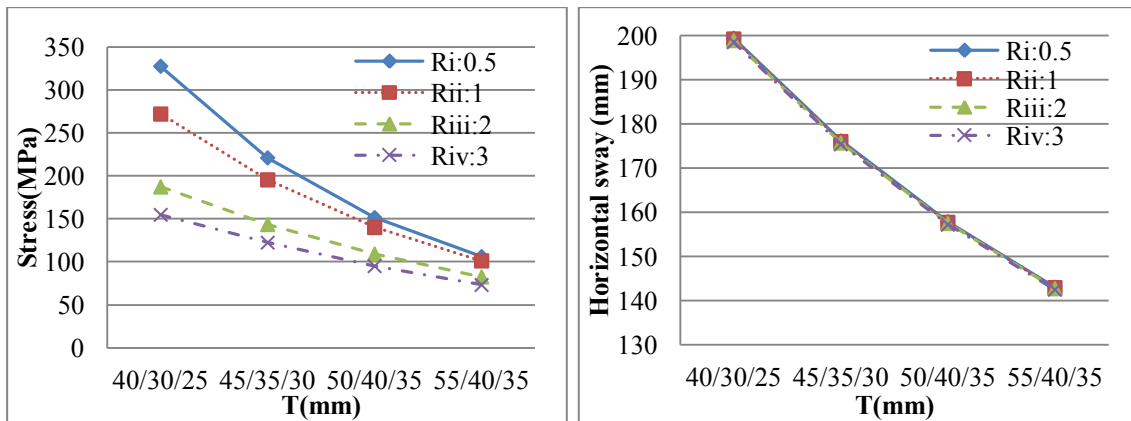
6.3.2 Effect of the thickness  $T$  on the overall structural response



a. Maximum von Mises stress

b. Maximum horizontal sway

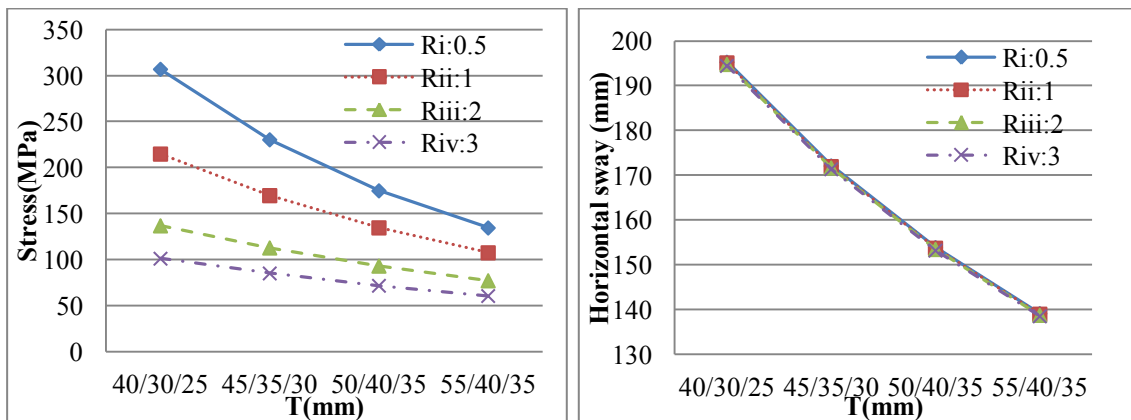
Figure 6.22 Maximum von Mises stress and horizontal sway versus  $T$  of the 150H<sub>i</sub>



a. Maximum von Mises stress

b. Maximum horizontal sway

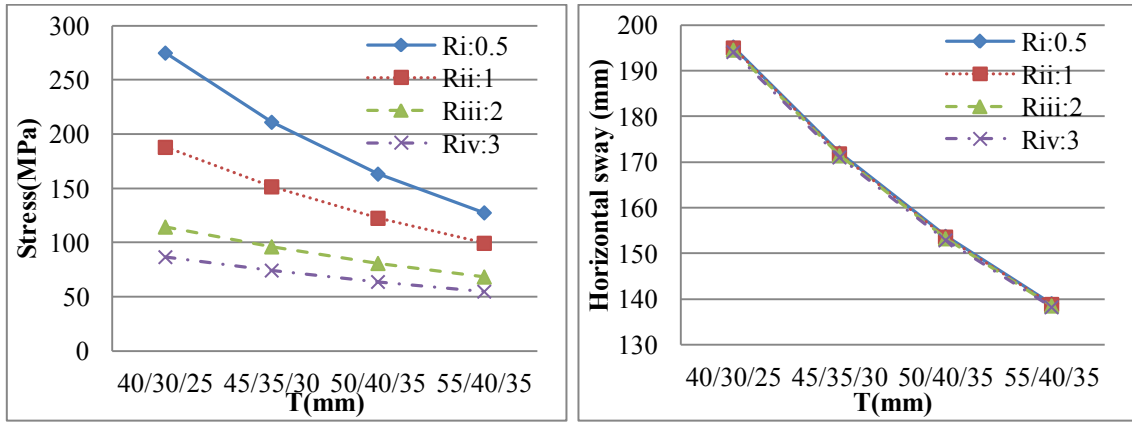
Figure 6.23 Maximum von Mises stress and horizontal sway versus  $T$  of the 150H<sub>ii</sub>



a. Maximum von Mises stress

b. Maximum horizontal sway

Figure 6.24 Maximum von Mises stress and horizontal sway versus T of the 150H<sub>iii</sub>



a. Maximum von Mises stress

b. Maximum horizontal sway

Figure 6.25 Maximum von Mises stress and horizontal sway versus T of the 150H<sub>iv</sub>

According to Figure 6.22 to 6.25, the horizontal axis refers to the thickness for the 150m-towers, and vertical axis refers to the maximum von Mises stresses and horizontal sways of the 150m-towers. Maximum von Mises stresses and horizontal sways of the 150H<sub>i</sub>/H<sub>ii</sub>/H<sub>iii</sub>/H<sub>iv</sub> decrease with wall thickness decreases. The maximum horizontal sway of 150m towers is close each other for each thickness case. Similarly, the rate of change of the maximum von Mises stress and the horizontal sway of the 50m-towers with respect to T can be also obtained by Eqs (6.1 to 6.2) and Table 6.6. The rate of change of maximum von Mises stresses and horizontal sways of the 150m-towers with respect to T are shown in Table 6.7.

Table 6.7 Rate of change  $\Delta S/\Delta T$  and  $\Delta D/\Delta T$  for the 150H<sub>i</sub>/H<sub>ii</sub>/H<sub>iii</sub>/H<sub>iv</sub> with respect to T

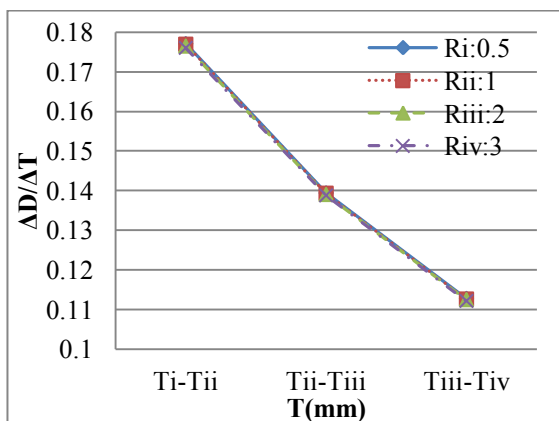
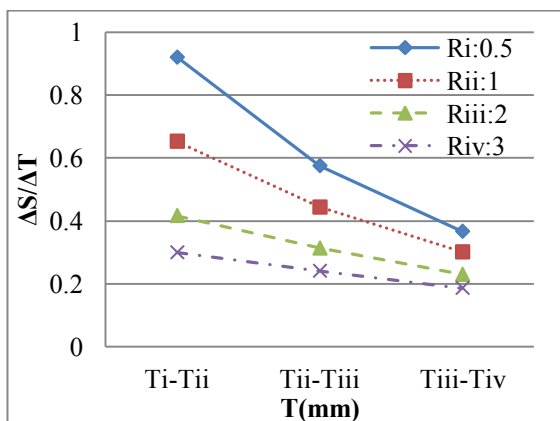
Types of rings	Ranges of thickness variations	$\Delta S/\Delta m$	$\Delta D/\Delta m$
R <sub>i</sub> H <sub>i</sub>	T <sub>i</sub> to T <sub>ii</sub>	0.92	0.18
	T <sub>ii</sub> to T <sub>iii</sub>	0.57	0.14
	T <sub>iii</sub> to T <sub>iv</sub>	0.37	0.11
R <sub>ii</sub> H <sub>i</sub>	T <sub>i</sub> to T <sub>ii</sub>	0.65	0.18

CHAPTER 7: VERTICAL STIFFENERS

	$T_{ii}$ to $T_{iii}$	0.44	0.14
	$T_{iii}$ to $T_{iv}$	0.30	0.11
$R_{iii}H_i$	$T_i$ to $T_{ii}$	0.42	0.18
	$T_{ii}$ to $T_{iii}$	0.31	0.14
	$T_{iii}$ to $T_{iv}$	0.23	0.11
$R_{iv}H_i$	$T_i$ to $T_{ii}$	0.30	0.18
	$T_{ii}$ to $T_{iii}$	0.24	0.14
	$T_{iii}$ to $T_{iv}$	0.19	0.11
$R_iH_{ii}$	$T_i$ to $T_{ii}$	0.81	0.18
	$T_{ii}$ to $T_{iii}$	0.53	0.14
	$T_{iii}$ to $T_{iv}$	0.35	0.11
$R_{ii}H_{ii}$	$T_i$ to $T_{ii}$	0.58	0.18
	$T_{ii}$ to $T_{iii}$	0.42	0.14
	$T_{iii}$ to $T_{iv}$	0.30	0.11
$R_{iii}H_{ii}$	$T_i$ to $T_{ii}$	0.33	0.18
	$T_{ii}$ to $T_{iii}$	0.26	0.14
	$T_{iii}$ to $T_{iv}$	0.20	0.11
$R_{iv}H_{ii}$	$T_i$ to $T_{ii}$	0.25	0.18
	$T_{ii}$ to $T_{iii}$	0.21	0.14
	$T_{iii}$ to $T_{iv}$	0.17	0.11
$R_iH_{iii}$	$T_i$ to $T_{ii}$	0.58	0.18
	$T_{ii}$ to $T_{iii}$	0.42	0.14
	$T_{iii}$ to $T_{iv}$	0.31	0.11
$R_{ii}H_{iii}$	$T_i$ to $T_{ii}$	0.34	0.18
	$T_{ii}$ to $T_{iii}$	0.27	0.14
	$T_{iii}$ to $T_{iv}$	0.21	0.11
$R_{iii}H_{iii}$	$T_i$ to $T_{ii}$	0.18	0.18

CHAPTER 7: VERTICAL STIFFENERS

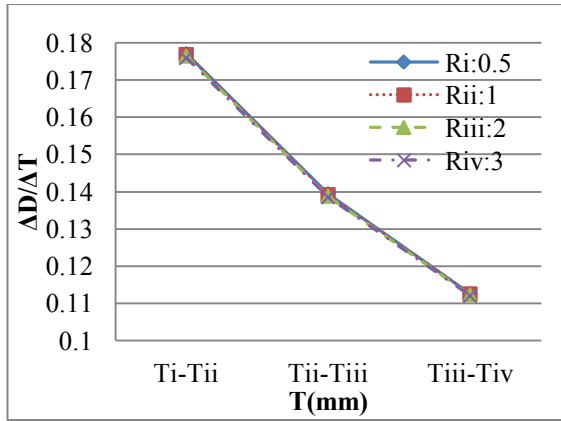
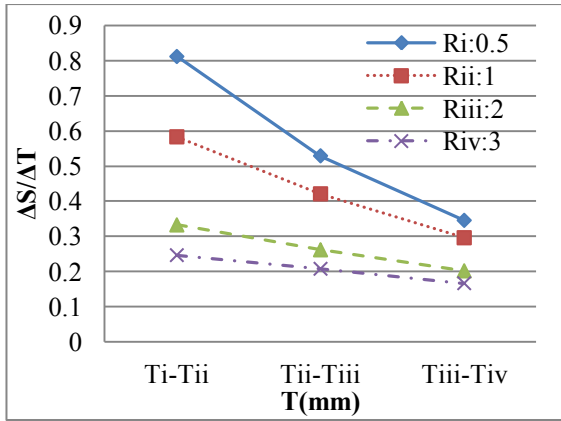
	$T_{ii}$ to $T_{iii}$	0.15	0.14
	$T_{iii}$ to $T_{iv}$	0.12	0.11
$R_{iv}H_{iii}$	$T_i$ to $T_{ii}$	0.12	0.18
	$T_{ii}$ to $T_{iii}$	0.10	0.14
	$T_{iii}$ to $T_{iv}$	0.08	0.11
$R_iH_{iv}$	$T_i$ to $T_{ii}$	0.49	0.18
	$T_{ii}$ to $T_{iii}$	0.36	0.14
	$T_{iii}$ to $T_{iv}$	0.27	0.11
$R_{ii}H_{iv}$	$T_i$ to $T_{ii}$	0.28	0.18
	$T_{ii}$ to $T_{iii}$	0.22	0.14
	$T_{iii}$ to $T_{iv}$	0.18	0.11
$R_{iii}H_{iv}$	$T_i$ to $T_{ii}$	0.14	0.18
	$T_{ii}$ to $T_{iii}$	0.12	0.14
	$T_{iii}$ to $T_{iv}$	0.095	0.11
$R_{iv}H_{iv}$	$T_i$ to $T_{ii}$	0.094	0.18
	$T_{ii}$ to $T_{iii}$	0.08	0.14
	$T_{iii}$ to $T_{iv}$	0.07	0.11



a. Rate of change of maximum von Mises stress

b. Rate of change of maximum horizontal sway

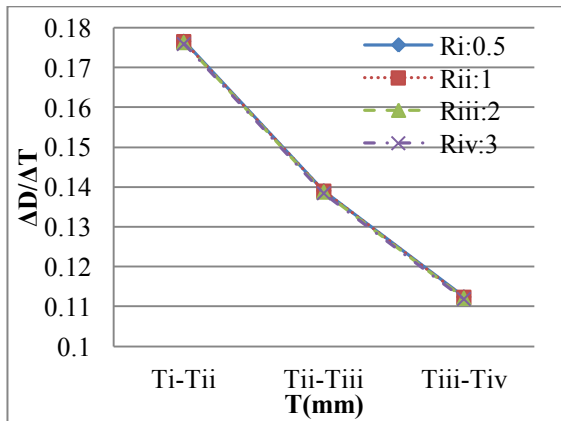
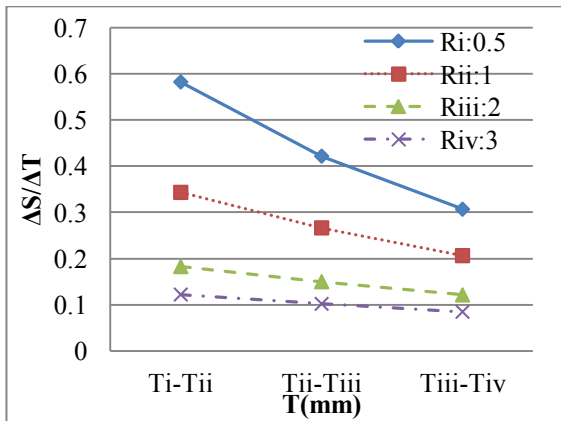
Figure 6.26  $\Delta S/\Delta T$  and  $\Delta D/\Delta T$  of the 150H<sub>i</sub> with respect to T



a. Rate of change of maximum von Mises stress

b. Rate of change of maximum horizontal sway

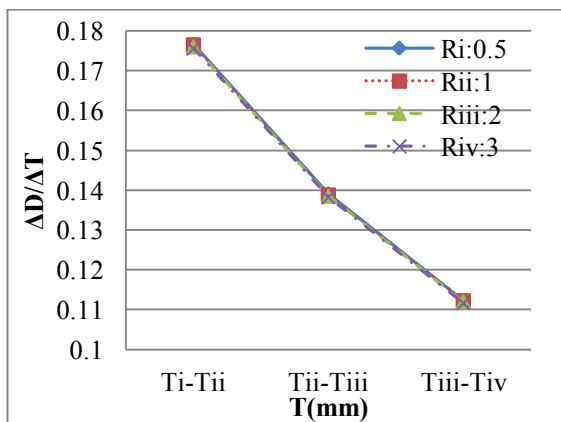
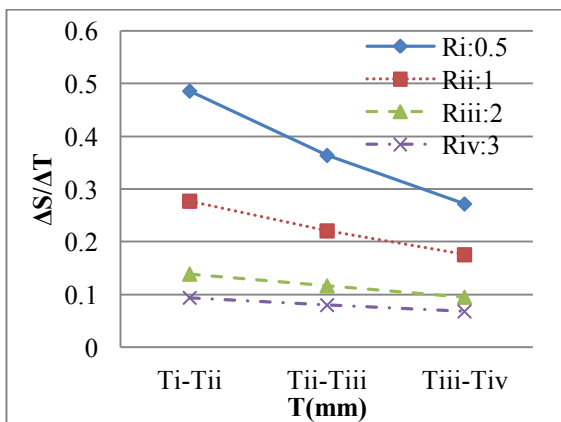
Figure 6.27  $\Delta S/\Delta T$  and  $\Delta D/\Delta T$  of the 150H<sub>ii</sub> with respect to T



a. Rate of change of maximum von Mises stress

b. Rate of change of maximum horizontal sway

Figure 6.28  $\Delta S/\Delta T$  and  $\Delta D/\Delta T$  of the 150H<sub>iii</sub> with respect to T



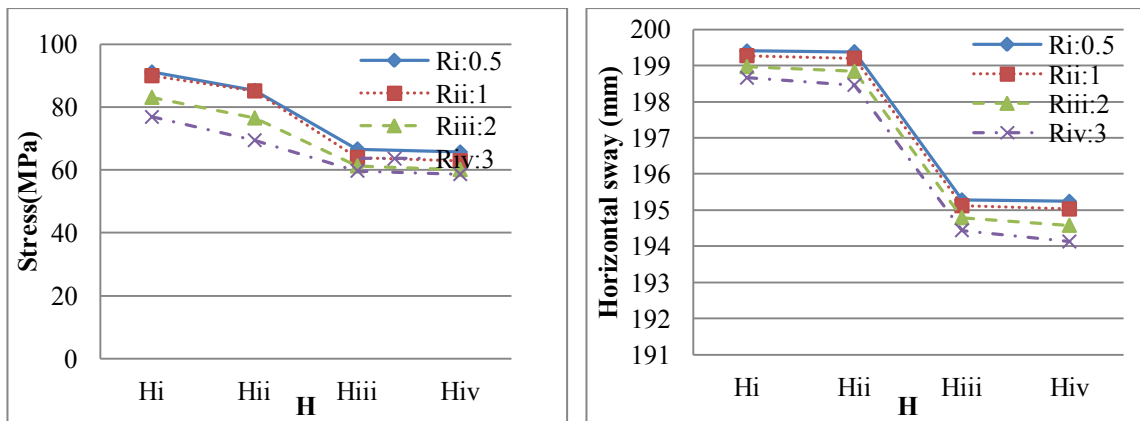
a. Rate of change of maximum von Mises stress

b. Rate of change of maximum horizontal sway

Figure 6.29  $\Delta S/\Delta T$  and  $\Delta D/\Delta T$  of the  $150H_{iv}$  with respect to T

For the 150m-towers, the rate of change of the 150m-towers when T varies from  $T_i$  to  $T_{ii}$  are also greater than those of the 150m towers when T increases from  $T_{ii}$  to  $T_{iv}$ . The rate of change of the maximum horizontal sway of the 150m-towers in each T variation range are also fairly close. According to Table 6.7, the rate of change of maximum horizontal sway tend to be linear curves with respect to each T variation for intermediate height towers. For the intermediate height tower, the efficiency range of thickness variation in thin walled towers is also more critical than that in thick walled towers in terms of the strengthening of the towers.

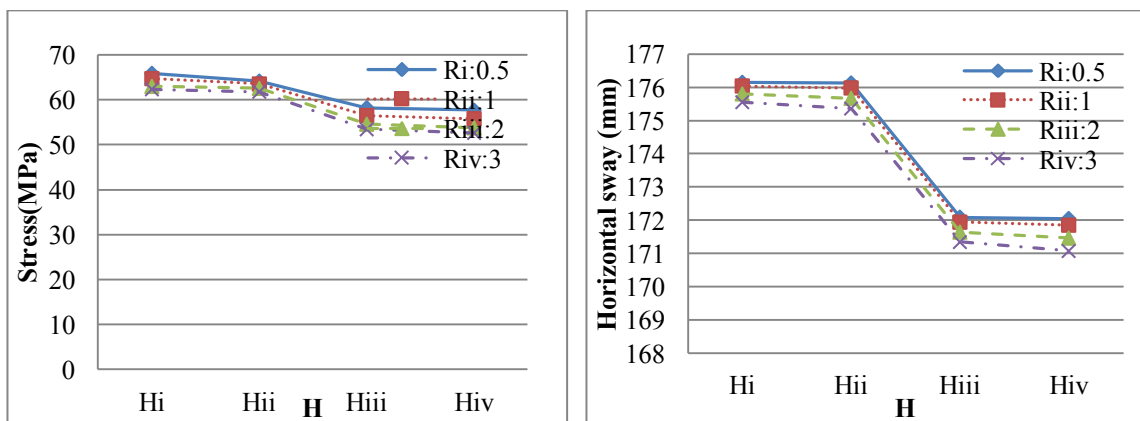
### 6.3.3 Effect of the spacing H of stiffening rings on the overall structural response



a. Maximum von Mises stress

b. Maximum horizontal sway

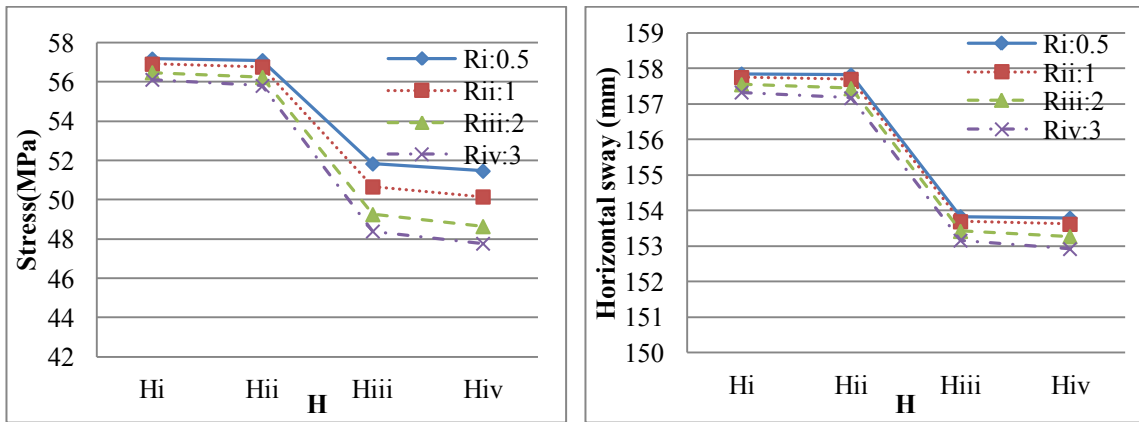
Figure 6.30 Maximum von Mises stresses and horizontal sways versus H of the  $150T_i$



a. Maximum von Mises stress

b. Maximum horizontal sway

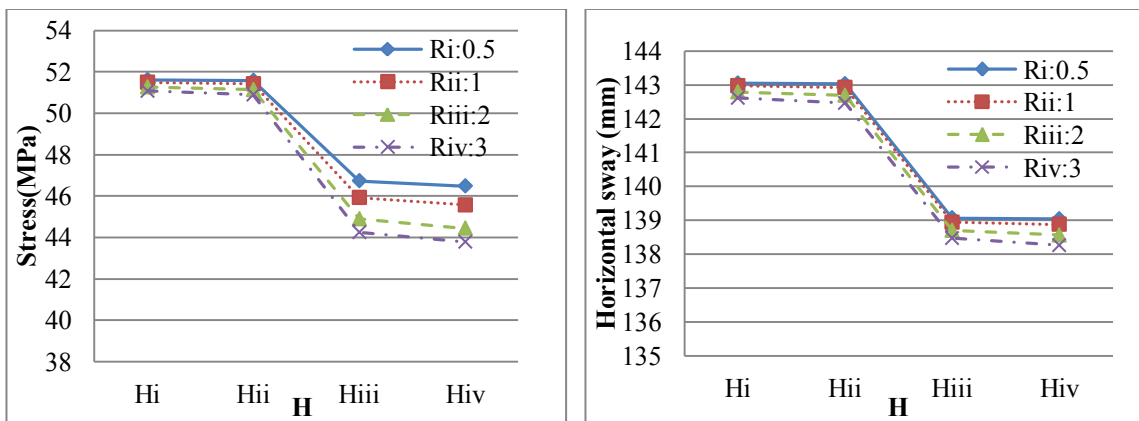
Figure 6.31 Maximum von Mises stresses and horizontal sways versus H of the 150T<sub>ii</sub>



a. Maximum von Mises stress

b. Maximum horizontal sway

Figure 6.32 Maximum von Mises stresses and horizontal sways versus H of the 150T<sub>iii</sub>



a. Maximum von Mises stress

b. Maximum horizontal sway

Figure 6.33 Maximum von Mises stresses and horizontal sways versus H of the 150T<sub>iv</sub>

The maximum von Mises stresses and horizontal sways versus ring distances of the 150T<sub>i</sub>/T<sub>ii</sub>/T<sub>iii</sub>/T<sub>iv</sub> are presented in Figure 6.30 to 6.33. The horizontal axis represents the H distance between two stiffening rings, and the vertical axis refers to the maximum von Mises stresses or the horizontal sways of each tower (Figure 6.30 to 6.33). Obviously, the maximum von Mises stresses and the horizontal sways reduce with the distances H decreasing in accordance to Table 6.7. Similarly, the rate of change of the maximum von Mises stress and the horizontal sway of 150m-towers with respect

CHAPTER 7: VERTICAL STIFFENERS

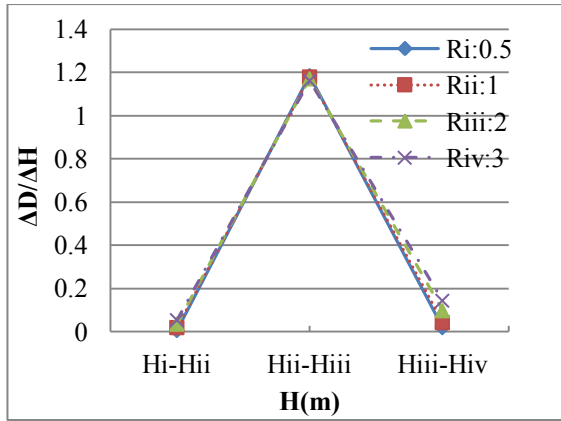
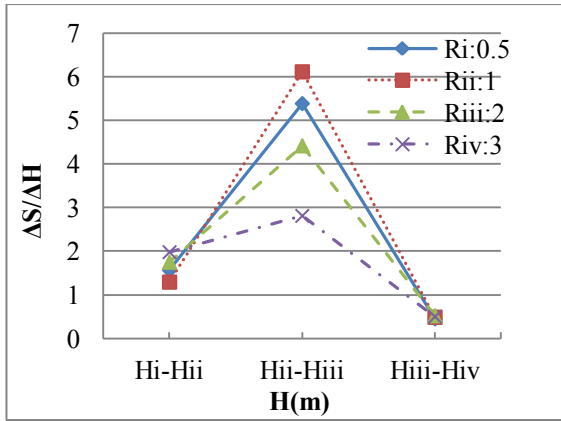
to the distance H should be obtained by referring to Eqs. (6.5, 6.6) and Table 6.7. The rate of change of maximum von Mises stresses and horizontal sways of 150m towers with respect to the distances H are displayed in Table 6.8.

Table 6.8 The  $\Delta S/\Delta H$  and  $\Delta D/\Delta H$  of the  $150T_i/T_{ii}/T_{iii}/T_{iv}$  with respect to H

Types of rings	Ranges of H variation	$\Delta S/\Delta H$	$\Delta D/\Delta H$
$T_i R_i$	$H_i$ to $H_{ii}$	1.56	0.62
	$H_{ii}$ to $H_{iii}$	5.38	0.017
	$H_{iii}$ to $H_{iv}$	0.45	0.138
$T_i R_{ii}$	$H_i$ to $H_{ii}$	1.29	0.56
	$H_{ii}$ to $H_{iii}$	6.11	0.027
	$H_{iii}$ to $H_{iv}$	0.48	0.169
$T_i R_{iii}$	$H_i$ to $H_{ii}$	1.75	0.528
	$H_{ii}$ to $H_{iii}$	4.42	0.054
	$H_{iii}$ to $H_{iv}$	0.52	0.22
$T_i R_{iv}$	$H_i$ to $H_{ii}$	1.98	0.51
	$H_{ii}$ to $H_{iii}$	2.81	0.073
	$H_{iii}$ to $H_{iv}$	0.50	0.25
$T_{ii} R_i$	$H_i$ to $H_{ii}$	0.46	0.00075
	$H_{ii}$ to $H_{iii}$	1.72	0.0043
	$H_{iii}$ to $H_{iv}$	0.25	0.12
$T_{ii} R_{ii}$	$H_i$ to $H_{ii}$	0.32	0.0012
	$H_{ii}$ to $H_{iii}$	2.03	0.0091
	$H_{iii}$ to $H_{iv}$	0.34	0.137
$T_{ii} R_{iii}$	$H_i$ to $H_{ii}$	0.12	0.0062
	$H_{ii}$ to $H_{iii}$	2.31	0.024
	$H_{iii}$ to $H_{iv}$	0.38	0.148

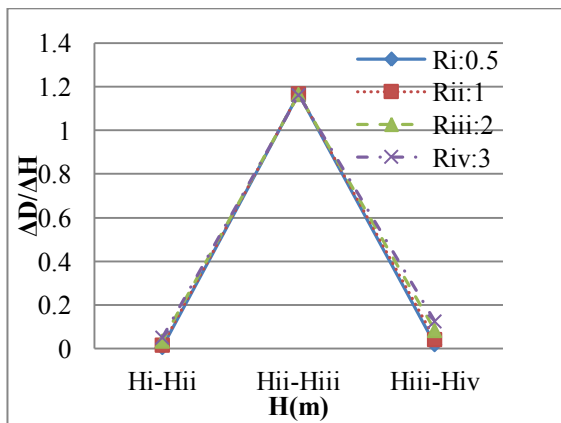
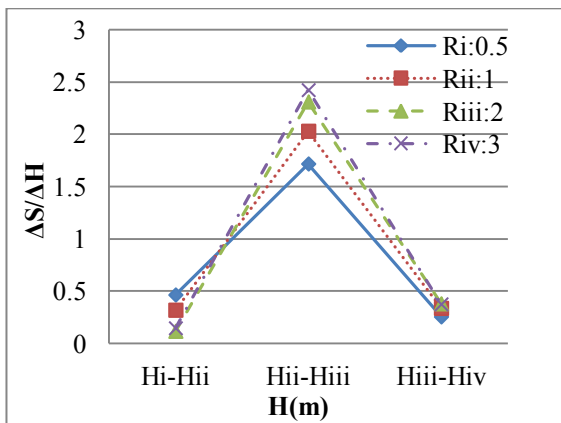
CHAPTER 7: VERTICAL STIFFENERS

$T_{ii}R_{iv}$	$H_i$ to $H_{ii}$	0.15	0.00915
	$H_{ii}$ to $H_{iii}$	2.42	0.035
	$H_{iii}$ to $H_{iv}$	0.37	0.16
$T_{iii}R_i$	$H_i$ to $H_{ii}$	0.02	0
	$H_{ii}$ to $H_{iii}$	1.52	0.0019
	$H_{iii}$ to $H_{iv}$	0.17	0.118
$T_{iii}R_{ii}$	$H_i$ to $H_{ii}$	0.039	0
	$H_{ii}$ to $H_{iii}$	1.76	0.0052
	$H_{iii}$ to $H_{iv}$	0.24	0.128
$T_{iii}R_{iii}$	$H_i$ to $H_{ii}$	0.064	0.0033
	$H_{ii}$ to $H_{iii}$	2.02	0.015
	$H_{iii}$ to $H_{iv}$	0.28	0.127
$T_{iii}R_{iv}$	$H_i$ to $H_{ii}$	0.083	0.0056
	$H_{ii}$ to $H_{iii}$	2.14	0.023
	$H_{iii}$ to $H_{iv}$	0.29	0.13
$T_{iv}R_i$	$H_i$ to $H_{ii}$	0.011	0
	$H_{ii}$ to $H_{iii}$	1.40	0.0016
	$H_{iii}$ to $H_{iv}$	0.12	0.117
$T_{iv}R_{ii}$	$H_i$ to $H_{ii}$	0.02	0.0003
	$H_{ii}$ to $H_{iii}$	1.59	0.0035
	$H_{iii}$ to $H_{iv}$	0.17	0.125
$T_{iv}R_{iii}$	$H_i$ to $H_{ii}$	0.035	0.0027
	$H_{ii}$ to $H_{iii}$	1.80	0.011
	$H_{iii}$ to $H_{iv}$	0.21	0.118
$T_{iv}R_{iv}$	$H_i$ to $H_{ii}$	0.047	0.0046
	$H_{ii}$ to $H_{iii}$	1.92	0.0168
	$H_{iii}$ to $H_{iv}$	0.21	0.119



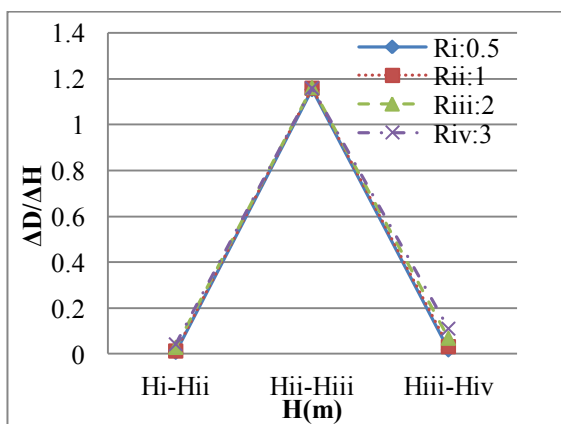
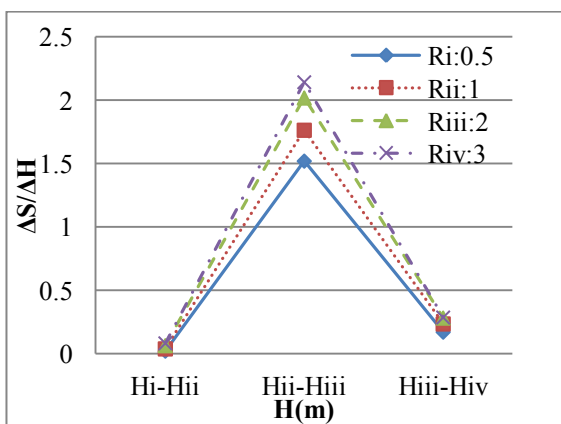
a. Rate of change of maximum von Mises stress      b. Rate of change of maximum horizontal sway

Figure 6.34 The  $\Delta S/\Delta H$  and  $\Delta D/\Delta H$  graphs of the  $150T_i$  with respect to  $H$



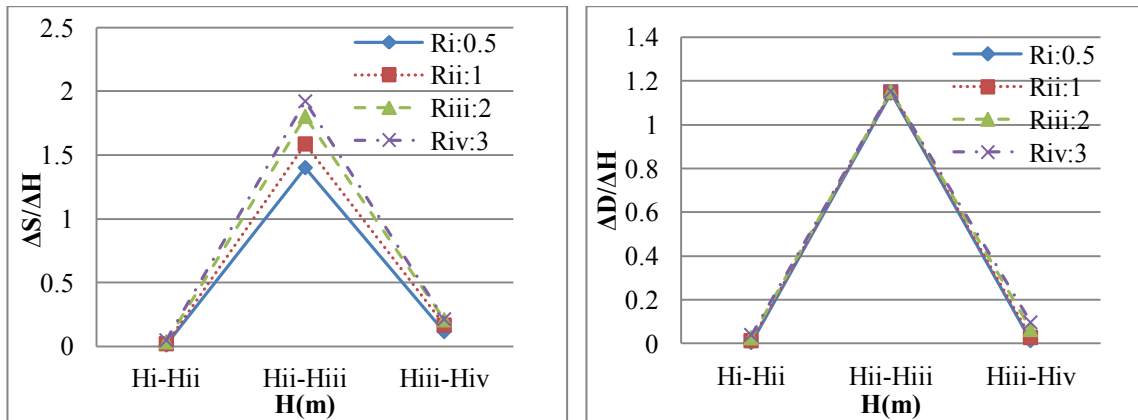
a. Rate of change of maximum von Mises stress      b. Rate of change of maximum horizontal sway

Figure 6.35 The  $\Delta S/\Delta H$  and  $\Delta D/\Delta H$  graphs of the  $150T_{ii}$  with respect to  $H$



a. Rate of change of maximum von Mises stress      b. Rate of change of maximum horizontal sway

Figure 6.36 The  $\Delta S/\Delta H$  and  $\Delta D/\Delta H$  graphs of the  $150T_{iii}$  with respect to H



- a. Rate of change of maximum von Mises stress      b. Rate of change of maximum horizontal sway

Figure 6.37 The  $\Delta S/\Delta H$  and  $\Delta D/\Delta H$  graphs of the  $150T_{iv}$  with respect to H

For the 150m-towers, the rate of change of the maximum von Mises stresses and of the horizontal sways of the  $150T_i/T_{ii}/T_{iii}/T_{iv}$  due to H variation are presented in Figure 6.34 to 6.37. As the peak of rate of change of the maximum von Mises stress and of the horizontal sway lie in the range of  $H_{ii}$  to  $H_{iii}$ , the most significant range of H variation for the 150m towers is from  $H_{ii}$  to  $H_{iii}$ . Concerning intermediate towers, the most significant ranges of two neighbouring rings are the intermediate distance.

## 6. 4 250m towers

### 6.4.1 Models of 250m towers

Four stiffening ring spacing distances for the 250m towers (2.5m, 16.667m, 11.364m and 8.612m, referred to as  $-H_i$ ,  $-H_{ii}$ ,  $-H_{iii}$  and  $-H_{iv}$  respectively) were investigated, as shown in Figure 6.38. The four widths of stiffening rings are 50mm, 100mm, 200mm and 300mm respectively (as shown in Figure 6.2). The mid-section thickness of all of the stiffening rings of the 250m-towers is 100mm. The R of the 250m towers are 0.5, 1, 2 and 3 respectively (referred to as  $-R_i$ ,  $-R_{ii}$ ,  $-R_{iii}$ ,  $-R_{iv}$ ). The thickness details for the 250m-towers are presented in Table 6.9, and the corresponding thickness groups are 60/50/45mm, 65/55/50mm, 70/60/55mm and 75/65/60mm respectively (referred to as  $-T_i$ ,

— $\mathbb{T}$ ”, — $\mathbb{T}_{iii}$ ”, — $\mathbb{T}_{iv}$ ”). The diameters of the tubular 250m towers gradually reduce from 14m to 9.5m as shown in Figure 6.38. The base of the 250m towers is considered as fixed, and the other parameters of the 250m-tower models are the same as those of the 50m and 150m towers.

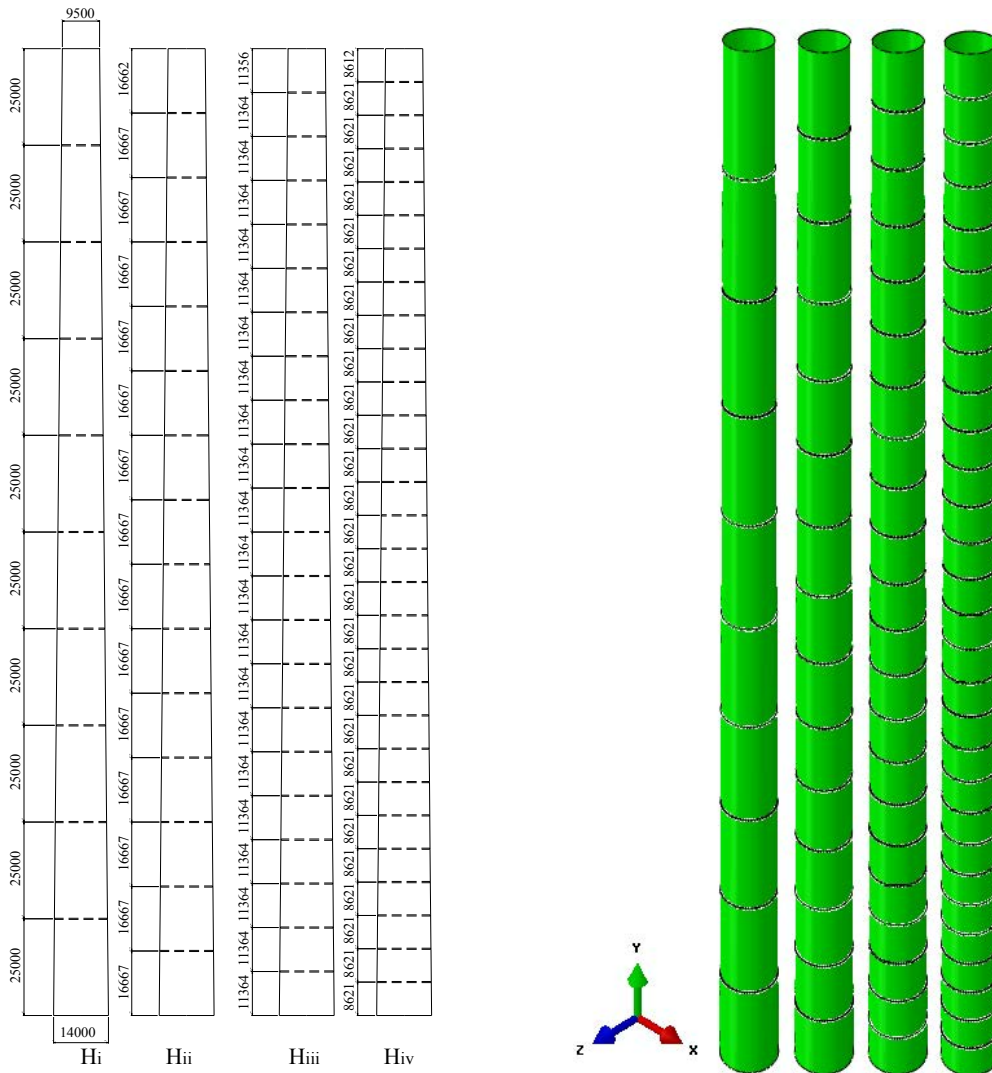
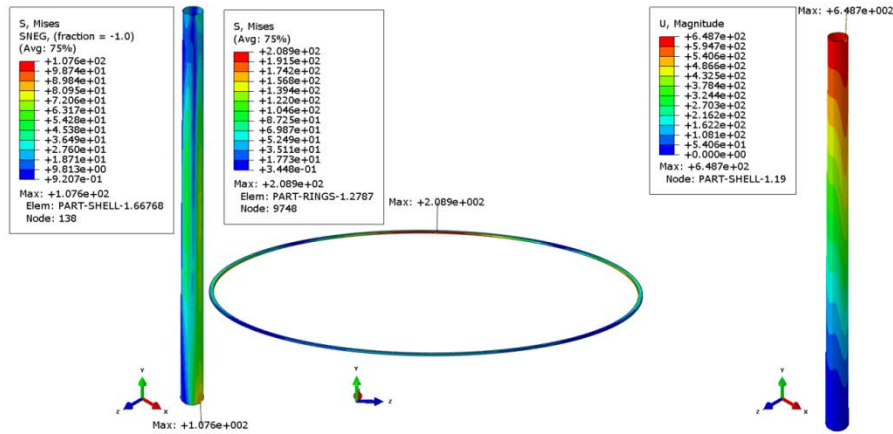


Figure 6.38 The 250m-towers: geometrical data and the FEM models (in mm)

## CHAPTER 7: VERTICAL STIFFENERS



a. von Mises stress: shell

b. von Mises stress: ring

c. Horizontal sway

Figure 6.39 The von Mises stress of the shell and the ring, and the horizontal sway of 250T<sub>i</sub>R<sub>i</sub>H<sub>i</sub> tower

Table 6.9 Parameter details of the 250m-towers

250m towers	Height range of the towers			Weight of the shell (t)	Ratio of mid-section width-to-thickness of rings		Spacing of rings (m)	
	0 to100m	100m to 200m	200m to 250m					
	Thickness	Thickness	Thickness					
T <sub>i</sub>	60mm	50mm	45mm	3884.04	R <sub>i</sub>	0.5	H <sub>i</sub>	2.5
T <sub>ii</sub>	65mm	55mm	50mm	4246.27	R <sub>ii</sub>	1	H <sub>ii</sub>	16.667
T <sub>iii</sub>	70mm	60mm	65mm	4608.50	R <sub>iii</sub>	2	H <sub>iii</sub>	11.364
T <sub>iv</sub>	75mm	65mm	60mm	4970.73	R <sub>iv</sub>	3	H <sub>iv</sub>	8.612

The contours of the von Mises stress in the shell and in the rings, as well as the horizontal sway of 250T<sub>i</sub>R<sub>i</sub>H<sub>i</sub> are displayed in Figure 6.39. The magnitude of the maximum von Mises stress in the shell is 107.6MPa, which occurs in the region near the base of the tower. The magnitude of the maximum von Mises stress in the rings is 208.9MPa, and the maximum horizontal sway is 648.7mm at the top of the tower. The maximum von Mises stresses and horizontal sways of 250m towers are shown in Table 6.10. The stiffener ring slenderness is also not regarded as the design parameter according to Table 6.10.

CHAPTER 7: VERTICAL STIFFENERS

Table 6.10 Maximum von Mises stress and horizontal sway of 250m towers

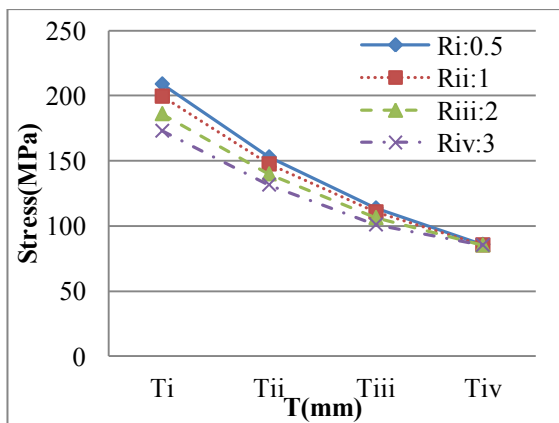
Types of towers	Max. Stress (MPa)	Max. Stress of shell (MPa)	Max. Horizontal sway (mm)
$T_i R_i H_i$	208.9	107.6	648.75
$T_{ii} R_i H_i$	152.9	98.74	598.28
$T_{iii} R_i H_i$	113.7	91.45	555.10
$T_{iv} R_i H_i$	85.79	85.39	517.76
$T_i R_{ii} H_i$	199.5	107.47	648.53
$T_{ii} R_{ii} H_i$	147.5	98.65	598.07
$T_{iii} R_{ii} H_i$	110.7	91.42	554.91
$T_{iv} R_{ii} H_i$	85.379	85.379	517.58
$T_i R_{iii} H_i$	186.1	107.16	648.00
$T_{ii} R_{iii} H_i$	139.9	98.498	597.57
$T_{iii} R_{iii} H_i$	106.4	91.348	554.44
$T_{iv} R_{iii} H_i$	85.36	85.36	517.15
$T_i R_{iv} H_i$	173.0	106.88	647.43
$T_{ii} R_{iv} H_i$	131.6	98.35	597.02
$T_{iii} R_{iv} H_i$	101.0	91.287	553.93
$T_{iv} R_{iv} H_i$	85.35	85.347	516.68
$T_i R_i H_{ii}$	308.2	96.47	636.62
$T_{ii} R_i H_{ii}$	243.5	88.356	586.11
$T_{iii} R_i H_{ii}$	195.7	81.64	542.93
$T_{iv} R_i H_{ii}$	159.8	76.0	505.6
$T_i R_{ii} H_{ii}$	266.8	95.246	636.59
$T_{ii} R_{ii} H_{ii}$	215.4	87.495	585.99
$T_{iii} R_{ii} H_{ii}$	175.9	81.023	542.77
$T_{iv} R_{ii} H_{ii}$	145.3	75.547	505.42

CHAPTER 7: VERTICAL STIFFENERS

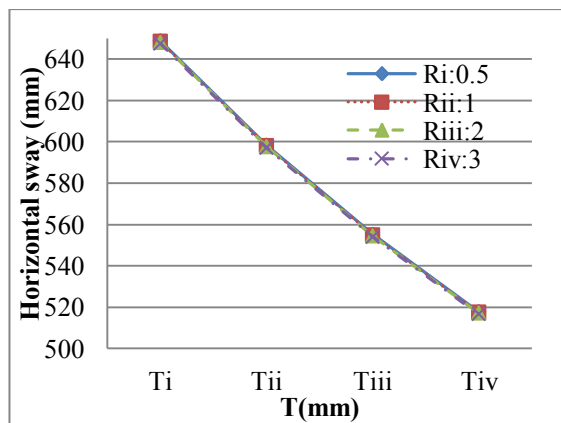
$T_i R_{iii} H_{ii}$	211.5	93.51	636.33
$T_{ii} R_{iii} H_{ii}$	175.1	86.23	585.64
$T_{iii} R_{iii} H_{ii}$	146.1	80.09	542.38
$T_{iv} R_{iii} H_{ii}$	123.2	74.85	505.02
$T_i R_{iv} H_{ii}$	176.6	92.3	635.95
$T_{ii} R_{iv} H_{ii}$	148.5	85.325	585.23
$T_{iii} R_{iv} H_{ii}$	125.9	79.41	541.96
$T_{iv} R_{iv} H_{ii}$	107.5	74.33	504.61
$T_i R_i H_{iii}$	290.6	95.81	636.61
$T_{ii} R_i H_{iii}$	232.7	87.9	586.07
$T_{iii} R_i H_{iii}$	188.8	81.32	542.87
$T_{iv} R_i H_{iii}$	155.1	75.764	505.52
$T_i R_{ii} H_{iii}$	241.4	94.21	636.48
$T_{ii} R_{ii} H_{iii}$	197.8	86.76	585.82
$T_{iii} R_{ii} H_{iii}$	163.5	80.485	542.58
$T_{iv} R_{ii} H_{iii}$	136.3	75.15	505.22
$T_i R_{iii} H_{iii}$	185.6	92.11	635.9
$T_{ii} R_{iii} H_{iii}$	156.3	85.187	585.18
$T_{iii} R_{iii} H_{iii}$	132.5	79.31	541.92
$T_{iv} R_{iii} H_{iii}$	112.9	74.26	504.56
$T_i R_{iv} H_{iii}$	147.7	90.75	635.18
$T_{ii} R_{iv} H_{iii}$	126.6	84.15	584.46
$T_{iii} R_{iv} H_{iii}$	109.0	78.504	541.21
$T_{iv} R_{iv} H_{iii}$	94.25	73.64	503.9
$T_i R_i H_{iv}$	279.5	95.203	636.6
$T_{ii} R_i H_{iv}$	225.0	87.47	586.00
$T_{iii} R_i H_{iv}$	183.4	81.01	542.77

$T_{iv}R_iH_{iv}$	151.1	75.54	505.43
$T_iR_{ii}H_{iv}$	224.0	93.32	636.34
$T_{ii}R_{ii}H_{iv}$	186.0	86.11	585.64
$T_{iii}R_{ii}H_{iv}$	155.6	80.01	542.38
$T_{iv}R_{ii}H_{iv}$	131.1	74.79	505.02
$T_iR_{iii}H_{iv}$	159.3	90.98	635.41
$T_{ii}R_{iii}H_{iv}$	136.4	84.34	584.68
$T_{iii}R_{iii}H_{iv}$	117.2	78.66	541.43
$T_{iv}R_{iii}H_{iv}$	101.2	73.76	504.1
$T_iR_{iv}H_{iv}$	128.1	89.57	634.32
$T_{ii}R_{iv}H_{iv}$	111.2	83.23	583.64
$T_{iii}R_{iv}H_{iv}$	96.80	77.8	540.44
$T_{iv}R_{iv}H_{iv}$	84.56	73.09	503.17

### 6.4.2 Effect of the thickness $T$ on the overall structural response

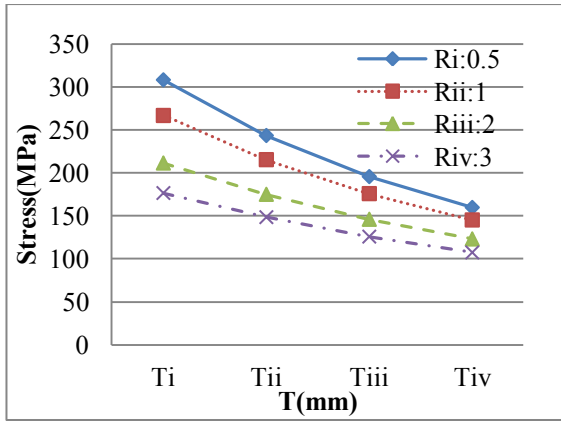


a. Maximum von Mises stress

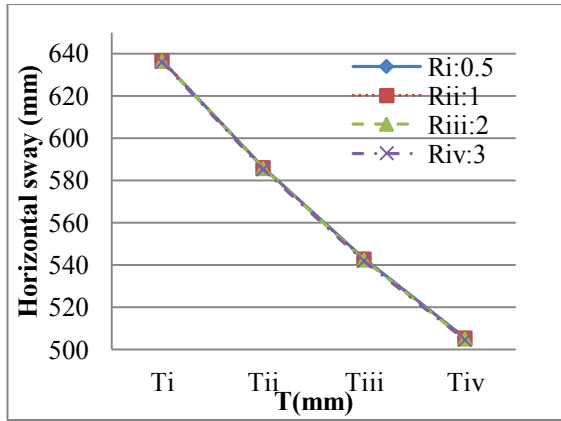


b. Maximum horizontal sway

Figure 6.40 Maximum von Mises stress and horizontal sway versus  $T$  of the  $250H_i$

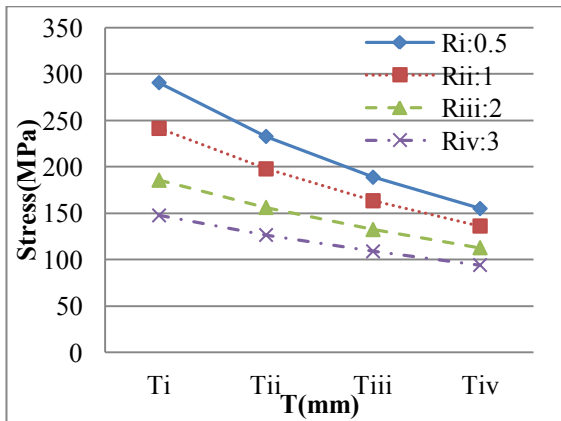


a. Maximum von Mises stress

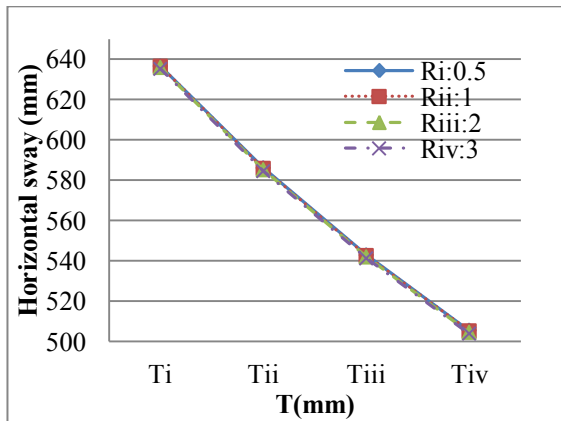


b. Maximum horizontal sway

Figure 6.41 Maximum von Mises stress and horizontal sway versus T of the 250Hii

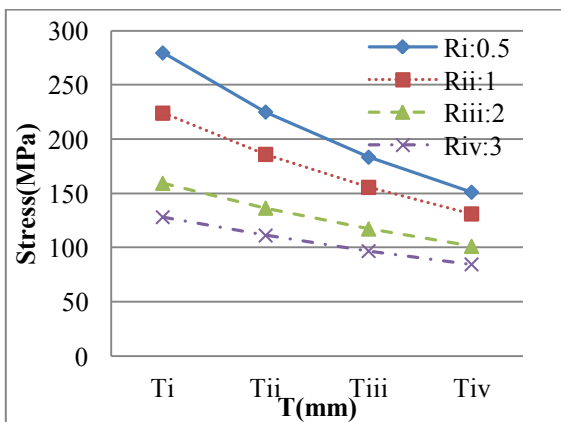


a. Maximum von Mises stress

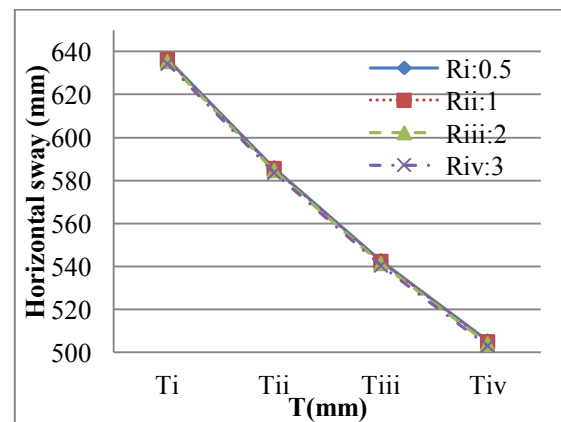


b. Maximum horizontal sway

Figure 6.42 Maximum von Mises stress and horizontal sway versus T of the 250Hiii



a. Maximum von Mises stress



b. Maximum horizontal sway

CHAPTER 7: VERTICAL STIFFENERS

Figure 6.43 Maximum von Mises stress and horizontal sway versus T of the 250H<sub>iv</sub>

In Figure 6.40 to 6.43, maximum von Mises stresses and horizontal sways of the 250H<sub>i</sub>/H<sub>ii</sub>/H<sub>iii</sub>/H<sub>iv</sub> are displayed. The strength of 250m-towers is negative with reference to wall thickness. The maximum horizontal sways of 250m-towers for each thickness case is close each other. More significant range of thickness variation can be obtained by calculating the rate of change of the maximum von Mises stress and horizontal sway of 250m-towers with respect to wall thickness. The rate of change  $\Delta S/\Delta m$  and  $\Delta D/\Delta m$  of 250m towers with respect to wall thickness are displayed in Table 6.11 obtained by Eqs. (6.1, 6.2) and Table 6.10.

Table 6.11 Rate of change  $\Delta S/\Delta T$  and  $\Delta D/\Delta T$  for the 250H<sub>i</sub>/H<sub>ii</sub>/H<sub>iii</sub>/H<sub>iv</sub> with respect to T

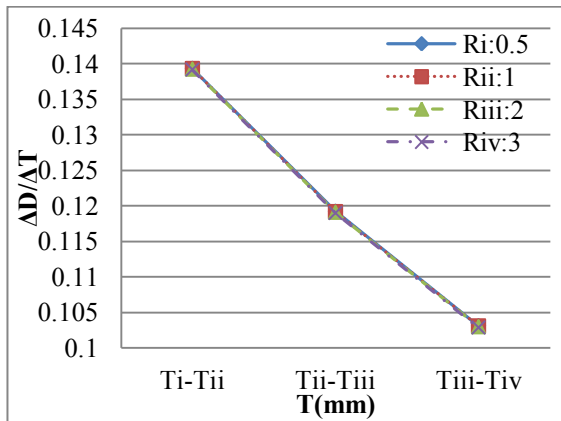
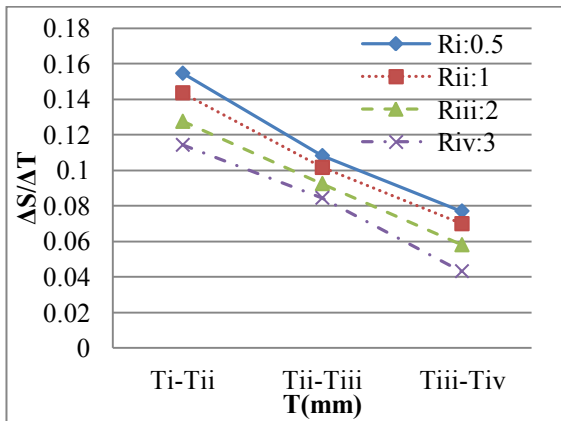
Types of rings	Ranges of thickness variations	$\Delta S/\Delta T$	$\Delta D/\Delta T$
R <sub>i</sub> H <sub>i</sub>	T <sub>i</sub> to T <sub>ii</sub>	0.15	0.14
	T <sub>ii</sub> to T <sub>iii</sub>	0.11	0.12
	T <sub>iii</sub> to T <sub>iv</sub>	0.08	0.10
R <sub>ii</sub> H <sub>i</sub>	T <sub>i</sub> to T <sub>ii</sub>	0.14	0.14
	T <sub>ii</sub> to T <sub>iii</sub>	0.10	0.12
	T <sub>iii</sub> to T <sub>iv</sub>	0.07	0.10
R <sub>iii</sub> H <sub>i</sub>	T <sub>i</sub> to T <sub>ii</sub>	0.13	0.14
	T <sub>ii</sub> to T <sub>iii</sub>	0.09	0.12
	T <sub>iii</sub> to T <sub>iv</sub>	0.06	0.10
R <sub>iv</sub> H <sub>i</sub>	T <sub>i</sub> to T <sub>ii</sub>	0.11	0.14
	T <sub>ii</sub> to T <sub>iii</sub>	0.08	0.12
	T <sub>iii</sub> to T <sub>iv</sub>	0.04	0.10
R <sub>i</sub> H <sub>ii</sub>	T <sub>i</sub> to T <sub>ii</sub>	0.18	0.14
	T <sub>ii</sub> to T <sub>iii</sub>	0.13	0.12
	T <sub>iii</sub> to T <sub>iv</sub>	0.099	0.10
R <sub>ii</sub> H <sub>ii</sub>	T <sub>i</sub> to T <sub>ii</sub>	0.14	0.14

CHAPTER 7: VERTICAL STIFFENERS

	$T_{ii}$ to $T_{iii}$	0.11	0.12
	$T_{iii}$ to $T_{iv}$	0.08	0.10
$R_{iii}H_{ii}$	$T_i$ to $T_{ii}$	0.10	0.14
	$T_{ii}$ to $T_{iii}$	0.08	0.12
	$T_{iii}$ to $T_{iv}$	0.06	0.10
$R_{iv}H_{ii}$	$T_i$ to $T_{ii}$	0.08	0.14
	$T_{ii}$ to $T_{iii}$	0.06	0.12
	$T_{iii}$ to $T_{iv}$	0.05	0.10
$R_iH_{iii}$	$T_i$ to $T_{ii}$	0.16	0.14
	$T_{ii}$ to $T_{iii}$	0.12	0.12
	$T_{iii}$ to $T_{iv}$	0.09	0.10
$R_{ij}H_{iii}$	$T_i$ to $T_{ii}$	0.12	0.14
	$T_{ii}$ to $T_{iii}$	0.09	0.12
	$T_{iii}$ to $T_{iv}$	0.075	0.10
$R_{iii}H_{iii}$	$T_i$ to $T_{ii}$	0.08	0.14
	$T_{ii}$ to $T_{iii}$	0.066	0.12
	$T_{iii}$ to $T_{iv}$	0.05	0.10
$R_{iv}H_{iii}$	$T_i$ to $T_{ii}$	0.06	0.14
	$T_{ii}$ to $T_{iii}$	0.049	0.12
	$T_{iii}$ to $T_{iv}$	0.04	0.10
$R_iH_{iv}$	$T_i$ to $T_{ii}$	0.15	0.14
	$T_{ii}$ to $T_{iii}$	0.11	0.12
	$T_{iii}$ to $T_{iv}$	0.089	0.10
$R_{ii}H_{iv}$	$T_i$ to $T_{ii}$	0.10	0.14
	$T_{ii}$ to $T_{iii}$	0.084	0.12
	$T_{iii}$ to $T_{iv}$	0.068	0.10
$R_{iii}H_{iv}$	$T_i$ to $T_{ii}$	0.06	0.14

CHAPTER 7: VERTICAL STIFFENERS

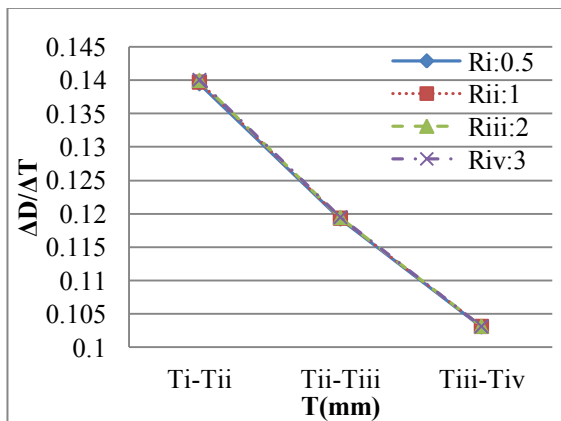
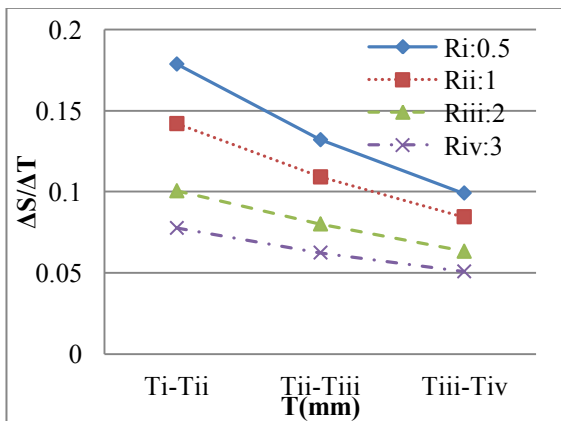
	$T_{ii}$ to $T_{iii}$	0.053	0.12
	$T_{iii}$ to $T_{iv}$	0.044	0.10
$R_{iv}H_{iv}$	$T_i$ to $T_{ii}$	0.047	0.14
	$T_{ii}$ to $T_{iii}$	0.04	0.12
	$T_{iii}$ to $T_{iv}$	0.034	0.10



a. Rate of change of maximum von Mises stress

b. Rate of change of maximum horizontal sway

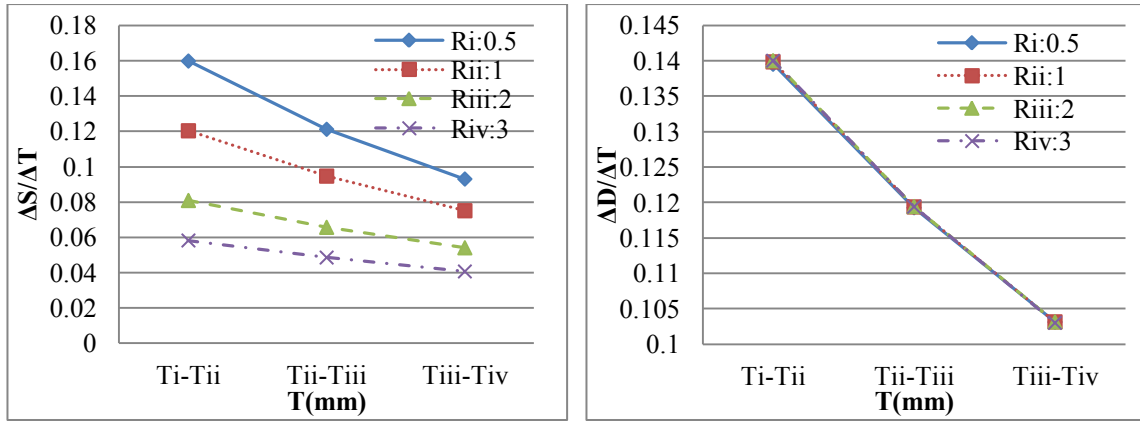
Figure 6.44  $\Delta S/\Delta T$  and  $\Delta D/\Delta T$  of the 250H<sub>i</sub> with respect to T



a. Rate of change of maximum von Mises stress

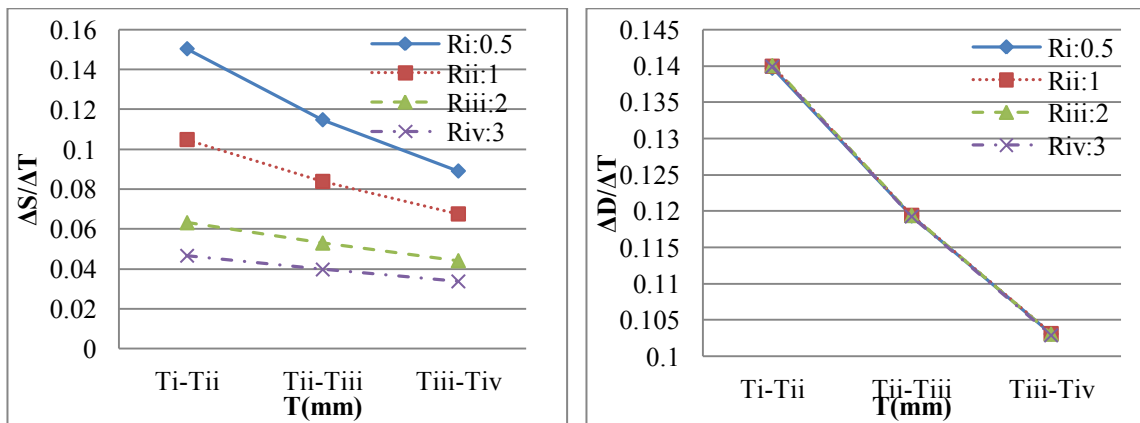
b. Rate of change of maximum horizontal sway

Figure 6.45  $\Delta S/\Delta T$  and  $\Delta D/\Delta T$  of the 250H<sub>ii</sub> with respect to T



a. Rate of change of maximum von Mises stress      b. Rate of change of maximum horizontal sway

Figure 6.46  $\Delta S/\Delta T$  and  $\Delta D/\Delta T$  of the 250H<sub>iii</sub> with respect to T

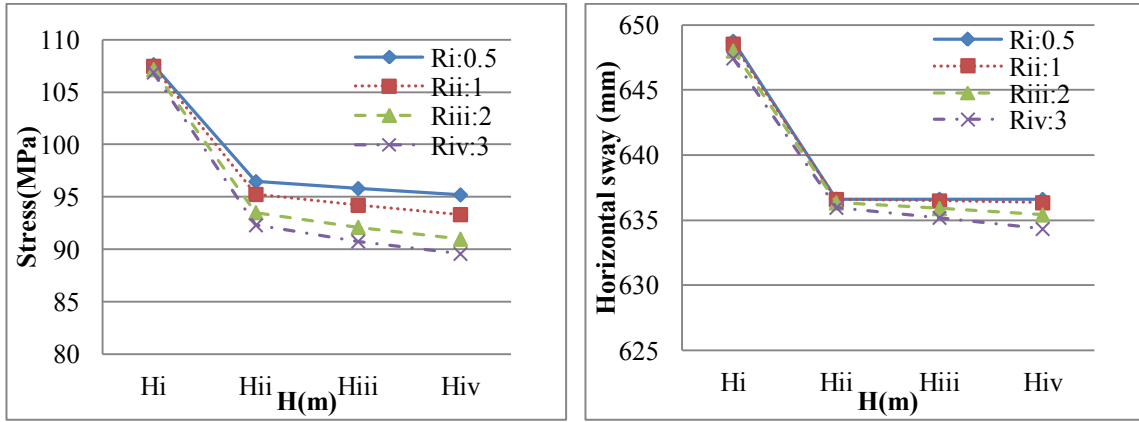


a. Rate of change of maximum von Mises stress      b. Rate of change of maximum horizontal sway

Figure 6.47  $\Delta S/\Delta T$  and  $\Delta D/\Delta T$  of the 250H<sub>iv</sub> with respect to T

For the 250m-towers, the rate of change of the 250m-towers with T variation from T<sub>i</sub> to T<sub>ii</sub> are also greater than those of the 250m towers with T increasing from T<sub>ii</sub> to T<sub>iv</sub> in accordance to Figure 6.44 to 6.47. The rate of change of maximum horizontal sway of the 250m-towers in each T variation range are also fairly close. According to Table 6.11, the rate of change of maximum horizontal sway also tend to be linear curves with respect to T variation for the high height tower. The efficiency range of thickness variation in low height and thin walled towers is more critical than that in high height and thick walled towers.

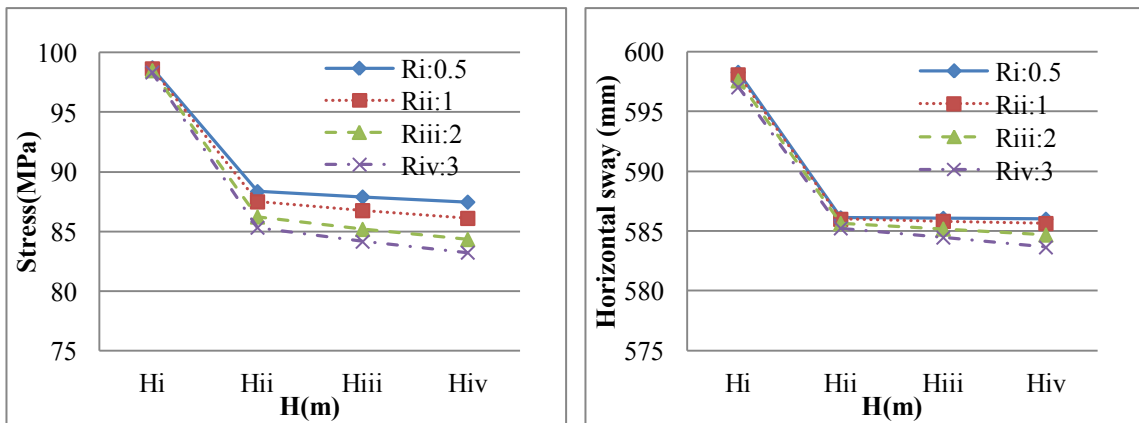
6.4.3 Effect of the spacing  $H$  of stiffening rings on the overall structural response



a. Maximum von Mises stress

b. Maximum horizontal sway

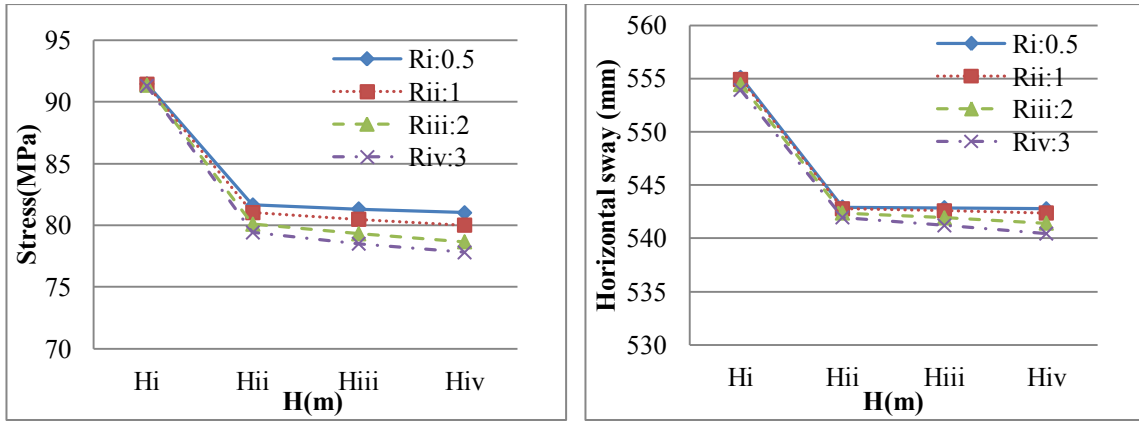
Figure 6.48 Maximum von Mises stresses and horizontal sways versus  $H$  of the 250T<sub>i</sub>



a. Maximum von Mises stress

b. Maximum horizontal sway

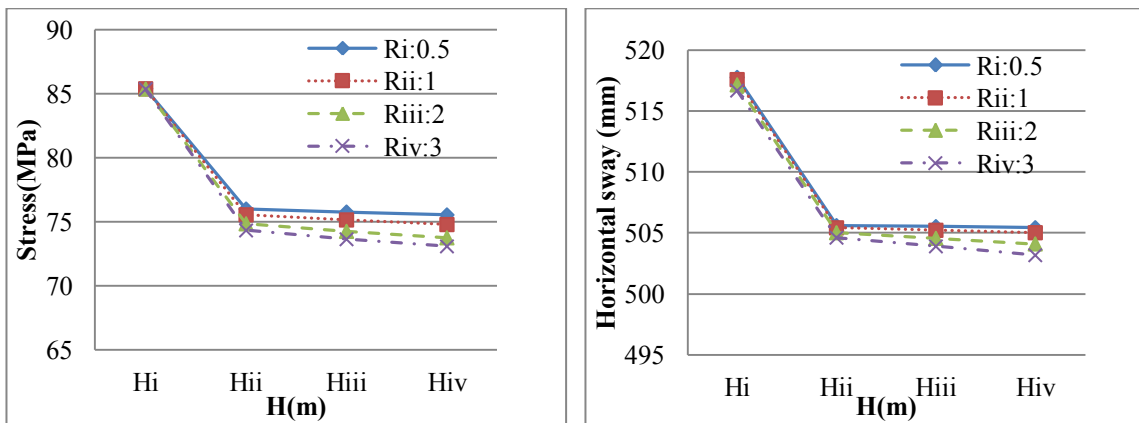
Figure 6.49 Maximum von Mises stresses and horizontal sways versus  $H$  of the 250T<sub>ii</sub>



a. Maximum von Mises stress

b. Maximum horizontal sway

Figure 6.50 Maximum von Mises stresses and horizontal sways versus H of the 250T<sub>iii</sub>



a. Maximum von Mises stress

b. Maximum horizontal sway

Figure 6.51 Maximum von Mises stresses and horizontal sways versus H of the 250T<sub>iv</sub>

Maximum von Mises stresses and horizontal sways of the 250T<sub>i</sub>/T<sub>ii</sub>/T<sub>iii</sub>/T<sub>iv</sub> are displayed in Figure 6.48 to 6.51. For each wall thickness, the maximum von Mises stresses and horizontal sways of the 250m-towers reduce with the distances H reduces. To study the changing efficiency of the distances H, the rate of change of maximum von Mises stresses and horizontal sways of the 250m-towers can be calculated by referring the Equations (6.5, 6.6) and Table 6.10. The  $\Delta S/\Delta H$  and  $\Delta D/\Delta H$  of 250m towers with respect to the distances H are shown in Table 6.12.

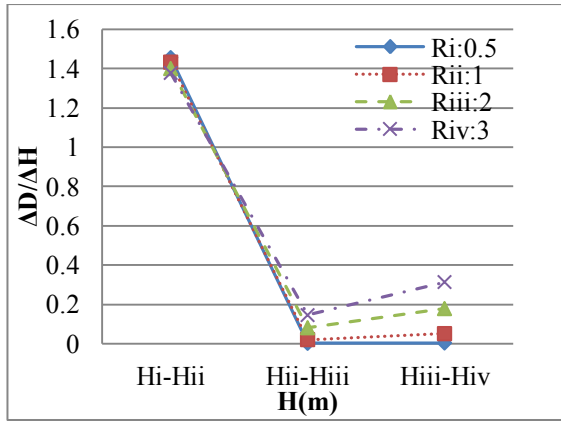
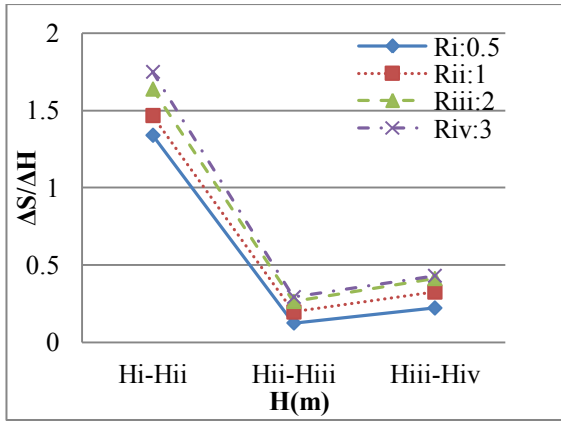
CHAPTER 7: VERTICAL STIFFENERS

Table 6.12 Rate of change  $\Delta S/\Delta H$  and  $\Delta D/\Delta H$  of the  $250T_i/T_{ii}/T_{iii}/T_{iv}$  with respect to H

Types of rings	Ranges of H variation	$\Delta S/\Delta H$	$\Delta D/\Delta H$
$T_i R_i$	$H_i$ to $H_{ii}$	1.34	1.46
	$H_{ii}$ to $H_{iii}$	0.12	0.002
	$H_{iii}$ to $H_{iv}$	0.22	0.004
$T_i R_{ii}$	$H_i$ to $H_{ii}$	1.47	1.43
	$H_{ii}$ to $H_{iii}$	0.20	0.02
	$H_{iii}$ to $H_{iv}$	0.32	0.05
$T_i R_{iii}$	$H_i$ to $H_{ii}$	1.64	1.40
	$H_{ii}$ to $H_{iii}$	0.26	0.08
	$H_{iii}$ to $H_{iv}$	0.41	0.18
$T_i R_{iv}$	$H_i$ to $H_{ii}$	1.75	1.38
	$H_{ii}$ to $H_{iii}$	0.29	0.145
	$H_{iii}$ to $H_{iv}$	0.43	0.31
$T_{ii} R_i$	$H_i$ to $H_{ii}$	1.25	1.46
	$H_{ii}$ to $H_{iii}$	0.09	0.0075
	$H_{iii}$ to $H_{iv}$	0.16	0.026
$T_{ii} R_{ii}$	$H_i$ to $H_{ii}$	1.34	1.45
	$H_{ii}$ to $H_{iii}$	0.14	0.03
	$H_{iii}$ to $H_{iv}$	0.24	0.066
$T_{ii} R_{iii}$	$H_i$ to $H_{ii}$	1.47	1.43
	$H_{ii}$ to $H_{iii}$	0.20	0.087
	$H_{iii}$ to $H_{iv}$	0.31	0.18
$T_{ii} R_{iv}$	$H_i$ to $H_{ii}$	1.56	1.41
	$H_{ii}$ to $H_{iii}$	0.22	0.145
	$H_{iii}$ to $H_{iv}$	0.34	0.3

CHAPTER 7: VERTICAL STIFFENERS

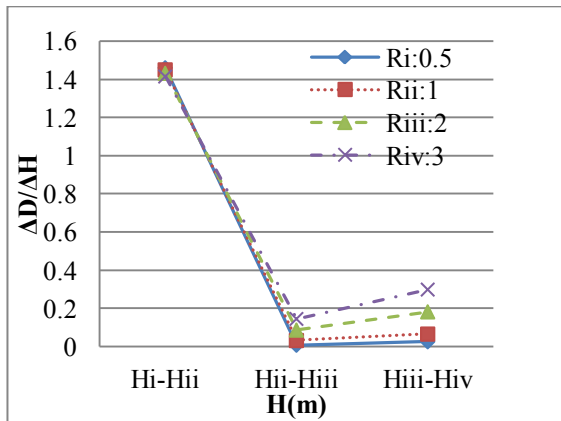
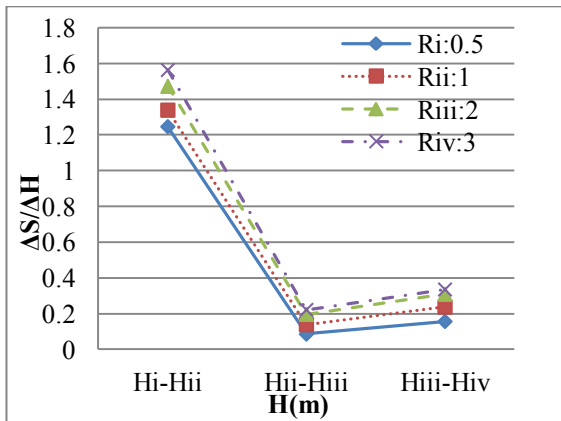
$T_{iii}R_i$	$H_i$ to $H_{ii}$	1.18	1.46
	$H_{ii}$ to $H_{iii}$	0.06	0.01
	$H_{iii}$ to $H_{iv}$	0.11	0.04
$T_{iii}R_{ii}$	$H_i$ to $H_{ii}$	1.25	1.46
	$H_{ii}$ to $H_{iii}$	0.10	0.036
	$H_{iii}$ to $H_{iv}$	0.17	0.073
$T_{iii}R_{iii}$	$H_i$ to $H_{ii}$	1.35	1.45
	$H_{ii}$ to $H_{iii}$	0.15	0.087
	$H_{iii}$ to $H_{iv}$	0.24	0.18
$T_{iii}R_{iv}$	$H_i$ to $H_{ii}$	1.43	1.44
	$H_{ii}$ to $H_{iii}$	0.17	0.14
	$H_{iii}$ to $H_{iv}$	0.26	0.28
$T_{iv}R_i$	$H_i$ to $H_{ii}$	1.13	1.46
	$H_{ii}$ to $H_{iii}$	0.04	0.015
	$H_{iii}$ to $H_{iv}$	0.08	0.033
$T_{iv}R_{ii}$	$H_i$ to $H_{ii}$	1.18	1.46
	$H_{ii}$ to $H_{iii}$	0.07	0.038
	$H_{iii}$ to $H_{iv}$	0.13	0.073
$T_{iv}R_{iii}$	$H_i$ to $H_{ii}$	1.26	1.46
	$H_{ii}$ to $H_{iii}$	0.11	0.087
	$H_{iii}$ to $H_{iv}$	0.18	0.17
$T_{iv}R_{iv}$	$H_i$ to $H_{ii}$	1.32	1.45
	$H_{ii}$ to $H_{iii}$	0.13	0.13
	$H_{iii}$ to $H_{iv}$	0.20	0.27



a. Rate of change of maximum von Mises stress

b. Rate of change of maximum horizontal sway

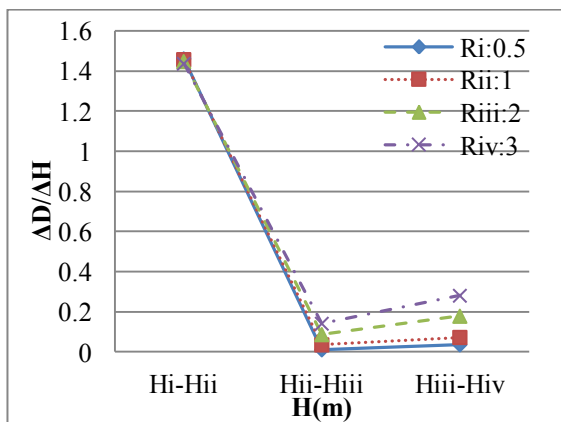
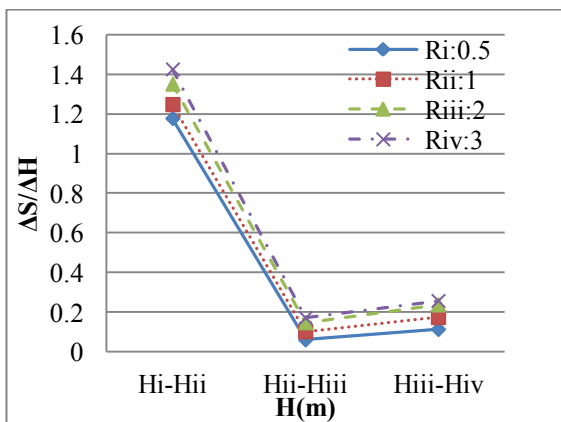
Figure 6.52 The  $\Delta S/\Delta H$  and  $\Delta D/\Delta H$  graphs of the  $250T_i$  with respect to  $H$



a. Rate of change of maximum von Mises stress

b. Rate of change of maximum horizontal sway

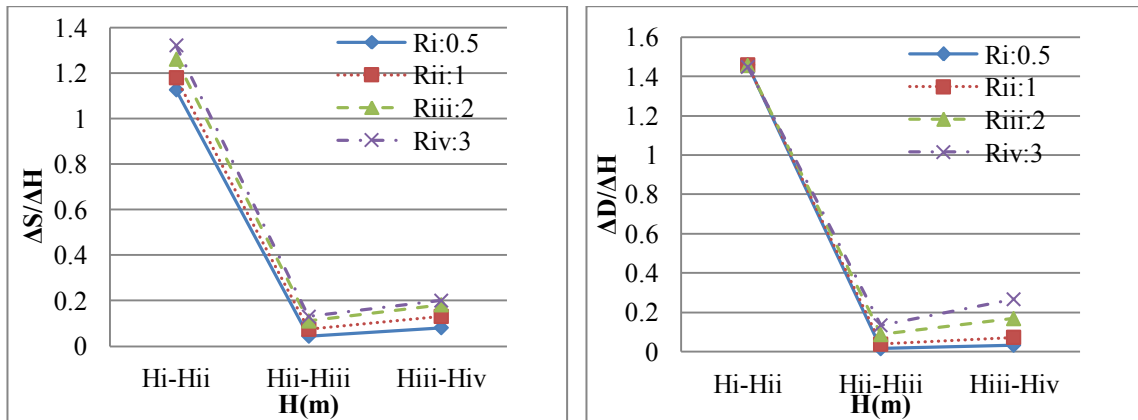
Figure 6.53 The  $\Delta S/\Delta H$  and  $\Delta D/\Delta H$  graphs of the  $250T_{ii}$  with respect to  $H$



a. Rate of change of maximum von Mises stress

b. Rate of change of maximum horizontal sway

Figure 6.54 The  $\Delta S/\Delta H$  and  $\Delta D/\Delta H$  graphs of the  $250T_{iii}$  with respect to H



a. Rate of change of maximum von Mises stress      b. Rate of change of maximum horizontal sway

Figure 6.55 The  $\Delta S/\Delta H$  and  $\Delta D/\Delta H$  graphs of the  $250T_{iv}$  with respect to H

Concerning the 250m-towers, Figure 6.52 to 6.55 shows the rate of change of the maximum von Mises stresses and of the horizontal sways of the  $250T_i/T_{ii}/T_{iii}/T_{iv}$  tower with respect to H. Clearly, H varying from  $H_i$  to  $H_{ii}$  is the most significant range with respect to the strengthening of the towers. Concerning high towers, the most significant ranges of two neighbouring rings are the long spans.

## 6.5 Conclusions

With reference to the parametric study, the tower shell thickness T and the ring spacing H were considered as design variables for each tower height case. For all three tower heights, the strengthening effect on the towers is positive with reference to the variations of wall thickness. In particular, the more significant range of wall thickness, T, for strength enhancement of the towers is at the thin walled category (e.g.  $T_i$  to  $T_{ii}$ ). Concerning the ring spacing, the more significant range for the low height level tower with thin walled thickness is at the greater height (e.g.  $H_i$  to  $H_{ii}$ ), but with intermediate and thick wall thickness, the range variation at the category of lower height (e.g.  $H_{iii}$  to  $H_{iv}$ ) is a better option in cost saving for the strengthening of the towers. The more significant design range for ring spacing for the intermediate and high height towers for increasing tower strength is at the level of intermediate distance and long distance respectively (e.g.  $H_{ii}$  to  $H_{iii}$  and  $H_i$  to  $H_{ii}$ ).

## CHAPTER 7: VERTICAL STIFFENERS

### 7.1 Introduction

As stiffening rings are traditionally employed to strengthen cylindrical shells, horizontal ring stiffeners are nowadays used extensively in engineering practice to enhance the strength of thin-walled structures against buckling. In 1998, J. F. Chen and Rotter (1998) proposed an integrated approach to predict the membrane and bending stresses of asymmetric stiffening rings on cylindrical shells under axisymmetric loadings. Some years later, Lemak and Studnicka (2005) investigated the effect of the spacing and stiffness of stiffening rings on a steel cylindrical shell, and concluded with the proposal of a method for the determination of the maximum distance between neighbouring stiffeners. Qu *et al.* (2013) studied the dynamic characteristics of conical-cylindrical-spherical shells enhanced by stiffening rings, and a good agreement between experimental and FEM results was achieved in terms of natural frequencies and mode shapes. Showkati and Shahandeh (2010) investigated the process of the collapse of ring-stiffened pipelines under hydrostatic pressure, and also studied the effect of stiffening rings on the buckling behaviours of the pipelines. Gong *et al.* (2013) studied the effect of stiffening rings on the critical harmonic settlement of thin-walled tanks. X Zhao *et al.* (2002) looked at the vibration of laminated circular cylindrical shells with orthogonal stiffeners by comparing numerical and experimental results. Sabouri-Ghomi *et al.* (2006) evaluated the effect of stiffening rings on the buckling behaviours of concrete cooling towers using numerical analysis. Lavassas *et al.* (2003) proposed the enhancement of the structural response of a 44m high tower with stiffening rings under gravity, seismic and wind loadings based on the relevant Eurocodes. Lupi *et al.* (2013) analysed a newly identified type of bistable flow around circular cross-section cylinders with stiffening rings through wind tunnel testing, and Ross *et al.* (2005) thoroughly investigated the plastic buckling of conical shells with stiffening rings under water pressure. T. K. Makarios and Baniotopoulos (2012) performed modal analysis by the continuous model method for a prototype of a 76m wind turbine tower. Baniotopoulos *et al.* (2011) systematically introduced the design of wind energy structures subjected to wind loadings.

Nowadays, wind turbines supported by high towers are extensively used to harvest wind energy due to their zero carbon dioxide emissions. These towers are often tubular steel structures with a relatively small wall thickness in relation to the diameter of the tower cross-section and height. Thus, these cylindrical tubular towers are considered to be typical slender structures. As all slender structures are vulnerable to local and overall buckling, stiffeners need to be added to the tower structure to enhance its structural response. Stiffeners are secondary sections used to strengthen the thin-walled structures against out-of-plane deformations. As previously mentioned, thin-walled towers are usually stiffened by stiffening rings. However, to improve the effect of the various stiffeners on the structural response of shell structures under wind loads, vertical stiffeners can be also added to the inside of towers. Hull (2012) proposed a three-dimensional analytical solution of a cylinder with vertical stiffeners and compared it with FEM results. Wójcik *et al.* (2011) assessed the linear and non-linear buckling behaviour of a cylindrical metal bin with vertical stiffeners under axisymmetric and non-axisymmetric loads, and the simulated buckling loads were compared with results based on existing guidelines. Xie and Sun (2009) investigated the vibration response of a cylindrical shell with vertical stiffeners excited by acoustic waves. Kyoung C. Lee and Yoo (2012) evaluated the effect of longitudinal stiffeners on the stability of concrete-filled tubes. In 2007, Ramachandran and Narayanan (2007) predicted the modal density and radiation efficiency of a cylinder with vertical stiffeners, and verified the predicted results by comparing them with experimental results. Bray and Egle (1970) carried out experiments on free vibrations of thin cylindrical shells stiffened with longitudinal stiffeners, and the experimental results were compared to theoretical results, and a close correlation between analytical and experimental results was found. Iwicki *et al.* (2011) studied the failure of cylindrical steel silos with vertical stiffeners by means of a linear and a non-linear buckling analysis taking into account geometric and material nonlinearities.

Actually, the horizontal and vertical stiffeners should be both included to form the connected flanges for the tower structures. Thus, some researchers focused on the combined effect of both horizontal and vertical stiffeners on the structural response of cylindrical shells. Rotter and Sadowski (2012) solved the equations of shell bending theory for stiffened orthotropic cylindrical shells under

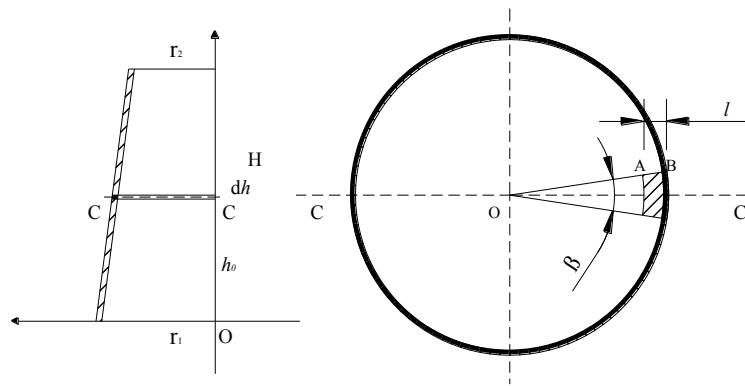
axisymmetric pressure. Torkamani *et al.* (2009) conducted the free vibration of orthogonally stiffened cylindrical shells by using structural similitude theory. To explore the effect of vertical stiffeners on the structural response of steel wind turbine towers under wind loads, only vertical stiffeners are assumed to be used in the inner tower wall. However, the combined effect of horizontal and vertical stiffeners should be also considered as future work. In realistic wind towers, the tower stem is divided into some sectors of a truncated cone, hence the vertical stiffeners should be also separated into several sectors. For taller tower, the cross-section of the low parts has to be bolted on site. In this Chapter, the tower wall and each vertical stiffener were considered to be continuous from the bottom to the top of the tower. Three representative towers of 50m, 150m and 250m in height were considered stiffened alternatively with horizontal rings and vertical stiffeners. To explore the effect of vertical stiffeners on the enhancement of the structural response of towers, the strength and buckling behaviour of vertically and horizontally stiffened towers under wind loads were compared with each other where the mass of the stiffening rings was equal to that of the vertical stiffeners. The maximum von Mises stresses and horizontal sways of these towers with vertical stiffeners were compared with the corresponding towers with horizontal stiffening rings. The buckling modes and eigenvalues of the 50m, 150m and 250m vertically stiffened towers were also compared with those of the horizontally stiffened towers. A parametric study of the effect of the vertical stiffeners on the overall structural response of each tower was also performed, which led to some useful comments on the efficiency of the proposed stiffening technique.

## 7.2 On the mass of the vertical stiffeners

To study the effect of vertical stiffeners on the structural response of wind towers, the maximum von Mises stress and horizontal sway of each height case should be compared where the mass of the vertical stiffeners is equal to that of the stiffening rings of the corresponding wind turbine tower. The formulas for the mass of each vertical stiffener can be obtained using the mathematical model presented schematically in Figure 7.1. Figure 7.1 shows the geometric profile of the tower, showing the longitudinal section and the cross section. The cross sectional radii of the tower at the base and at the top of the vertical stiffener are  $r_1$  and  $r_2$  respectively.  $dh$  is the differential height of the cross-

CHAPTER 7: VERTICAL STIFFENERS

section C-C at height,  $h_0$  from the bottom of the vertical stiffener to the cross-section C-C (Figure 7.1a). The central angle of the arc of the vertical stiffener at this point is  $\beta$ , and the thickness of the vertical stiffener at this point is  $l$ , as shown in Figure 7.1b.



a. Longitudinal profile of tower

b. Cross section

Figure 7.1 Profile of the wind turbine tower in two perpendicular planes

According to the geometry of the tower (Figure 7.1), the following formulas are obtained:

$$r_{OB} = \frac{r_2 - r_1}{H} \cdot h + r_1 \quad (7.1)$$

$$r_{OB} - r_{OA} = l \quad (7.2)$$

$$S = 0.5 \cdot \beta \cdot r_{OB}^2 - 0.5 \cdot \beta \cdot r_{OA}^2 \quad (7.3)$$

where  $S$  is the cross-sectional area of the vertical stiffener at the cross-section C-C;

$r_{OA}$  is the inner radius of the vertical stiffener;

$r_{OB}$  is the outer radius of the vertical stiffener;

$H$  is the height of the vertical stiffener;

$\rho_s$  is the density of steel.

According to Equations (7.1 to 7.3), the mass of each vertical stiffener can be obtained by Equation (7.4):

$$m = \rho \cdot \int_0^H S dh = 0.5 \cdot \rho_s \cdot \beta \cdot l \cdot H \cdot (r_1 + r_2 - l) \quad (7.4)$$

## 7.3 Towers of 50m height

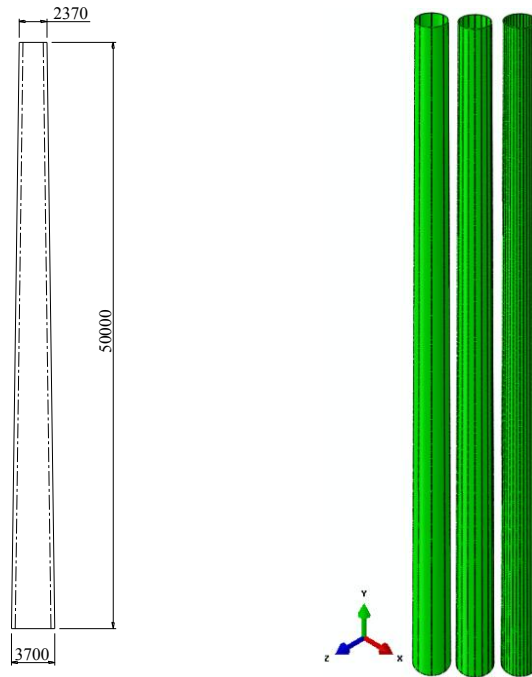
### 7.3.1 Model description

The 50m tower contains eight, sixteen or thirty-two vertical stiffeners uniformly distributed on the inner side of the cylindrical tower as shown in Figure 7.2, and referred to as “tower a”, “tower b” and “tower c”. The height of each vertical stiffener is 50m from the bottom to the top of the tower as shown in Figure 7.2a. The central angle,  $\beta$  of each vertical stiffener was selected to be 4°, 5° or 6° (referred to as “V<sub>i</sub>”, “V<sub>ii</sub>” and “V<sub>iii</sub>”). As the diameter of the 50m tower varies linearly from 3.7m at the base to 2.37m at the top, the mid-arc-length of the cross-section of each vertical stiffener also varies linearly. The wall thickness of the 50m towers *a*, *b* and *c* is identical to that of the 50m ring-stiffened tower. For wind loading, the magnitudes for the 50m towers *a*, *b* and *c* are identical to those described by Hu *et al.* (2014). A typical cross-section and vertical stiffener distribution of the 50m tower *a* is shown in Figure 7.3. The tower wall was simulated using S4R shell elements and the vertical stiffeners were simulated using C3D10 solid elements.

Table 7.1 Thickness of the vertical stiffeners of the 50m towers

Types of vertical stiffeners	Thickness of vertical stiffeners (mm)		
	tower <i>a</i>	tower <i>b</i>	tower <i>c</i>
V <sub>i</sub>	72	49	18
V <sub>ii</sub>	59	39	14
V <sub>iii</sub>	49	32	12

CHAPTER 7: VERTICAL STIFFENERS



a. Geometrical data

b. FEM model

Figure 7.2 Prototypes of the 50m towers *a*, *b* and *c* (mm)

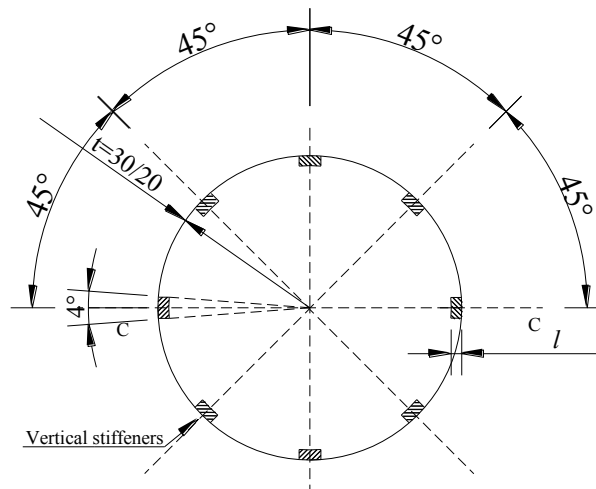


Figure 7.3 Typical cross-section of the 50m tower *a* with  $V_i$

According to the Chapter 6, the mass of the 50m ring-stiffened tower ( $50T_{iv}R_{iv}H_{iv}$ ) is 24t, and the maximum von Mises stress and horizontal sway of the 50m ring-stiffened tower are 11.72MPa and 6.52mm, respectively. To analyse the effect of the vertical and horizontal stiffeners, the mass of the vertical stiffeners has been selected to be equal to that of the stiffening rings of the 50m ring-stiffened tower. Therefore, the thickness of the stiffeners in the three vertical stiffened cases can be obtained by

means of the given parameters and Equation (7.4), and the magnitudes of the vertical stiffeners are shown in Table 7.1. Specifically, the thicknesses  $l$  of the 50m towers  $a$ ,  $b$  and  $c$  with  $V_i$  are 72mm, 49mm and 18mm, respectively. The thicknesses  $l$  of the 50m towers  $a$ ,  $b$  and  $c$  with  $V_{ii}$  are 59mm, 39mm and 14mm, respectively, and the thicknesses  $l$  of the 50m towers  $a$ ,  $b$  and  $c$  with  $V_{iii}$  are 49mm, 32mm and 12mm, respectively.

### 7.3.2 Effect of the number of vertical stiffeners

Figure 7.4 to 7.6 shows the contour plots of the von Mises stresses and the horizontal sways of the 50m towers  $a$  with  $V_i$ . The maximum von Mises stresses of the 50m towers  $a$ ,  $b$  and  $c$  with  $V_i$  are 23.23MPa, 22.68MPa and 20.32MPa, respectively. The maximum horizontal sways of the 50m towers  $a$ ,  $b$  and  $c$  with  $V_i$  are 5.683mm, 5.617mm and 5.601mm. The horizontal sways of the three heights of tower with vertical stiffeners increase as the height of the tower increases, as shown in Figure 7.4 to 7.6.

As the mass of the vertical stiffeners has been selected to be equal to that of the stiffening rings, the efficiency in strength variation of the 50m towers can be obtained by comparing the maximum von Mises stress and horizontal sway of the 50m vertically- and horizontally-stiffened towers. The maximum von Mises stresses of the three vertically stiffened towers are all greater than those of the 50m towers with stiffening rings, but the maximum horizontal sways of the towers  $a$ ,  $b$  and  $c$  are less than those of the horizontally stiffened towers as shown in Figure 7.4 to 7.6. Therefore, the use of stiffening rings appears to be a more efficient way to strengthen the tower compared to the use of vertical stiffeners in the case where the mass of the vertical stiffeners is equal to that of the stiffening rings.

## CHAPTER 7: VERTICAL STIFFENERS

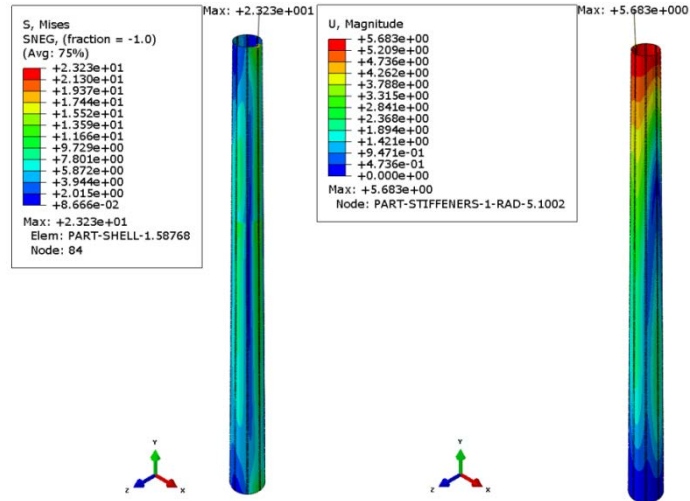


Figure 7.4 Contour plots of 50m tower *a* with  $V_i$

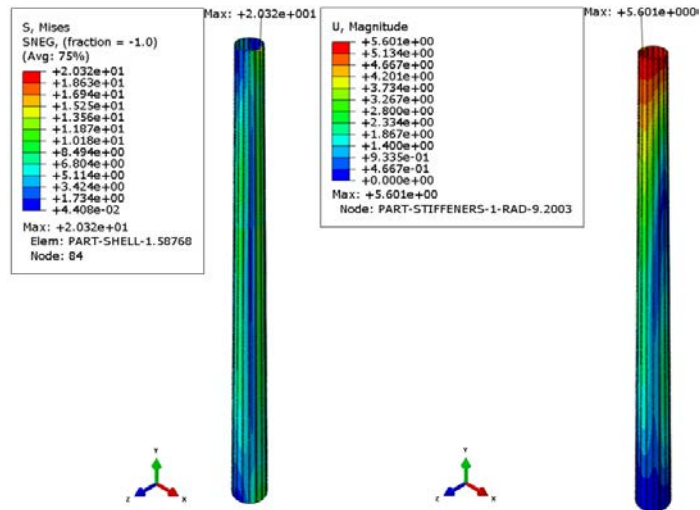


Figure 7.5 Contour plots of 50m tower *b* with  $V_i$

## CHAPTER 7: VERTICAL STIFFENERS

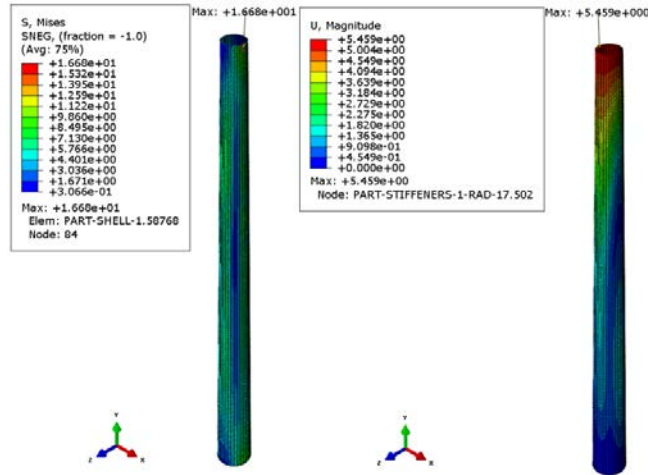


Figure 7.6 Contour plots of 50m tower  $c$  with  $V_i$

For each vertical stiffener, the maximum von Mises stresses and horizontal sways of the 50m towers  $a$ ,  $b$  and  $c$  are shown in Table 7.2. The maximum von Mises stresses and horizontal sways of the 50m towers  $a$ ,  $b$  and  $c$  with respect to the numbers of vertical stiffeners are plotted in Figure 7.7. The horizontal axis represents the number of vertical stiffeners in the 50m heights of tower, and the vertical axis refers to the maximum von Mises stresses and the horizontal sways of the 50m heights of tower.

Table 7.2 Maximum von Mises stress and horizontal sway of the 50m towers  $a$ ,  $b$  and  $c$

Types of vertical stiffeners	Types of towers	Maximum von Mises stress (MPa)	Maximum horizontal sway (mm)
$V_i$	$a$	23.23	5.68
	$b$	20.32	5.60
	$c$	16.68	5.46
$V_{ii}$	$a$	23.02	5.643
	$b$	17.43	5.54
	$c$	16.19	5.46
$V_{iii}$	$a$	22.07	5.64
	$b$	16.61	5.48

	$c$	15.64	5.43
--	-----	-------	------

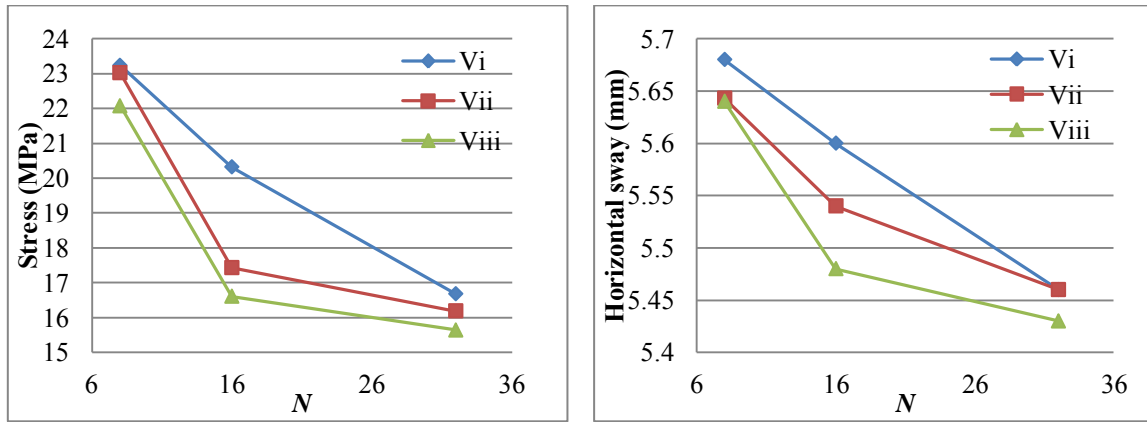


Figure 7.7 Maximum von Mises stresses and horizontal sways of the 50m towers with  $V_i$ ,  $V_{ii}$  and  $V_{iii}$

As shown in Figure 7.7, the maximum von Mises stresses of the 50m vertically stiffened towers  $a$ ,  $b$  and  $c$  reduce as the number of vertical stiffeners increases, where the stiffeners have the same mass as the horizontal rings. The maximum horizontal sways of the 50m towers with  $V_i$ ,  $V_{ii}$  and  $V_{iii}$  also reduce as the number of vertical stiffeners increases. The maximum horizontal sways of the 50m towers  $a$ ,  $b$  and  $c$  are almost identical. Therefore, the strength of the 50m towers increases as the number of vertical stiffeners increases, where the masses of the horizontal and vertical stiffeners are equal to each other as shown in Table 7.2 and Figure 7.7.

### 7.3.3 Effect of the central angle of the vertical stiffeners

Considering the same prototype of the tower stiffened with vertical stiffeners, the central angle,  $\beta$  of the vertical stiffeners is considered to be the design variable in terms of Equation (7.4), and its effect on the strength of the towers has been studied. The maximum von Mises stresses and horizontal sways of the 50m towers  $a$ ,  $b$  and  $c$  are depicted in Figure 7.8. The horizontal axis refers to the central angle of the arc of each vertical stiffener for each tower height, and the vertical axis represents the maximum von Mises stresses and horizontal sways of the 50m towers  $a$ ,  $b$  and  $c$ .

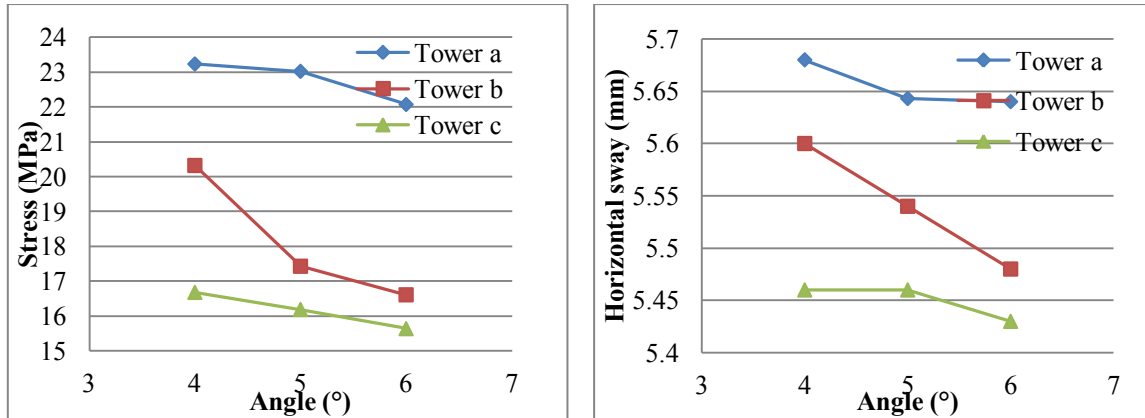


Figure 7.8 Maximum von Mises stresses and horizontal sways of the 50m towers *a*, *b* and *c*

According to Figure 7.8, the maximum von Mises stress reduces, and the maximum horizontal sway of the 50m tower *a*, *b* and *c* increases with an increase in the central angle,  $\beta$  of the cross-sectional arc of each vertical stiffener. Therefore, the strength of the 50m towers increases with an increase in the central angle,  $\beta$  of the cross-sectional arc of each vertical stiffener.

### 7.3.4 Buckling analysis

A linear buckling analysis was performed to investigate the effect of the vertical stiffeners on the stability of the 50m vertically stiffened towers under wind loadings. The load states include axial, transverse and torsional loads at the top of the tower and wind loading around the circumference. The thickness,  $l$  and the central angle,  $\beta$  of each vertical stiffener were considered as design parameters, and the effect of the various vertical stiffeners on the buckling behaviour of the 50m towers were obtained. Additionally, the local buckling modes and the eigenvalues of the 50m ring-stiffened tower ( $50T_{iv}R_{iv}H_{iv}$ ) are also compared with those of the 50m towers *a*, *b* and *c* to estimate a better approach to strengthen the 50m towers.

CHAPTER 7: VERTICAL STIFFENERS

The local buckling modes of the 50m towers  $a$ ,  $b$  and  $c$  with  $V_i$  are displayed in Figure 7.9. The local buckling eigenvalues of the  $50T_{iv}R_{iv}H_{iv}$  is 79.06 and the local buckling modes of the  $50T_{iv}R_{iv}H_{iv}$  is shown in Figure 7.10. As can be seen, the first local buckling modes of the 50m towers  $a$ ,  $b$  and  $c$  with  $V_i$  all occur in the vicinity of the base of the towers. The absolute values of the buckling eigenvalues of the 50m towers  $a$ ,  $b$  and  $c$  are presented in Table 7.3.

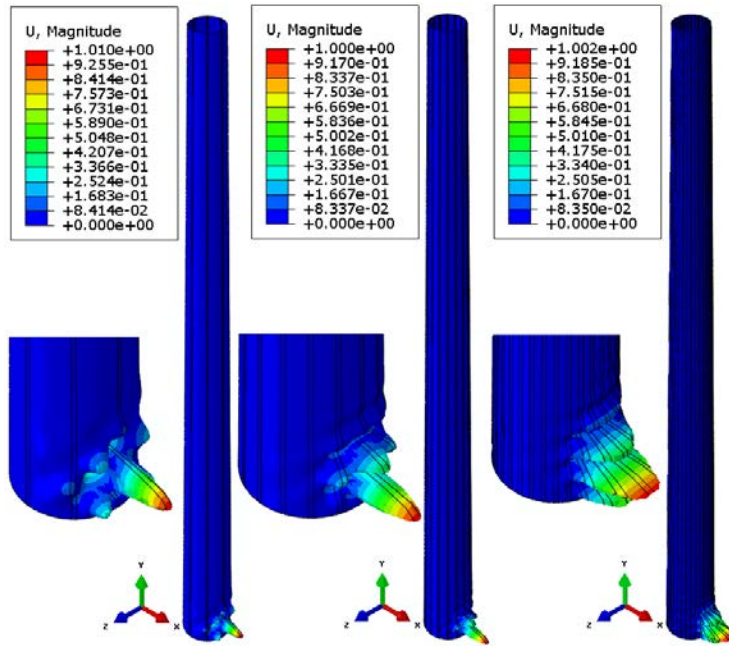


Figure 7.9 First local buckling modes of the 50m towers  $a$ ,  $b$  and  $c$  with  $V_i$

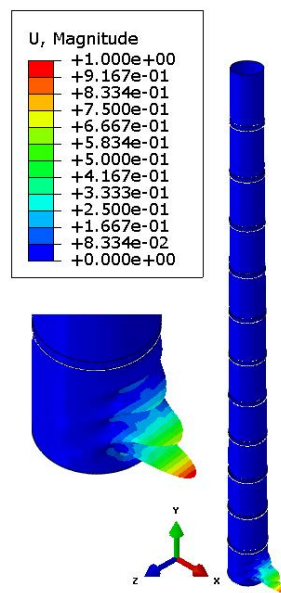
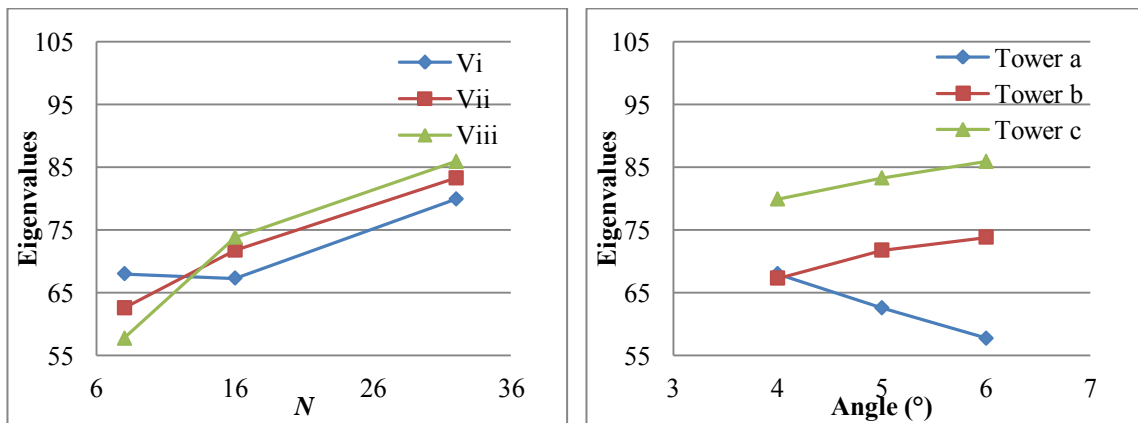


Figure 7.10 First local buckling modes of the  $50T_{iv}R_{iv}H_{iv}$

CHAPTER 7: VERTICAL STIFFENERS

Table 7.3 First buckling eigenvalues of the 50m towers *a*, *b* and *c*

Type of vertical stiffeners	Type of tower	Eigenvalues
$V_i$	<i>a</i>	68.031
	<i>b</i>	67.324
	<i>c</i>	79.933
$V_{ii}$	<i>a</i>	62.588
	<i>b</i>	71.784
	<i>c</i>	83.286
$V_{iii}$	<i>a</i>	57.737
	<i>b</i>	73.85
	<i>c</i>	85.908



a. Eigenvalues of the 50m towers with  $V_i$ ,  $V_{ii}$  and  $V_{iii}$       b. Eigenvalues of the 50m towers *a*, *b* and *c*

Figure 7.11 Local buckling eigenvalues of the 50m towers

The buckling eigenvalues of the 50m towers with respect to each central angle, and the number of vertical stiffeners are presented in Figure 7.11. For each central angle,  $\beta$  of the arc of the vertical stiffener, the buckling eigenvalues of the 50m towers *a*, *b* and *c* increase with the number of vertical stiffeners, as shown in Figure 7.11a. For each number of vertical stiffeners, the buckling eigenvalues

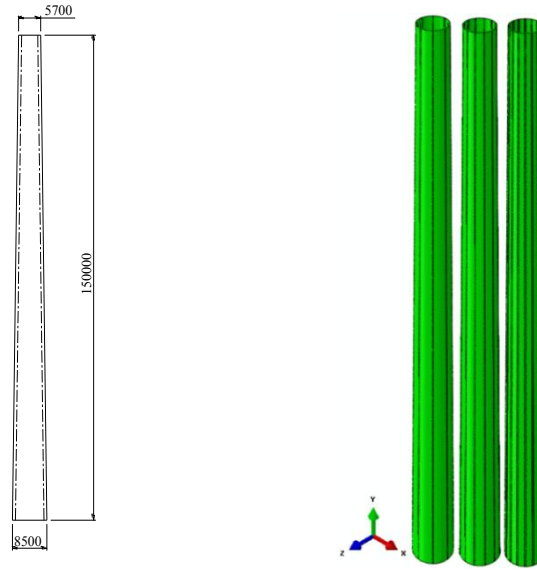
of the 50m towers  $b$  and  $c$  increase as the central angle,  $\beta$  of the vertical stiffener increases. However, the buckling eigenvalues of the 50m towers  $a$  reduce as the central angle of the vertical stiffeners increases. Compared with the 50m ring-stiffened towers, the absolute value of the corresponding buckling eigenvalues of the vertically stiffened 50m towers  $a$  and  $b$  (shown in Table 7.3) are less than the eigenvalue of the 50m ring-stiffened tower, but the absolute eigenvalues of the 50m towers  $c$  are greater than those of the 50m ring-stiffened tower. Thus, the stability strength of the 50m towers can be improved more efficiently by using vertical stiffeners which have the same mass as the stiffening rings.

## 7.4 Towers of 150m height

### 7.4.1 Model description

The geometry and the FEM model of the 150m towers with vertical stiffeners are depicted in Figure 7.12. The models of the 150m tower with eight, twelve or sixteen vertical stiffeners are shown in Figure 7.12b and are referred to as “tower  $a$ ”, “tower  $b$ ” and “tower  $c$ ”. The sixteen vertical stiffeners are uniformly distributed on the inner side of the tower as shown in Figure 7.13, however, the vertical stiffeners are too closely spaced in engineering practice. The diameters of the 150m towers  $a$ ,  $b$  and  $c$  reduce linearly from 8.5m at the base to 5.7m at the top. The length of each vertical stiffener of the 150m towers is 150m. The central angles,  $\beta$  of each vertical stiffener are  $2^\circ$ ,  $3^\circ$  and  $4^\circ$  respectively, (referred to as  $V_i$ ”,  $V_{ii}$ ” and  $V_{iii}$ ”). The masses of the vertical stiffeners for the 150m towers  $a$ ,  $b$  and  $c$  are all equal to those of the 150m ring-stiffened tower. Therefore, the thicknesses  $l$  of the vertical stiffeners of the 150m towers with  $V_i$  are 68mm, 45mm and 33mm respectively, obtained by applying Equation (7.4). The thicknesses of the 150m towers with  $V_{ii}$  are 45mm, 30mm and 22mm respectively, and those of the 150m towers with  $V_{iii}$  are 33mm, 22mm and 17mm respectively, as shown in Table 7.4. The wall thickness of the 150m towers  $a$ ,  $b$  and  $c$  is 55mm from the height of 0m to 50m, 45mm from the height of 50m to 100m, and 40mm from the height of 100m to 150m. The loading states of the 150m towers  $a$ ,  $b$  and  $c$  are identical to those described by Chapter 3.

CHAPTER 7: VERTICAL STIFFENERS



a. Geometrical data

b. FE model

Figure 7.12 Prototypes of the 150m towers *a*, *b* and *c* (mm)

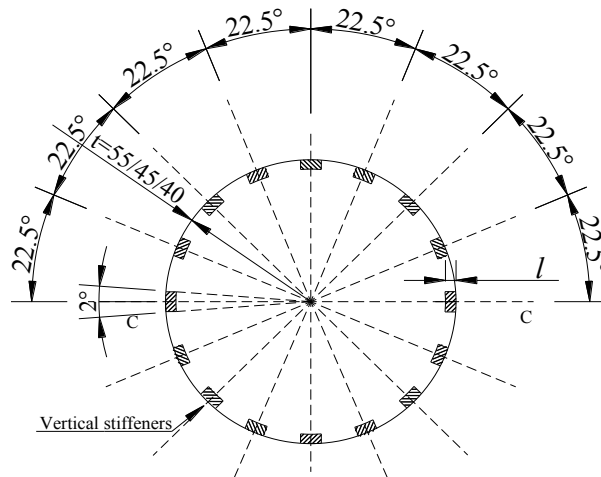


Figure 7.13 Typical cross-section of the 150m tower *c* with  $V_i$

Table 7.4 Thickness of the vertical stiffeners of the 150m towers

Types of vertical stiffeners	Thickness of vertical stiffeners (mm)		
	Tower <i>a</i>	Tower <i>b</i>	Tower <i>c</i>
$V_i$	68	45	33
$V_{ii}$	45	30	22
$V_{iii}$	33	22	17

### 7.4.2 Effect of the number of vertical stiffeners

The contour plots of the von Mises stress and the horizontal sway of the 150m towers *a*, *b* and *c* with  $V_i$  are presented in Figure 7.14 to 7.16. The maximum von Mises stresses of the 150m towers *a*, *b* and *c* are 48.63MPa, 47.82MPa and 47.1MPa respectively, occurring in the vicinity of the base of the 150m towers. However, the maximum horizontal sways of the 150m towers *a*, *b* and *c* appear at the top of the towers, with magnitudes of 136.2mm, 134.5mm and 134.6mm respectively. The horizontal sways for each tower increase with the height of tower increases as shown in Figure 7.14 to 7.16.

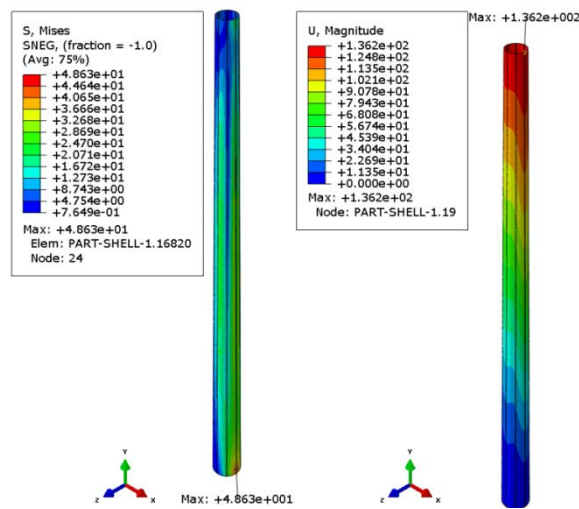


Figure 7.14 Contour plots of the 150m towers *a* with  $V_i$

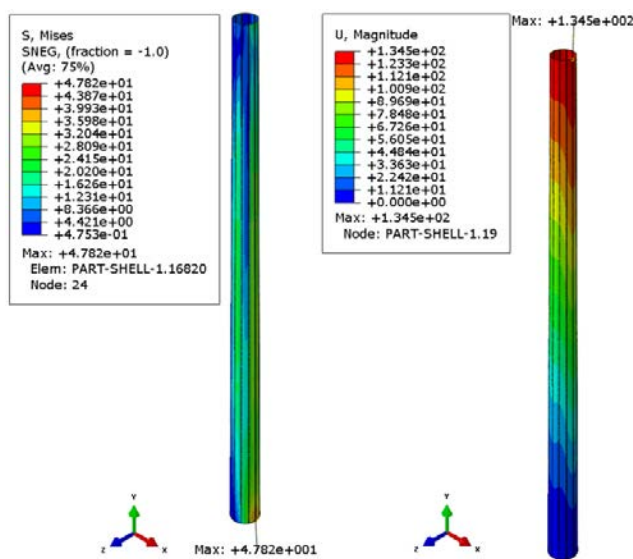


Figure 7.15 Contour plots of the 150m towers *b* with  $V_i$

CHAPTER 7: VERTICAL STIFFENERS

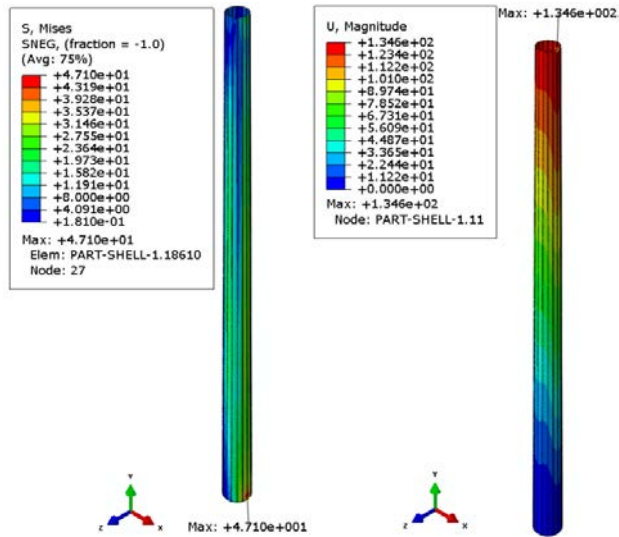


Figure 7.16 Contour plots of the 150m towers *c* with  $V_i$

For the 150m tower with stiffening rings, the maximum von Mises stresses in the rings and shell are 54.95MPa and 43.78MPa respectively, and its maximum horizontal sway is 138.26mm as shown in Table 6.2. According to Figure 7.14 to 7.16, the maximum von Mises stresses of the 150m towers *a*, *b* and *c* are all less than the maximum von Mises stresses in the rings, and are all close to those in the shell of the 150m horizontally stiffened tower. The maximum horizontal sways of 150m towers *a*, *b* and *c* are less than those of the 150m ring-stiffened tower. Therefore, vertical stiffeners effectively increase the strength of the 150m towers *a*, *b* and *c* compared with stiffening rings which have the same mass as the vertical stiffeners.

Table 7.5 Maximum von Mises stress and horizontal sway of the 150m towers *a*, *b* and *c*

Types of vertical stiffeners	Types of towers	Maximum von Mises stress (MPa)	Maximum horizontal sway (mm)
$V_i$	<i>a</i>	48.63	136.2
	<i>b</i>	47.82	134.5
	<i>c</i>	47.1	134.6
$V_{ii}$	<i>a</i>	47.38	134.6
	<i>b</i>	47.14	134.5

CHAPTER 7: VERTICAL STIFFENERS

	<i>c</i>	46.02	134.5
$V_{iii}$	<i>a</i>	47.09	134.8
	<i>b</i>	46.95	134.7
	<i>c</i>	46.20	134.4

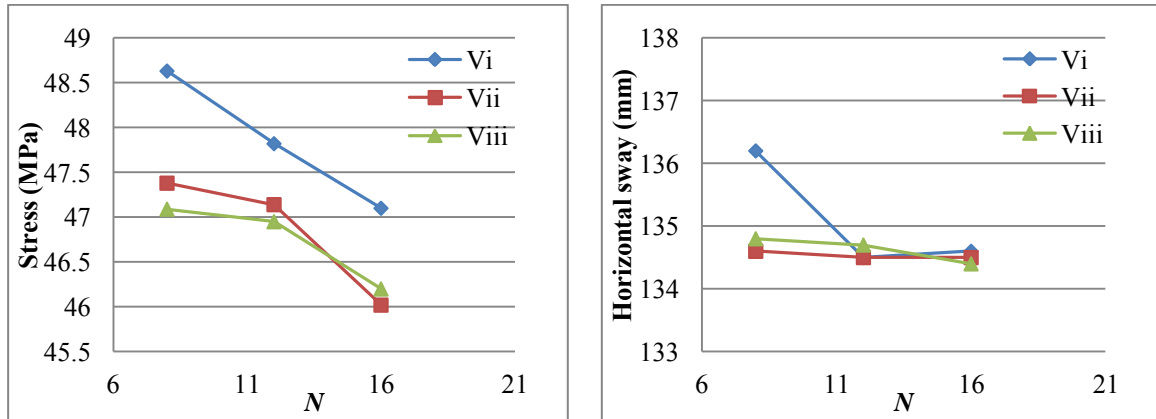


Figure 7.17 Maximum von Mises stresses and horizontal sways of 150m towers with  $V_i$ ,  $V_{ii}$  and  $V_{iii}$

Table 7.5 and Figure 7.17 present the maximum von Mises stresses and the horizontal sways of the 150m towers *a*, *b* and *c*. The horizontal axis refers to the numbers of the vertical stiffeners and vertical axis refers to the maximum von Mises stresses and the maximum horizontal sways of the 150m towers *a*, *b* and *c*. Maximum von Mises stresses of the 150m towers *a*, *b* and *c* reduce with numbers of vertical stiffeners increase for the stiffeners in the same mass with horizontal rings. The same results can be obtained in terms of maximum horizontal sway of the 150m towers *a*, *b* and *c* with respect to numbers of vertical stiffeners. Thus, the strength of tower increases with quantity of vertical stiffener increases in accordance to Figure 7.17.

### 7.4.3 Effect of the central angle of the vertical stiffeners

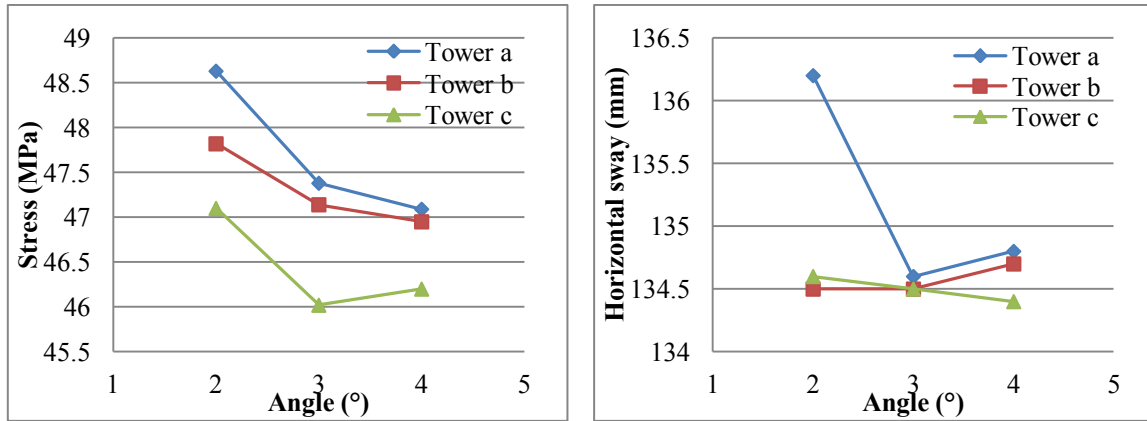


Figure 7.18 Maximum von Mises stresses and horizontal sways of the 150m towers *a*, *b* and *c*

For the 150m towers, the maximum von Mises stresses and horizontal sways of towers *a*, *b* and *c* are shown in Figure 7.18. The maximum von Mises stresses of the 150m tower types *a* and *b* reduce with an increase in the central angle of each vertical stiffener. The maximum von Mises stress of the 150m tower *c* with  $V_{ii}$  is less than those of the 150m tower *c* with  $V_i$  and  $V_{iii}$ . The maximum von Mises stresses of the 150m tower *c* with  $V_{ii}$  and  $V_{iii}$  are similar. The maximum von Mises stress of the 150m towers *a*, *b* and *c* decreases with an increase in the central angle of the vertical stiffeners. The maximum horizontal sway of the 150m tower *a* with  $V_{ii}$  is less than that of the 150m tower *a* with  $V_{ii}$  and  $V_{iii}$ , and the maximum horizontal sways of the 150m tower *b* increase with an increase in the central angle of the vertical stiffener. However, the maximum horizontal sway of the 150m tower *c* reduces as the central angle of the vertical stiffener increases. As the magnitudes of the maximum horizontal sway are almost identical for the 150m towers *a*, *b* and *c*, the strength variation of the 150m tower can be determined by considering the variation of the maximum von Mises stress. Thus, the strength of the 150m tower can be enhanced by increasing the central angle  $\beta$  of the vertical stiffener.

### 7.4.4 Buckling analysis

The buckling analysis is also performed for the 150m towers. The first buckling modes of 150m towers *a*, *b* and *c* with  $V_i$  are shown in Figure 7.19. The first buckling modes of 150T<sub>iv</sub>R<sub>iv</sub>H<sub>iv</sub> are given in Figure 7.20. The absolute values of the buckling eigenvalues for each 150m vertically stiffened

tower case are displayed in Table 7.6. The absolute value of the buckling eigenvalues of the 150T<sub>iv</sub>R<sub>iv</sub>H<sub>iv</sub> is 29.8 in the positive direction of horizontal axis, which is less than those of the 150m towers *b* with V<sub>iii</sub>, towers *c* with V<sub>ii</sub> and V<sub>iii</sub>. According to Figure 7.19 to 7.20, the first buckling modes of the 150m towers occur in the vicinity of the tower bottom in the positive direction of the horizontal axis. The magnitudes of the buckling eigenvalues are negative being in accordance to the reverse load direction.

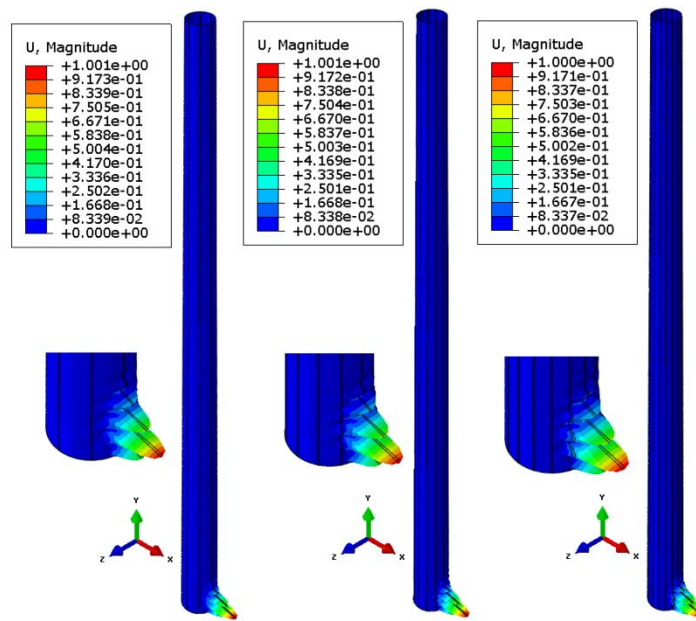


Figure 7.19 Local buckling modes of the 150m towers *a*, *b* and *c* with V<sub>i</sub>

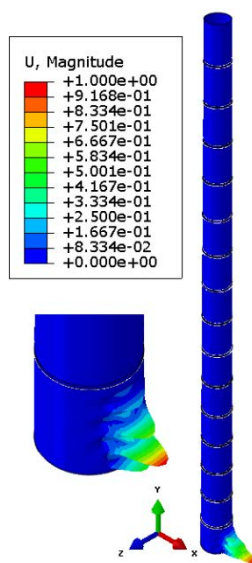
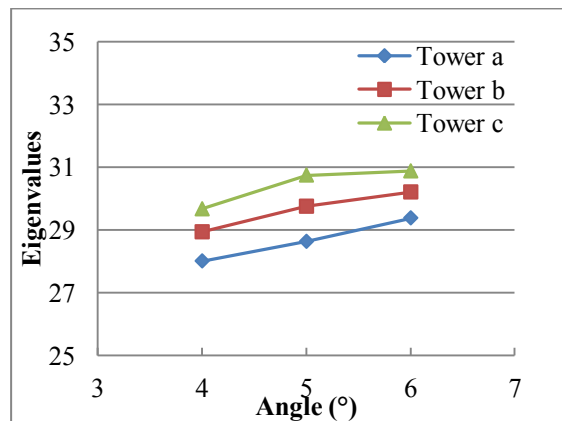
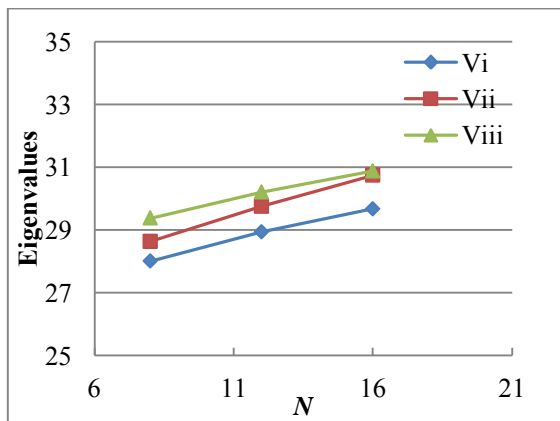


Figure 7.20 First local buckling modes of the 150T<sub>iv</sub>R<sub>iv</sub>H<sub>iv</sub>

CHAPTER 7: VERTICAL STIFFENERS

Table 7.6 Buckling eigenvalues of the 150m towers *a*, *b* and *c*

Type of vertical stiffeners	Type of towers	Eigenvalues
$V_i$	<i>a</i>	28.01
	<i>b</i>	28.937
	<i>c</i>	29.67
$V_{ii}$	<i>a</i>	28.633
	<i>b</i>	29.753
	<i>c</i>	30.746
$V_{iii}$	<i>a</i>	29.381
	<i>b</i>	30.207
	<i>c</i>	30.878



a. Eigenvalues of 50m towers with  $V_i$ ,  $V_{ii}$  and  $V_{iii}$

b. Eigenvalues of the 50m towers *a*, *b* and *c*

Figure 7.21 Buckling eigenvalues of the 150m towers

For the 150m ring-stiffened towers, the first local buckling eigenvalues are shown in Figure 7.21. The first local buckling eigenvalues of the 150m towers increase as the number and the central angle of the vertical stiffeners increases. The absolute values of the eigenvalues of the 150m towers *b* and *c* with  $V_{iii}$  are greater than those of the 150m horizontally stiffened tower. Therefore, using vertical stiffeners

of the same mass as the stiffening rings is a more appropriate option to strengthen the stability of the 150m towers than using stiffening rings.

## 7.5 Towers of 250m height

### 7.5.1 Model description

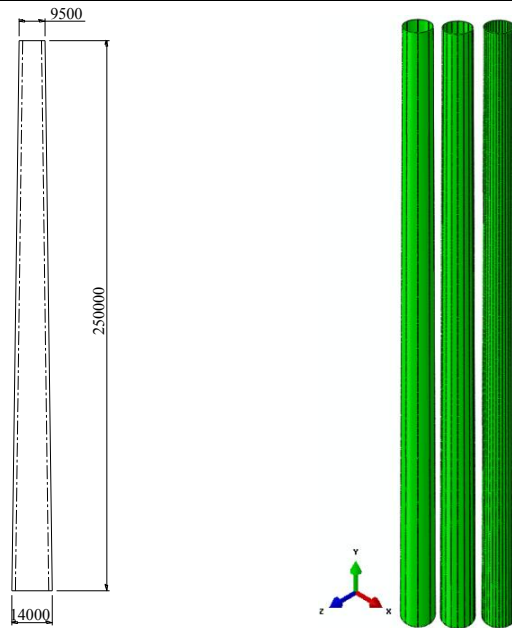
The geometrical data and the FE models of the 250m towers with eight, sixteen or thirty-two vertical stiffeners (referred to as “tower *a*”, “tower *b*” and “tower *c*”) are shown in Figure 7.22. The diameter of the 250m towers reduces linearly from 14m at the base to 9.5m at the top. The vertical stiffeners of the 250m towers *a*, *b* and *c* are equally distributed around the circumference and they are spaced in very close distances for practical application, from the base to the top of the tower as shown in Figure 7.23. For each vertical stiffener, the central angles,  $\beta$  of the vertical stiffener are  $1^\circ$ ,  $1.5^\circ$  and  $2^\circ$  respectively (referred to as “ $V_i$ ”, “ $V_{ii}$ ” and “ $V_{iii}$ ”) as shown in Figure 7.23. The mass of the stiffeners for each of the three vertical stiffened towers is 241.34t, equal to that of the stiffening rings of the 250m ring-stiffened tower. According to Equation (7.4), the thicknesses of the vertical stiffeners of the 250m towers with  $V_i$  are 152mm, 75mm and 38mm respectively, and those of the 250m tower with  $V_{ii}$  are 101mm, 50mm and 25mm, respectively. The thicknesses of the vertical stiffeners for the 250m tower with  $V_{iii}$  are 75mm, 38mm and 19mm, respectively, as shown in Table 7.7. The wall thickness of the 250m towers *a*, *b* and *c* is 75mm from the height of 0m to 100m, 65mm from the height of 100m to 200m, and 60mm from the height of 200m to 250m. The wall thickness and the wind loadings of the 250m towers *a*, *b* and *c* are identical to those of the 250m ring-stiffened tower (250T<sub>iv</sub>R<sub>iv</sub>H<sub>iv</sub>).

Table 7.7 Thickness of the vertical stiffeners of the 250m towers

Type of vertical stiffeners	Thickness of vertical stiffeners (mm)		
	Tower <i>a</i>	Tower <i>b</i>	Tower <i>c</i>
$V_i$	152	75	38
$V_{ii}$	101	50	25

CHAPTER 7: VERTICAL STIFFENERS

$V_{iii}$	75	38	19
-----------	----	----	----



a. Geometrical data

b. FE model

Figure 7.22 Prototypes of 250m towers *a*, *b* and *c* (mm)

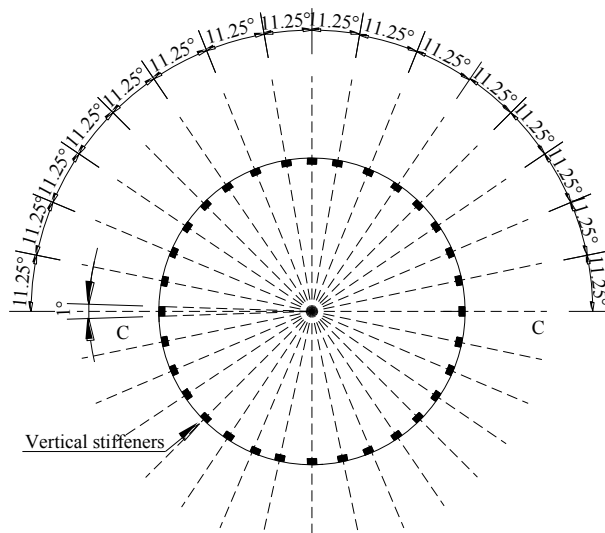


Figure 7.23 Typical cross-section of the 250m tower *b* with  $V_i$

### 7.5.2 Effect of the number of vertical stiffeners

The contour plots of the maximum von Mises stresses and the horizontal sways of the 250m towers *a*, *b* and *c* are displayed in Figure 7.24 to 7.26. The maximum von Mises stresses of the three 250m vertically stiffened towers are 83.03MPa, 82.35MPa and 81.54MPa respectively, which are less than those in the rings of the 250m ring-stiffened tower previously described. The maximum horizontal sways of the 250m towers *a*, *b* and *c* are 505.5mm, 504.9mm and 504.9mm respectively, which are slightly greater than the 503.17mm maximum horizontal sway of the 250m ring-stiffened tower. Maximum von Mises stresses occur in the vicinity of the bottom of the 250m towers *a*, *b* and *c*, and maximum horizontal sways are at the top of the tower in accordance to Figure 7.24 to 7.26. The horizontal sways of the 250m towers gradually increase with the height increases.

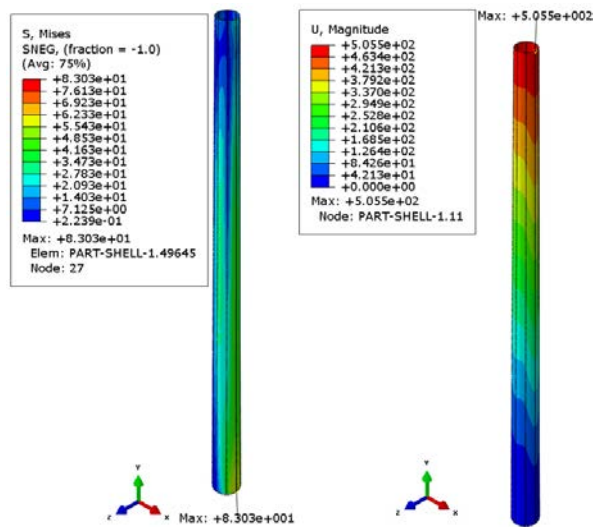


Figure 7.24 Contour plots of the 250m tower *a* with  $V_i$

## CHAPTER 7: VERTICAL STIFFENERS

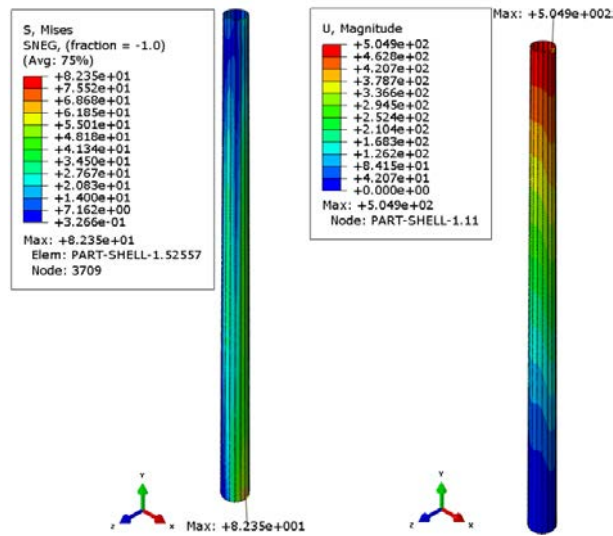


Figure 7.25 Contour plots of the 250m tower *b* with  $V_i$

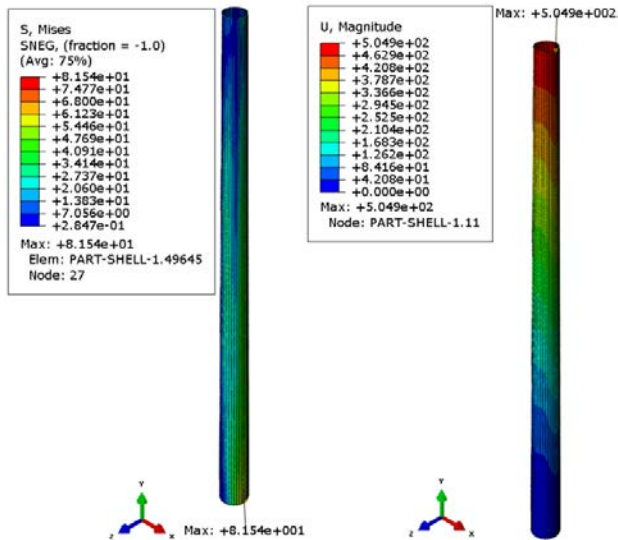


Figure 7.26 Contour plots of the 250m tower *c* with  $V_i$

As shown in Figure 7.24 to 7.26, the maximum von Mises stresses and horizontal sways of the 250m towers *a*, *b* and *c* reduce as the number of vertical stiffeners increases in the case where the mass of the vertical stiffeners is equal to that of the stiffening rings of the 250m tower with stiffening rings. For the 250m towers *a*, *b* and *c* with  $V_{ii}$  and  $V_{iii}$ , the maximum von Mises stresses and horizontal sways are less than those of the 250m ring-stiffened tower. Therefore, the vertical stiffeners seem to be a better choice in increasing the strength of towers than the horizontal stiffening rings with the same mass as the vertical stiffeners, when comparing the 250m towers.

CHAPTER 7: VERTICAL STIFFENERS

Table 7.8 Maximum von Mises stress and horizontal sway of the 150m towers *a*, *b* and *c*

Type of vertical stiffeners	Type of towers	Maximum von Mises stress (MPa)	Maximum horizontal sway (mm)
$V_i$	<i>a</i>	83.03	505.5
	<i>b</i>	82.35	504.9
	<i>c</i>	81.54	504.9
$V_{ii}$	<i>a</i>	82.29	499.1
	<i>b</i>	80.79	492.9
	<i>c</i>	79.33	492.6
$V_{iii}$	<i>a</i>	81.53	493.5
	<i>b</i>	80.07	492.8
	<i>c</i>	78.91	492.6

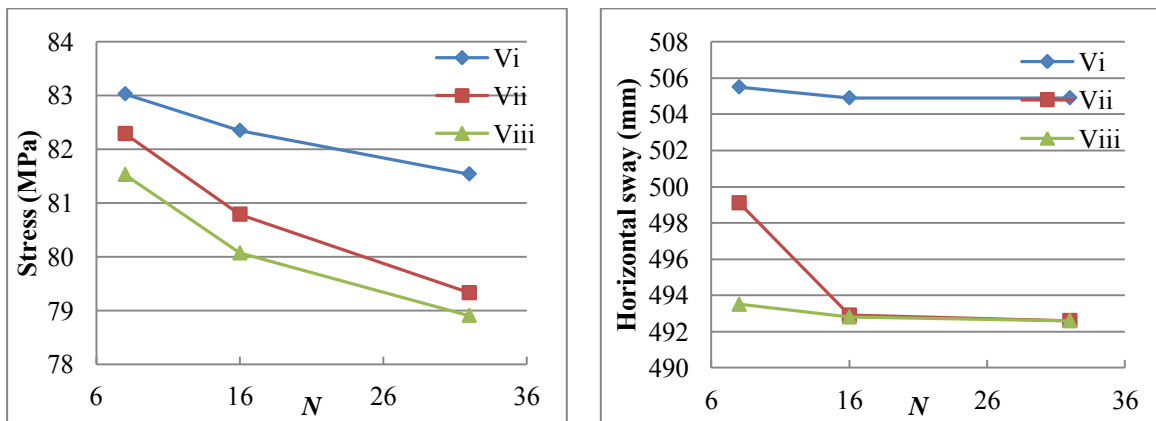


Figure 7.27 Maximum von Mises stresses and horizontal sways of the 250m towers with  $V_i$ ,  $V_{ii}$  and  $V_{iii}$

Maximum von Mises stresses and horizontal sways of the 250m towers with  $V_i$ ,  $V_{ii}$  and  $V_{iii}$  are displayed in Figure 7.27. The horizontal axis presents the numbers of vertical stiffeners for the 250m towers, and the vertical axis refers to the maximum von Mises stresses and horizontal sways of the 250m towers. Obviously, the maximum von Mises stresses and horizontal sways of the 250m towers *a*, *b* and *c* reduces with the number of the vertical stiffeners increase. Thus, the strength of the 250m

towers increases as the number of vertical stiffeners increases in the case that the mass between horizontal and vertical stiffeners is equal each other.

### 7.5.3 Effect of the central angle of the vertical stiffeners

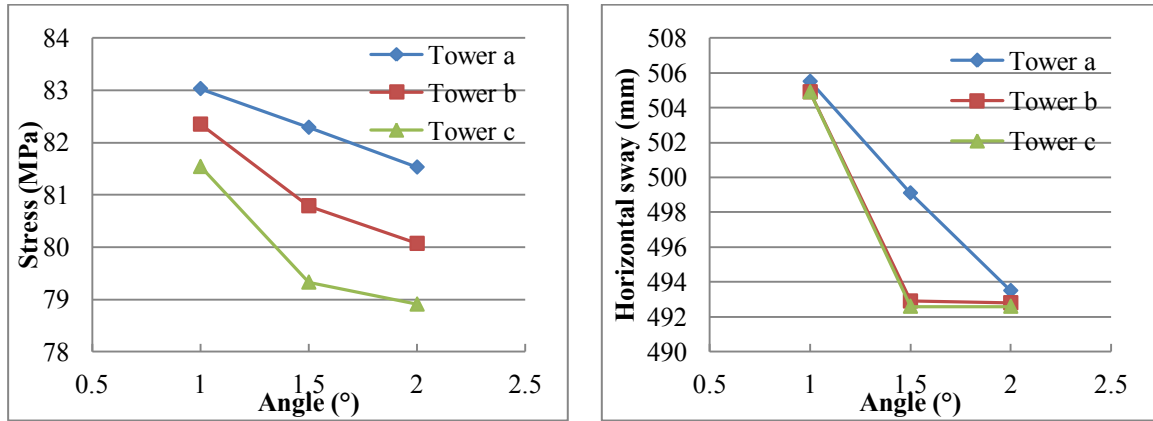


Figure 7.28 Maximum von Mises stresses and horizontal sways of the 250m towers *a*, *b* and *c*

The maximum von Mises stresses and the horizontal sways of the 250m towers *a*, *b* and *c* with respect to the central angle,  $\beta$  of each vertical stiffener are depicted in Figure 7.28. The maximum von Mises stresses and horizontal sways of the 250m towers *a*, *b* and *c* reduce as the central angle,  $\beta$  of each vertical stiffener increases. The maximum horizontal sways of the 250m tower *b* and *c* show a similar trend as the central angle,  $\beta$  of each vertical stiffener increases. It is concluded that an increase in the central angle,  $\beta$  of each vertical stiffener significantly improves the strength of the 250m towers.

### 7.5.4 Buckling analysis

Similarly, the linear buckling analysis of the 250m towers is performed by using the finite element software ABAQUS, and the local buckling modes and eigenvalues of the 250m towers *a*, *b* and *c* are obtained. The first local buckling modes of the 250m towers with  $V_i$  are shown in Figure 7.29. The first local buckling modes of the 250T<sub>iv</sub>R<sub>iv</sub>H<sub>iv</sub> are displayed in Figure 7.30. Also, the first local buckling modes of the 250m towers appear at the near base of the towers in accordance to Figure 7.29 and 7.30. The absolute value of buckling eigenvalues of the 250T<sub>iv</sub>R<sub>iv</sub>H<sub>iv</sub> is 12.48 less than those of the 250m towers as shown in Table 7.9. The corresponding first buckling eigenvalues of the 250m

towers are negative indicating the direction of the local buckling modes is opposite to the load direction.

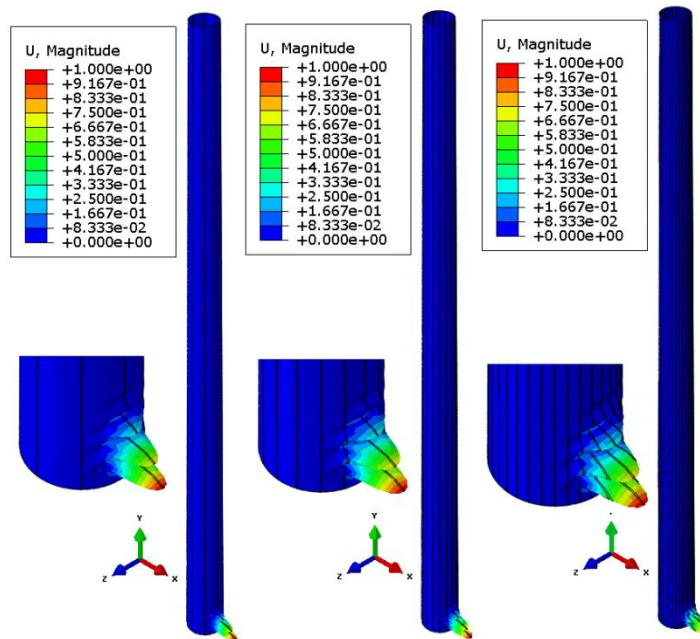


Figure 7.29 First local buckling modes of 250m towers *a*, *b* and *c* with  $V_i$

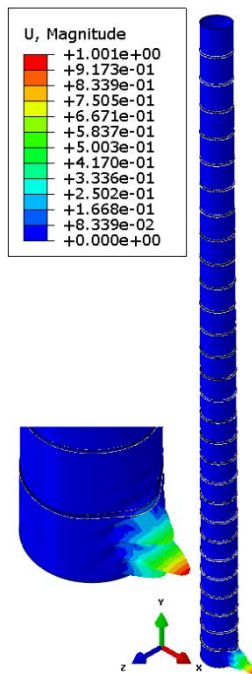
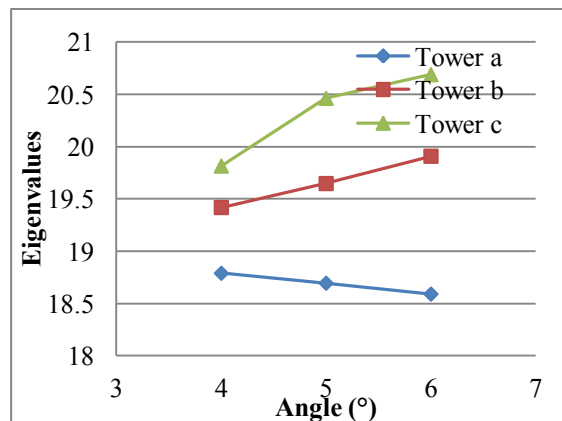
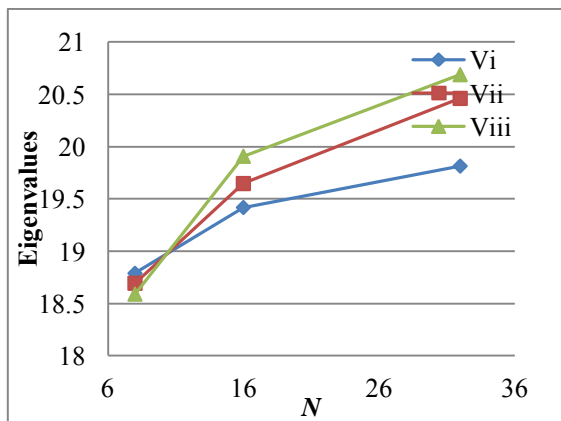


Figure 7.30 First local buckling modes of  $250T_{iv}R_{iv}H_{iv}$

CHAPTER 7: VERTICAL STIFFENERS

Table 7.9 Buckling eigenvalues of the 250m towers *a*, *b* and *c*

Type of vertical stiffeners	Type of towers	Eigenvalues
$V_i$	<i>a</i>	18.789
	<i>b</i>	19.418
	<i>c</i>	19.814
$V_{ii}$	<i>a</i>	18.694
	<i>b</i>	19.647
	<i>c</i>	20.461
$V_{iii}$	<i>a</i>	18.59
	<i>b</i>	19.908
	<i>c</i>	20.688



a. Eigenvalues of 250m towers with  $V_i$ ,  $V_{ii}$  and  $V_{iii}$       b. Eigenvalues of the 250m towers *a*, *b* and *c*

Figure 7.31 Buckling eigenvalues of the 250m towers

Table 7.9 shows the absolute values of the buckling eigenvalues of the 250m towers, and the buckling eigenvalues are given in Figure 7.31. The eigenvalues of the 250m towers, for each central angle  $\beta$  of the vertical stiffeners, increase with an increase in the number of vertical stiffeners. The eigenvalues of the 250m towers, for each number of vertical stiffeners, increase as the central angle  $\beta$  of the vertical stiffeners increases. In other words, the stability of the 250m vertically stiffened towers

increases as the number and the central angle of the vertical stiffeners increase. Vertical stiffeners can be utilised as a better design approach to improve the stability of the 250m towers than an approach using stiffening rings, where the mass is equal to that of the vertical stiffeners.

## 7.6 Conclusions

In this Chapter, the number of vertical stiffeners and the central angle of each vertical stiffener for the three height cases was considered as design parameters. In each case, the mass of the vertical stiffeners is equal to the mass of the stiffening rings that would have employed otherwise in the same towers. The effect of vertical stiffeners and of horizontal rings on the structural response of these towers under wind loading is compared, and a parametric study with respect to the vertical stiffeners was carried out. It is concluded that the use of stiffening rings is a more efficient approach than the use of vertical stiffeners for the low height towers in terms of strength enhancement, whereas for the intermediate and higher tower, vertical stiffeners are a more efficient way to enhance the strength of towers than horizontal stiffening rings of equal mass. The strength of all tower heights is increased with an increase in the number and the central angle of the vertical stiffeners.

Concerning the buckling analysis, the buckling strength of the low height towers with more vertical stiffeners increases as the quantity and the central angle  $\beta$  of the vertical stiffeners increases. The buckling strength of the low height towers with fewer vertical stiffeners reduces as the central angle  $\beta$  of the vertical stiffeners increases and as the number of vertical stiffeners is reduced. However, for the intermediate and high towers, their buckling strength increases as the number and the central angle of the vertical stiffeners increases. The use of vertical stiffeners is a more efficient approach to enhance the stability of the low, intermediate and high towers than the use of horizontal rings.

## **CHAPTER 8: CONCLUSIONS AND RECOMMENDATIONS**

### **8.1 Conclusions**

In the present thesis, the structural response of steel wind turbine towers with stiffeners subjected to wind loading has been investigated. Certain knowledge gaps have been identified from a critical review of the literature on wind turbine systems. Although in a number of papers, the serviceability and strength of wind turbine assemblies is scrutinised, the effect of stiffening rings on the structural response of wind turbine towers of various heights is almost always ignored. A more efficient approach to strengthening the towers whilst at the same time reducing the manufacturing costs should also be developed. For the design of wind turbine towers, the inherent relationships between the different parameters involving the distribution and the dimensions of the stiffening rings, and the wall thickness had not previously been explored. Likewise, the effect of the vertical stiffeners on the strength and on the buckling behaviour of wind turbine towers had not previously been considered.

To address these knowledge gaps, advanced numerical FE models of towers have been developed to simulate the structural response of the towers under wind loading. Wind loads are simulated in a simplified form along the tower height and around the circumference, in accordance with the relevant Eurocodes. The numerical method to simulate the structural response of towers was validated by comparing the models' results with the existing monitoring data. Based on the outcome, the three towers of height 50m, 150m, and 250m were chosen as representative cases in order to study their structural response comprehensively. The effect of stiffening rings and wall thickness on the structural response of the three towers was obtained for each height case by comparing the 50m, 150m and 250m towers I, II and III, and the most efficient approach to strengthening the tower, whilst saving manufacturing costs for each height case has been proposed. The most efficient range of variation for the relevant parameters, in terms of their effect on tower stability, was also obtained for each of the three height cases. In addition, the structural response of the 50m, 150m and 250m towers with

## CONCLUSIONS AND RECOMMENDATIONS

vertical stiffeners subjected to wind loads was investigated and compared with the previously mentioned corresponding horizontally stiffened  $T_{iv}R_{iv}H_{iv}$  in Chapter 6. The angle and the number of vertical stiffeners were considered as the design variables to obtain the effect of the parameter variation on the strength and buckling behaviour of the 50m, 150m and 250m towers. The main findings of this research project can be summarised as follows:

1. A method to simplify wind loading in a quasi-static way and to develop an effective discrete tower model composed of shell elements and solid elements has been proposed. The numerical modelling results have been compared with existing experimental data. By means of this approach, the optimum element size has also been obtained by comparing the results of the tower models meshed with various element sizes.
2. Three tower heights, 50m, 150m and 250m, were considered and their structural response was simulated by using the validated numerical models described above. The maximum von Mises stresses and horizontal sways of each height of tower I, II and III were obtained. The variation ratios of maximum von Mises stresses and horizontal sways of the 50m, 150m and 250m towers I and III were then compared with those of the corresponding towers II. In addition, the mass reduction ratios of towers I and III to tower II for each tower height were calculated. Then, the differential von Mises stress and horizontal sways were divided by the corresponding differential masses to estimate the marginal increase or decrease. For the 50m and 250m towers, reducing the number of rings is a more efficient way to save material and to reduce the relevant cost. For the 150m towers, reducing the wall thickness is a more efficient way to increase the strength of the towers whilst saving manufacturing costs.
3. In the framework of the dynamic analysis, both the independent towers, without the nacelle-rotor system, and the towers with a concentrated mass at the top of the tower were considered in turn. Concerning the independent towers, the 50m towers designed as ‘stiff-stiff’ towers will not experience resonance during the start-up and shut-down of wind turbines. The 150m towers and 250m towers were designed as ‘soft-stiff’ and ‘soft-soft’ towers, respectively. A significant conclusion is that the turbines on the 150m and 250m towers should be controlled

## CONCLUSIONS AND RECOMMENDATIONS

to avoid resonance effects during start-up and shut-down. Concerning towers with a concentrated mass, the 50m and 150m towers were designed as ‘soft-stiff’ towers and the 250m towers were designed as ‘soft-soft’ towers. Therefore, the 50m, 150m and 250m towers with a concentrated mass should be operated to distance their blade passing frequencies from the corresponding natural frequencies during start-up and shut-down of the wind turbines.

4. A linear buckling analysis of the 50m, 150m and 250m towers was performed to study the effect of the stiffening rings and the wall thickness on the stability of the tubular towers. For the 50m height level, increasing the quantity of rings is a more efficient way to strengthen the stability in terms of cost saving, whereas for the 150m and 250m towers, increasing the wall thickness is the more efficient way to reinforce the towers.
5. A parametric study was performed, taking into consideration the wall thickness  $T$  and the spacing of the stiffening rings for the 50m, 150m and 250m towers. The effect of the parameter variations on the structural response of the different height towers was investigated by calculating the rate of change of the maximum von Mises stress, and of the maximum horizontal sway of the three height cases with reference to the two types of parameter. The most significant range in the strength enhancement of the towers with respect to each of the design variables was then obtained, based on the rate of change of the maximum von Mises stress and of the horizontal sway of the towers. In particular, the more significant range of wall thickness,  $T$ , for strength enhancement of the towers is within the thin walled category (e.g.  $T_i$  to  $T_{ii}$ ). Concerning the ring spacing, the more significant range for the low height tower with thin walled thickness is within the greater ring spacing range (e.g.  $H_i$  to  $H_{ii}$ ), but for towers with intermediate and thick wall thickness, the range variation within the category of lower ring spacing (e.g.  $H_{iii}$  to  $H_{iv}$ ) is a more economical option for the strengthening of the towers. The more significant design range for ring spacing for the intermediate and high height towers for increasing tower strength is within the level of intermediate distance and long distance respectively (e.g.  $H_{ii}$  to  $H_{iii}$  and  $H_i$  to  $H_{ii}$ ).
6. The structural responses of vertically stiffened towers were compared with those of horizontally stiffened towers in order to explore the effect of vertical stiffeners on the strength

## CONCLUSIONS AND RECOMMENDATIONS

and buckling behaviour of the towers. The mass of the vertical stiffeners for each height case was equal to that of the corresponding height  $T_{iv}R_{iv}H_{iv}$ . The angle and the number of vertical stiffeners were then considered as design variables. The effect of the design parameters of the vertical stiffeners on the structural response of the three towers heights was examined. For the 50m towers, the stiffening rings seem to be a more efficient way to stiffen the tower wall than the vertical stiffeners, in the case where the mass of the stiffening rings and that of the vertical stiffeners are the same. However, the vertical stiffeners in the 150m and 250m towers are the more efficient option to strengthen the towers than the horizontal stiffening rings. The strength of the 50m, 150m and 250m towers  $a$ ,  $b$  and  $c$  is positive with reference to the numbers and angle of the vertical stiffeners.

7. The stability strength of the 50m towers  $b$  and  $c$  increases with reference to the quantities and angle of the vertical stiffeners, but the stability strength of the 50m tower  $a$  decreases with reference to the angle of the vertical stiffeners, and increases with reference to the numbers of the vertical stiffeners. For the 150m and 250m towers, the stability strength increases when the number and angle of the vertical stiffeners increase. The use of vertical stiffeners is a more efficient way to strengthen the 50m, 150m and 250m towers with respect to stability criteria, compared to the use of horizontal rings.

Overall, for low height towers with stiffening rings, the wall thickness is designed within the category of 'thin' thickness (e.g.  $T_i$  to  $T_{ii}$ ), and the distance between two neighbouring stiffening rings designed to be within the category of long distances (e.g. 16.67m to 10m) appears to be the most significant one. Varying the number of stiffening rings is a more efficient way to change the strength and stability of the low height towers. The use of stiffening rings is a more efficient way to strengthen a low height tower than the use of vertical stiffeners.

For an intermediate height tower with stiffening rings, the wall thickness, and the distance between stiffening rings are designed within the category of thin thickness (e.g.  $T_i$  to  $T_{ii}$ ) and intermediate distance (e.g. 11.54m to 15m) respectively, as the most significant ranges. Varying the thickness is a more efficient way to improve the strength and stability of the intermediate height towers. For the

## CONCLUSIONS AND RECOMMENDATIONS

intermediate height tower with vertical stiffeners, the use of vertical stiffeners is more efficient for strengthening than the use of stiffening rings in terms of cost saving. The numbers and angle of the vertical stiffeners have a positive effect on the strength and stability of the intermediate height towers.

For high towers with stiffening rings, the most efficient range of wall thickness is considered to be within the category of 'thin' thickness (e.g.  $T_i$  to  $T_{ii}$ ), and the optimum distance of two neighbouring stiffening rings is within the category of long distance (e.g. 16.67m to 25m). Varying the number of rings is more efficient for the strength enhancement of the high height towers. For high height towers with vertical stiffeners, vertical stiffeners are the more efficient option to strengthen the towers when comparing the stiffening rings of the same mass with vertical stiffeners. The increase in the number and angle of vertical stiffeners leads to an increase in the efficiency of material use.

### **8. 2 Recommendations for future work**

Although a lot of research effort has been invested in the field of wind turbine tower design by using finite element software as previously described, there is still a plethora of research issues to be studied. As future research topics for investigation on wind turbines, the following are recommended:

1. As the wind turbine towers have to be capable of resisting strong wind loads, the failure of a wind turbine tower may occur in a lifetime of operation. A fatigue strength analysis of the towers should be carried out to estimate the lifetime of the towers, and the effect of the parameter variations on the fatigue strength of the towers needs to be explored. Some stiffeners are welded onto tower walls in engineering practice, hence the effect of welded stiffeners on the fatigue response should be also considered.
2. The foundations of wind turbine towers should be considered as a part of the wind turbine tower system. Therefore, a serviceability analysis of the tower-foundation system should be performed to study the vibration behaviour of the entire tower system. The strength and stability of tower-foundation systems need to be assessed to optimise the foundation design.

## CONCLUSIONS AND RECOMMENDATIONS

3. During the operating life of wind turbines, the benefits resulting from the power that wind turbines produce can be estimated and compared with the investment costs, including the maintenance and manufacturing costs, in order to optimise the towers in terms of material use.
4. The towers of wind turbines are connected by the flange-bolt system, but in this paper the flanges and rings were simplified and considered as one solid, whereas the effect of pre-stressed bolts on the structural response of the flange-bolt system have been ignored. Therefore, the pre-stressing of bolts should be considered as a design variable, and the dimensions and distributions of bolts around the circumference should be assessed to reduce the local maximum stress of the flange-bolt system.
5. In engineering practice, there may be door openings in the vicinity of the tower base. The door opening area of the wind turbine towers under wind loads experience stress concentration, so the effect of the door opening on the strength and buckling behaviours of wind turbine towers should be thoroughly investigated and the methods to stiffen the door opening should be studied.
6. In this paper, the effect of vertical stiffeners and horizontal stiffening rings on the towers were respectively evaluated and compared with each other. The effect of orthogonal stiffeners on the structural response of the towers could also be obtained and compared with those of the vertical and horizontal stiffeners. Towers manufactured in cylindrical sections should be also compared with towers composed of various types of polygonal sections in future research.
7. The taper angle for the three height towers can be considered to be a design parameter, and the effect of taper angle on the structural response of steel tubular wind turbine towers under wind loads can be studied.
8. The geometrically and materially nonlinear analysis including the effect of geometric imperfections (GMNIA) can be performed as future work, and their possible magnitudes and shapes and their expected effect on the structural response can be studied in future work. The conclusions drawn in the present thesis should be rechecked in the light of the future work.

## REFERENCES

- ABAQUS (2008) *ABAQUS/Standard and ABAQUS/Explicit-Version 6.8-1. Abaqus Theory Manual*, Dassault System.
- Abdalla, K.M.A., Efthymiou, E. and Baniotopoulos, C.C. (2014) On the Design of Steel Lattice Telecommunication Structures. *Journal of Structural Engineering*, 41: (3): 214-226.
- Ackermann, T. and Soder, L. (2000) Wind energy technology and current status: a review. *Renewable and Sustainable Energy Reviews*, 4: 315-374.
- Adams, D., White, J., Rumsey, M. and Farrar, C. (2011) Structural health monitoring of wind turbines: method and application to a HAWT. *Wind Energy*, 14: (4): 603-623.
- Adhikaria, S. and Bhattacharya, S. (2012) Dynamic Analysis of Wind Turbine Towers on Flexible Foundations. *Shock and Vibration*, 19: 37-56.
- Agbayani, N.A. and Vega, R.E. (2012) The Rapid Evolution of Wind Turbine Tower Structural Systems: A history and technical overview. *Structures Congress 2012*, 1201-1212.
- Al-Bahadly, I. (2009) Building a wind turbine for rural home. *Energy for Sustainable Development*, 13: (3): 159-165.
- AlHamaydeh, M. and Hussain, S. (2011) Optimized frequency-based foundation design for wind turbine towers utilizing soil–structure interaction. *Journal of the Franklin Institute*, 348: (7): 1470-1487.
- Ancona, D.F. (1989) *Power generation, wind ocean*. In: *Wilk's encyclopedia of architecture: design, engineering and construction*. New York: Wiley.
- Andersen, L.V., Vahdatirad, M.J., Sichani, M.T. and Sørensen, J.D. (2012) Natural frequencies of wind turbines on monopile foundations in clayey soils—A probabilistic approach. *Computers and Geotechnics*, 43: 1–11.

## REFERENCES

- Antunes, P., Travanca, R., Varum, H. and André, P. (2012) Dynamic monitoring and numerical modelling of communication towers with FBG based accelerometers. *Journal of Constructional Steel Research*, 74: 58-62.
- Baker, L.T. (1982) *A field guide to American windmills*. Norman, Oklahoma: USA: University of Oklahoma Press.
- Baniotopoulos, C., Borri, C. and Stathopoulos, T. (2011) *Environmental wind engineering and design of wind energy structures, CISM Courses and Lectures Udine*. Italy: Springer Verlag.
- Bañuelos-Ruedas, F., Angeles-Camacho, C. and Rios-Marcuello, S. (2010) Analysis and validation of the methodology used in the extrapolation of wind speed data at different heights. *Renewable and Sustainable Energy Reviews*, 14: (8): 2383-2391.
- Bazeos, N., Hatzigeorgiou, G.D., Hondros, I.D., Karamaneas, H., Karabalis, D.L. and Beskos, D.E. (2002) Static, seismic and stability analyses of a prototype wind turbine steel tower. *Engineering Structures*, 24: 1015-1025.
- Bhattacharya, S. and Adhikari, S. (2011) Experimental validation of soil–structure interaction of offshore wind turbines. *Soil Dynamics and Earthquake Engineering*, 31: 805–816.
- Bilgili, M., Yasar, A. and Simsek, E. (2011) Offshore wind power development in Europe and its comparison with onshore counterpart. *Renewable and Sustainable Energy Reviews*, 15: (2): 905-915.
- Binh, L.V., Ishihara, T., Phuc, P.V. and Fujino, Y. (2008) A peak factor for non-Gaussian response analysis of wind turbine tower. *Journal of Wind Engineering and Industrial Aerodynamics*, 96: (10-11): 2217-2227.
- Bisoi, S. and Haldar, S. (2014) Dynamic analysis of offshore wind turbine in clay considering soil–monopile–tower interaction. *Soil Dynamics and Earthquake Engineering*, 63: 19-35.

## REFERENCES

- Bray, F.M. and Egle, D.M. (1970) An experimental investigation of the free vibration of thin cylindrical shells with discrete longitudinal stiffening. *Journal of Sound and Vibration*, 12: (2): 153-164.
- Breeze, P. (2004) *The future of global offshore wind power: the technology economics and impact of wind power generation*. London: Business insights.
- Breeze, P. (2008) *The future of wind power: increasing economic competitiveness as the technology matures*. London: Business insights.
- Brodersen, M.L. and Høgsberg, J. (2014) Damping of Offshore Wind Turbine Tower Vibrations by a Stroke Amplifying Brace. *Energy Procedia*, 53: 258-267.
- Carmoy, D. (1978) The USA faces the energy challenge *Energy Policy*, 36-52.
- Chang, S.J. (2013) Solving the problem of carbon dioxide emissions. *Forest Policy and Economics*, 35: 92-97.
- Chen, J.F. and Rotter, J.M. (1998) Effective cross sections of asymmetric rings on cylindrical shells. *Journal of Structural Engineering*, 124: 1074-1080.
- Chen, K., Song, M.X. and Zhang, X. (2014) The iteration method for tower height matching in wind farm design. *Journal of Wind Engineering and Industrial Aerodynamics*, 132: 37-48.
- Chen, L. and Rotter, J.M. (2012) Buckling of anchored cylindrical shells of uniform thickness under wind load. *Engineering Structures*, 41: 199-208.
- Chen, W.H., Lu, Z.R., Lin, W., Chen, S.H., Ni, Y.Q., Xia, Y. and Liao, W.Y. (2011) Theoretical and experimental modal analysis of the Guangzhou New TV Tower. *Engineering Structures*, 33: (12): 3628-3646.
- Chen, X.-b., Li, J. and Chen, J.-y. (2009) Wind-induced response analysis of a wind turbine tower including the blade-tower coupling effect. *Journal of Zhejiang University SCIENCE A*, 10: (11): 1573-1580.

## REFERENCES

- Chou, J.-S. and Tu, W.-T. (2011) Failure analysis and risk management of a collapsed large wind turbine tower. *Engineering Failure Analysis*, 18: (1): 295-313.
- Ciang, C.C., Lee, J.-R. and Bang, H.-J. (2008) Structural health monitoring for a wind turbine system: a review of damage detection methods. *Measurement Science and Technology*, 19: (12): 122001.
- Corona, E., Lee, L.H. and Kyriakides, S. (2006) Yield anisotropy effects on buckling of circular tubes under bending. *International Journal of Solids and Structures*, 43: (22-23): 7099-7118.
- CWIF (2005) "Caithness windfarm information forum 2005 wind turbine accident data", [online]. <http://www.caithnesswindfarms.co.uk> [Accessed 31/08/ 2014]
- DEA (2006) *Offshore wind farms and the environment, Danish experiences from Horns Rev and Nysted*. Copenhagen: Danish Energy Agency.
- Dimopoulos, C.A. and Gantes, C.J. (2012) Experimental investigation of buckling of wind turbine tower cylindrical shells with opening and stiffening under bending. *Thin-Walled Structures*, 54: 140-155.
- Dimopoulos, C.A. and Gantes, C.J. (2013) Comparison of stiffening types of the cutout in tubular wind turbine towers. *Journal of Constructional Steel Research*, 83: 62-74.
- Dixon, S.L. and Hall, C.A. (2014) "*Wind Turbines*". Fluid Mechanics and Thermodynamics of Turbomachinery. Elsevier 419-485.
- Do, T.Q., Lindt, J.W.v.d. and H.N.Mahmoud (2014a) Fatigue Life Model Including Crack Propagation for Wind Turbine Tower Base Connections. *Structures Congress 2014*, 1606-1615.
- Do, T.Q., Mahmoud, H. and van de Lindt, J.W. (2014b) Fatigue Life of Wind Turbine Tower Bases throughout Colorado. *Journal of Performance of Constructed Facilities*, 04014109.
- Do, T.Q., van de Lindt, J.W. and Mahmoud, H. (2014c) Fatigue Life Fragilities and Performance-Based Design of Wind Turbine Tower Base Connections. *Journal of Structural Engineering*, 04014183.

## REFERENCES

- EN 1991-01-04: Actions on structures, CEN, Brussels 1991.
- EN 1991-01-06: Strength and Stability of Shell Structures, CEN, Brussels 1991.
- Erdos, P. (2012) Have oil and gas prices got separated? . *Energy Policy*, 707-718.
- Esteban, M. and Leary, D. (2012) Current developments and future prospects of offshore wind and ocean energy. *Applied Energy*, 90: (1): 128-136.
- Esteban, M.D., Diez, J.J., López, J.S. and Negro, V. (2011) Why offshore wind energy? *Renewable Energy*, 36: (2): 444-450.
- EWEA (2008) "Pure power: wind energy scenarios up to 2030", [online]. [www.ewea.org](http://www.ewea.org) European Wind Energy Association [Accessed 27/08/ 2014]
- EWEA (2009a) "The economics of wind energy", [online]. <http://www.ewea.org> European Wind Energy Association [Accessed 30/08/ 2014]
- EWEA (2009b) "Wind at work", [online]. <http://www.ewea.org> European Wind Energy Association [Accessed 30/08/ 2014]
- Farshidianfar, A., Farshidianfar, M.H., Crocker, M.J. and Smith, W.O. (2011) Vibration analysis of long cylindrical shells using acoustical excitation. *Journal of Sound and Vibration*, 330: (14): 3381-3399.
- Garratt, J.R. (1992) *The atmospheric boundary layer*. New York: Cambridge University Press.
- Gasch, R. and Tvele, J. (2012) *Wind Power Plants*. Second. Berlin: Springer.
- Geernaert, G.L. (2003) Surface layer. *Encyclopedia of Atmospheric Sciences*, 305–311.
- Gencturk, B., Attar, A. and Tort, C. (2014) Design Optimization of Lattice Wind Turbine Towers Subjected to Earthquake Forces. *Structures Congress 2014*, 1694-1703.

## REFERENCES

- Gervásio, H., Rebelo, C., Moura, A., Veljkovic, M. and Simões da Silva, L. (2014) Comparative life cycle assessment of tubular wind towers and foundations – Part 2: Life cycle analysis. *Engineering Structures*, 74: 292–299.
- Gettel, M. and Schneider, W. (2007) Buckling strength verification of cantilevered cylindrical shells subjected to transverse load using Eurocode 3. *Journal of Constructional Steel Research*, 63: (11): 1467-1478.
- GEWEC (2014) "Global Wind Energy Council (GWEC)", [online]. [www.gwec.net](http://www.gwec.net) [Accessed 01/09/2014]
- Ghanbari Ghazijahani, T., Jiao, H. and Holloway, D. (2015) Structural behavior of shells with different cutouts under compression: An experimental study. *Journal of Constructional Steel Research*, 105: 129-137.
- Ghanbari Ghazijahani, T. and Showkati, H. (2013) Experiments on cylindrical shells under pure bending and external pressure. *Journal of Constructional Steel Research*, 88: 109-122.
- Gipe, P. (1995) *Wind energy comes of age*. USA: Wiley.
- Golding, E. (1991) *Renewable energy sources for fuels and electricity*. Washinton, DC: Island Press.
- Gong, J., Tao, J., Zhao, J., Zeng, S. and Jin, T. (2013) Effect of top stiffening rings of open top tanks on critical harmonic settlement. *Thin-Walled Structures*, 65: 62-71.
- Grant, I., M.Mo, Pan, X., Parkin, P., Powell, J., Reinecke, H., Shuang, K., Coton, F. and Lee, D. (2000) An experimental and numerical study of the vortex filaments in the wake of an operational, horizontal-axis, wind turbine. *Journal of Wind Engineering and Industrial Aerodynamics*, 85: 177-189.
- Green, R. and Vasilakos, N. (2011) The economics of offshore wind. *Energy Policy*, 39: (2): 496-502.
- Guo, L., Uang, C.-M., Elgamal, A., Prowell, I. and Zhang, S. (2011) Pushover Analysis of a 53 m High Wind Turbine Tower. *Advanced Science Letters*, 4: (3): 656-662.

## REFERENCES

- Guo, L., Yang, S. and Jiao, H. (2013) Behavior of thin-walled circular hollow section tubes subjected to bending. *Thin-Walled Structures*, 73: 281-289.
- GWEC (2011a) "The global wind energy council. Germany", [online]. <http://www.gwec.net> [Accessed 11/11/ 2012]
- GWEC (2011b) "The global wind energy council. Spain", [online]. <http://www.gwec.net> [Accessed 11/11/ 2012]
- Häckell, M.W. and Rolfes, R. (2013) Monitoring a 5MW offshore wind energy converter—Condition parameters and triangulation based extraction of modal parameters. *Mechanical Systems and Signal Processing*, 40: (1): 322-343.
- Haenler, M., Ritschel, U. and Warnke, I. (2006) "Systematic modelling of wind turbine dynamics and earthquake loads on wind turbines", *European Wind Energy Conference Exhibition, European Wind Energy Association*, Brussels, Belgium
- Harte, M., Basu, B. and Nielsen, S.R.K. (2012) Dynamic analysis of wind turbines including soil-structure interaction. *Engineering Structures*, 45: 509-518.
- Harte, R. and Van Zijl, G.P.A.G. (2007) Structural stability of concrete wind turbines and solar chimney towers exposed to dynamic wind action. *Journal of Wind Engineering and Industrial Aerodynamics*, 95: (9-11): 1079-1096.
- Hartmann, D., Smarsly, K. and Law, K.H. (2011) "Coupling sensor-based structural health monitoring with finite element model updating for probabilistic lifetime estimation of wind energy converter structures.", [online]. <http://eil.stanford.edu/publications> [Accessed 30/09/ 2014]
- Herman, S.A., Kooijman, H.J.T. and Hendriks, H.B. (2003) "Variations on a 500MW offshore wind farm design", *Offshore Wind Energy in Mediterranean and Other Europeans Seas Conference*, Naples, Italy

## REFERENCES

- Hills, R.L. (1994) *Power from Wind: A History of Windmill Technology*. UK: Cambridge University Press.
- Houliara, S. and Karamanos, S.A. (2010) Stability of long transversely-isotropic elastic cylindrical shells under bending. *International Journal of Solids and Structures*, 47: (1): 10-24.
- Hu, Y., Baniotopoulos, C. and Yang, J. (2014) Effect of internal stiffening rings and wall thickness on the structural response of steel wind turbine towers. *Engineering Structures*, 81: 148-161.
- Hull, A.J. (2012) Elastic response of a cylinder containing longitudinal stiffeners. *Journal of Sound and Vibration*, 331: (3): 588-604.
- IEA (2006) "Wind energy annual report 2006". Spain, International Energy Agency
- IEA (2010a) *International Energy Agency. Key world energy statistics*. Paris: IEA.
- IEA (2010b) *International Energy Agency. World energy outlook 2010 factsheet*. Paris: IEA.
- IPCC (2011) *Summary for policymakers. In: IPCC special report on renewable energysources and climate change mitigation*. Cambridge, United Kingdom and New York, NY, USA: Cambridge University Press.
- Islam, M.R., Mekhilef, S. and Saidur, R. (2013) Progress and recent trends of wind energy technology. *Renewable and Sustainable Energy Reviews*, 21: 456-468.
- Iwicki, P., Wójcik, M. and Tejchman, J. (2011) Failure of cylindrical steel silos composed of corrugated sheets and columns and repair methods using a sensitivity analysis. *Engineering Failure Analysis*, 18: (8): 2064-2083.
- Javidruzi, M., Vafai, A., Chen, J.F. and Chilton, J.C. (2004) Vibration, buckling and dynamic stability of cracked cylindrical shells. *Thin-Walled Structures*, 42: (1): 79-99.
- Jay, A. and Myers, A. (2014) Design of Conical Steel Wind Turbine Towers Manufactured with Automated Spiral Welding. *Structures Congress 2014*, 1675-1683.

## REFERENCES

- Jerath, S. and Austin, S. (2013) Response of Wind Turbine Towers to Seismic Loading At Different Damping Ratios. *Structures Congress 2013*.
- Jiang, W., Fan, Q. and Gong, J. (2010) Optimization of welding joint between tower and bottom flange based on residual stress considerations in a wind turbine. *Energy*, 35: (1): 461-467.
- Johnson, G.L. (1985) *Wind energy systems*. . NewYork: Prentice Hall.
- Joselin Herbert, G.M., Iniyan, S., Sreevalsan, E. and Rajapandian, S. (2007) A review of wind energy technologies. *Renewable and Sustainable Energy Reviews*, 11: (6): 1117-1145.
- Kaldellis, J.K. and Zafirakis, D. (2011) The wind energy (r)evolution: A short review of a long history. *Renewable Energy*, 36: (7): 1887-1901.
- Karpat, F. (2013) A Virtual Tool for Minimum Cost Design of a Wind Turbine Tower with Ring Stiffeners. *Energies*, 6: (8): 3822-3840.
- Kealey, E.J. (1987) *Harvesting the air: Windmill pioneers in 12th century England*. Berkeley, CA: University of California Press.
- Kilic, G. and Unluturk, M.S. (2015) Testing of wind turbine towers using wireless sensor network and accelerometer. *Renewable Energy*, 75: 318-325.
- Kim, D.H., Lee, S.G. and Lee, I.K. (2014) Seismic fragility analysis of 5MW offshore wind turbine. *Renewable Energy*, 65: 250-256.
- Kim, Y.T., Haghpanah, B., Ghosh, R., Ali, H., Hamouda, A.M.S. and Vaziri, A. (2013) Instability of a cracked cylindrical shell reinforced by an elastic liner. *Thin-Walled Structures*, 70: 39-48.
- Kjørlaug, R.A., Kaynia, A.M. and Elgamal, A. (2014) "Seismic Response of Wind Turbines due to Earthquake and Wind Loading", *Proceedings of the 9th International Conference on Structural Dynamics, EURO DYN 2014*, Porto, Portugal

## REFERENCES

- Knight, S. (2014) "FWT installs 2.5MW machine on 140-metre lattice tower", [online]. <http://www.windpowermonthly.com/article/1230277/fwt-installs-25mw-machine-140-metre-lattice-tower> [Accessed 10/10/ 2014]
- Koepl, G.W. (1982) *Putnam's power from the wind*. Second. New York, USA: Van Nostrand Reinhold.
- Krohn, S., Morthorst, P.-E. and Awerbuch, S. (2009) "Economics of Wind Energy". European Wind Energy Association.
- Kuhn, M. (1997) "Soft or Stiff a Fundamental Question for Designers of Offshore Wind Energy Converters", *Proceedings European Wind Energy Conference EWEC'97*, Dublin, Ireland
- Kwon, D.K., Kareem, A. and Butler, K. (2012) Gust-front loading effects on wind turbine tower systems. *Journal of Wind Engineering and Industrial Aerodynamics*, 104-106: 109-115.
- Lavassas, I., Nikolaidis, G., Zervas, P., Efthimiou, E., Doudoumis, I.N. and Baniotopoulos, C.C. (2003) Analysis and design of the prototype of a steel 1-MW wind turbine tower. *Engineering Structures*, 25: (8): 1097-1106.
- Lee, K.-S. and Bang, H.-J. (2012) A study on the prediction of lateral buckling load for wind turbine tower structures. *International Journal of Precision Engineering and Manufacturing*, 13: (10): 1829-1836.
- Lee, K.C. and Yoo, C.H. (2012) Longitudinal Stiffeners in Concrete-Filled Tubes. *Journal of Structural Engineering*, 138: 753-758.
- Lemak, D. and Studnicka, J. (2005) Influence of Ring Stiffeners on a Steel Cylindrical Shell. *Acta Polytechnica*, 45: 56-63.
- Leung, D.Y.C. and Yang, Y. (2012) Wind energy development and its environmental impact: A review. *Renewable and Sustainable Energy Reviews*, 16: (1): 1031-1039.

## REFERENCES

- Li, Z.-q., Chen, S.-j., Ma, H. and Feng, T. (2013) Design defect of wind turbine operating in typhoon activity zone. *Engineering Failure Analysis*, 27: 165-172.
- Lim, S., Kong, C. and Park, H. (2013) A Study on Optimal Design of Filament Winding Composite Tower for 2MW Class Horizontal Axis Wind Turbine Systems. *International Journal of Composite Materials*, 3: 15-23.
- Lindvig, K. (2010) "The installation and servicing of offshore wind farms", [online]. [http://www.eufores.org/fileadmin/eufores/Events/Parliamentary\\_Events/Offshore\\_September\\_2010/The%20installation%20and%20servicing\\_A2SEA.pdf](http://www.eufores.org/fileadmin/eufores/Events/Parliamentary_Events/Offshore_September_2010/The%20installation%20and%20servicing_A2SEA.pdf) [Accessed 03/09/ 2014]
- Liu, W., Tang, B. and Jiang, Y. (2010) Status and problems of wind turbine structural health monitoring techniques in China. *Renewable Energy*, 35: (7): 1414-1418.
- Liu, W.Y. (2013) The vibration analysis of wind turbine blade-cabin-tower coupling system. *Engineering Structures*, 56: 954-957.
- Lopatin, A.V. and Morozov, E.V. (2015) Fundamental frequency of a cantilever composite cylindrical shell. *Composite Structures*, 119: 638-647.
- Lupi, F., Borri, C., Facchini, L., Niemann, H.J. and Peil, U. (2013) A new type of bistable flow around circular cylinders with spanwise stiffening rings. *Journal of Wind Engineering and Industrial Aerodynamics*, 123: 281-290.
- Maalawi, K.Y. (2007) A model for yawing dynamic optimization of a wind turbine structure. *International Journal of Mechanical Sciences*, 49: (10): 1130-1138.
- Makarios, T. and Baniotopoulos, C. (2015) Modal analysis of wind turbine tower via its continuous model with partially fixed foundation. *International Journal of Innovative Research in Advanced Engineering*, 2: (1): 14-25.
- Makarios, T.K. and Baniotopoulos, C.C. (2012) Wind energy structures: modal analysis by the continuous model approach. *Journal of Vibration and Control*, 20: (3): 395-405.

## REFERENCES

- Malcolm, D.J. (2004) "Windpact rotor design study: hybrid tower design", [online]. <http://www.nrel.gov> National Renewable Energy Laboratory, Washington [Accessed 04/09/ 2014]
- Manenti S., P.F. (2010) Dynamic Analysis of an Offshore Wind Turbine\_ Wind-Waves Nonlinear Interaction. *Earth and Space* 2010.
- Manwell, J.F., McGowan, J.G. and Rogers, A.L. (2009) *Wind Energy Explained: Theory, Design and Application*. 2nd Edition. Wiley.
- Mensah, A.F. and Dueñas-Osorio, L. (2014) Improved reliability of wind turbine towers with tuned liquid column dampers (TLCs). *Structural Safety*, 47: 78-86.
- Meyer, N.I. (1995) Danish wind power development *Energy Sustain Development*, 18-25.
- Murtagh, P.J., Basu, B. and Broderick, B.M. (2004) Simple models for natural frequencies and mode shapes of towers supporting utilities. *Computers & Structures*, 82: (20-21): 1745-1750.
- Murtagh, P.J., Basu, B. and Broderick, B.M. (2005) Along-wind response of a wind turbine tower with blade coupling subjected to rotationally sampled wind loading. *Engineering Structures*, 27: (8): 1209-1219.
- Negm, H.M. and Maalawi, K.Y. (2000) Structural design optimization of wind turbine towers. *Computers & Structures*, 74: 649-666.
- Ni, Y.Q., Xia, Y., Liao, W.Y. and Ko, J.M. (2009) Technology innovation in developing the structural health monitoring system for Guangzhou New TV Tower. *Structural Control and Health Monitoring*, 16: (1): 73-98.
- Nuta, E., Christopoulos, C. and Packer, J.A. (2011) Methodology for seismic risk assessment for tubular steel wind turbine towers: application to Canadian seismic environment. *Canadian Journal of Civil Engineering*, 38: (3): 293-304.
- Oh, C.H. and Reuveny, R. (2010) Climatic natural disasters, political risk, and international trade. *Global Environmental Change*, 20: (2): 243-254.

## REFERENCES

- Ozbek, M., Rixen, D.J., Erne, O. and Sanow, G. (2010) Feasibility of monitoring large wind turbines using photogrammetry. *Energy*, 35: (12): 4802-4811.
- Patel, A. (2014) Onshore wind projects dominate. *Renewable Energy Focus*, 15: (4): 12-13.
- Perelmuter, A. and Yurchenko, V. (2013) Parametric Optimization of Steel Shell Towers of High-Power Wind Turbines. *Procedia Engineering*, 57: 895-905.
- Perveen, R., Kishor, N. and Mohanty, S.R. (2014) Off-shore wind farm development: Present status and challenges. *Renewable and Sustainable Energy Reviews*, 29: 780-792.
- Petersen, F. and Thorndahl, J. (1993) *Som vinden blaeser*. Elmuseet.
- Pieraccini, M., Parrini, F., Fratini, M., Atzeni, C. and Spinelli, P. (2008) In-service testing of wind turbine towers using a microwave sensor. *Renewable Energy*, 33: (1): 13-21.
- Polyzois, D.J., Raftoyiannis, I.G. and Ungkurapinan, N. (2009) Static and dynamic characteristics of multi-cell jointed GFRP wind turbine towers. *Composite Structures*, 90: (1): 34-42.
- Price, T.J. (2005) James Blyth – Britain's first modern wind power pioneer *Wind Engineering*, 29: 191-200.
- Prowell, I., Uang, C.-M., Elgamal, A., Luco, J.E. and Guo, L. (2012) Shake Table Testing of a Utility-Scale Wind Turbine. *Journal of Engineering Mechanics*, 138: (7): 900-909.
- Prowell, I., Veletzos, M., Elgamal, A. and Restrepo, J. (2009) Experimental and Numerical Seismic Response of a 65 kW Wind Turbine. *Journal of Earthquake Engineering*, 13: (8): 1172-1190.
- Qu, Y., Wu, S., Chen, Y. and Hua, H. (2013) Vibration analysis of ring-stiffened conical–cylindrical–spherical shells based on a modified variational approach. *International Journal of Mechanical Sciences*, 69: 72-84.
- Quilligan, A., O'Connor, A. and Pakrashi, V. (2012) Fragility analysis of steel and concrete wind turbine towers. *Engineering Structures*, 36: 270-282.

## REFERENCES

- Rajgor, G. (2010) EU renewables: will the decade belong to onshore wind. *Renewable Energy Focus*, 12-20.
- Ramachandran, P. and Narayanan, S. (2007) Evaluation of modal density, radiation efficiency and acoustic response of longitudinally stiffened cylindrical shell. *Journal of Sound and Vibration*, 304: (1-2): 154-174.
- Rebelo, C., Moura, A., Gervásio, H., Veljkovic, M. and Simões da Silva, L. (2014) Comparative life cycle assessment of tubular wind towers and foundations – Part 1: Structural design. *Engineering Structures*, 74: 283–291.
- Rebelo, C., Simões, R., Matos, R., Silva, L.S.d., Veljkovic, M. and Pircher, M. (2012a) "Structural monitoring of a wind turbine steel tower", *15th International Conference on Experimental Mechanics*, Porto, Portugal
- Rebelo, C., Veljkovic, M., Matos, R. and Silva, L.S.d. (2012b) Structural monitoring of a wind turbine steel tower Part II monitoring results. *Wind and Structures*, 15: 301-311.
- Rebelo, C., Veljkovic, M., Silva, L.S.d., Simões, R. and Henriques, J. (2012c) Structural monitoring of a wind turbine steel tower Part I system description and calibration. *Wind and Structures*, 15: 285-299.
- REN21 (2012) "Renewables 2012 global status report", [online]. <http://www.ren21.net> Paris REN21 Secretariat [Accessed 01/09/ 2014]
- Righter, R. (1996) *Wind energy in America: a history*. USA: University of Oklahoma Press.
- Rolfes, R., Tsiapoki, S. and Häckell, M.W. (2014) "*Sensing solutions for assessing and monitoring wind turbines*". Elsevier Ltd 565-604.
- Ross, C.T.F., Little, A.P.F. and Adeniyi, K.A. (2005) Plastic buckling of ring-stiffened conical shells under external hydrostatic pressure. *Ocean Engineering*, 32: (1): 21-36.

## REFERENCES

- Rotter, J.M. and Sadowski, A.J. (2012) Cylindrical shell bending theory for orthotropic shells under general axisymmetric pressure distributions. *Engineering Structures*, 42: 258-265.
- RRB-Energy-Limited (2009) "World Wide Wind Turbines: Technical specification RRB Energy 500kW wind turbine PS 500", [online]. <http://www.stirling.gov.uk/PABS/> [Accessed 03/09/ 2014]
- Sabouri-Ghomi, S., Kharrazi, M.H.K. and Javidan, P. (2006) Effect of stiffening rings on buckling stability of R.C. hyperbolic cooling towers. *Thin-Walled Structures*, 44: (2): 152-158.
- Sahu, B.K., Hiloidhari, M. and Baruah, D.C. (2013) Global trend in wind power with special focus on the top five wind power producing countries. *Renewable and Sustainable Energy Reviews*, 19: 348-359.
- Schneider, W. and Zahlten, W. (2004) Load-bearing behaviour and structural analysis of slender ring-stiffened cylindrical shells under quasi-static wind load. *Journal of Constructional Steel Research*, 60: (1): 125-146.
- Seçer, M., Efthymiou, E. and Baniotopoulos, C.C. (2013) "Wind Loading Evaluation on Steel Wind Turbine Towers Codified Provisions and Standards", *Proceedings of the Conference on Wind Energy Science and Technology*, Ankara, Turkey
- Sharma, A., Srivastava, J., Kar, S.K. and Kumar, A. (2012) Wind energy status in India: A short review. *Renewable and Sustainable Energy Reviews*, 16: (2): 1157-1164.
- Sharma, P.K., Warudkar, V. and Ahmed, S. (2014) Design and Optimization of 150 m Higher Wind Monitoring Tower. *International Journal of Scientific Engineering and Technology*, 3: 85 - 89.
- Sheng, J.D. (2008) Offshore wind energy: the next North sea soil. *Journal Sea Technology*, 33-37.
- Shepherd, D.G. (1990) *Historical development of the windmill*. Washinton, DC: US Department of Energy (DOE/NASA-5266-2).

## REFERENCES

- Shi, G., Jiang, X., Zhou, W., Chan, T.-M. and Zhang, Y. (2014) Experimental study on column buckling of 420MPa high strength steel welded circular tubes. *Journal of Constructional Steel Research*, 100: 71-81.
- Showkati, H. and Shahandeh, R. (2010) Experiments on the Buckling Behavior of Ring-Stiffened Pipelines under Hydrostatic Pressure. *Journal of Engineering Mechanics*, 136: 464-471.
- Silva, M.A., Reyolando and Arora, J.S. (2008) "Formulations for the Optimal Design of RC Wind Turbine Towers", *Proceedings International Conference on Engineering Optimization*, Rio de Janeiro, Brazil
- Silvestre, N. and Gardner, L. (2011) Elastic local post-buckling of elliptical tubes. *Journal of Constructional Steel Research*, 67: (3): 281-292.
- Sim, H.-B., Prowell, I., Elgamal, A. and Uang, C.-M. (2014) Flexural Tests and Associated Study of a Full-Scale 65-kW Wind Turbine Tower. *Journal of Structural Engineering*, 140: (5): 04013110.
- Sim, H.-B. and Uang, C.-M. (2011) Welded Sleeve Connection Design of Cantilevered Steel Sign Structures. *Journal of Structure Engineering*, 1303-1310.
- Smarsly, K., Law, K.H. and Hartmann, D. (2012) "Structural health monitoring of wind turbines observed by autonomous software components", [online]. <http://eil.stanford.edu/publications/> [Accessed 23/09/ 2014]
- Swartz, R.A., Lynch, J.P., Zerbst, S., Sweetman, B. and Rolfes, R. (2010) Structural monitoring of wind turbines using wireless sensor networks. *Smart structures and Systems*, 6: 1-14.
- Tabassum, A., Premalatha, M., Abbasi, T. and Abbasi, S.A. (2014) Wind energy: Increasing deployment, rising environmental concerns. *Renewable and Sustainable Energy Reviews*, 31: 270-288.
- Tafreshi, A. and Bailey, C.G. (2007) Instability of imperfect composite cylindrical shells under combined loading. *Composite Structures*, 80: (1): 49-64.

## REFERENCES

- Tempel, J.v.d. and Molenaar, D.-P. (2002) Wind turbine structural dynamics – A review of the principles for modern power generation, onshore and offshore. *Wind Engineering*, 26: 211-220.
- Thomas, R.L. and Robbins, W.H. (1980) Large wind-turbine projects in the United States wind energy program *Wind Eng Ind Aerodyn*, 323-325.
- Timilsina, G.R., Cornelis van Kooten, G. and Narbel, P.A. (2013) Global wind power development: Economics and policies. *Energy Policy*, 61: 642-652.
- Tondini, N., Hoang, V.L., Demonceau, J.F. and Franssen, J.M. (2013) Experimental and numerical investigation of high-strength steel circular columns subjected to fire. *Journal of Constructional Steel Research*, 80: 57-81.
- Torkamani, S., Navazi, H.M., Jafari, A.A. and Bagheri, M. (2009) Structural similitude in free vibration of orthogonally stiffened cylindrical shells. *Thin-Walled Structures*, 47: (11): 1316-1330.
- Tran, A.T., Veljkovic, M., Rebelo, C. and Silva, L.S.d. (2013) "Resistance of door openings in towers for wind turbines", *Third South-East European Conference on Computational Mechanics*, Kos Island, Greece
- UN (2014) "United Nations: World Population to 2300", [online]. <http://www.un.org/esa/population> [Accessed 01/09/ 2014]
- UNEP Centre, F. (2013) "Global trends in renewable energy investment.", [online]. <http://fs-unep-centre.org> [Accessed 30/08/ 2014]
- UNFCCC (2013) "United Nations Framework Convention on Climate Change, Kyoto Protocol", [online]. [http://unfccc.int/kyoto\\_protocol](http://unfccc.int/kyoto_protocol) [Accessed 11/08/ 2014]
- Urbano, R.B., Savini, B. and Dobbin, J. (2013) "Optimising wind turbine design for the brazilian wind climate", *Brazil windpower conference & exhibition 2013*, Rio de Janeiro, Brazil
- Uys, P.E., Farkas, J., Jármai, K. and van Tonder, F. (2007) Optimisation of a steel tower for a wind turbine structure. *Engineering Structures*, 29: (7): 1337-1342.

## REFERENCES

- Valamanesh, V. and Myers, A.T. (2014) Aerodynamic Damping and Seismic Response of Horizontal Axis Wind Turbine Towers. *Journal of Structural Engineering*, 04014090.
- Van der Woude, C. and Narasimhan, S. (2014) A study on vibration isolation for wind turbine structures. *Engineering Structures*, 60: 223-234.
- Veljkovic, M., Feldmann, M., Naumes, J., Pak, D., Rebelo, C. and Simões da Silva, L. (2010a) Friction connection in tubular towers for a wind turbine. *Stahlbau*, 79: (9): 660-668.
- Veljkovic, M., Limam, M., Heistermann, C., Rebelo, C. and Silva, L.S.d. (2010b) "Feasibility study of friction connection in tubular towers for wind turbines", *International Symposium Steel Structures*, Istanbul, Turkey Turkish Constructional Steelwork Association.
- WB (2014) "The World Bank: GDP Ranking, PPP Based", [online]. <http://data.worldbank.org/data-catalog/GDP-PPP-based-table>. [Accessed 01/09/ 2014]
- Wikipedia (2014a) "Smith-Putnam wind turbine", [online]. [http://en.wikipedia.org/wiki/Smith-Putnam\\_wind\\_turbine](http://en.wikipedia.org/wiki/Smith-Putnam_wind_turbine) [Accessed 10/10/ 2014]
- Wikipedia (2014b) "Wind power", [online]. [http://en.wikipedia.org/wiki/Wind\\_power](http://en.wikipedia.org/wiki/Wind_power) [Accessed 10/10/ 2014]
- Winterstetter, T.A. and Schmidt, H. (2002) Stability of circular cylindrical steel shells under combined loading. *Thin-Walled Structures*, 40: 893-909.
- WMO (1981) "Meteorological aspects of the utilisation of wind as an energy resource". Geneva.
- Wójcik, M., Iwicki, P. and Tejchman, J. (2011) 3D buckling analysis of a cylindrical metal bin composed of corrugated sheets strengthened by vertical stiffeners. *Thin-Walled Structures*, 49: (8): 947-963.
- Wu, J., Wang, Z.-X. and Wang, G.-Q. (2014) The key technologies and development of offshore wind farm in China. *Renewable and Sustainable Energy Reviews*, 34: 453-462.

## REFERENCES

- Xie, W. and Sun, L. (2009) "Structural Noise of Longitudinal Stiffened Concrete Cylindrical Shell", *ICCTP 2009: Critical Issues in Transportation Systems Planning, Development, and Management*, Harbin, China
- Zaaijer, M.B. (2006) Foundation modelling to assess dynamic behaviour of offshore wind turbines. *Applied Ocean Research*, 28: (1): 45-57.
- Zhao, X., Liew, K.M. and Ng, T.Y. (2002) Vibrations of rotating cross-ply laminated circular cylindrical shells with stringer and ring stiffeners. *International Journal of Solids and Structures*, 39: 529-545.
- Zhao, Y. and Lin, Y. (2014) Buckling of cylindrical open-topped steel tanks under wind load. *Thin-Walled Structures*, 79: 83-94.
- Zhao, X. (2010) "The development of modern power system and power power system technology", *APPEEC 2010 Conference*, China
- Zhu, J.-H. and Young, B. (2012) Design of cold-formed steel oval hollow section columns. *Journal of Constructional Steel Research*, 71: 26-37.